

# **Air-liquid interface exposure of *in vitro* lung models**

**Improvement and application to study  
inhalation toxicity of aircraft-related air pollutants**

**Ruiwen He**

# Air-liquid interface exposure of *in vitro* lung models

Improvement and application to study  
inhalation toxicity of aircraft-related air pollutants

Air-liquid interface blootstelling van *in vitro* longmodellen

Verbetering en toepassing voor de studie van inhalatie  
toxiciteit van vliegtuig-gerelateerde luchtverontreinigingen

(met een samenvatting in het Nederlands)

## Proefschrift

ter verkrijging van de graad van doctor aan de  
Universiteit Utrecht  
op gezag van de  
rector magnificus, prof.dr. H.R.B.M. Kummeling,  
ingevolge het besluit van het college voor promoties  
in het openbaar te verdedigen op

dinsdag 14 september 2021 des ochtends te 10.15 uur

door

**Ruiwen He**

geboren op 16 juli 1991  
Anhui, China

©copyright Ruiwen He, 2021

Printing and layout: Guus Gijben | Proefschrift-aio.nl

Cover design: Eric Gremmer and Ruiwen He

ISBN:

All rights reserved. No part of this publication may be reproduced, stored in a retrieval system or transmitted, in any form or by any means, electronic, mechanical, photocopying, recording or otherwise, without prior permission of the author or the copyright-owning journals for previous published chapters.

**Promotor:**

Prof. dr. F.R. Cassee

**Copromotor:**

Dr. R.H.S. Westerink

**Table of contents**

<b>Chapter 1</b>	
General introduction	7
<b>Chapter 2</b>	
Pro-inflammatory responses to PM <sub>0.25</sub> from airport and urban traffic emissions	35
<b>Chapter 3</b>	
<b>Part I</b>	
An air-liquid interface bronchial epithelial model for realistic, repeated inhalation exposure to airborne particles for toxicity testing	59
<b>Chapter 3</b>	
<b>Part II</b>	
Optimization of an air-liquid interface <i>in vitro</i> cell co-culture model to estimate the hazard of aerosol exposures	81
<b>Chapter 4</b>	
Comparative toxicity of ultrafine particles around a major airport in human bronchial epithelial (Calu-3) cell model at the air-liquid interface	113
<b>Chapter 5</b>	
<i>In vitro</i> hazard characterization of simulated aircraft cabin bleed-air contamination in lung models using an air-liquid interface (ALI) exposure system	139
<b>Chapter 6</b>	
General Discussion and Future Perspectives	171
Summary	187
Nederlandse Samenvatting	193
Acknowledgements	199
Curriculum Vitae	203

# Chapter 1

## **General introduction**



## Background

It has been calculated that an adult human at rest can inhale 10,000 to 15,000 L of ambient air per day (Harkema and Wagner, 2019). Therefore, inhalation of polluted air can result in a significant deposition of xenobiotics. Inhaled polluted air may contain various gaseous and solid and soluble particulate pollutants present in outdoor air (e.g. ozone, particulate matters (PM)) and occupational settings (e.g. asbestos and engineered nanomaterials, process generated particles) (Kelly and Fussell, 2012). Since aviation industry has expanded rapidly in the past years, aircraft-related air pollution, including ultrafine particles (UFPs, particle size < 100 nm) near and at airports and bleed-air contamination in aircraft cabins, is considered as an increasing health risk (Bendtsen et al., 2021; NRC, 2002). Understanding inhalation toxicity of aircraft-related air pollutants is thus of major importance for prediction of their potential health impact.

To evaluate inhalation toxicity of gaseous and particulate pollutants, experiments can be performed using *in vivo* exposure. However, there is a continuous ethical debate on using animals to test the toxicity of chemicals. Interspecies difference is another limitation of *in vivo* models, which makes it challenging to interpret results of *in vivo* experiments for the human situation. Those issues can be avoided by the use of *in vitro* exposure, since cell models are mainly isolated from human tissues or transformed from human cells (BéruBé et al., 2010). Therefore, *in vitro* exposure systems have become a promising alternative method for toxicity testing.

## Part I: The respiratory system

It has been reported that inhalation exposure to air pollutants is associated with a wide range of public health problems such as chronic respiratory diseases (e.g. asthma and pulmonary fibrosis) (Samet and Krewski, 2007; Savolainen et al., 2010). Based on its structure and function, the respiratory tract (**Figure 1**) can be divided into the upper conducting and lower respiratory zones (Harkema and Wagner, 2019). The upper conducting airways make up the majority of the human respiratory tract and consist of nose, pharynx, larynx and tracheobronchial airways (trachea, bronchi, bronchioles, and terminal bronchioles). It not only conducts gases into and out of the lungs, but also filters, warms, and moisturizes the inhaled air before it enters the alveolar portions of the lungs. The lower respiratory tract is divided into respiratory bronchioles, alveolar ducts, and alveoli, which are functional units of gas exchange (Harkema and Wagner, 2019; Parent, 2015).

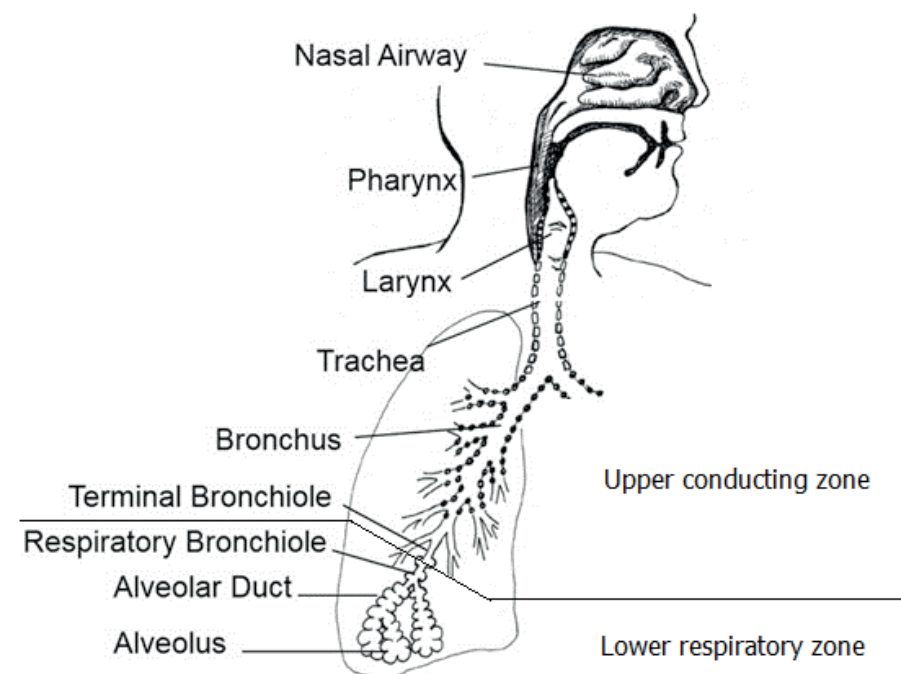


**Figure 1.** Illustration of the respiratory tract including the upper and lower respiratory zones, adapted from Harkema and Wagner (2019).

The human respiratory tract is covered by a epithelial cell layer, in which cell types vary with zones depending on their functions (**Table 1**). The bronchial tracts are covered by a pseudo-stratified columnar epithelium, which consists of undifferentiated basal cells, secretory goblet cells, and ciliated cells. The bronchioles have a cuboidal epithelium, which is mainly composed of secretory Clara cells (BéruBé et al., 2010). During inhalation, the bronchial epithelium functions as a physical barrier against inhaled materials such as particles and bacteria. Mucus clearance contributes significantly to the barrier function of the bronchial epithelium, which is regulated by different types of cells. Mucus synthesized by the secretory cells (e.g. serous cells and mucous cells) is a watery, sticky material lining on the surface of the epithelium to trap inhaled substances (e.g. particles and bacteria). Mucus containing the entrapped foreign substances are subsequently swept from the lungs to the oral cavity via mucociliary clearance by ciliated cells, and then swallowed into the esophagus (Antunes and Cohen, 2007; Knowles and Boucher, 2002; Randell and Boucher, 2006). Tight junctions are important in the barrier function of the bronchial epithelium (Ganesan et al., 2013), which can restrict paracellular permeability, regulate the flow of molecules and control homeostasis of the respiratory tract (Heijink et al., 2010; Schneeberger

and Lynch, 2004). In addition, barrier function can not only prevent inhaled foreign materials from injuring the lungs, but can also act as a signaling platform for, for example, activation of immune cells in lungs (Ganesan et al., 2013; Godfrey, 1997).

The alveolus (**Figure 1** and **Table 1**), the functional unit of gas exchange, consists of an air space with thin walls that are surrounded by a rich network of pulmonary capillaries for blood transport. Alveolar type (AT) I and type II cells, fibroblasts, and a small population of macrophages together constitute the alveolar squamous epithelium (BéruBé et al., 2010; Féréol et al., 2008). Fibroblasts act as scaffold; the attached AT I cells cover 95% of the alveolar surface. The main function of AT I cells is to form a barrier that allows gases to exchange freely (Williams, 2003). AT II cells that form the remaining 5% of the surface are involved in lung defense, immune regulation, transepithelial solute transport and epithelial repair (Fehrenbach, 2001). Pulmonary macrophages are the most abundant immune-cell type present in the alveolar compartment. They also play a critical role in the defense against foreign substances, especially inhaled particles (Joshi et al., 2018).

**Exposure methods of *in vitro* lung models**

Traditionally, *in vitro* exposure is performed under submerged conditions. More recently, air-liquid interface (ALI) exposure via ALI exposure systems has become widely applied (Antherieu et al., 2017; Mühlhopt et al., 2016; Paur et al., 2011). In the following section submerged and ALI exposure methods are described, including their advantages and disadvantages, and summarized in **Table 2**.

**Submerged exposure**

Submerged exposure involves adding particle or fibre suspensions or dissolving chemicals into the culture medium to expose cells. Submerged exposure is easy to perform and requires a relatively low amount of test substance for exposure. Due to the immediate (high dose rate) exposure, this approach could not be considered as being realistic for airborne exposures (BeruBe et al., 2009). For example, inhaled substances (e.g. particles) will directly deposit onto the respiratory epithelium mainly by diffusion, whereas under submerged conditions cells are covered by the thick layer of fluid (cell culture medium) in which particles can either reach the cells by sedimentation or diffusion. Besides, characteristics and kinetics of test substances can be changed by the culture medium and the relevance of biological responses observed following submerged exposure have consequently been debated (Limbach et al., 2005; Maier et al., 2008). In addition, cells under submerged condition do not tend to differentiate and secrete the epithelial lining fluid.

	Anatomy	Structure	Cell Types *
Conducting zone		Larynx	1, 2, 3
		Trachea	1, 2, 3, 4, 5, 6
		Primary bronchi	
		Secondary bronchi	1, 2, 3, 4
		Tertiary bronchi	
		Small bronchi	
		Bronchioles	
			Terminal bronchioles
Respiratory zone		Respiratory bronchioles	1, 3, 7, 8, 9
		Alveolar sacs	8, 9

\* 1. Ciliated cells  
 2. Goblet cells  
 3. Basal cells  
 4. Serous cells  
 5. Serous gland cells  
 6. Mucous gland cells  
 7. Clara cells  
 8. Alveolar type I cells  
 9. Alveolar type II cells

**Table 1.** Overview of the different structures and cell types of the conducting and respiratory zones in the lung, adapted from BéruBé, et al. (2010).

**Air-liquid interface (ALI) exposure systems**

To minimize the limitations of submerged exposure and to accurately mimic inhalation exposure, ALI culture and ALI exposure systems have been developed. For ALI culture, cells are cultured on a permeable membrane on an insert fitted into culture plates with the apical side (eventually) being exposed to air (Braakhuis et al., 2020; Paur et al., 2011). Culture medium is added to the basolateral side of the insert (BéruBé et al., 2010; Upadhyay and Palmberg, 2018). The cells on the inserts stay in contact with air on the apical side to induce cell differentiation and mimic *in vivo* conditions, as well as with medium on the basolateral side to absorb nutrients. During ALI exposure, cells can be directly exposed to generated aerosols, reflecting realistic inhalation conditions (Antherieu et al., 2017; Mühlhopt et al., 2016; Paur et al., 2011).

In comparison to submerged exposure, ALI exposure places demand on the careful selection of cell models, as not many cell types can remain viable for a long period of time under ALI conditions.

Among different types of ALI exposure systems for *in vitro* study, the cloud exposure system has been widely used in recent studies (Fizeşan et al., 2019; Wang et al., 2019). The cloud system normally consists of a polycarbonate aerosol chamber, a base module for placing culture inserts, and a nebulizer that generates liquid aerosols (one example shown in **Figure 2A**). During exposure, a dense cloud of droplets containing the test substance is generated by a single nebulization, which is uniformly distributed at the base of the exposure chamber. Within 10 minutes, droplets settle onto the bottom of the base module, where cell inserts are positioned. The deposited mass can be monitored with the use of a quartz crystal microbalance (QCM) that is installed in the base module. To rapidly remove the residual gaseous phase after sedimentation of the test material, the cloud PowerVent exposure system has been developed on the basis of the cloud system, equipped with a vacuum system. However, such “one-hit” cloud exposure does not fully reflect realistic inhalation exposure. As such, another type of ALI exposure system, the continuous flow exposure system, has been developed (Jeannet et al., 2015; Jonsdottir et al., 2019; Mülhopt et al., 2016). ALI continuous exposure systems can be connected to different aerosol sources, allowing cells to be continuously exposed to pre-heated aerosols under ALI conditions for a long period with an adjustable flow rate (Braakhuis et al., 2020). In addition, those systems can also be coupled with additional equipment for monitoring characteristics of test atmospheres during ALI exposure, including chemical composition, particle number concentration (PNC), particle size distribution (PSD). The VITROCELL<sup>®</sup> continuous flow exposure station (**Figure 2B**) is an example of this kind of system, which is commercially available. This exposure station includes 3 levels with exposure modules: the top level for clean air exposures and the middle and bottom level for aerosol exposures. The exposure modules contain inserts with cells. Using compressed air, the spray nozzle nebulizes the test suspension (e.g. particle suspension), which can be heated in a mixing chamber and is subsequently led to the exposure modules.

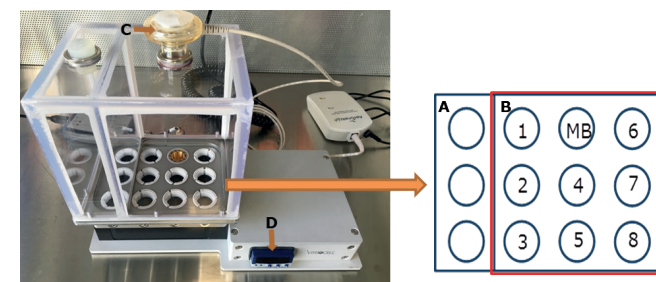


**Figure 2A.** The VITROCELL<sup>®</sup> cloud exposure system as an example of ALI cloud exposure systems includes A: Chamber for exposure of controls; B: Chamber for exposure of aerosolized substances, number 1-8 represents where cell inserts are positioned, MB represents a microbalance; C: Aerosol nebulizer; D: Temperature controller.

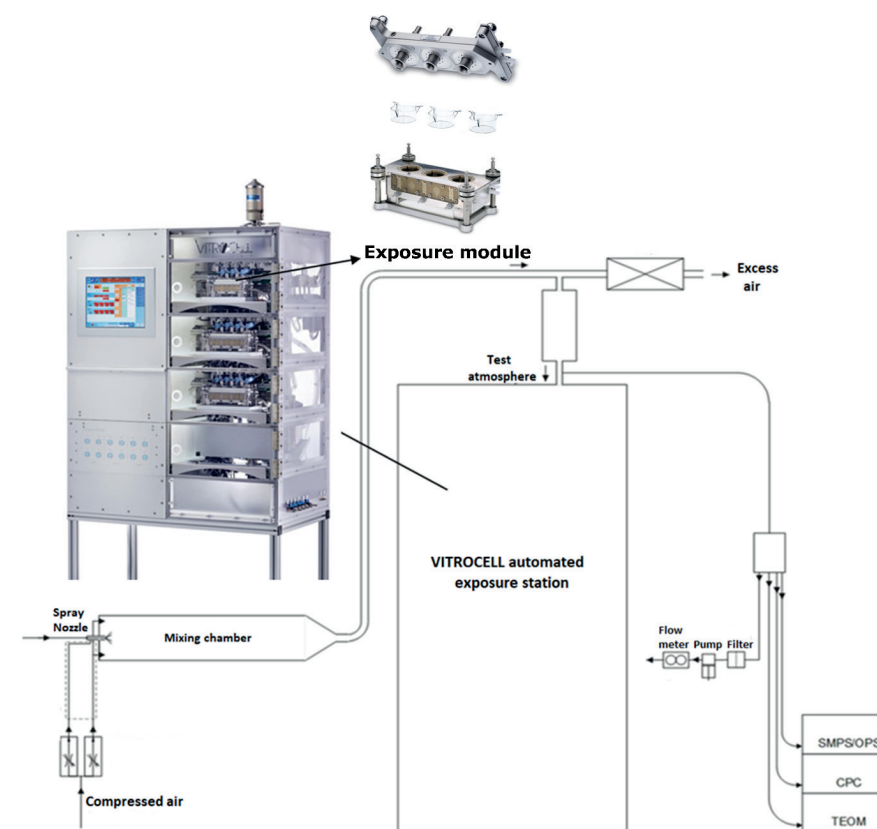


**Figure 2B.** The VITROCELL<sup>®</sup> continuous flow exposure station as an example of ALI continuous exposure systems, adapted from Braakhuis et al. (2020), includes 3 levels with exposure modules: the top level for clean air exposures and the middle and bottom level for aerosol exposures. The exposure modules contain inserts with cells. Aerosol characterization instruments can be connected, such as the scanning mobility particle sizer (SMPS), condensation particle counter (CPC), and tapered element oscillating microbalance (TEOM).



**Table 2.** Advantages and disadvantages of submerged and ALI exposure methods for toxicity testing of particles.

Exposure methods	Exposure systems	Advantages	Disadvantages
Submerged Exposure	–	Easy to operate; Various cell models can be used	Not representative of human inhalation dynamics; Deposited mass could not be measured; Characteristics of test substance can be changed due to the cell culture medium
ALI exposure	Cloud	More representative of human inhalation dynamics than submerged exposure; Easy to operate; Dose of solid particles can be assessed gravimetrically	Fewer cell models can be used; Less representative of human inhalation dynamics than continuous exposure system
	Continuous flow	<i>In-vivo</i> like exposure conditions; Dose of solid particles can be assessed gravimetrically; Aerosols characterization available	Fewer cell models have been shown to be resistant to air flow; Relatively more test substance is needed compared to submerged or cloud exposures

### Lung models for *in vitro* ALI studies

To study inhalation toxicity via *in vitro* exposure, it is critical to choose an appropriate cell model that mimics the region of interest of the respiratory tract. Characteristics of cell models can differ, depending on the origin, differentiation ability and culture conditions. Identifying those characteristics is thus of great importance for the application of cell models in *in vitro* experiments. *In vitro* lung models are usually divided based upon the use of either primary cells or immortalized cell lines (BeruBe et al., 2009; Gordon et al., 2015). Primary cells are isolated from healthy or even diseased human tissues, which can be obtained from lung resection or donation. Cell lines are mainly derived from lung cancer cells or transformed from primary cells by viruses to immortalize those cells. Both types of cell models have specific advantages and disadvantages, which should be weighed before use. For example, primary cells with the ability of complete differentiation and tight junction formation can represent the *in vivo* airway epithelium more closely compared to cell lines. Their use also has some disadvantages such as high(er) cost, difficult handling procedures and donor variations (Hiemstra et al., 2018). Cell lines are more convenient because they are readily available and can be passaged continually over a long period of

time. Conversely, they do not retain many differentiation features of primary cells. Moreover, as cell lines do not have inter-donor variability, results derived from cell lines are often more reproducible (BeruBe et al., 2009).

A number of commonly-used lung cell models is selected for detailed introduction in the following section and summarized in **Table 3**, including advantages and disadvantages.

### Human primary lung epithelial cells

#### 1. Normal human bronchial epithelial (NHBE) cells:

Normal human bronchial epithelial (NHBE) cells are isolated from bronchus samples of donors. When in submerged culture, NHBE cells form a monolayer of undifferentiated bronchial epithelium. While under ALI conditions, NHBE cells can form a pseudostratified bronchial epithelium-like tissue and fully differentiate to ciliated cells and goblet cells located at the apical side, as well as basal cells at the basolateral side (Mathis et al., 2013). Tight junctions play a crucial role in epithelial barrier function. NHBE cells show a high transepithelial electrical resistance (TEER) value that exceeds 800 ohm × cm<sup>2</sup> with well-defined zonula occludens protein-1 (ZO-1) expression under ALI culture (Lin et al., 2007; Oshima et al., 2011), indicating formation of tight junctions. However, donor differences in NHBE cells have been observed in cell viability tests and transporter expression levels (Sakamoto et al., 2013; Scheffler et al., 2015). The relatively short lifespan is another disadvantage of NHBE cells (Scheffler et al., 2015). Currently, there are some commercially available NHBE-based cell models (e.g. Epithelix and MucilAir model) that can retain a pseudostratified morphology and functional characteristics for up to 6 months (BeruBe et al., 2009).

#### 2. Human alveolar epithelial cells (hAEPc):

AT I cells cover the major part of the alveolar surface, however, it is very hard to build primary an AT I cell model under laboratory conditions. Up to now, the commonly-used primary alveolar cell model is the human alveolar epithelial cell (hAEPc) (Elbert et al., 1999; Forbes and Ehrhardt, 2005). Primary hAEPc can have an AT I-like squamous appearance as well as AT II-like lamellar bodies (Lehmann et al., 2011). Under ALI conditions, the hAEPc model shows clear expression of ZO-1 proteins and has a high TEER value (> 1000 ohm×cm<sup>2</sup>) (Forbes and Ehrhardt, 2005; Lehmann et al., 2011). However, the isolation and culture of hAEPc is very time-consuming and the cells need 14 days to reach confluence (Lehmann et al., 2011). Also, the hAEPc model is not yet commercially available, which limits its application in inhalation exposure studies. To overcome those disadvantages, a modified hAEPc model, human alveolar epithelial

lentivirus immortalized (CI-hAELVi) cell model, has been recently developed (Kuehn et al., 2016). This CI-hAELVi cell model may be a promising alternative to hAEPc as a model for the alveolar epithelium.

## Human lung epithelial cell lines

### 1. Human bronchial epithelial cell line (Calu-3):

Calu-3 cells were derived from a 25-year old Caucasian male with lung adenocarcinoma (Ong et al., 2013). Grainger et al. (2006) reported that Calu-3 cells grow fast and consistently, and can generate a more representative morphology of the airway epithelium under ALI conditions compared to cells under submerged conditions. Also, Calu-3 cells can form polarized monolayers with functional tight junctions under ALI culture (Gordon et al., 2015; Ong et al., 2013). However, TEER values of Calu-3 cells differ widely between different laboratories, varying from 100 to 2500 ohm $\times$ cm<sup>2</sup> (Srinivasan et al., 2015). As an important mechanism of airway defense, mucin release and swelling are observed in Calu-3 cells after long-term ALI culture (Kreda et al., 2007; Shumilov et al., 2014). However, it has been reported that different culture conditions can significantly affect characteristics of Calu-3 cells, including cell differentiation, barrier integrity and permeability properties (Kreft et al., 2015).

### 2. Human bronchial epithelial cell line (16HBE140-):

16HBE140- (16HBE) is a cell line transformed from normal bronchial epithelial cells with SV40 large T antigen (Ehrhardt et al., 2002). Under submerged culture, 16HBE cells grow fast and can form layers of polarized cells with microvilli and cilia, comparable with bronchial epithelium *in vivo*. Also, 16HBE cells exhibit good intercellular integrity with well-defined tight junctions, adherent junctions, and gap junctions and high TEER values ( $\approx$  800 ohm $\times$ cm<sup>2</sup>) (Ehrhardt et al., 2002; Forbes et al., 2003; Heijink et al., 2010). However, when changing to ALI conditions, 16HBE cells build layers of 10-16 cells in thickness without a clear polarity organization (Ehrhardt et al., 2002). Their TEER values also drop accordingly to below 130 ohm  $\times$  cm<sup>2</sup>, with an irregular staining pattern of ZO-1 and E-cadherin (Ehrhardt et al., 2002).

### 3. Human bronchial epithelial cell line (BEAS-2B):

BEAS-2B cells are transformed from bronchial epithelial cell with adenovirus 12-SV40 virus hybrid (Reddel et al., 1988). Although BEAS-2B cells generate a confluent monolayer more rapidly than 16HBE cells, they cannot form intercellular junctions. Only faint staining for ZO-1 proteins can be observed, and E-cadherin proteins are rarely detected (Heijink et al., 2010). Courcot et al. (2012) have shown that BEAS-2B cells exhibit a high similarity in gene expression pattern with primary cells, which

makes them widely-used for studying cytokine responses. However, as BEAS-2B cells contain polyomavirus DNA sequences, a high safety level of laboratory (Biosafety Level 2) is required for their culture.

### 4. Human alveolar type II epithelial cell line (A549):

A549 cells derived from alveolar type II carcinoma cells are a commonly used alveolar model in *in vitro* studies (Lieber et al., 1976). A549 cells grow rapidly and can express AT II-like lamellar bodies (Foster et al., 1998; Heijink et al., 2010). The low TEER value of A549 cells indicates poor formation of tight junctions (Srinivasan et al., 2015), although Foster et al. (1998) have shown that the permeability of Lucifer yellow (a fluorescent dye) across A549 cells monolayers decreases under ALI conditions compared to submerged conditions, indicating the barrier resistance to Lucifer yellow at the ALI.

### 5. Human mucoepidermoid carcinoma cell line (NCI-H292):

NCI-H292 (H292) cells are generated from salivary gland carcinoma cells (Courcot et al., 2012). The fact that H292 cells are not derived from lung tissues could be a disadvantage. H292 cells have high reactivity and tolerance to PM and gas/vapor phases, they are therefore widely used as a lung model in inhalation studies (Schamberger et al., 2015). The ability of H292 cells to form intercellular junction is better than BEAS-2B cells, but still relatively weak. Expression of ZO-1 and E-cadherin proteins can be detected in H292 cells, though it is fragmented and irregular (Heijink et al., 2010). Passage number is an important factor for H292 cells in toxicity testing as it can cause a significant variety of cell viability and inflammatory responses upon exposure (Azzopardi et al., 2015).

**Table 3.** Advantages and disadvantages of the commonly-used lung cell models.

	Cell models	Advantages	Disadvantages
Primary cells	NHBE	<i>In vivo</i> -like morphology of airway epithelium under ALI culture; Epithelial membrane integrity; Some NHBE-based models (e.g. Epithelix and MucilAir model) are commercially available	Relatively short lifespan; High price
	hAEPc	AT I-like squamous appearance and AT II-like lamellar bodies; Epithelial membrane integrity	Time-consuming for cell isolation and culture; Not commercially available
Cell lines	Calu-3	Grow fast; Representative morphology of airway epithelium; Epithelial membrane integrity; Mucociliary differentiation under ALI culture	Variability dependent on culture conditions
	16HBE	Grow fast; <i>In vivo</i> -like airway epithelium under submerged culture; Epithelial membrane integrity under submerged culture	Not suitable for ALI culture
	BEAS-2B	Grow fast; High homology in gene expression pattern with primary cells	Weak formation of tight junctions; Need high safety level laboratory
	A549	Grow fast; AT II-like lamellar bodies	Cannot form tight junctions;
	H292	High reactivity and tolerance to PM and gas/vapor phases	Not derived from lung cells; Weak formation of tight junctions; Variability dependent on passage number

### Other relevant lung cell models

The human lungs contain more than 50 cell types (BéruBé et al., 2010). Each area/zone of the lungs consists of different cell types and compositions. It can, therefore, be useful to develop cell models that represent a certain part of the respiratory tract. During inhalation exposure, human airway epithelium serves not only as a barrier, but also a pro-inflammatory signaling platform for recruitment and activation of immune cells such as macrophages and dendritic cells (Faber and McCullough, 2018; Rothen-Rutishauser et al., 2005). Communication between immune cells and epithelial cells in response to the inhaled substances have been reported. For example, during endocytosis of inhaled particles, macrophages are intended to produce inflammatory responses that can affect cellular responses from epithelial cells (Dagvadorj et al., 2015; Ishii et al., 2005; Wottrich et al., 2004). To mimic the *in vivo* situation more closely and

obtain insight in interactions between cells (Fröhlich and Salar-Behzadi, 2014; Klein et al., 2011), it would be meaningful to build multi-culture cell models combine lung epithelial cells with immune cells for inhalation studies.

Macrophages have a strong phagocytic function and are the most abundant immune cells in the lungs. Macrophages differentiated from human peripheral-blood monocytes, so called monocyte-derived macrophages (MDMs), are a good option for co-cultures (Lehmann et al., 2011). However, MDMs have some disadvantages that limit their application, including donor variability and the difficulty to obtain MDMs. Another type of macrophages differentiated from THP-1 human monocytes (THP-1 derived macrophages, TDMs) has also been extensively used as an alternative to MDMs in co-cultures. TDMs have an easy-handling culture protocol and show high reproducibility, although they only show few characteristics of *in vivo* macrophages (Chanput et al., 2014; Tedesco et al., 2018). By adding macrophages on top of the epithelial layer, co-culture models can be created. Several types of macrophage/epithelial cell co-culture models have been designed using macrophages in combination with lung epithelial cells such as primary bronchial epithelial cells (Ji et al., 2018), CI-hAELVi cells (Kletting et al., 2018) and A549 cells (Müller-Quernheim et al., 2012; Wottrich et al., 2004). Besides the co-culture models of the respiratory tract, some triple-culture models have also been designed and applied in the past ten years, represented by macrophages and lung epithelial cells with dendritic cells (Lehmann et al., 2011), fibroblasts (Barosova et al., 2020) or pulmonary endothelial cells (Dekali et al., 2014; Zhang et al., 2019).

Overall, various lung cell models, including monoculture and multi-culture models, have been developed to mimic the region of interest of the respiratory tract in *in vitro* studies. When selecting these lung cell models for *in vitro* exposure, the tested substances, exposure methods, and region of the lung that relates to the objectives of the study need to be taken into consideration.

## Part II: Aircraft-related air pollutants and their adverse health effects

Due to the rapid development of civil aviation, concerns on the potential health impacts of aircraft-related air pollutants have been raised in recent years. High levels of air pollutants, mainly nitrogen oxides and PM, are detected near busy airports. Most of these are typically related to aviation emissions (Masiol and Harrison, 2014). Among those pollutants, UFPs from aircraft emission have received increasing attention, as they may pose a serious threat to public health. Meanwhile, it has also

been reported that bleed-air contamination events occurred in aircraft cabin, which are potential causes of the alleged aerotoxic syndrome of cabin crews and passengers (Michaelis et al., 2017).

### Ultrafine particles

UFPs are particles with a mobility diameter < 100 nanometers (nm) that are of natural origin (volcanos and sea) or from anthropogenic emissions (engine exhaust, welding, and high-temperature processes in general). UFPs have a negligible mass compared to micron sized particles in the same mixture, thus making up only a small proportion of the weight of measured PM<sub>10</sub> and PM<sub>2.5</sub> concentrations (Kwon et al., 2020). Due to unique characteristics (e.g. small particle size and large surface-to-volume ratio), UFPs are associated with noticeable inhalation risks (Heinzerling et al., 2016; Leikauf et al., 2020). Upon inhalation, particles will deposit in the respiratory tract mainly by diffusion, which increases with decreasing air velocity. Model calculation using the Multiple Path Particle Dosimetry model (MPPD model, ARA Inc., 2014; Braakhuis et al., 2014) suggests that UFPs can deposit onto the epithelial surface of both tracheobronchial and alveolar regions. Inhalation exposure to UFPs has therefore been correlated with a wide range of chronic respiratory diseases (Heinzerling et al., 2016; Leikauf et al., 2020). Meanwhile, the small size of UFPs also increases the likelihood of particles to translocate into the human microvasculature and systemic circulation, eventually diffusing throughout the body including the brain (Miller et al., 2017; Terzano et al., 2010). Moreover, the large surface-to-volume ratio allows UFPs to absorb more organic and inorganic substances compared to fine particles with micrometer dimensions, thereby increasing the toxicity of UFPs per unit mass (Li et al., 2003). In this thesis, we focus on effects of UFPs emitted by aircrafts, both within (cabin/cockpit/flight deck) as well as outside (exhaust).

### Aviation as source of UFPs emissions

UFPs in the range of 10-30 nm dominated the particle number concentration (PNC) of particles from aviation emissions (Keuken et al., 2015; Riley et al., 2016; Stacey, 2019). Particles emitted from aircrafts during takeoff and landing are predominantly in the ultrafine range (4 - 100 nm), whereas aircraft ground movements generate predominantly large particles (1 and 10  $\mu$ m) from aircraft tire wear (Mazaheri et al., 2013). Also, aircraft activities can influence PNCs of UFPs. A study on Los Angeles International Airport (LAX) reported that take-off events correlated with the highest spikes of UFP number concentrations, some of which exceed  $10^7$  particles/cm<sup>3</sup> (Zhu et al., 2011). UFPs from aircraft emissions have large surface-to-volume ratios and high reactivity, enabling them to absorb chemical substances from the incomplete combustion of fuel and lubricating oil (Masiol and Harrison, 2014). Sulphur (S) is identified as the most abundant element in airport UFPs, since a large amount of

sulfur content is added to aviation fuel (Agrawal et al., 2008; Kinsey et al., 2011). High concentrations of soluble transition metals (e.g. Ni, V, Fe, and Cu) and PAHs are also detected in UFPs collected from airport surroundings (Lai et al., 2013; Shirmohammadi et al., 2018).

Inhalation exposure to airport UFPs may have potential adverse effects on airport employees and residential population in airport surrounding areas (Marie-Desvergne et al., 2016; Touri et al., 2013). A study on UFPs at Copenhagen Airport (CPH) reported occupational exposure levels of UFPs among 5 airport-employee groups, including baggage handlers, catering drivers, cleaning staff, airside security, and landside security (Møller et al., 2014). They found that the average exposure level of UFPs at the airport can reach to  $3.7 \times 10^4$  UFPs/cm<sup>3</sup> (baggage handlers) depending on working positions. A few epidemiological studies conducted outside the airport areas reported that the average exposure PNC of UFPs is around  $5.4 \times 10^4$  particles/cm<sup>3</sup> at Amsterdam Airport and  $5.3 \times 10^4$  particles/cm<sup>3</sup> at Los Angeles International Airport (LAX) (Habre et al. 2018; Lammers et al. 2020). Health risks upon inhalation exposure to airport UFPs are summarized in **Table 4A**. According to those studies, short-term exposure to airport UFPs may be associated with increased acute systemic inflammation and decreased lung and heart functions (Habre et al., 2018; Lammers et al., 2020). However, there is still a general lack of data on inhalation risk of exposure to airport UFPs, in particular for their *in vitro* toxicity.

### Bleed-air contamination in aircraft cabins

In most commercial jet aircrafts, the compressed air drawn from the compressor stage of the engine is mainly used for air supply during flights, so called “bleed air”. Bleed air passes through the Environmental Control System (ECS), where the air is conditioned to meet the required temperature before being distributed to the flight deck and the passenger cabin. From the air compression to the air distribution into the aircraft cabin, bleed-air contamination may happen in the aircraft cabin on some occasions. For example, if seals within the engine are not performing effectively, oil from oil leaks may be pyrolyzed at high temperature. These oil leaks and resulting thermal degradation products could lead to bleed-air contamination, subsequently contaminating the aircraft cabin (Day, 2015). This type of contamination in an aircraft cabin is commonly referred to as “fume events”. Due to the widespread use of jet engines and the occasionally occurring fume events, concerns have been raised over the composition of pyrolyzed aircraft engine oils and their potential to cause short- and long-term health effects (NRC, 2002; Michaelis, 2011).



**Table 4.** Epidemiological studies for evaluating health risks of inhalation exposure to UFPs from aircraft emissions (A) and to bleed-air contaminants in aircraft cabins (B), including the study design, data set, results and main conclusions.

(A) Health risks of inhalation exposure to aircraft-related UFPs				
Study design	Data set	Results	Conclusions	Reference
To investigate if the acute systemic inflammation in individuals with asthma is associated with short-term exposure to UFPs in a busy airport area.	22 non-smoking adults with mild to moderate asthma conducted the scripted and mild walking activity for 2 hrs, having a rest every 15 mins, on two locations in public parks inside (exposure) and outside (control) of the high UFPs zone at the LAX.	A standard deviation increase in the airport UFPs factor is significantly associated with IL-6 cytokine level in blood samples.	Exposure to UFPs in airport area had distinct effects on the induction of acute inflammation in individuals, using IL-6 level in blood sample as a marker.	Habre et al. (2018)
To investigate the health effects (lung and heart functions) of the controlled short-term exposure to UFPs near a major airport.	21 healthy non-smoking volunteers (age: 18–35 years) performed intermittent moderate exercise (i.e. cycling) for 5 hrs (2–5 visits) near Amsterdam Schiphol Airport.	An increase in exposure to airport UFPs is associated with a decrease in forced vital capacity (FVC) and a prolongation of the corrected QT (QTc) in healthy volunteers.	Short-term (5 hrs) exposure to airport UFPs are associated with decreased lung and heart function in healthy volunteers. Those effects are associated with particles < 20 nm (mainly UFP from aviation), but not with particles > 50 nm (mainly UFP from road traffic).	Lammers et al. (2020)
To investigate if ischemic heart disease (IHD) and cerebrovascular disease are linked to long-term occupational exposure to UFPs outdoors at an airport.	Exposed group comprises 6515 unskilled employees at Copenhagen Airport, and 6,617 unskilled employees in other companies in Copenhagen as a reference group during 1990–2012. For the exposed group, the proportion of time spent on the airport apron for each year was recorded.	No associations between the cumulative time on the airport apron and the risk of IHD (incidence rate ratio (IRR), 1.00; 95% CI, 0.97–1.03) or cerebrovascular disease (IRR, 1.00; 95% CI, 0.98–1.02) when adjusted for confounders.	No association was observed between long-term occupational exposure to UFPs at Copenhagen Airport outdoor and the risk of IHD and cerebrovascular disease.	Møller et al. (2020)

(B) Health risks of inhalation exposure to bleed-air contaminants in aircraft cabins				
Study design	Data set	Results	Conclusions	Reference
Summary of aircraft cabin air quality incident, symptoms, exposures, and possible solutions.	Symptoms were reported by aircrew members in a MD-80 aircraft and by aircrews in a mixed fleet of aircraft.	Exposure to contaminated aircraft bleed air varied due to differences of air supply in the cockpit (100% fresh bleed air) compared to the flight deck (60/40 recirculated/fresh bleed air). Central nervous system symptoms were predominantly reported, followed by gastrointestinal and respiratory system problems.	Most of the aircraft air quality incidents can be traced to contamination of the bleed air with jet engine oil and/or hydraulic fluid. Symptoms reported by aircrews may be related to CO and TCP levels. Long-term chronic effects are difficult to trace back to exposure events, because the symptoms are a result of exposure to low levels of contaminated bleed air for a long period of time.	Van Netten (2005)
To investigate associations between neurological deficits and elevated autoantibodies levels in flight crews.	There are 34 flight crew members (pilot and attendant) who experienced bleed air contamination and had medical attention compared to 12 healthy controls. Also, a case study of a single pilot was included who was followed for 21 months and suffered health problems after exposure to contaminated cabin air.	The most common symptoms reported by 34 flight aircrew members were memory deficits (78%), headaches (62%), fatigue (53%), muscle weakness (42%) and imbalance (35%).	An association between self-reported neurologic deficits and levels of autoantibodies against neuro- and glia-specific proteins in serum from 34 flight crew members was observed compared to the control group. However, the small sample size and the lack of chemical identification and quantification of contaminated cabin air are limitations of this study.	Abou-Donia et al. (2013)
A health survey on 4011 flight attendants from two airline companies was compared to data from a health survey of a general population (data used from the National Health and Nutrition Examination Surveys (NHANES)).	Addresses were randomly chosen from union provided lists of flight attendants. The mean age of flight attendants was 47 years. 41% of them had more than 20 years of working experiences. 9% were current smokers and 2.2–30% were former smokers.	The largest number of work-related injuries were musculoskeletal (33%), respiratory (23%), neurological problem (17%), psychological problems (14%). Significantly elevated standardized prevalence ratios (SPR) were observed for chronic bronchitis, cardiac disease, diagnosed sleep disorders, fatigue and depression for flight attendants compared to the general population.	Almost 50% of flight attendants reported one or more work related injuries. In comparison, the reference value is 4.2% for all industries and 10.2% for the transportation.	OHRCA (2014)
To investigate the exposure of helicopter crews to engine exhaust fumes, including clinical signs of CO intoxication, and the level of carboxyhemoglobin saturation (SpCO) after standard operation training flights.	69 completed surveys of crew pilots (n=18), system operators (n=14), engineers (n=11), rescuers (n=11), flight physicians (n=15) were collected over a 2-week period. The median duration of the training session was 80 minutes.	64% reported subjective exposure to engine exhaust during the training sessions. 8.6% reported clinical symptoms such as exhaustion (n=4), headache (n=1) and nausea (n=1).	Exposure to engine exhaust fumes is common mainly during open cargo door operations. However, clinical symptoms reported are infrequent. Toxic SpCO levels are not reached, but 29% of SpCO levels are outside the normal range (>4%).	Busch (2015)
To investigate cognitive impairment in aircrews by an extensive neuropsychological test battery and if a neurobiological substrate can be found for complaints using magnetic resonance imaging techniques.	12 aircrew members (10 male, average age of 44 years, 8130 flight hours) compared to the matching control group including 11 racing-car drivers (10 male, average age of 43 years, 233 flight hours).	The aircrew group reported complaints regarding cognitive impairment.	Aircrews reported more (no significant difference) cognitive complaints and depressive symptoms than controls. Subtle differences in brain white matter compared to controls, but the sample size is small. The estimated flight hours are not associated with cognitive impairment nor with reductions in white matter microstructure.	Reneman et al. (2016)



The Civil Aviation Authority (CAA) (2004) reported that breakdown products of aircraft engine oil contain more than 40 different potentially harmful chemicals. Carbon monoxide (CO) and volatile organic compounds (VOCs) have been suggested as potential indicators of bleed-air contamination in aircraft cabins (Michaelis, 2011). Organophosphates (OPs) are also one of abundant byproducts from pyrolysis of aircraft engine oils. Among OPs, tricresyl phosphates (TCPs) are the most frequently detected compounds in cabin air (Denola et al., 2011; Solbu et al., 2011). In accordance with a recent study (Howard et al., 2018), UFPs in aircraft cabins can also be abundantly formed by pyrolysis of engine oils, combustion of fossil fuels and chemical reactions. Therefore, an increase of UFP counts in cabin air would be expected under bleed-air contamination, in particular accompanied by visible fumes. A lot of sampling work has been performed in an attempt to measure and identify bleed-air contaminants in aircraft cabins. Van Netten (1998) measured air quality on three aircrafts during normal commercial flights and found no detectable levels of CO above the limit of detection (LOD) of 1 ppm in any of the airplanes. Also, TCPs were not detected in either cockpit or cabin air in airplanes that suffered from smoke odor and oil leakage (Van Netten, 1998). Solbu et al. (2011) sampled in 40 aircrafts (cockpit and passenger cabins) from 4 airline companies in Norway, including jet engine airplanes, propeller airplanes and helicopters. They noticed that TCP levels are an order of magnitude higher in cabin air samples collected from an airplane that experienced turbine oil leakage compared to samples collected after engine replacement. Wang et al. (2014) collected 84 air samples during 14 flights and selected 19 VOCs for chemical analysis of samples. According to source apportionments of VOCs, cabin service and humans contributed the most (29%) to VOC emissions in aircraft cabins. Denola et al. (2011) took 78 air samples from 3 different airplanes (a fighter trainer, a cargo transporter and a fighter bomber) to monitor TCP in the cockpit and cabin air. Only 11 samples showed total TCP levels slightly above the limit of quantitation (LOQ) ranging from 0.12 to 4.99  $\mu\text{g}/\text{m}^3$ , with levels in 2 samples (21.7 and 51.3  $\mu\text{g}/\text{m}^3$ ) 10 times higher than the LOQ. The general non-detectable or low levels of those indicators is mainly due to the difficulties of capturing the fume events in real time in aircraft cabins.

Cabin crews and passengers have reported a wide number of symptoms during flights including cough, sore throat, dizziness, nausea, disorientation, confusion, lethargy, tremors, and tingling of the arms and legs, so called “aerotoxic syndrome” (Michaelis et al., 2017). Those symptoms have been associated with inhalation exposure to bleed-air contaminants at low levels (Brown et al., 2001; Hocking, 2000; Michaelis, 2011). CO is a toxic gas which has an affinity for hemoglobin (Hb) to forming COHb, reducing blood  $\text{O}_2$ -carrying capacity (Kao and Nañagas, 2004). The presence of CO in aircraft cabin may be associated with the neurological complaints reported by aircrews and passengers after fume events (Van Netten, 2005). TCPs in cabin air, particularly tri-

*ortho*-cresyl phosphate (ToCP), has been suggested to be associated with the reported CNS-related symptoms in aircraft crews after fume events (Van Netten, 2005). Additionally, it has been reported that exposure to VOCs and UFPs is related to noticeable inhalation risks on e.g. the respiratory systems (Pappas et al., 2000; Soni et al., 2018).

Many epidemiological studies have been performed to evaluate adverse health effects of bleed-air contamination in aircraft cabins on aircrews and passengers, some of which are summarized in **Table 4B** including the study design, data set, reported symptoms and conclusions. Notably, most of those epidemiological studies could not fully reveal the cause-effect relationship between fume events and health outcomes for several reasons. 1) The broad variety in reported symptoms and the lack of clustered symptoms in crews and passengers make it difficult to attribute reported symptoms to specific diseases; 2) Some of the reported symptoms may result from exposure to low levels of contaminated bleed-air for a long period of time, however, those long-term chronic effects are difficult to trace back to exposure events; 3) Some of the reported symptoms can also be caused by other environmental factors in aircraft cabins such as low humidity, hypoxia and high level of passenger occupancy, which may affect well-being and sensory perception of aircrews and passengers. Therefore, toxicological data of inhalation exposure during fume events is required. The need for improved understanding of *in vitro* toxicity of aircraft engine oil fumes is the prime basis for the current need for in-depth expertise of the risk assessment of fume events.

## Objectives and thesis outline

Inhalation exposure to aircraft-related air pollutants such as UFPs from airport emissions and bleed air contaminants in aircraft cabins is associated with a wide range of public health problems. However, information on their toxicity (e.g. *in vitro* toxicity) following inhalation is still lacking, which hampers establishing a clear cause-effect relationship. In addition, physicochemical characteristics of those air pollutants including PNC, particle size distribution (PSD) and chemical composition may affect their toxic potency. It is thus necessary to investigate the *in vitro* toxicity of aircraft-related air pollutants together with their physicochemical characteristics to identify the most toxic fractions or compounds. In this thesis, conventional (submerged) and advanced (ALI) exposure systems have been applied to study the adverse effects of aircraft-related air pollutants in the lung cell culture models *in vitro*. The main goal of this thesis is to optimize the lung cell models under ALI conditions to assess inhalation toxicity of aircraft-related air pollutants *in vitro*.

To achieve this goal, the specific objectives are formulated as follows:

**To investigate the chemical composition, potential sources, and *in vitro* toxicity of airport PM, in comparison to PM collected from urban traffic emissions.**

Compared to our understanding of vehicle emissions, there is limited knowledge on physicochemical characteristics and *in vitro* toxicity of airport PM. Therefore, we measured the chemical composition and oxidative potential of PM<sub>0.25</sub> collected in airport areas, in comparison to well-analyzed urban traffic PM. By comparing to the chemical composition of PM collected directly from diesel engine and aircraft turbine engine emissions, the potential sources of urban traffic PM and airport PM were identified. Furthermore, effects of urban traffic PM and airport PM samples on reactive oxygen species (ROS) activity, pro-inflammatory responses, and cell viability in the human bronchial epithelial cell model were assessed under submerged exposure conditions (**Chapter 2**).

**To optimize the *in vitro* mono-/co-culture models of human airway barrier for aerosol exposure under ALI conditions.**

In order to avoid some of the limitations of the submerged exposure method used in **Chapter 2**, we optimized and evaluated the *in vitro* mono-/co-culture models of human airway barrier under prolonged ALI conditions for toxicity testing at more realistic exposure conditions in **Chapter 3**. Four types of the human bronchial epithelial cell model were evaluated with respect to the epithelial morphology, barrier function and cytotoxicity over prolonged ALI culture. One of those cell models that can retain the monolayer structure and maintain a strong tight junction was selected to create co-culture models with macrophages. The co-culture protocol under ALI conditions was improved and the sensitivity of the co-culture models to aerosolized LPS was evaluated.

**To apply the optimized lung cell models for *in vitro* toxicity testing of aircraft-related air pollutants under ALI exposure conditions.**

**Chapter 4 and 5** focus on inhalation toxicity of aircraft-related air pollutants, including UFPs from airport emissions and fumes generated from aircraft engine oil and hydraulic fluid. With the optimized *in vitro* cell model in **Chapter 3**, we evaluated inhalation toxicity of both airport UFPs with a Cloud exposure system (**Chapter 4**) and generated oil fumes with a continuous aerosol exposure system (**Chapter 5**).

A general discussion of the main findings and future perspectives in relation to the objectives is presented in **Chapter 6**, following by an overall **summary**.

## Reference

- Abou-Donia, M.B., M.M. Abou-Donia, E.M. ElMasry, J.A. Monro, and M.F. Mulder. 2013. Autoantibodies to nervous system-specific proteins are elevated in sera of flight crew members: biomarkers for nervous system injury. *Journal of Toxicology and Environmental Health, Part A*. 76:363-380.
- Agrawal, H., A.A. Sawant, K. Jansen, J.W. Miller, and D.R. Cocker. 2008. Characterization of chemical and particulate emissions from aircraft engines. *Atmospheric Environment*. 42:4380-4392.
- Antherieu, S., A. Garat, N. Beauval, M. Soyez, D. Allorge, G. Garcon, and J.-M. Lo-Guidice. 2017. Comparison of cellular and transcriptomic effects between electronic cigarette vapor and cigarette smoke in human bronchial epithelial cells. *Toxicology in vitro*. 45:417-425.
- Antunes, M.B., and N.A. Cohen. 2007. Mucociliary clearance—a critical upper airway host defense mechanism and methods of assessment. *Current opinion in allergy and clinical immunology*. 7:5-10.
- Azzopardi, D., L.E. Haswell, G. Foss-Smith, K. Hewitt, N. Asquith, S. Corke, and G. Phillips. 2015. Evaluation of an air-liquid interface cell culture model for studies on the inflammatory and cytotoxic responses to tobacco smoke aerosols. *Toxicology in Vitro*. 29:1720-1728.
- Barosova, H., B.B. Karakocak, D. Septiadi, A. Petri-Fink, V. Stone, and B. Rothen-Rutishauser. 2020. An *In Vitro* Lung System to Assess the Proinflammatory Hazard of Carbon Nanotube Aerosols. *International journal of molecular sciences*. 21:5335.
- Bendtsen, K.M., E. Bengtson, A.T. Saber, and U. Vogel. 2021. A review of health effects associated with exposure to jet engine emissions in and around airports. *Environmental Health*. 20:1-21.
- BeruBe, K., M. Aufderheide, D. Breheny, R. Clothier, R. Combes, R. Duffin, B. Forbes, M. Gaca, A. Gray, and I. Hall. 2009. *In vitro* models of inhalation toxicity and disease. *Alternatives to Laboratory Animals*. 37:89-141.
- BéruBé, K., Z. Prytherch, C. Job, and T. Hughes. 2010. Human primary bronchial lung cell constructs: the new respiratory models. *Toxicology*. 278:311-318.
- Braakhuis, H.M., R. He, R.J. Vandebriel, E.R. Gremmer, E. Zwart, J.P. Vermeulen, P. Fokkens, J. Boere, I. Gosens, and F.R. Cassee. 2020. An Air-liquid Interface Bronchial Epithelial Model for Realistic, Repeated Inhalation Exposure to Airborne Particles for Toxicity Testing. *Journal of Visualized Experiments*:e61210.
- Braakhuis, H.M., M.V. Park, I. Gosens, W.H. De Jong, and F.R. Cassee. 2014. Physicochemical characteristics of nanomaterials that affect pulmonary inflammation. *Particle and fibre toxicology*. 11:18.
- Brown, T.P., L.K. Shuker, L. Rushton, F. Warren, and J. Stevens. 2001. The possible effects on health, comfort and safety of aircraft cabin environments. *The journal of the Royal Society for the Promotion of Health*. 121:177-184.
- Busch, M. 2015. Carbon monoxide exposure in Norwegian rescue helicopters. *Air medical journal*. 34:328-332.
- CAA. 2004. Safety Regulation Group: cabin air quality. *Report No. Civil Aviation Authority (CAA) Paper 2004/04*.
- Chanput, W., J.J. Mes, and H.J. Wichers. 2014. THP-1 cell line: an *in vitro* cell model for immune modulation approach. *International immunopharmacology*. 23:37-45.
- Courcot, E., J. Leclerc, J.-J. Lafitte, E. Mensier, S. Jaillard, P. Gosset, P. Shirali, N. Pottier, F. Broly, and J.-M. Lo-Guidice. 2012. Xenobiotic metabolism and disposition in human lung cell models: comparison with *in vivo* expression profiles. *Drug Metabolism and Disposition*. 40:1953-1965.
- Dagvadorj, J., K. Shimada, S. Chen, H.D. Jones, G. Tumurkhuu, W. Zhang, K.A. Wawrowsky, T.R. Crother, and M. Arditi. 2015. Lipopolysaccharide induces alveolar macrophage necrosis via CD14 and the P2X7 receptor leading to interleukin-1 $\alpha$  release. *Immunity*. 42:640-653.
- Day, G.A. 2015. Aircraft cabin bleed air contaminants: A review. Federal Aviation Administration: Report No. DOT/FAA/Am-15/20.
- Dekali, S., C. Gamez, T. Kortulewski, K. Blazy, P. Rat, and G. Lacroix. 2014. Assessment of an *in vitro* model of pulmonary barrier to study the translocation of nanoparticles. *Toxicology reports*. 1:157-171.
- Denola, G., P. Hanhela, and W. Mazurek. 2011. Determination of tricresyl phosphate air contamination in aircraft. *Annals of occupational hygiene*. 55:710-722.
- Ehrhardt, C., C. Kneuer, J. Fiegel, J. Hanes, U. Schaefer, K.-J. Kim, and C.-M. Lehr. 2002. Influence of apical fluid volume on the development of functional intercellular junctions in the human epithelial cell line 16HBE140-: implications for the use of this cell line as an *in vitro* model for bronchial drug absorption studies. *Cell and tissue research*. 308:391-400.

- Elbert, K.J., U.F. Schäfer, H.-J. Schäfers, K.-J. Kim, V.H. Lee, and C.-M. Lehr. 1999. Monolayers of human alveolar epithelial cells in primary culture for pulmonary absorption and transport studies. *Pharmaceutical research*. 16:601-608.
- Faber, S.C., and S.D. McCullough. 2018. Through the Looking Glass: *In Vitro* Models for Inhalation Toxicology and Interindividual Variability in the Airway. *Applied In Vitro Toxicology*. 4:115-128.
- Fehrenbach, H. 2001. Alveolar epithelial type II cell: defender of the alveolus revisited. *Respiratory research*. 2:33.
- Féréol, S., R. Fodil, G. Pelle, B. Louis, and D. Isabey. 2008. Cell mechanics of alveolar epithelial cells (AECs) and macrophages (AMs). *Respiratory physiology & neurobiology*. 163:3-16.
- Fizeşan, I., S. Cambier, E. Moschini, A. Chary, I. Nelissen, J. Ziebel, J.-N. Audinot, T. Wirtz, M. Kruszewski, and A. Pop. 2019. *In vitro* exposure of a 3D-tetraculture representative for the alveolar barrier at the air-liquid interface to silver particles and nanowires. *Particle and fibre toxicology*. 16:14.
- Forbes, B., and C. Ehrhardt. 2005. Human respiratory epithelial cell culture for drug delivery applications. *European journal of pharmaceuticals and biopharmaceutics*. 60:193-205.
- Forbes, B., A. Shah, G.P. Martin, and A.B. Lansley. 2003. The human bronchial epithelial cell line 16HBE140- as a model system of the airways for studying drug transport. *International journal of pharmaceuticals*. 257:161-167.
- Foster, K.A., C.G. Oster, M.M. Mayer, M.L. Avery, and K.L. Audus. 1998. Characterization of the A549 cell line as a type II pulmonary epithelial cell model for drug metabolism. *Experimental cell research*. 243:359-366.
- Fröhlich, E., and S. Salar-Behzadi. 2014. Toxicological assessment of inhaled nanoparticles: role of *in vivo*, *ex vivo*, *in vitro*, and *in silico* studies. *International journal of molecular sciences*. 15:4795-4822.
- Ganesan, S., A.T. Comstock, and U.S. Sajjan. 2013. Barrier function of airway tract epithelium. *Tissue barriers*. 1:e24997.
- Godfrey, R. 1997. Human airway epithelial tight junctions. *Microscopy research and technique*. 38:488-499.
- Gordon, S., M. Daneshian, J. Bouwstra, F. Caloni, S. Constant, D.E. Davies, G. Dandekar, C.A. Guzman, E. Fabian, and E. Haltner. 2015. Non-animal models of epithelial barriers (skin, intestine and lung) in research, industrial applications and regulatory toxicology. *Altex*. 32:327-378.
- Grainger, C.I., L.L. Greenwell, D.J. Lockley, G.P. Martin, and B. Forbes. 2006. Culture of Calu-3 cells at the air interface provides a representative model of the airway epithelial barrier. *Pharmaceutical research*. 23:1482-1490.
- Habre, R., H. Zhou, S.P. Eckel, T. Enebish, S. Fruin, T. Bastain, E. Rappaport, and F. Gilliland. 2018. Short-term effects of airport-associated ultrafine particle exposure on lung function and inflammation in adults with asthma. *Environment international*. 118:48-59.
- Harkema, J.R., and J.G. Wagner. 2019. Pathology of the Respiratory System. *In Toxicologic Pathology for Non-Pathologists*. Springer. 311-354.
- Heijink, I.H., S.M. Brandenburg, J.A. Noordhoek, D.S. Postma, D.-J. Slebos, and A.J. van Oosterhout. 2010. Characterisation of cell adhesion in airway epithelial cell types using electric cell-substrate impedance sensing. *European Respiratory Journal*. 35:894-903.
- Heinzerling, A., J. Hsu, and F. Yip. 2016. Respiratory health effects of ultrafine particles in children: A literature review. *Water, Air, & Soil Pollution*. 227:32.
- Hiemstra, P.S., G. Grootaers, A.M. van der Does, C.A. Krul, and I.M. Kooter. 2018. Human lung epithelial cell cultures for analysis of inhaled toxicants: Lessons learned and future directions. *Toxicology in vitro*. 47:137-146.
- Hocking, M.B. 2000. Passenger aircraft cabin air quality: trends, effects, societal costs, proposals. *Chemosphere*. 41:603-615.
- Howard, C., D. Johnson, J. Morton, S. Michaelis, D. Supplee, and J. Burdon. 2018. Is a Cumulative Exposure to a Background Aerosol of Nanoparticles Part of the Causal Mechanism of Aerotoxic Syndrome. *J Nanomed Nanosci: JNAN-139*. DOI. 10.
- Ishii, H., S. Hayashi, J.C. Hogg, T. Fujii, Y. Goto, N. Sakamoto, H. Mukae, R. Vincent, and S.F. Van Eeden. 2005. Alveolar macrophage-epithelial cell interaction following exposure to atmospheric particles induces the release of mediators involved in monocyte mobilization and recruitment. *Respiratory research*. 6:1-12.
- Jeannot, N., M. Fierz, M. Kalberer, H. Burtscher, and M. Geiser. 2015. Nano aerosol chamber for *in-vitro* toxicity (NACIVT) studies. *Nanotoxicology*. 9:34-42.
- Ji, J., S. Upadhyay, X. Xiong, M. Malmlöf, T. Sandström, P. Gerde, and L. Palmberg. 2018. Multi-cellular human bronchial models exposed to diesel exhaust particles: assessment of inflammation, oxidative stress and macrophage polarization. *Particle and fibre toxicology*. 15:19.
- Jonsdottir, H.R., M. Delaval, Z. Leni, A. Keller, B.T. Brem, F. Siegerist, D. Schönenberger, L. Durdina, M. Elser, and H. Burtscher. 2019. Non-volatile particle emissions from aircraft turbine engines at ground-idle induce oxidative stress in bronchial cells. *Communications biology*. 2:1-11.
- Joshi, N., J.M. Walter, and A.V. Misharin. 2018. Alveolar macrophages. *Cellular immunology*. 330:86-90.
- Kao, L.W., and K.A. Nañagas. 2004. Carbon monoxide poisoning. *Emergency Medicine Clinics*. 22:985-1018.
- Kelly, F.J., and J.C. Fussell. 2012. Size, source and chemical composition as determinants of toxicity attributable to ambient particulate matter. *Atmospheric environment*. 60:504-526.
- Keuken, M., M. Moerman, P. Zandveld, J. Henzing, and G. Hoek. 2015. Total and size-resolved particle number and black carbon concentrations in urban areas near Schiphol airport (the Netherlands). *Atmospheric Environment*. 104:132-142.
- Kinsey, J., M. Hays, Y. Dong, D. Williams, and R. Logan. 2011. Chemical characterization of the fine particle emissions from commercial aircraft engines during the aircraft particle emissions experiment (APEX) 1 to 3. *Environmental science & technology*. 45:3415-3421.
- Klein, S.G., J. Hennen, T. Serchi, B. Blömeke, and A.C. Gutleb. 2011. Potential of coculture *in vitro* models to study inflammatory and sensitizing effects of particles on the lung. *Toxicology in vitro*. 25:1516-1534.
- Kletting, S., S. Barthold, U. Repnik, G. Griffiths, B. Loretz, N. Schneider-Daum, C. de Souza Carvalho-Wodarz, and C.-M. Lehr. 2018. Co-culture of human alveolar epithelial (hAELVi) and macrophage (THP-1) cell lines. *ALTEX - Alternatives to animal experimentation*. 35:pp. 211-222.
- Knowles, M.R., and R.C. Boucher. 2002. Mucus clearance as a primary innate defense mechanism for mammalian airways. *The Journal of clinical investigation*. 109:571-577.
- Kreda, S.M., S.F. Okada, C.A. Van Heusden, W. O'Neal, S. Gabriel, L. Abdullah, C.W. Davis, R.C. Boucher, and E.R. Lazarowski. 2007. Coordinated release of nucleotides and mucin from human airway epithelial Calu-3 cells. *The Journal of physiology*. 584:245-259.
- Kreft, M.E., U.D. Jerman, E. Lasič, N. Hevir-Kene, T.L. Rižner, L. Peternel, and K. Kristan. 2015. The characterization of the human cell line Calu-3 under different culture conditions and its use as an optimized *in vitro* model to investigate bronchial epithelial function. *European Journal of Pharmaceutical Sciences*. 69:1-9.
- Kuehn, A., S. Kletting, C. de Souza Carvalho-Wodarz, U. Repnik, G. Griffiths, U. Fischer, E. Meese, H. Huwer, D. Wirth, and T. May. 2016. Human alveolar epithelial cells expressing tight junctions to model the air-blood barrier. *ALTEX - Alternatives to animal experimentation*. 33:pp. 251-260.
- Kwon, H.-S., M.H. Ryu, and C. Carlsten. 2020. Ultrafine particles: unique physicochemical properties relevant to health and disease. *Experimental & Molecular Medicine*:1-11.
- Lai, C.-H., K.-Y. Chuang, and J.-W. Chang. 2013. Characteristics of nano-/ultrafine particle-bound PAHs in ambient air at an international airport. *Environmental Science and Pollution Research*. 20:1772-1780.
- Lammers, A., N. Janssen, A. Boere, M. Berger, C. Longo, S. Vijverberg, A. Neerinx, A. Maitland-van der Zee, and F. Cassee. 2020. Effects of short-term exposures to ultrafine particles near an airport in healthy subjects. *Environment International*. 141:105779.
- Lehmann, A.D., N. Daum, M. Bur, C.-M. Lehr, P. Gehr, and B.M. Rothen-Rutishauser. 2011. An *in vitro* triple cell co-culture model with primary cells mimicking the human alveolar epithelial barrier. *European Journal of Pharmaceuticals and Biopharmaceutics*. 77:398-406.
- Leikauf, G.D., S.-H. Kim, and A.-S. Jang. 2020. Mechanisms of ultrafine particle-induced respiratory health effects. *Experimental & Molecular Medicine*:1-9.
- Li, N., C. Sioutas, A. Cho, D. Schmitz, C. Misra, J. Sempf, M. Wang, T. Oberley, J. Froines, and A. Nel. 2003. Ultrafine particulate pollutants induce oxidative stress and mitochondrial damage. *Environmental health perspectives*. 111:455.
- Lieber, M., G. Todaro, B. Smith, A. Szakal, and W. Nelson-Rees. 1976. A continuous tumor-cell line from a human lung carcinoma with properties of type II alveolar epithelial cells. *International journal of cancer*. 17:62-70.
- Limbach, L.K., Y. Li, R.N. Grass, T.J. Brunner, M.A. Hintermann, M. Müller, D. Gunther, and W.J. Stark. 2005. Oxide nanoparticle uptake in human lung fibroblasts: effects of particle size, agglomeration, and diffusion at low concentrations. *Environmental science & technology*. 39:9370-9376.



- Lin, H., H. Li, H.-J. Cho, S. Bian, H.-J. Roh, M.-K. Lee, J.S. Kim, S.-J. Chung, C.-K. Shim, and D.-D. Kim. 2007. Air-liquid interface (ALI) culture of human bronchial epithelial cell monolayers as an *in vitro* model for airway drug transport studies. *Journal of pharmaceutical sciences*. 96:341-350.
- Maier, K.L., F. Alessandrini, I. Beck-Speier, T.P. Josef Hofer, S. Diabaté, E. Bitterle, T. Stöger, T. Jakob, H. Behrendt, and M. Horsch. 2008. Health effects of ambient particulate matter—biological mechanisms and inflammatory responses to *in vitro* and *in vivo* particle exposures. *Inhalation toxicology*. 20:319-337.
- Marie-Desvergne, C., M. Dubosson, L. Touri, E. Zimmermann, M. Gaude-Môme, L. Leclerc, C. Durand, M. Klerlein, N. Molinari, and I. Vachier. 2016. Assessment of nanoparticles and metal exposure of airport workers using exhaled breath condensate. *Journal of breath research*. 10:036006.
- Masiol, M., and R.M. Harrison. 2014. Aircraft engine exhaust emissions and other airport-related contributions to ambient air pollution: A review. *Atmospheric Environment*. 95:409-455.
- Mathis, C., C. Poussin, D. Weissensee, S. Gebel, A. Hengstermann, A. Sewer, V. Belcastro, Y. Xiang, S. Ansari, and S. Wagner. 2013. Human bronchial epithelial cells exposed *in vitro* to cigarette smoke at the air-liquid interface resemble bronchial epithelium from human smokers. *American Journal of Physiology-Lung Cellular and Molecular Physiology*. 304:L489-L503.
- Mazaheri, M., T.E. Bostrom, G.R. Johnson, and L. Morawska. 2013. Composition and morphology of particle emissions from in-use aircraft during takeoff and landing. *Environmental science & technology*. 47:5235-5242.
- Michaelis, S. 2011. Contaminated aircraft cabin air. *J. Biol. Phys. Chem.* 11:132-145.
- Michaelis, S., J. Burdon, C.V. Howard, and W.H. Organization. 2017. Aerotoxic syndrome: a new occupational disease? *Public health panorama*. 3:198-211.
- Miller, M.R., J.B. Raftis, J.P. Langrish, S.G. McLean, P. Samutrtai, S.P. Connell, S. Wilson, A.T. Vesey, P.H. Fokkens, and A.J.F. Boere. 2017. Inhaled nanoparticles accumulate at sites of vascular disease. *ACS nano*. 11:4542-4552.
- Møller, K.L., C. Brauer, S. Mikkelsen, J.P. Bonde, S. Loft, K. Helweg-Larsen, and L.C. Thygesen. 2020. Cardiovascular disease and long-term occupational exposure to ultrafine particles: A cohort study of airport workers. *International Journal of Hygiene and Environmental Health*. 223:214-219.
- Møller, K.L., L.C. Thygesen, J. Schipperijn, S. Loft, J.P. Bonde, S. Mikkelsen, and C. Brauer. 2014. Occupational exposure to ultrafine particles among airport employees—combining personal monitoring and global positioning system. *PloS one*. 9:e106671.
- Mülhopt, S., M. Dilger, S. Diabaté, C. Schlager, T. Krebs, R. Zimmermann, J. Buters, S. Oeder, T. Wäscher, and C. Weiss. 2016. Toxicity testing of combustion aerosols at the air-liquid interface with a self-contained and easy-to-use exposure system. *Journal of Aerosol Science*. 96:38-55.
- Müller-Quernheim, U.C., L. Potthast, J. Müller-Quernheim, and G. Zissel. 2012. Tumor-cell co-culture induced alternative activation of macrophages is modulated by interferons *in vitro*. *Journal of Interferon & Cytokine Research*. 32:169-177.
- NRC. 2002. The airliner cabin environment and the health of passengers and crew. National Academies Press. <https://doi.org/10.17226/10238>.
- OHRCA. 2014. <http://www.ohrca.org/wpcontent/uploads/2014/08/finalreport.pdf>.
- Ong, H.X., D. Traini, and P.M. Young. 2013. Pharmaceutical applications of the Calu-3 lung epithelia cell line. *Expert opinion on drug delivery*. 10:1287-1302.
- Oshima, T., K. Gedda, J. Koseki, X. Chen, J. Husmark, J. Watari, H. Miwa, and S. Pierrou. 2011. Establishment of esophageal-like non-keratinized stratified epithelium using normal human bronchial epithelial cells. *American Journal of Physiology-Cell Physiology*. 300:C1422-C1429.
- Pappas, G.P., R.J. Herbert, W. Henderson, J. Koenig, B. Stover, and S. Barnhart. 2000. The respiratory effects of volatile organic compounds. *International Journal of Occupational and Environmental Health*. 6:1-8.
- Parent, R.A. 2015. Comparative biology of the normal lung. Academic Press.
- Paur, H.-R., F.R. Cassee, J. Teeguarden, H. Fissan, S. Diabate, M. Aufderheide, W.G. Kreyling, O. Hänninen, G. Kasper, and M. Riediker. 2011. In-vitro cell exposure studies for the assessment of nanoparticle toxicity in the lung—A dialog between aerosol science and biology. *Journal of Aerosol Science*. 42:668-692.
- Randell, S.H., and R.C. Boucher. 2006. Effective mucus clearance is essential for respiratory health. *American journal of respiratory cell and molecular biology*. 35:20-28.
- Reddel, R.R., Y. Ke, B.I. Gerwin, M.G. McMenamin, J.F. Lechner, R.T. Su, D.E. Brash, J.-B. Park, J.S. Rhim, and C.C. Harris. 1988. Transformation of human bronchial epithelial cells by infection with SV40 or adenovirus-12 SV40 hybrid virus, or transfection via strontium phosphate coprecipitation with a plasmid containing SV40 early region genes. *Cancer research*. 48:1904-1909.
- Reneman, L., S.B. Schagen, M. Mulder, H.J. Mutsaerts, G. Hageman, and M.B. de Ruiter. 2016. Cognitive impairment and associated loss in brain white microstructure in aircrew members exposed to engine oil fumes. *Brain imaging and behavior*. 10:437-444.
- Riley, E.A., T. Gould, K. Hartin, S.A. Fruin, C.D. Simpson, M.G. Yost, and T. Larson. 2016. Ultrafine particle size as a tracer for aircraft turbine emissions. *Atmospheric Environment*. 139:20-29.
- Rothen-Rutishauser, B.M., S.G. Kiama, and P. Gehr. 2005. A three-dimensional cellular model of the human respiratory tract to study the interaction with particles. *American journal of respiratory cell and molecular biology*. 32:281-289.
- Sakamoto, A., T. Matsumaru, N. Yamamura, Y. Uchida, M. Tachikawa, S. Ohtsuki, and T. Terasaki. 2013. Quantitative expression of human drug transporter proteins in lung tissues: Analysis of regional, gender, and interindividual differences by liquid chromatography–tandem mass spectrometry. *Journal of pharmaceutical sciences*. 102:3395-3406.
- Samet, J., and D. Krewski. 2007. Health effects associated with exposure to ambient air pollution. *Journal of toxicology and environmental health, Part A*. 70:227-242.
- Savolainen, K., L. Pyllkänen, H. Norppa, G. Falck, H. Lindberg, T. Tuomi, M. Vippola, H. Alenius, K. Hämeri, and J. Koivisto. 2010. Nanotechnologies, engineered nanomaterials and occupational health and safety—A review. *Safety science*. 48:957-963.
- Schamberger, A.C., C.A. Staab-Weijnitz, N. Mise-Racek, and O. Eickelberg. 2015. Cigarette smoke alters primary human bronchial epithelial cell differentiation at the air-liquid interface. *Scientific reports*. 5:8163.
- Scheffler, S., H. Dieken, O. Krischenowski, and M. Aufderheide. 2015. Cytotoxic evaluation of e-liquid aerosol using different lung-derived cell models. *International journal of environmental research and public health*. 12:12466-12474.
- Schneeberger, E.E., and R.D. Lynch. 2004. The tight junction: a multifunctional complex. *American Journal of Physiology-Cell Physiology*. 286:C1213-C1228.
- Shirmohammadi, F., C. Lovett, M.H. Sowlat, A. Mousavi, V. Verma, M.M. Shafer, J.J. Schauer, and C. Sioutas. 2018. Chemical composition and redox activity of PM<sub>2.5</sub> near Los Angeles International Airport and comparisons to an urban traffic site. *Science of the Total Environment*. 610:1336-1346.
- Shumilov, D., A. Popov, R. Fudala, I. Akopova, I. Gryczynski, J. Borejdo, Z. Gryczynski, and R. Grygorczyk. 2014. Real-time imaging of exocytotic mucin release and swelling in Calu-3 cells using acridine orange. *Methods*. 66:312-324.
- Solbu, K., H.L. Daae, R. Olsen, S. Thorud, D.G. Ellingsen, T. Lindgren, B. Bakke, E. Lundanes, and P. Molander. 2011. Organophosphates in aircraft cabin and cockpit air—method development and measurements of contaminants. *Journal of Environmental Monitoring*. 13:1393-1403.
- Soni, V., P. Singh, V. Shree, and V. Goel. 2018. Effects of VOCs on human health. In *Air pollution and control*. Springer. 119-142.
- Srinivasan, B., A.R. Kolli, M.B. Esch, H.E. Abaci, M.L. Shuler, and J.J. Hickman. 2015. TEER measurement techniques for *in vitro* barrier model systems. *Journal of laboratory automation*. 20:107-126.
- Stacey, B. 2019. Measurement of ultrafine particles at airports: A review. *Atmospheric Environment*. 198:463-477.
- Tedesco, S., F. De Majo, J. Kim, A. Trenti, L. Trevisi, G.P. Fadini, C. Bolego, P.W. Zandstra, A. Cignarella, and L. Vitiello. 2018. Convenience versus biological significance: are PMA-differentiated THP-1 cells a reliable substitute for blood-derived macrophages when studying *in vitro* polarization? *Frontiers in pharmacology*. 9:71.
- Terzano, C., F. Di Stefano, V. Conti, E. Graziani, and A. Petroianni. 2010. Air pollution ultrafine particles: toxicity beyond the lung. *Eur Rev Med Pharmacol Sci*. 14:809-821.
- Touri, L., H. Marchetti, I. Sari-Minodier, N. Molinari, and P. Chanez. 2013. The airport atmospheric environment: respiratory health at work. *European respiratory review*. 22:124-130.
- Upadhyay, S., and L. Palmberg. 2018. Air-liquid interface: relevant *in vitro* models for investigating air pollutant-induced pulmonary toxicity. *Toxicological Sciences*. 164:21-30.
- Van Netten, C. 1998. Air quality and health effects associated with the operation of BAe 146-200 aircraft. *Applied Occupational and Environmental Hygiene*. 13:733-739.

- Van Netten, C. 2005. Aircraft air quality incidents, symptoms, exposures and possible solutions. *In Air Quality in Airplane Cabins and Similar Enclosed Spaces*. 193-210.
- Wang, C., X. Yang, J. Guan, Z. Li, and K. Gao. 2014. Source apportionment of volatile organic compounds (VOCs) in aircraft cabins. *Building and environment*. 81:1-6.
- Wang, Y., Q. Wu, L. Muskhelishvili, K. Davis, M. Bryant, and X. Cao. 2019. Assessing the respiratory toxicity of dihydroxyacetone using an *in vitro* human airway epithelial tissue model. *Toxicology in Vitro*. 59:78-86.
- Williams, M.C. 2003. Alveolar type I cells: molecular phenotype and development. *Annual review of physiology*. 65:669-695.
- Wottrich, R., S. Diabaté, and H.F. Krug. 2004. Biological effects of ultrafine model particles in human macrophages and epithelial cells in mono- and co-culture. *International journal of hygiene and environmental health*. 207:353-361.
- Zhang, F., G.V. Aquino, A. Dabi, and E.D. Bruce. 2019. Assessing the translocation of silver nanoparticles using an *in vitro* co-culture model of human airway barrier. *Toxicology in Vitro*. 56:1-9.
- Zhu, Y., E. Fanning, R.C. Yu, Q. Zhang, and J.R. Froines. 2011. Aircraft emissions and local air quality impacts from takeoff activities at a large International Airport. *Atmospheric Environment*. 45:6526-6533.

# Chapter 2

## **Pro-inflammatory responses to PM<sub>0.25</sub> from airport and urban traffic emissions**

Rui-Wen He <sup>a</sup>, Farimah Shirmohammadi <sup>c</sup>, Miriam E. Gerlofs-Nijland <sup>a</sup>, Constantinos Sioutas <sup>c</sup>, Flemming R. Cassee <sup>a,b\*</sup>

<sup>a</sup> National Institute for Public Health and the Environment (RIVM), P.O. Box, 2720 BA, Bilthoven, The Netherlands.

<sup>b</sup> Institute for Risk Assessment Sciences, Utrecht University, P.O. Box 80178, 3508 TD Utrecht, The Netherlands

<sup>c</sup> University of Southern California, Department of Civil and Environmental Engineering, 3620 S Vermont Ave, Los Angeles, CA 90089, USA

(Science of The Total Environment, 2018, Volumes 640–641, Pages 997-1003, ISSN 0048-9697)

## Highlights

Aviation emission was the main contributor to  $PM_{0.25}$  from a major airport

Urban area  $PM_{0.25}$  were dominated by road traffic (traffic emission and road dust)

Airport-related  $PM_{0.25}$  exerts similar toxicity compared to  $PM_{0.25}$  from urban traffic

## Abstract

Air traffic is rapidly growing, raising concerns about the air pollution its impact on public health. However, little is known about the impact of air pollution sources on air quality and health in the vicinity of airports. In this study, the sources and adverse health effects of airport-related particulate matter (PM) were investigated and compared to those of urban traffic emissions. Ambient  $PM_{0.25}$  were collected at the Los Angeles International Airport (LAX) and at a central Los Angeles USC campus), along with  $PM_{2.5}$  collected directly from turbine and diesel engines. The particle chemical composition, oxidative potential (OP) (ascorbic acid (AA), and electron spin resonance (ESR) assay) as well as their reactive oxygen species (ROS) activity, inflammatory potential (interleukin (IL) 6 and 8 and tumor necrosis factor (TNF)  $\alpha$ ) and cytotoxicity on human bronchial epithelial (16HBE) cells were assessed. Chemical composition measurements confirmed that aircraft emissions were the major source to LAX  $PM_{0.25}$ , while the sources of the USC samples were more complex, including traffic emissions, suspended road and soil dust, and secondary aerosols. The traffic-related transition metals (Fe and Cu) in LAX and USC samples mainly affected OP values of particles, while multiple factors such as composition, size distribution and internalized amount of particles contributed to the promotion of ROS generation in 16HBE cells during 4 h exposure. Internalized particles in cells might also play an important role in activating inflammatory responses during cell recovery period, with LAX particles being more potent. Our results demonstrated considerable toxicity of airport-related particles, even at low exposure concentrations, suggesting that airport emission as source of  $PM_{0.25}$  may also contribute to the adverse effects on public health attributable to PM. The potency of such particles is in the same range as those collected at a site in urban area impacted heavily by traffic emissions.

**Keywords:**  $PM_{0.25}$ ; Aviation emission; Traffic emission; Oxidative potential; Pro-inflammation.

## Introduction

Due to the rapid development of the aviation industry and high demand for air transportation, the concomitant airport pollution has attracted increasing attention in recent years (Masiol and Harrison, 2014). Airport particulate matter (PM) emissions are the known source of air pollution in the proximity of an airport (Hu et al., 2009; Hudda et al., 2014). These particles, however, are not only from aircraft emissions (engine exhaust and non-exhaust emissions from aircraft), but also emissions from other sources like the ground traffic operations for transporting people and goods (Masiol and Harrison, 2014). However, current information regarding contributions of the relevant sources to airport PM emissions is inadequate, which hinders our ability to accurately assess the population risks associated with the exposure to these emissions.

Large airports are often located in the proximity of metropolises, consequently airport emissions may have considerable impact on public health in the surrounding urban areas. Barrett et al. (2010) estimated that around 8000 premature mortalities were attributable to aircraft cruise emissions globally every year (Barrett et al., 2010). Touri and colleagues (2013) examined the impact of airport pollution exposure on respiratory health by evaluation of studies on occupational exposure. Although the link between respiratory health effects and airport pollution exposure was shown in a few occupational studies, the correlation was weak and needs further research (Touri et al., 2013). Therefore, understanding the associated risks of exposure to airport-related PM in comparison with other major contributors to urban PM such as vehicle emissions are of great significance to public health officials and legislators.

PM is a rather complex mixture that could differ in size distribution and chemical composition depending on emission sources. Both size distribution and composition are major critical factors influencing particle toxicity (Kelly and Fussell 2012). Particles in the nanometer-size range typically account for the majority of total particle number concentrations in airport areas (Masiol and Harrison, 2014). A recent LAX airport study shown that the mean diameter of particles from the LAX is around 20 nm that is distinctly smaller than particles emitted from the urban traffic area (USC samples: mean diameter  $\approx$  35 nm) (Shirmohammadi et al., 2017b). These nano-sized airport-related particles result in a higher surface area/mass ratio compared to micron-sized PM, which allows more organic and inorganic species to be adsorbed and/or absorbed on their surface. This, in turn, could increase the particle toxicity per unit inhaled mass (Li et al., 2003; Nel et al., 2006). Many relevant toxic effects of PM might be triggered through PM-induced oxidative stress due to reactive oxygen species (ROS) generation in cells (Ayres et al., 2008; Xiang et al., 2016a). PM-induced ROS can oxidize lipids and

damage DNA, thereby impairing natural defense mechanisms, and lead to excessive production of inflammatory mediators, which are highly related to many respiratory and lung inflammatory diseases. In particular, small particle size and PM species including elemental carbon (EC), a number of organics as well as soluble transition metals (including Ni, V, Fe, and Cu) can have significant effects on the toxicity of PM as evidenced by previous studies (Aust et al., 2002, Kelly and Fussell 2012, Loxham et al., 2013). However, there is a general lack of information on the health hazards of aviation-released PM compared to that of other mobile transportation sources such as road traffic.

The primary goal of the study presented here was to explore the health hazards of two important PM sources in relation to their PM composition. We hypothesized that airport-related PM<sub>0.25</sub> can induce comparable cytotoxicity to particles collected from an urban area, impacted mostly by road traffic emissions. To test this hypothesis, we collected PM<sub>0.25</sub> samples downwind the Los Angeles International airport and in the downtown area of Los Angeles, CA, along with PM samples directly collected from the exhaust of a turbine and a diesel engine, then examined how these different PM samples affect the biological responses in human bronchial epithelial (16HBE) cells.

## Materials and methods

### PM sampling

#### *Urban air PM samples*

Ambient PM<sub>0.25</sub> samples were collected in two locations in Los Angeles, as discussed in more detail by Shirmohammadi et al., (2017a). One sampling site was near the residential area of Playa del Rey, at a South Coast Air Quality Management District (AQMD) LAX Hastings monitoring site, which is located adjacent to the downwind Los Angeles International Airport (LAX). The PM<sub>0.25</sub> collected in this site was mainly influenced by the airport emissions and to a lesser extent by shore ocean breeze, and are less affected by traffic emissions (Shirmohammadi et al., 2017a). The other site was in central Los Angeles, at the University of Southern California (USC), roughly 150 meters from -and immediately downwind the major freeway (I-110). Samples collected here mainly represent urban mixed particles, mostly dominated by road traffic emissions (Minguillón et al. 2008; Sowlat et al 2016).

Personal Cascade Impactor Samplers (PCIS) (SKC, Inc., Eighty-Four, PA, USA) were used for sampling PM at the flow rate of 9 lpm (Misra et al, 2002). The sampling duration for each sample was 7 days from late October to early December of 2016 (for a total of 5 weeks). Each site was visited once a week to collect samples and load new

filters. Flow rates were checked during the visit to ensure proper performance of the PCIS samplers. PM was classified in two particle collection size ranges: accumulation mode (0.25 - 2.5  $\mu\text{m}$ , PM<sub>2.5</sub> - 0.25) and quasi-ultrafine mode (< 0.25  $\mu\text{m}$ , PM<sub>0.25</sub>). Only PM<sub>0.25</sub> samples have been used for the work discussed in this paper, as they were considered more representative of direct primary emissions compared to the accumulation mode range that contains a higher fraction of regional aerosols (Shirmohammadi et al, 2017a). During the sampling period, one PCIS loaded with 37-mm quartz filters (Whatman International Ltd, Maidstone, England) was used for organic chemical speciation measurements (details can be found in Shirmohammadi et al, 2017a). The other three PCISs were loaded with 37 mm Teflon filters (Pall Life Sciences, 3- $\mu\text{m}$  pore, Ann Arbor, MI) for gravimetric measurements to determine mass concentration as well as for the additional chemical and biological analyses discussed in this study.

#### *Turbine and diesel samples*

Turbine and diesel samples were collected directly from diluted exhaust of a Fighting Falcon turbine engine (F100, Pratt & Whitney, East Hartford, Connecticut, USA) and a low-sulfur fuel diesel (EN 590) engine (Bredenoord, 35 KVA Silent, Apeldoorn, Netherlands), respectively, by means of a versatile aerosol concentration enrichment system (VACES) (Kim et al., 2001) as well as a high-volume cascade impactor (HVCI) sampler (Demokritou et al., 2002) in this study. Minor flows of the VACES were used to collect droplets containing particles into a BioSampler (SKC, Inc., Eighty-Four, PA, USA) as well as passing the concentrated aerosol through a diffusion dryer and subsequently collect PM on 47-mm Teflon filters (Pall Life Sciences, 2- $\mu\text{m}$  pore, Ann Arbor, MI, USA) for the biological and chemical analyses, respectively. Albeit that the VACES was equipped with a PM<sub>2.5</sub> size selective inlet, the vast majority of the particles from both test engines were < 0.1  $\mu\text{m}$ . Sampling time for each day lasted for eight hours and a filter was collected in parallel to the BioSampler, then a new filter was loaded for the next sampling day, resulting in 1 turbine sample and 3 diesel samples were collected. Flow rates, heating and cooling temperatures, and particle number concentration as well as concentration enrichment of the VACES were checked every 2 hours to ensure proper performance. The HVCI consists different impaction stages to collect particles in different size ranges. 3 impaction stages (cut-points at 10, 2.5 and 0.1  $\mu\text{m}$ , respectively) were selected in this study, and downstream of the third stage, a backup TE 38 filter (Whatman, 5- $\mu\text{m}$  pore, Dassel, Niedersachsen, Germany) was placed for collecting the ultrafine particles (<0.1  $\mu\text{m}$ ) for chemical analysis. All filters were weighed before and after sampling to determine particle mass loadings and then stored in petri dishes at 4°C in the dark.



## Filters extraction

Teflon filters (5 LAX and 5 USC filters from PCIS, 1 turbine and 3 diesel filters from VACES) were immersed by 2mL methanol (HPLC grade) in a petri dish, followed by sonication (Sonorex RK-52, 60/120 KW, 35 KHz, Bandelin, Berlin, Germany) for 1 minute. The filters were then flipped over with clean tweezers and were sonicated again for 1 minute, a process that was repeated for three consecutive times. The extract was transferred into a vial, then 5 LAX extracts, 5 USC extracts and 1 turbine extract were dried respectively overnight at 30°C in an incubator. For diesel samples, 3 diesel extracts were combined before drying. All the filters were also weighed after the extraction process to determine the extraction efficiency, which was around 90% in this study. Dried extracts (5 LAX, 5 USC, 1 turbine and 1 diesel samples) were re-suspended in 1mL Hanks' Balanced Salt solution (HBSS, Thermo Fisher Scientific Inc., the Netherlands), which can maintain cells osmotic balance during *in vitro* assay.

## Chemical analysis

Filter samples (details in 2.1) collected at LAX and USC as well as from the exhaust of the turbine and diesel engines (from HVCI) were analyzed to quantify the chemical PM constituents. The analytical procedures were described in more detail by Shirmohammadi et al., (2017a). Briefly, both EC and OC content of all weekly samples were quantified using 1 cm<sup>2</sup> punch of each quartz filters. The United States National Institute for Occupational Safety and Health Thermal Optical Transmission method was applied in EC and OC analysis (Birch and Cary, 1996). To measure the total elemental composition of the PM, a section of each Teflon filter was digested in a mixture of 1.5 mL of 16 M nitric acid, 0.5 mL of 12 M hydrochloric acid and 0.2 mL of hydrofluoric acid using a microwave-aided solubilization protocol (Shirmohammadi et al., 2017a). The digests were then analyzed using a high resolution (magnetic sector) inductively coupled plasma mass spectrometer (SF-ICPMS, Thermo-Finnigan Element 2).

## Oxidative potential assays

### Ascorbic acid (AA) depletion assay

The AA assay measures the rate of AA consumption by a known amount of PM and was used to measure the redox activity of the ambient and engine exhaust PM samples of this study. 200µg/mL PM re-suspensions (in HBSS) were diluted in ultrapure water (1:15) to a concentration of 12.5 µg/mL. Briefly, 160 µL of 12.5 µg/mL PM suspension was added to a 96-well flat-bottomed UV plates (VWR, Breda, Netherlands). All samples were incubated in a spectrophotometer (spectraMAX 190: Molecular Devices, Sunnyvale, USA) for 10 minutes at 37 °C. 20 µl of 2 mM AA was then added and measured by a microplate reader at 265 nm every 2 minutes for 2 hours. For AA depletion assay experiment, 160 µL of domestic oil burning furnace particles (DOFA,

US EPA, RTP, NC) suspension at 12.5 µg/mL and HBSS diluted in dH<sub>2</sub>O (1:15) were used as the positive, and negative controls, respectively. The results were expressed as nmol/s of AA depletion per µg PM.

## Electron spin resonance (ESR) assay

ESR assay is selected to detect the PM-induced hydroxyl radical (OH·) generation, which is mainly generated via Fenton-type reaction. Spin trap 5,5-dimethyl-1-pyrroline-N-oxide (DMPO) was applied in presence of hydrogen peroxide. In brief, 25 µL of 200 µg/mL PM re-suspension (in HBSS) was mixed with 50 µL of 0.05M DMPO (kept in the dark) and 25 µL 0.5 M hydrogen peroxide (H<sub>2</sub>O<sub>2</sub>) in a vortex mixer for 5 seconds and then placed in shaking water bath at 37 °C for 15 minutes' incubation. The suspension was then placed in the vortex mixer again for 15 seconds followed by a transfer into a 50 µl glass capillary to measure. A MS-300 ESR spectrometer (Magnettech, Berlin, Germany) was utilized to measure the DMPO-OH quartet signal. The following ESR settings at room temperature were used for all measurements: magnetic field: 337 mT, range: 7mT, sweep time: 30 s, number of scans: 3, modulation amplitude: 0.2 mT, receiver gain: 2E2. For ESR assay, DOFA suspension at 1000 µg/mL and HBSS were used as the positive, and negative control, respectively. The results were expressed as the total amplitudes of DMPO-OH quartet in arbitrary units (A.U.) per µg PM.

## Cell culture

Human bronchial epithelial (16HBE) cells used in Braakhuis et al., (2016) were cultured in Dulbecco Modified Eagle Medium<sup>†</sup> (DMEM)/F-12 medium, L-Glutamine (1%), fungizone (1%), fetal bovine serum (5%), and 1% weight per volume penicillin/streptomycin in an incubator with 5% CO<sub>2</sub> at 37 °C. All culture media and supplements were purchased from Life Technologies (Thermo Fisher Scientific Inc., the Netherlands).

## Cell viability

MTS assay, a colorimetric method for determining the number of viable cells, was used to study cytotoxicity due to exposure to PM according to the manufacturer procedure (Promega, Fitchburg, Wisconsin, USA). Briefly, 16HBE cells were seeded into 96-well plates with 2 × 10<sup>5</sup> cells/mL and cultured for 24 h to reach ~ 80% confluence. Subsequently, the medium was replaced by the 100 µL non-serum fresh culture medium to prevent a protein corona around the particles. Two samples with relatively high mass filter loadings (L4: LAX week4 and U4: USC week4) were firstly chosen to establish the range for a concentration-response relationship (5 to 160 µg/mL). Cells were exposed to PM for 4 h after which the culture media was refreshed with serum-free fresh culture medium without PM for a 20h recovery period. The

culture media from recovery period were collected and stored at  $-20^{\circ}\text{C}$  for testing cytokine release. Next, cells were washed with HBSS and incubated with serum-free fresh culture medium containing MTS reagent (medium: MTS reagent = 10:1) for 1 h following absorbance measurement by a microplate reader at 490 nm (SpectraMax M2; Molecular Devices, Sunnyvale CA, USA). Fresh HBSS (containing no PM) was used as negative control. Based on the concentration-response curve, the concentration points corresponding to 80% of viability were set as the exposure concentration for the repetition of MTS assay for all PM samples (**Figure S2**).

### Reactive oxygen species (ROS) activity

Changes in intracellular ROS level after PM exposure were detected using the fluorescent dye 2', 7'- dichlorodihydrofluorescein diacetate ( $\text{H}_2\text{-DCFDA}$ ) (Thermo Fisher Scientific Inc., the Netherlands) methodology, which is based on the oxidation of nonfluorescent  $\text{H}_2\text{-DCFDA}$  by intracellular ROS to highly fluorescent 2',7'-dichlorofluorescein (DCF).  $\text{H}_2\text{-DCFDA}$  in the assay is used as an indicator for intracellular generated reactive oxygen species (ROS). Similarly, to the seeding process followed for cell viability testing, cells were washed with HBSS before adding 100 $\mu\text{L}$   $\text{H}_2\text{-DCFDA}$  (10 $\mu\text{M}$ , dilute in HBSS) probe (in the dark). After 45 minutes incubation, the probe was removed, and cells were washed again, and the plate was measured with 100 $\mu\text{L}$  HBSS using microplate reader (SpectraMax M2; Molecular Devices, Sunnyvale CA, USA) to determine the basal ROS production over the time. The cells were then exposed to all PM samples with serum-free fresh colorless culture medium and the plate was measured after 1 h, 2 h, 4 h exposure and 20 h recovery. 0.5%  $\text{H}_2\text{O}_2$  and fresh HBSS (no PM) were used as positive and negative controls, respectively.

### Release of inflammatory mediators

To test the effects of particles on pro-inflammatory mediator expression, the release of IL-6, IL-8 and tumor necrosis factor  $\alpha$  (TNF- $\alpha$ ) proteins from 16HBE cells was determined for LAX and USC samples with the supernatants collected from MTS assay using Luminex multiplex kit (Millipore, Merck, Darmstadt, Germany). For turbine and diesel samples, only IL-8 release was determined using the enzyme-linked immunosorbent assay (ELISA) Kit (eBioscience, San Diego, USA). Fresh HBSS (no PM) was used as the negative control.

### Statistical analysis

Correlations between elemental composition and oxidative potential (OP) were analyzed using Spearman rank correlation coefficient. Statistical comparison test was conducted using one-way ANOVA, significant differences were defined as  $p < 0.05$ .

## Results

### Characteristics of particles

The measured elements were assigned to four categories, each representing a specific emission source; these categories were aviation, ocean spray, road dust, and traffic. S, as the most abundant element in aircraft emissions, was considered as the aviation-related species (Kinsey et al., 2011). As the LAX site is located near the Pacific Ocean, particle-bound Na was considered as the ocean-related element in the form of sea salt. Al, Ca, Ti and K reported as the trace elements for suspended road dust (Marcazzan et al., 2001) were considered as road dust elements for LAX and USC particles (Al, Ca, and Ti were considered as road dust elements for turbine and diesel particles without K). While Mn, Fe, Cu, Zn, Ba, Pb, Ni, and Mg were elements associated with the traffic emissions, including combustion of fuel and lubricating oil as well as abrasion of brake, engine and tire wear (Maier et al., 2010; Pant and Harrison, 2013). For the LAX samples, aviation-related element (S) accounted for the largest fraction at 49.5%, followed by road dust elements (Al, Ca, Ti and K) and traffic-related elements (Mn, Fe, Cu, Zn, Ba, Pb, Ni and Mg) at 21.8% and 15.9%, respectively. In contrast, the emissions from traffic (28.5%), road dust (31.5%) and aviation (33.4%) were represented equally in the USC samples. In addition, ocean-related element had a higher contribution to the total elemental fraction for the LAX samples (12.8%) than in USC samples (6.60%) (**Figure 1a**), which can be explained by the proximity of the LAX to the Pacific Ocean, as noted earlier.

As presented in **Figure 1b**, aviation element contributed to the largest fraction in turbine sample at 82.9%, which corroborated the use of this element (S) as a tracer of aviation-related emissions in the smaller PM size range. Road dust (Al, Ca, and Ti), traffic and ocean markers accounted for much smaller fractions of 9.53%, 6.54%, and 1.04%, respectively. For diesel samples, traffic-related elements were the major contributors (54.1%) to the total elemental fraction, followed by ocean marker at 23.2%. The remainder was divided by aviation and road dust markers, with similar fractions of 12.2% and 10.4%, respectively. The mass fractions of the  $\text{PM}_{0.25}$  measured species, including trace elements and metals as well as organic carbon (OC) and elemental carbon (EC) can be found in **Table S1**. The ambient concentrations of these species are reported in detail in Shirmohammadi et al (2017a). EC and OC were omitted from our statistical analyses because their mass fractions in the USC and LAX samples were virtually identical (as seen in **Table S1**) and their inclusion to the statistical analysis did not provide any meaningful insight or conclusions.

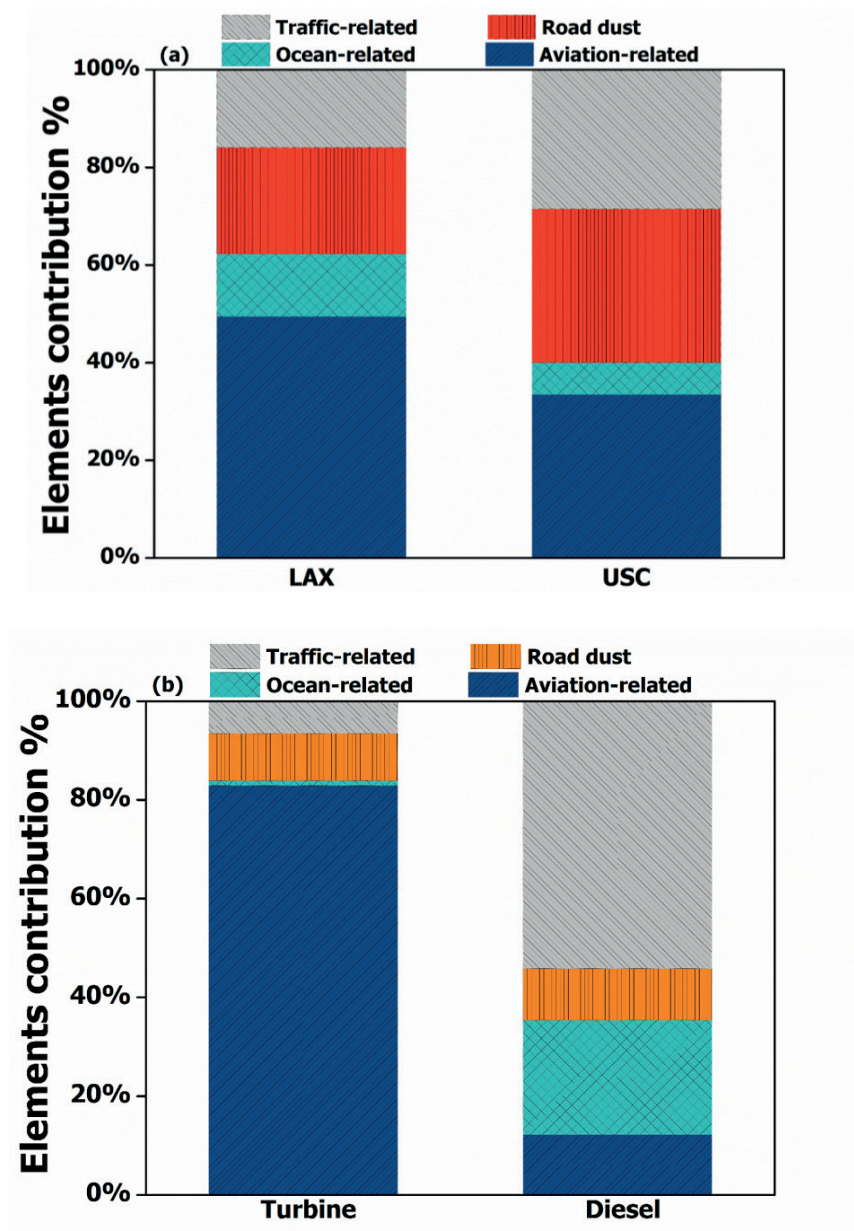


**Figure 1.** Elemental contributions in PM from LAX and USC (a) as well as turbine and diesel engines (b). S was considered as aviation-related element, Na as ocean-related element, and Mn, Fe, Cu, Zn, Ba, Pb, Ni and Mg as traffic-related elements in both (a) and (b). Al, Ca, Ti and K were considered as road dust elements in a (red), while Al, Ca, and Ti as road dust elements in b (orange).

### Oxidative potential assays (AA and ESR)

The oxidative potentials (OP) measured by AA and ESR of PM<sub>0.25</sub> sampled at LAX and USC are illustrated in **Figure S1**, using the ratios of PM samples divided by negative control (NC) values of each assay. A significant positive correlation was observed between  $OP_{AA}$  and  $OP_{ESR}$  ( $R=0.81$ ,  $p<0.05$ ,  $n=10$ , **Table S2**).

To evaluate and compare the OP level of different PM samples, the geometric mean (GM) values of  $OP_{AA}$  and  $OP_{ESR}$  are presented in **Table 1** for all PM samples. For both LAX and USC samples,  $OP_{AA}$  and  $OP_{ESR}$  values were significantly higher than the value of negative control ( $p<0.05$ ), with LAX samples showing relatively lower values compared to USC samples ( $0.33 \pm 0.10$  vs  $1.14 \pm 0.18$  for AA,  $1.97 \pm 0.51$  vs  $3.58 \pm 0.24$  for ESR).  $OP_{AA}$  and  $OP_{ESR}$  levels in turbine samples were higher than the levels of diesel samples ( $1.11 \pm 0.04$  vs  $0.53 \pm 0.06$  for AA,  $0.83 \pm 0.07$  vs  $0.59 \pm 0.11$  for ESR). Both PM samples showed significant OP except the diesel PM  $OP_{ESR}$  value, which was comparable to OP value of the NC.

**Table 1.** Geometric mean of oxidative potential (AA and ESR) values of LAX, USC, turbine, and diesel samples as well as negative and positive controls.

	AA (nmol AA/s/ $\mu$ g)	ESR (A.U/1000/ $\mu$ g)
LAX (n=5)	$0.33 \pm 0.10$	$1.97 \pm 0.51$
USC (n=5)	$1.14 \pm 0.18$	$3.58 \pm 0.24$
Turbine	$1.11 \pm 0.04$	$0.83 \pm 0.07$
Diesel	$0.53 \pm 0.06$	$0.59 \pm 0.11$
Negative control (dH <sub>2</sub> O)	$0.08 \pm 0.02$	$0.49 \pm 0.02$
Positive control (DOFA)	$1.36 \pm 0.13$	$11.4 \pm 0.37$

### Cell viability

Cell viability, an important indicator of toxicity, was measured after 24 h, including 4 h particle exposure and 20 h recovery period. One low (10  $\mu$ g/mL) and one high (100  $\mu$ g/mL) exposure level were used for all samples, as shown in **Figure 2**. Overall, 16HBE cells treated at 10 and 100  $\mu$ g/mL particles showed little cytotoxic effects, with the exceptions of U1(81.8%) and U2 (79.6%) at 100  $\mu$ g/mL, for which cell viabilities were around 80%, implying more cell deaths. To further study cellular responses after exposure, the lower exposure dose (10  $\mu$ g/mL) was used in subsequent study tests.



## Reactive oxygen species (ROS) activity

Intracellular ROS generation was measured after 1, 2, and 4 h exposure and 20 h recovery for all the samples to examine the oxidative potential of the particles by an additional method. The level of ROS was illustrated using ratios between samples and negative control (**Figure 3** and **Figure S3**). After exposure to 10  $\mu\text{g/mL}$  particles, the ROS levels in 16HBE cells were significantly elevated ( $p < 0.05$ ), and a slowly increasing trend was observed from 1h to 4h in all samples. On average, USC samples caused a slightly higher ROS generation than LAX samples per unit mass, while turbine samples showed a greater effect on ROS induction than diesel samples ( $p < 0.05$ ). After 20-h recovery, ROS production decreased to comparable level to the negative control for LAX, and USC samples.

## Correlation between oxidative potential indicators and PM composition

We selected  $OP_{AA}$ ,  $OP_{ESR}$  and  $OP_{ROS}$  at 1, 2, and 4 h to calculate the Spearman's correlation coefficient with chemical species in LAX and USC samples (**Table 2**). It was shown that  $OP_{AA}$ ,  $OP_{ESR}$  and  $OP_{ROS}$  at 1, 2, and 4 h significantly correlated with traffic-related transition metals (Fe and Cu, Spearman R: 0.65–0.87;  $p < 0.05$ ). Some trace elements that are ingredients of road and soil dust (e.g. Ti, Pb and Ca) also showed positive correlation with  $OP_{AA}$  and  $OP_{ESR}$  (Spearman R: 0.65–0.77;  $p < 0.05$ ) but not with the  $OP_{ROS}$ .

**Table 2.** Spearman's correlation coefficients (R) between the OP measures (AA, ESR and ROS) and chemical species for LAX and USC samples.

Species	AA	ESR	ROS <sub>1h</sub>	ROS <sub>2h</sub>	ROS <sub>4h</sub>
Cu	0.87*	0.80*	0.81*	0.78*	0.71*
Fe	0.85*	0.76*	0.77*	0.73*	0.65*
Ca	0.77*	0.72*	0.64	0.60	0.50
Ti	0.71*	0.65*	0.59	0.53	0.41
Pb	0.70*	0.46	0.60	0.65*	0.67*
Sum of traffic-related elements	0.78*	0.71*	0.67*	0.64	0.55

\* =  $p < 0.05$ .

## Inflammatory mediators

The induction and release of inflammatory mediators (IL-6, IL-8 and TNF- $\alpha$ ) was observed in 16HBE cells, and is expressed as ratios between samples and negative control (**Figure 4**). The LAX samples induced higher release of the inflammatory mediators in 16HBE cells at 1.7, 1.8, and 1.4-fold increase for IL-6, IL-8 and TNF- $\alpha$ ,

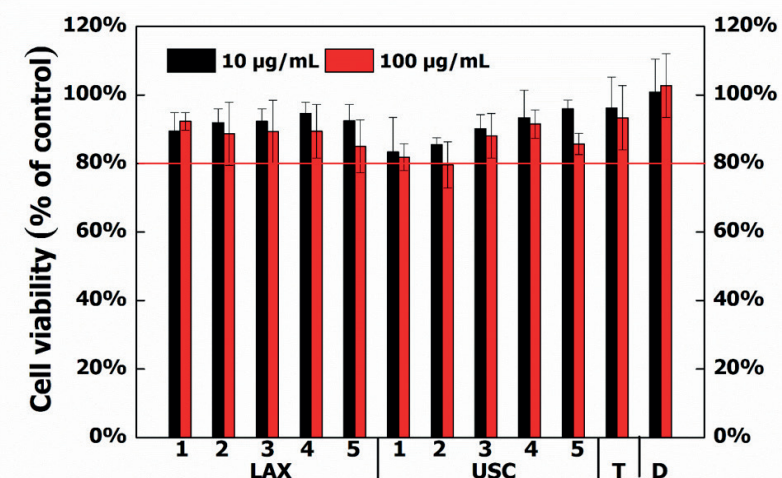


**Figure 2.** 16HBE cell viability tested by MTS assay for PM samples at 10 and 100  $\mu\text{g/mL}$ . T and D denote turbine and diesel samples, respectively. 1, 2, 3, 4 and 5 refer to the sampling week at LAX and USC.

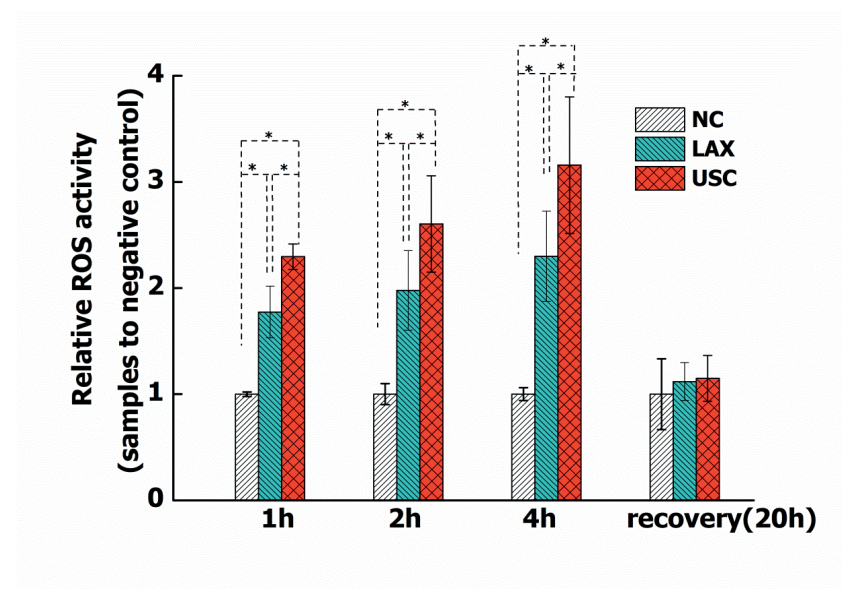


**Figure 3.** Average relative ROS activity in 16HBE cells after 1, 2, 4 h exposure and 20 h recovery to PM<sub>0.25</sub> from LAX, and USC (compared to negative control, NC), \* represents significant difference at  $p < 0.05$ .

respectively, while the release of IL-6, IL-8 and TNF- $\alpha$  induced by USC samples were at 1.3, 1.3, and 1.1-fold increase, respectively. However, no significant changes of IL-8 release were seen for turbine and diesel samples at 10  $\mu\text{g}/\text{mL}$ .

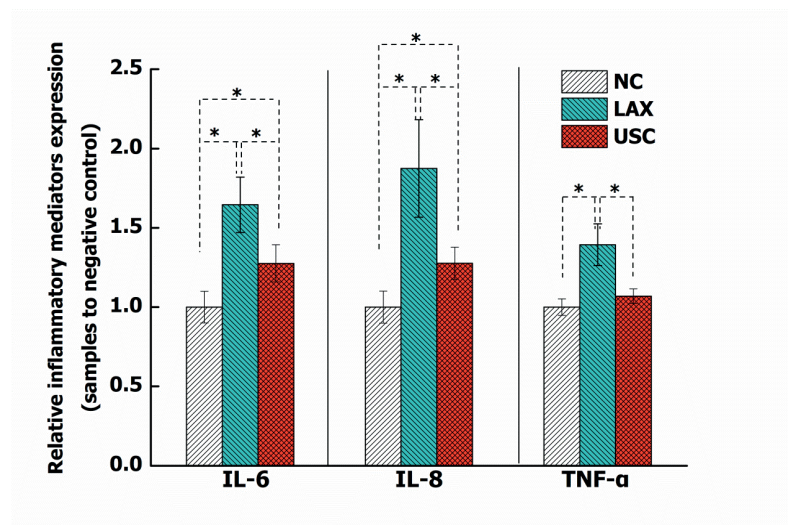


**Figure 4.** Relative expression of inflammatory mediators (IL-6, IL-8, and TNF- $\alpha$ ) after 20 h recovery on 16HBE cells for LAX and USC samples (compared to the negative control, NC). \* represents significant difference at  $p < 0.05$ .

## Discussion

Our results demonstrate the adverse responses in human bronchial cells (16HBE), including effects on cell viability/cytotoxicity, ROS activity and inflammatory mediators release, after exposure to ambient PM<sub>0.25</sub> collected near airport and urban sites as well as PM directly sampled from diluted exhaust of turbine and diesel engines. Elemental composition and oxidative potential of the PM samples seem to explain these biological responses.

Combustion of different fuels and the use of diverse engine types result in the emission of PM with distinctly different elemental composition. In line with several previous studies, S was found to be the most dominant element (82.9%) for turbine engine particles in this study due to the abundant S content in aviation fuel (Agrawal et al., 2008; Kinsey et al., 2011). In comparison, diesel exhaust particles were dominated (54.1%) by elemental markers of fuel and lubricant oil combustion, such as Mn, Fe, Cu,

Zn, Ba, Ni, Pb, and Mg (Lin et al., 2005; Wang et al., 2003). An appreciable (although lower than that of turbine engines) S fraction (12.2%) was measured in diesel samples, probably due to the S content in diesel oil and fuel (Shields et al., 2007).

The elemental composition of PM<sub>0.25</sub> from LAX showed some differences compared to aircraft turbine engine samples. S (49.5%) was still the most abundant element for LAX samples, while the contributions of road dust (21.8%), vehicle emissions (15.9%), and ocean related elements (12.9%) were higher than those of the engine samples. This was a result of the influence of not only aircraft emissions, but also ground support transportation at the airport as well as the seaside location of LAX on the composition of these urban samples (Masiol and Harrison, 2014, Shirmohammadi et al., 2017a). This suggests that, besides aviation activities, the contributions from surrounding traffic emissions and re-suspended road-dust to the airport-related particles are not negligible. In contrast, the elemental contributions in USC sample differed considerably compared to diesel engine sample. Traffic, road dust related elements as well as S accounted for similar large fractions of the PM mass underscoring the contributions of emission sources such as suspended road dust and atmospheric secondary sulfate to urban particles besides exhaust emissions (Marcazzan et al., 2001; Pant and Harrison, 2013).

The oxidative potential (OP) assays, AA and ESR, used in this study mainly represent the level of metal mediated reactive oxygen species (ROS) in particles such as OH $\cdot$  by Fenton reaction. The values of OP<sub>ESR</sub> and OP<sub>AA</sub> both showed significant positive correlations with some dominate traffic-related metals such as Fe and Cu (Spearman  $R > 0.75$ ,  $p < 0.05$ , **Table 2**). Janssen et al. (2014) reported similar high correlations between OP<sub>ESR</sub> and OP<sub>AA</sub> (Spearman  $R > 0.85$ ), as well as the correlations with such transition metals (Janssen et al., 2014). This indicates that the level of transition metals in PM have a major impact on the induction of ROS. This in turn, might explain the higher OP<sub>ESR</sub> and OP<sub>AA</sub> levels for PM from USC and turbine engine as they contain more abundant traffic-related elements compared to LAX and diesel PM samples (**Table 1**).

In contrast, ROS regulation in cells relates to more components. When particles deposit on surface of cells after exposure, a number of particle-cell physicochemical interactions could take place, including catalysis of surface compositions, particle wrapping, intracellular uptake and biocatalysts (Nel et al., 2009; Øvrevik et al., 2015). Certain particle characteristics such as chemical composition, size distribution and surface area contribute actively to these interactions, often leading to oxidative stress due to access ROS generation (Øvrevik et al., 2015). It has been reported that transition metals play an important role in ROS generation; PM with higher level

of transition metals such as Fe and Cu are capable of amplifying intracellular ROS generation (Aust et al., 2002; Schwarze et al., 2006), while the large surface area of ultrafine PM can provide more opportunities for catalyzing redox reactions (Nel et al., 2006). Similar findings were shown in our study, in that, the USC as well as turbine particle samples that were more abundant in transition metals induced greater intracellular ROS generation during the exposure period compared to LAX and diesel samples, respectively ( $p < 0.05$ , **Figure 3** and **Figure S3**).

To determine the influence of transition metals on ROS generation during the whole exposure period, the correlations between levels of  $OP_{ROS}$  at 1, 2, and 4 h and the dominant transition metals (Fe and Cu) in  $PM_{0.25}$  were calculated (**Table 2**). The significant and positive correlations between  $OP_{ROS}$  at 1, 2, and 4 h and such metals at the first 1 h exposure ( $OP_{ROS}$  at 1 h: Spearman  $R = 0.77$  to  $0.81$ ) confirmed the importance of these transition metals in ROS production. At the beginning of exposure, the release of redox active transition metals from particles might activate redox cycling (e.g. Fenton reaction) and promote a great intracellular ROS generation (Øvrevik et al., 2015). This similar ROS-formation principle may also explain the higher correlation coefficients between  $OP_{ROS}$  at 1 h and  $OP_{AA}$  and  $OP_{ESR}$  ( $R = 0.95$  and  $0.84$ , **Table S2**). However, with cellular internalization of particles taking place, the size, surface area and internalized amount of particles might gradually dominate in intracellular ROS generation (Hussain et al., 2009; Li et al., 2008). Several studies reported that particles with smaller size have a higher likelihood entering into cells (Braakhuis et al., 2015; Gratton et al., 2008); their interaction with cellular membrane, subcellular organelles and biological systems can catalyze greater ROS production (Hussain et al., 2009; Li et al., 2008; Øvrevik et al., 2015). While the transition metals showed less influence on ROS generation during the cellular internalization period, this might explain the decrease in the correlation coefficients between  $OP_{ROS}$  and these traffic-related metals over the course of the exposure ( $OP_{ROS}$  at 2 h: Spearman  $R = 0.73$  to  $0.78$ , 4 h:  $R = 0.65$  to  $0.67$ , **Table 2**).

Furthermore, it has been reported that oxidative stress can activate transcription factors such as NF- $\kappa$ B and AP-1 (Reuter et al., 2010; Rincon and Irvin, 2012). This can lead to the transcription of pro-inflammatory mediators such as IL-6, IL-8 and TNF- $\alpha$ , the expression of which is directly related with asthma and some inflammatory pulmonary diseases. However, results from our study showed that inflammatory responses (IL-6, IL-8 and TNF- $\alpha$ ) could also be elicited after 20 h recovery even when ROS generation induced by PM was balanced to the control level. Although PM suspensions used for cell exposure were changed to particle-free culture media followed by a 20 h recovery period, several *in vitro* studies showed that small PM can cross the cell membrane and remain in cells (Gratton et al., 2008; Braakhuis et al.,

2015), which may play an important role in inflammatory mediators' induction during the recovery period (Hussain et al., 2009). The smaller size distribution of LAX samples (Shirmohammadi et al 2017a) might lead to greater internalized amount of particles, thus promoting the release of IL-6, IL-8 and TNF- $\alpha$  in 16HBE cells (**Figure 4**).

The enhancement of ROS may disrupt the cellular oxidant-antioxidant balance, leading to inflammation and cytotoxicity. Excessive inflammation can result in the programmed cell death (Elmore, 2007). In this study, MTS values were all above 80%, indicating that cells showed low mortality after particles exposure ( $10 \mu\text{g/mL}$ ) in spite of at high level of oxidative stress. On the other hand, the results are also in accordance with the growing awareness that significant toxicity in cells such as enhanced ROS production and inflammatory responses can be induced even at high cell viability level (Valberg, 2004).

## Summary and Conclusions

In this study, we found that the aviation emissions were the major contributor to the total mass of  $PM_{0.25}$  collected downwind a major airport. In contrast, PM collected in a busy urban area have more complex chemistry due to the contribution of multiple sources, including traffic emissions, suspended road dust and atmospheric secondary sulfates, which accounted for similar contributions. Moreover, elemental carbon and organic carbon content was very similar for these two locations. In addition, our results demonstrated that airport-related  $PM_{0.25}$ , even at relatively low exposure concentrations, possess toxic properties similar to the  $PM_{0.25}$  emissions from urban traffic, suggesting that airport activity as a pollution source of  $PM_{0.25}$  may also contribute to adverse effects on public health.

**Disclaimer:** The content of this paper does not necessarily reflect the views and policies of the RIVM or those of the Netherlands Ministry of Infrastructures and Water Management. The authors have no conflict of interest to disclose.

## Acknowledgements

We thank Eric Gremmer, Daan L.A.C. Leseman, A. John F. Boere, Paul H. B. Fokkens from the National Institute for Public Health and the Environment (RIVM), Bilthoven, The Netherlands, and Yi-Xuan Li from the Institute for Risk Assessment Sciences, Utrecht University, Utrecht, The Netherlands, for their valuable assistance with the PM sampling and *in vitro* experiments. The support provided by China Scholarship Council (CSC) during the PhD period of Rui-Wen He in Utrecht University-Institute for Risk Assessment Studies is also acknowledged.



## References

- Agrawal H, Sawant AA, Jansen K, Miller JW, Cocker DR. 2008. Characterization of chemical and particulate emissions from aircraft engines. *Atmos. Environ.* 42: 4380-92
- Aust AE, Ball JC, Hu AA, Lighty J, Smith KR, Straccia AM, Veranth JM, Young WC. 2002. Particle characteristics responsible for effects on human lung epithelial cells. Research Report (Health Effects Institute): 1-65; discussion 67-76
- Ayres JG, Borm P, Cassee FR, Castranova V, Donaldson K, Ghio A, Harrison RM, Hider R, Kelly F, Kooter IM, Marano F, Maynard RL, Mudway I, Nel A, Sioutas C, Smith S, Baeza-Squiban A, Cho A, Duggan S, Froines J. 2008. Evaluating the toxicity of airborne particulate matter and nanoparticles by measuring oxidative stress potential—a workshop report and consensus statement. *Inhal Toxicol* 20: 75-99
- Barrett SR, Britter RE, Waitz IA. 2010. Global mortality attributable to aircraft cruise emissions. *Environ. Sci. Technol* 44: 7736-42
- Birch M, Cary R. 1996. Elemental carbon-based method for monitoring occupational exposures to particulate diesel exhaust. *Aerosol. Sci. Tech* 25: 221-41
- Braakhuis HM, Giannakou C, Peijnenburg WJ, Vermeulen J, van Loveren H, Park MV. 2016. Simple *in vitro* models can predict pulmonary toxicity of silver nanoparticles. *Nanotoxicology* 10:770-779.
- Braakhuis HM, Kloet SK, Kezic S, Kuper F, Park MV, Bellmann S, van der Zande M, Le Gac S, Krystek P, Peters RJ. 2015. Progress and future of *in vitro* models to study translocation of nanoparticles. *Arch Toxicol* 89:1469-1495.
- Demokritou P, Kavouras IG, Ferguson ST, Koutrakis P. 2002. Development of a High-Volume Cascade Impactor for Toxicological and Chemical Characterization Studies. *Aerosol. Sci. Tech.* 36:925-933.
- Elmore S. 2007. Apoptosis: a review of programmed cell death. *Toxicol Pathol* 35: 495-516
- Gratton SE, Ropp PA, Pohlhaus PD, Luft JC, Madden VJ, Napier ME, DeSimone JM. 2008. The effect of particle design on cellular internalization pathways. *P Natl Acad Sci* 105: 11613-18
- Hu S, Fruin S, Kozawa K, Mara S, Winer AM, Paulson SE. 2009. Aircraft emission impacts in a neighborhood adjacent to a general aviation airport in Southern California. *Environ. Sci. Technol* 43: 8039-45
- Hussain S, Boland S, Baeza-Squiban A, Hamel R, Thomassen LC, Martens JA, Billon-Galland MA, Fleury-Feith J, Moisan F, Pairon J-C. 2009. Oxidative stress and proinflammatory effects of carbon black and titanium dioxide nanoparticles: Role of particle surface area and internalized amount. *Toxicology* 260:142-149.
- Hudda N, Gould T, Hartin K, Larson TV, Fruin SA. 2014. Emissions from an international airport increase particle number concentrations 4-fold at 10 km downwind. *Environ. Sci. Technol* 48:6628-6635.
- Janssen NA, Yang A, Strak M, Steenhof M, Hellack B, Gerlofs-Nijland ME, Kuhlbusch T, Kelly F, Harrison R, Brunekreef B. 2014. Oxidative potential of particulate matter collected at sites with different source characteristics. *Sci. Total Environ* 472: 572-81
- Kelly, F. J. and J. C. Fussell. 2012. "Size, source and chemical composition as determinants of toxicity attributable to ambient particulate matter." *Atmos. Environ* 60: 504-526.
- Kim S, Jaques PA, Chang M, Froines JR, Sioutas C. 2001. Versatile aerosol concentration enrichment system (VACES) for simultaneous *in vivo* and *in vitro* evaluation of toxic effects of ultrafine, fine and coarse ambient particles Part I: Development and laboratory characterization. *J Aerosol Sci* 32: 1281-97
- Kinsey J, Hays M, Dong Y, Williams D, Logan R. 2011. Chemical characterization of the fine particle emissions from commercial aircraft engines during the aircraft particle emissions experiment (APEX) 1 to 3. *Environ. Sci. Technol* 45: 3415-21
- Li N, Sioutas C, Cho A, Schmitz D, Misra C, Sempf J, Wang M, Oberley T, Froines J, Nel A. 2003. Ultrafine particulate pollutants induce oxidative stress and mitochondrial damage. *Environ Health Persp* 111: 455
- Li N, Xia T, Nel AE. 2008. The role of oxidative stress in ambient particulate matter-induced lung diseases and its implications in the toxicity of engineered nanoparticles. *Free Radical Bio Med* 44:1689-1699.
- Lin C-C, Chen S-J, Huang K-L, Hwang W-I, Chang-Chien G-P, Lin W-Y. 2005. Characteristics of metals in nano/ultrafine/fine/coarse particles collected beside a heavily trafficked road. *Environ. Sci. Technol* 39: 8113-22
- Loxham M, Cooper MJ, Gerlofs-Nijland ME, Cassee FR, Davies DE, Palmer MR, Teagle DA. 2013. Physicochemical characterization of airborne particulate matter at a mainline underground railway station. *Environ. Sci. Technol* 47: 3614-22
- Maier N, Nickel KG, Engel C, Mattern A. 2010. Mechanisms and orientation dependence of the corrosion of single crystal Cordierite by model diesel particulate ashes. *J Eur Ceram Soc* 30: 1629-40
- Marcazzan GM, Vaccaro S, Valli G, Vecchi R. 2001. Characterisation of PM10 and PM2.5 particulate matter in the ambient air of Milan (Italy). *Atmos. Environ.* 35: 4639-50
- Masiol M, Harrison RM. 2014. Aircraft engine exhaust emissions and other airport-related contributions to ambient air pollution: a review. *Atmos. Environ.* 95: 409-55
- Minguillón, M.C., Arhami, M., Schauer, J.J., Sioutas, C., 2008. Seasonal and spatial variations of sources of fine and quasi-ultrafine particulate matter in neighborhoods near the Los Angeles–Long Beach harbor. *Atmos. Environ.* 42, 7317–7328.
- Misra, C., Singh, M., Shen, S., Sioutas, C., Hall, P.M., 2002. Development and evaluation of a personal cascade impactor sampler (PCIS). *J. Aerosol Sci.* 33, 1027–1047.
- Nel A, Xia T, Mädler L, Li N. 2006. Toxic potential of materials at the nanolevel. *science* 311: 622-27
- Nel AE, Mädler L, Velegol D, Xia T, Hoek EM, et al. 2009. Understanding biophysicochemical interactions at the nano-bio interface. *Nat Mater* 8: 543
- Øvrevik J, Refsnes M, Låg M, Holme J, Schwarze P. 2015. Activation of proinflammatory responses in cells of the airway mucosa by particulate matter: Oxidant- and non-oxidant-mediated triggering mechanisms. *Biomolecules* 5:1399.
- Pant P, Harrison RM. 2013. Estimation of the contribution of road traffic emissions to particulate matter concentrations from field measurements: a review. *Atmos. Environ.* 77: 78-97
- Reuter S, Gupta SC, Chaturvedi MM, Aggarwal BB. 2010. Oxidative stress, inflammation, and cancer: how are they linked? *Free Radical Bio Med* 49: 1603-16
- Rincon M, Irvin CG. 2012. Role of IL-6 in asthma and other inflammatory pulmonary diseases. *Int J Biol Sci* 8: 1281
- Schwarze P, Øvrevik J, Låg M, Refsnes M, Nafstad P, Hetland R, Dybing E. 2006. Particulate matter properties and health effects: consistency of epidemiological and toxicological studies. *Hum Exp Toxicol* 25: 559-79
- Shields LG, Suess DT, Prather KA. 2007. Determination of single particle mass spectral signatures from heavy-duty diesel vehicle emissions for PM 2.5 source apportionment. *Atmos. Environ.* 41: 3841-52
- Shirmohammadi F, Lovett C, Sowlat M, Mousavi A, Verma V, Shafer M, Schauer J, Sioutas C. 2017a. Chemical composition and redox activity of PM<sub>0.25</sub> near Los Angeles International Airport and comparisons to an urban traffic site. *Sci. Total Environ* 610: 1336
- Shirmohammadi F, Sowlat MH, Hasheminassab S, Saffari A, Ban-Weiss G, Sioutas C. 2017b. Emission rates of particle number, mass and black carbon by the Los Angeles International Airport (LAX) and its impact on air quality in Los Angeles. *Atmos. Environ.* 151: 82-93
- Sowlat, M.H., Hasheminassab, S., Sioutas, C., 2016. Source apportionment of ambient particle number concentrations in central Los Angeles using positive matrix factorization (PMF). *Atmos Chem Phys* 16, 4849–4866. doi:10.5194/acp-16-4849-2016
- Touri L, Marchetti H, Sari-Minodier I, Molinari N, Chanez P. 2013. The airport atmospheric environment: respiratory health at work. *Eur Respir Review* 22: 124-30
- Unal A, Hu Y, Chang ME, Odman MT, Russell AG. 2005. Airport related emissions and impacts on air quality: Application to the Atlanta International Airport. *Atmos. Environ.* 39: 5787-98
- Valberg PA. 2004. Is PM more toxic than the sum of its parts? Risk-Assessment toxicity factors vs. PM-mortality "effect functions". *Inhal Toxicol* 16: 19-29
- Wang Y-F, Huang K-L, Li C-T, Mi H-H, Luo J-H, Tsai P-J. 2003. Emissions of fuel metals content from a diesel vehicle engine. *Atmos. Environ.* 37: 4637-43
- Xiang P, He R-W, Han Y-H, Sun H-J, Cui X-Y, Ma LQ. 2016a. Mechanisms of housedust-induced toxicity in primary human corneal epithelial cells: Oxidative stress, proinflammatory response and mitochondrial dysfunction. *Environ Int* 89: 30-37

## Supplementary Material

**Table S1.** Average mass fractions (with standard deviations, SD) of organic carbon (OC), elemental carbon (EC), metals and trace elements elements. OC and EC mass fractions are in units of  $\mu\text{g}/\mu\text{g}$  PM, whereas mass fractions of all other trace elements and metals are in  $\text{ng}/\mu\text{g}$  PM

Species	LAX		USC		Turbine		Diesel	
	Ave	SD	Ave	SD	Ave	SD	Ave	SD
OC( $\mu\text{g}/\mu\text{g}$ )	0.31	0.04	0.31	0.09	-	-	-	-
EC( $\mu\text{g}/\mu\text{g}$ )	0.12	0.01	0.12	0.05	-	-	-	-
S( $\text{ng}/\mu\text{g}$ )	34.31	4.50	22.57	3.71	328	41.0	9.35	0.83
Na	8.92	1.96	4.48	1.66	4.11	0.50	17.9	0.58
Fe	7.48	3.43	13.37	6.33	17.0	1.51	0.72	0.02
Al	5.32	2.44	7.03	4.77	17.9	2.21	0.20	0.07
K	5.51	2.06	6.06	2.32	-	-	-	-
Ca	3.86	1.73	7.36	4.09	19.2	2.26	7.80	0.18
Mg	1.26	0.50	1.83	1.20	2.00	0.32	3.74	0.18
Ba	0.67	0.34	1.08	0.49	0.13	0.01	0.01	0.001
Zn	0.63	0.20	1.03	0.43	2.72	0.28	36.8	0.81
Cu	0.51	0.21	1.21	1.07	2.62	0.19	0.10	0.002
Ti	0.41	0.23	0.78	0.55	0.68	0.12	0.02	0.003
Pb	0.30	0.10	0.42	0.22	0.93	0.10	0.06	0.001
Mn	0.15	0.05	0.25	0.09	0.12	0.01	0.08	0.002
Ni	0.05	0.01	0.05	0.01	0.38	0.06	0.08	0.003

**Table S2.** Spearman's correlation coefficients (R) between the oxidative potential (OP) measures (AA, ESR, and ROS) for LAX and USC samples (n=10).

Measures	AA	ESR	ROS <sub>1h</sub>	ROS <sub>2h</sub>	ROS <sub>4h</sub>
AA	-	0.81*	0.95*	0.94*	0.88*
ESR	0.81*	-	0.84*	0.81*	0.79*
ROS <sub>1h</sub>	0.95*	0.84*	-	0.99*	0.95*
ROS <sub>2h</sub>	0.94*	0.81*	0.99*	-	0.98*
ROS <sub>4h</sub>	0.88*	0.79*	0.95*	0.98*	-

\* =  $p < 0.05$

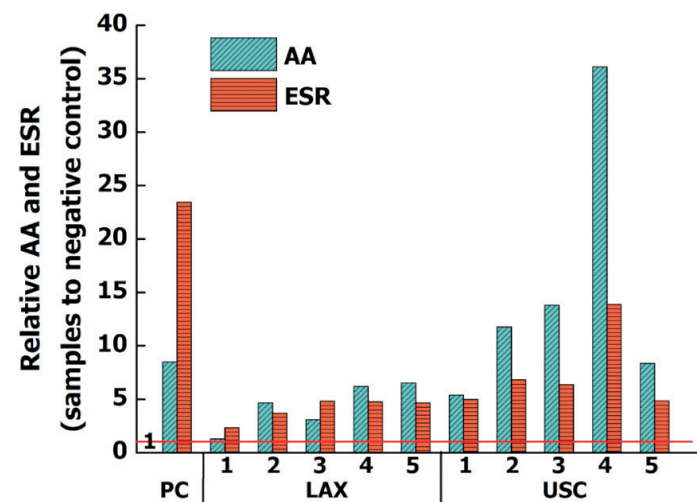


**Figure S1.** Relative ratios of oxidative potential measured by AA and ESR in LAX, and USC samples, adjusted for negative control. Domestic oil burning furnace (DOFA) is used as a positive control (PC), 1,2,3,4, and 5 refer to the sampling week at LAX and USC.

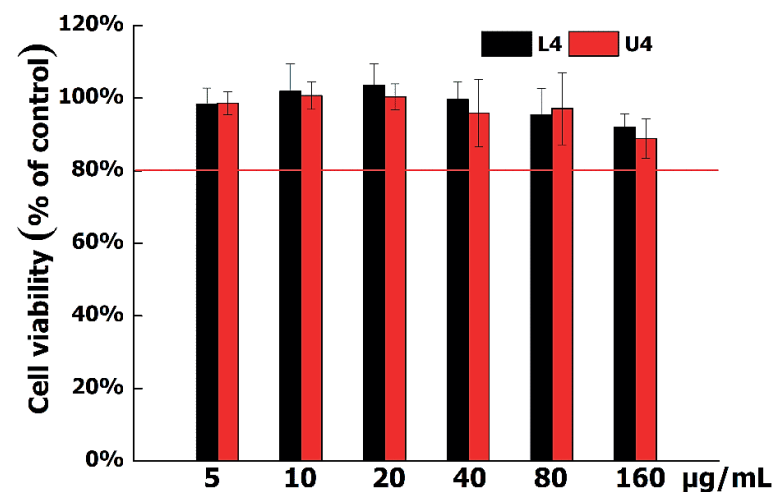


**Figure S2.** 16HBE cell viability tested by MTS assay at L4 (LAX week 4) and U4 (USC week 4) from 5 to 160  $\mu\text{g}/\text{mL}$ .



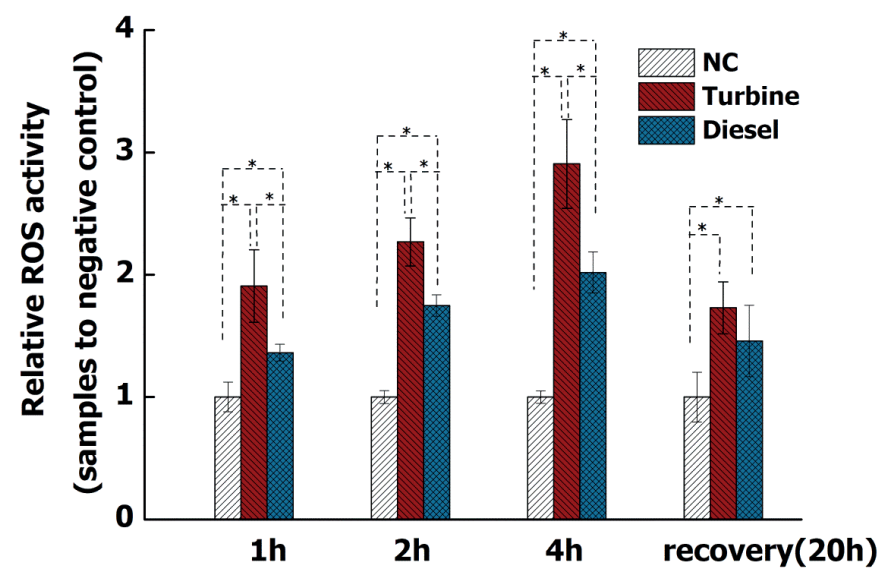


**Figure S3.** Relative average ROS activity (compared to the negative control, NC) in 16HBE cells after 1, 2, 4 h exposure and 20 h recovery for turbine, and diesel PMs, adjusted for NC (negative control). \* represents significant difference at  $p < 0.05$ .

# Chapter 3

## Part I

### **An air-liquid interface bronchial epithelial model for realistic, repeated inhalation exposure to airborne particles for toxicity testing**

Hedwig M. Braakhuis <sup>1</sup>, Ruiwen He <sup>1,2</sup>, Rob J. Vandebriel <sup>1</sup>, Eric R. Gremmer <sup>1</sup>, Edwin Zwart <sup>1</sup>, Jolanda P. Vermeulen <sup>1</sup>, Paul Fokkens <sup>1</sup>, John Boere <sup>1</sup>, Ilse Gosens <sup>1</sup>, Flemming R. Cassee<sup>1,2</sup>

<sup>1</sup> National Institute for Public Health and the Environment (RIVM)

<sup>2</sup> Institute for Risk Assessment Sciences (IRAS)

(Journal of Visualized Experiments, 2020, Issue 159, e61210)

(Video: <https://www.jove.com/t/61210>)

## Abstract

For toxicity testing of airborne particles, air-liquid interface (ALI) exposure systems have been developed for *in vitro* tests in order to mimic realistic exposure conditions. This puts specific demands on the cell culture models. Many cell types are negatively affected by exposure to air (e.g., drying out) and only remain viable for a few days. This limits the exposure conditions that can be used in these models: usually relatively high concentrations are applied as a cloud (i.e., droplets containing particles, which settle down rapidly) within a short period of time. Such experimental conditions do not reflect realistic long-term exposure to low concentrations of particles. To overcome these limitations the use of a human bronchial epithelial cell line, Calu-3 was investigated. These cells can be cultured at ALI conditions for several weeks while retaining a healthy morphology and a stable monolayer with tight junctions. In addition, this bronchial model is suitable for testing the effects of repeated exposures to low, realistic concentrations of airborne particles using an ALI exposure system. This system uses a continuous airflow in contrast to other ALI exposure systems that use a single nebulization producing a cloud. Therefore, the continuous flow system is suitable for repeated and prolonged exposure to airborne particles while continuously monitoring the particle characteristics, exposure concentration, and delivered dose. Taken together, this bronchial model, in combination with the continuous flow exposure system, is able to mimic realistic, repeated inhalation exposure conditions that can be used for toxicity testing.

**Keywords:** air-liquid interface, bronchial model, inhalation exposure, toxicity, realistic exposure, *in vitro*, nanomaterials;

## Introduction

The lungs are vulnerable to inhalation exposure to airborne particles. To assess the potential toxicity of airborne particles, progress has been made to develop air-liquid interface (ALI) exposure systems<sup>1,2,3,4,5</sup>. ALI exposure systems allow more relevant and realistic exposure models compared to traditional submerged exposure via culture medium that alters the characteristics and kinetics of the particles<sup>6</sup>. The ALI exposure systems place specific demands on the cell culture models, as the models lack culture medium and thus nutrients at the apical side. Many cell models are negatively affected by being cultured and exposed at the air (e.g., drying out) and only remain viable for a few days. This limits the exposure conditions that can be used in these models: usually relatively high concentrations are applied within a short period of time as a cloud (i.e., droplets containing particles, which settle down rapidly). Such experimental conditions do not reflect realistic long-term exposure to low concentrations of particles; thus, the relevance of the results can be questioned. To overcome these limitations, the culture and exposure protocol for a bronchial model consisting of the human bronchial epithelial cell line Calu-3<sup>7</sup> was optimized.

Most *in vitro* lung models used for ALI exposure contain other cell lines such as A549, BEAS-2B, and 16HBE140- (16HBE) or primary cells as a basis<sup>8</sup>. These cell lines have the disadvantage that they remain viable for only a few days when cultured at the ALI. In addition, some of these cell lines overgrow when cultured for a period longer than 5 days. Finally, A549 cells miss functional tight junctions and can therefore not form a tight barrier that is needed to mimic the lungs<sup>9,10</sup>. Primary epithelial cells might be a good option for ALI exposure as they can be cultured at the ALI for weeks. However, primary cells differ from batch to batch, are more difficult to maintain, and are more expensive compared to cell lines, which makes them less suitable for toxicity testing and screening. When comparing different human bronchial epithelial cell lines (16HBE, Calu-3, H292, and BEAS-2B), only the Calu-3 cells fulfill all criteria needed for realistic, repeated ALI exposure: they remain viable for weeks while cultured at the ALI, provide a high barrier integrity, do not overgrow, and are easy to culture and maintain. Calu-3 cells originate from an adenocarcinoma and are able to produce mucus<sup>11,12</sup>. There are inconsistencies as to whether the cells can develop cilia<sup>11,13</sup>. Calu-3 cells are also a suitable model to study respiratory syncytial virus (RSV) infections that infect ciliated airway epithelial cells<sup>14</sup>.

Besides the cell model, an automated exposure system (AES) is used for the air-liquid exposure to aerosols<sup>15,16</sup>. The AES has the advantage that it uses a continuous airflow to expose the cell model to aerosols. This is in contrast to other air-liquid exposure systems that usually use relatively high concentrations within a short period of time as

a cloud (i.e., droplets containing particles that settle down rapidly)<sup>17,18,19</sup>. These cloud systems do not reflect realistic long-term exposure to low concentrations of particles. By applying a continuous airflow using the AES, the cell model can be exposed to a low concentration of particles over a longer time period, reflecting realistic exposure conditions. Another advantage over cloud systems is that the AES has the option to connect particle characterization instruments, allowing the measurements of particle size, number concentration, and mass over time. A limitation of the AES is that it uses relatively high airflows between 10 mL/min and 100 mL/min.

## Protocol

### 1. Preparing cell culture medium (CCM)

1. Prepare a bottle of 500 mL of minimum essential medium (MEM) supplemented with glutamine.
2. Add 5 mL of penicillin-streptomycin (i.e., 100 U/mL penicillin and 100 µg/mL streptomycin).
3. Add 5 mL of non-essential amino acids (NEAA) solution.
4. Add 10 mL of amphotericin B (optional).
5. Add 50 mL of FBS (heat inactivated, please follow the ATCC protocol for heat inactivation; ([https://www.atcc.org/~media/PDFs/Culture%20Guides/AnimCellCulture\\_Guide.ashx](https://www.atcc.org/~media/PDFs/Culture%20Guides/AnimCellCulture_Guide.ashx), page 19)).

### 2. Sub-culturing of Calu-3 cells

NOTE: Calu-3 cells are cultured in T75 or T175 cell culture flasks at 37 °C and 5% CO<sub>2</sub>. Cells are passaged at 60–80% confluency every 7 days with CCM renewal every 2–3 days. CCM is poured off and fresh CCM (T25 = 5 mL, T75 = 15 mL, and T175 = 25 mL) is pipetted into the flask and the flask is placed back into the incubator. Cells should be passaged at least 2x after thawing, before using in experiments, or before freezing, and they should be passaged no more than 25x in total.

1. Confirm if flask is 60–80% confluent by checking under a light microscope.
2. Pour off the CCM from the flask.
3. Wash the cells 2x with 5 mL of 1x Hanks' Balanced Salt Solution (HBSS) without calcium and without magnesium. Discard the HBSS after each wash. HBSS removes serum, which inhibits trypsin.
4. Add 3 mL of trypsin-EDTA for a T75 (4 mL for a T175) and place the flask back into the incubator at 37 °C and 5% CO<sub>2</sub> for 10–15 min. Check after 10 min, ensuring the cells have become detached from the flask surface. In case the cells are grown to >80% confluency, they will not detach using trypsin 0.05% and trypsin 0.25% could be used.

5. Add 6 mL (i.e., double the trypsin-EDTA volume originally added) of CCM to the flask and gently rock the flasks to ensure proper mixing. This is to ensure the trypsin has been neutralized by the FBS in the CCM and its activity on the cells halted. If trypsin is allowed to remain in contact with the cells for too long they will not reattach when put into a new cell culture flask.
6. Pour the complete contents of the flask into a 50 mL centrifuge tube.
7. Centrifuge the cells for 5 min at 130 x g, ensuring that the centrifuge is correctly balanced.
8. Return the vial containing the cells back to aseptic conditions and remove the supernatant gently, without disturbing the pellet. The supernatant can be poured off and the remainder pipetted off, ensuring the pellet is not disturbed.
9. Resuspend the cell pellet in 1 mL of CCM by pipetting up and down until all cells are suspended (i.e., no pellet or cell agglomerates are observed). Additional CCM can be added to dilute the cell suspension.
10. Count the cells, both dead and alive, in 1 mL of CCM using a hemocytometer. If needed for proper counting, dilute the cells in 3 or 4 mL.
11. Suspend the cells into the CCM volume required and add the cell suspension into each flask. To achieve about 80% confluency in a week, seed 2 x 10<sup>6</sup> cells in a T75 or 6 x 10<sup>6</sup> cells in a T175.
12. Gently rock the flask and then place it back into the incubator at 37 °C and 5% CO<sub>2</sub>.
13. Replace with fresh CCM every 2–3 days and subculture when the cells reach 60–80% confluency.

### 3. Seeding Calu-3 cells onto culture inserts

NOTE: Inserts are available with different pore sizes. Small pore sizes (e.g., 0.4 µm) have the advantage that the cells grow more easily and can achieve a good barrier already after 5 days culturing under submerged conditions, as measured by Trans Epithelial Electrical Resistance (TEER). However, when interested in particle translocation, these pores are too small and will trap the particles. Therefore, larger pore sizes (e.g., 3 µm) are usually chosen to test particles. When using a larger pore size, the cells need longer time periods (e.g., 7–10 days culturing under submerged conditions) to achieve a good TEER.

1. Prepare cell suspension with known concentration following steps 2.1–2.10.
2. Dilute cells to a concentration of 5 x 10<sup>5</sup> cells/mL in prewarmed CCM for 6 well inserts or 2.5 x 10<sup>5</sup> cells/mL for 12 well inserts.
3. Take a cell culture plate with inserts and place under aseptic conditions.
4. Fill the basolateral side with 2 mL of prewarmed CCM for 6 well inserts, or 1 mL for 12 well inserts. While adding the culture medium, take the insert out using tweezers.

5. Carefully mix the cell suspension by pipetting up and down. Pipette 1.0 mL for 6 well inserts and 500  $\mu$ L for 12 wells inserts (equivalent to 100,000 cells/cm<sup>2</sup>) on the top of the membrane in the cell culture insert with 0.4  $\mu$ m pores. For 3.0  $\mu$ m pores, increase the cell density to 128,000 cell/cm<sup>2</sup>.
6. Cover the cell culture plate and incubate at 37 °C and 5% CO<sub>2</sub>.
7. Change the CCM every 2–3 days.
8. Let the cells become confluent for 7 days under submerged conditions before continuing to culture at the ALI.
9. Measure TEER.
  1. Take an Epithelial Voltohmmeter supplemented with Chopstick Electrode Set and charge the battery system overnight.
  2. Disconnect the Voltohmmeter from the charger and connect the chopstick electrode.
  3. Clean the electrode with 70% ethanol.
  4. Place the electrode in the CCM by putting the longer electrode in the external culture media until it touches the bottom of the dish and putting the shorter electrode in the media without touching the membrane.
  5. Start with an empty insert without cells. Wait until the measurement stabilizes and write down the resistance in Ohms. This measurement is the resistance of the insert membrane without any cells (i.e., blank resistance).
  6. Repeat the measurement for each insert and subtract the blank resistance to obtain the true resistance.
  7. For data analysis, multiply the resistance values by the surface area of the insert into  $\Omega \times \text{cm}^2$ . For a 6 well insert, the surface area is 4.67 cm<sup>2</sup>. Thus, if a resistance of 600 Ohm is measured and the background is 120 Ohm, the resistance is 480 Ohm, which is then multiplied by the surface area of 4.67 cm<sup>2</sup> for a total of 2,241.6 Ohm  $\times$  cm<sup>2</sup>. The TEER should be >1,000  $\Omega \times \text{cm}^2$  to continue.
10. Remove the CCM from the apical side of the inserts.
11. Add 2 mL of prewarmed CCM for 6 well and 1 mL for 12 well inserts to the basolateral side of the well (i.e., under the cell culture insert). The CCM should touch the membrane from the bottom, but not leak onto the top of the insert.
12. At this point cells are apically exposed to air, which is referred to as culturing at the ALI.
13. Culture cells at the ALI in the incubator at 37 °C and 5% CO<sub>2</sub> for 7 days prior to exposure.
14. Change the basolateral CCM every 2–3 days. The cells can be used at the ALI for 6 weeks.

#### 4. Preparing the exposure setup

NOTE: Sections 5–7 describe preparations for particle exposure using an automated exposure station (AES, see Table of Materials). The setup for particle nebulization and characterization is also compatible with other ALI exposure systems from other manufacturers. As an example, the exposure to particles is described below. Such systems can also be used for other exposures, such as sensitizers, cigarette smoke, and diesel exhaust. Figure 1 shows the AES and an exposure module. **Figure 2** shows a schematic representation of the exposure setup including all other instruments.

1. Before starting an exposure using the AES, connect the system to several instruments to measure aerosol characteristics; these are measured in a side stream just before the aerosols enter the cabinet.

NOTE: A flow splitter is used to connect the side stream to the exposure characterization equipment. Generally, the following equipment is used: scanning mobility particle sizer (SMPS), optical particle sizer (OPS), condensation particle counter (CPC), tapered element oscillating microbalance (TEOM). The SMPS and OPS measurements are performed 1x per hour and use the same tubing from the flow splitter. The CPC and TEOM perform continuous measuring and data from both are logged on a Squirrel model 2020 data logger. In addition, gravimetric mass concentration is determined using a microbalance in controlled relative humidity (40–70%) and temperature (21–23 °C) conditions.

Teflon filters are weighed before and after each exposure to confirm the exposure concentration. To capture the exhaust, a HEPA filter is used. The setup including engineered nanomaterial (ENM) suspensions and nebulizer are all placed in a flow cabinet to prevent any exposure to people. The AES can be used for testing many different types of ENMs, including metals and metal oxides.

2. Prepare a nanomaterial suspension shortly before exposure. Usually a 1% suspension is prepared as a stock solution. For example, suspend 100 mg of nanomaterial in 10 mL of pure water.

NOTE: For DQ12 exposure, 300 mg is used to achieve about 2  $\mu$ g/cm<sup>2</sup>. This amount can be used in a single exposure or divided over repeated exposures (e.g., 300 mg is suspended in 30 mL for a single exposure or 21.5 mg is suspended in 2.15 mL freshly every day for 3 weeks of repeated exposure). The suspension is freshly prepared on each exposure day. The particle suspension is sonicated for 16 min using probe sonication. The volume of the 1% stock solution is adjusted to a total volume of 100 mL by adding pure water.

3. Put the ENM suspension in a small bottle with a cap and a magnetic stirrer to prevent settling of the particles. Connect the bottle to a peristaltic pump via a small tube and adjust the flow to 25 mL/h.
4. Connect the peristaltic pump to a spray nozzle and adjust the settings to allow continuous aerosolization.
5. The spray nozzle is mounted to a 60 cm long aluminium tube (mixing chamber, diameter 15 cm, heated to 60 °C). The setup is connected to the AES via a 1.5-meter-long copper tube (diameter 15 cm). On top of the AES an impactor removes all aerosols larger than 2.5 µm.
6. Connect the spray nozzle to 3 bar compressed air through two mass flow controllers (MFC) to allow nebulization of suspensions. One flow of 14 L/min is used for the spray nozzle, the other MFC for mixing of the air in the tube.
7. The day before the start of the exposure, turn on the AES to allow the cabinet to reach a temperature of 37 °C.
8. Turn on the air flow and the humidity in the cabinet 2 h before start of the exposure, to reach 85% humidity. Turn on the heating of the exposure chambers in which the inserts with the cells will be placed.
9. Turn on the quartz microbalance (QCM) and set the initial value at 0 using the software. Start logging. Every 10 s the mass is measured and expressed as ng/cm<sup>2</sup>.
10. Warm the cell culture media to 37 °C in a water bath (~20 – 30 min).

### 5. Preparing Calu-3 cells for exposure

NOTE: For a typical ALI exposure using the AES, 15–20 inserts with a confluent cell layer are needed. These consist of 3 clean air controls, 3 incubator controls that will be handled similarly to the other inserts without exposure in the AES, 6–8 inserts for aerosol exposure (depending on the use of 0, 1, or 2 microbalances), 1–3 inserts for control measurements (such as maximum LDH release), and 3 spare inserts in case the TEER of some of the inserts is not sufficient. The cells should have a TEER of >1,000 Ω x cm<sup>2</sup> to continue.

1. On the first day of exposure, wash cells 1x with CCM, check cell morphology, and measure the TEER of the cell model using a Voltohmmeter. The cells should form a tight monolayer without gaps.
2. Put 2 mL/1 mL of HEPES buffered CCM without FCS to the basolateral side of 6 well/12 well plates and transfer the culture inserts with cells to the new plates.  
NOTE: During exposure, no CO<sub>2</sub> is present in the AES. Therefore, HEPES buffered culture medium (25 mM HEPES) is used during transport and exposure. This medium is used for both the exposed cells in the AES as well as the incubator control cells.

3. In case the time to transport the cell cultures to the AES is more than 5 min, put the cells in a portable incubator of 37 °C during transport.

### 6. Handling the AES during an exposure

1. At the AES, fill the exposure modules with HEPES-buffered CCM without fetal calf serum (FCS). The amount of CCM depends on the unit used, and the type of cell culture insert. Keep in mind that to keep cells at the ALI, the medium should reach the bottom of the membrane, but should not leak on top of the membrane. When using 6 well inserts, add 6 mL of HEPES-buffered CCM to the exposure modules.
2. Transfer the inserts with cells from the plates to the exposure modules using sterile tweezers. Check that there are no air bubbles at the basolateral side of the cells and remove any CCM on the apical side of the inserts. In case there are some air bubbles at the basolateral side, gently turn the inserts using the sterile tweezers until they are removed. Keep the plates containing CCM in an incubator for transfer after an exposure.
3. Use the touchscreen display to choose exposure duration, air flow rate, and electrostatic deposition enhancement. The display can also be used to check humidity and temperature. Usually, an exposure duration of 4 h is chosen, with a flow rate of 50 mL/min on the inserts at 37 °C and 85% humidity.  
NOTE: The modules in the first level (**Figure 1**) are used for clean air exposure; inserts in this level are used as clean air exposure controls. The other modules in the second and third level can be used for aerosol exposure, including two modules for quartz crystal microbalances (QCM) to measure deposition online.
4. The leak test should be conducted before starting exposure. The leakage needs to be less than 5 mL/min. Follow the instructions on the AES display. When the leak test has finished, the exposure can be started. In case of a leak, the tubing should be checked.
5. At the end of exposure, open the door of an AES module, open the exposure modules, place the cell culture inserts back to the cell culture plates, and transfer the plates to the portable incubator.
6. Collect the media from the modules (i.e., exposed samples) and from the plates (i.e., incubator controls) for later analysis, such as lactate dehydrogenase (LDH) measurement.
7. Back at the cell culture lab, transfer the cell culture inserts to plates filled with fresh standard CCM. Put the cell culture plates in the incubator until the next exposure or until analysis.
8. After the final exposure day, put the inserts in the incubator until the next day.
9. At the day after the final exposure, add CCM to the apical side to measure TEER using a Voltohmmeter. Collect both the apical and the basolateral CCM separately for analysis of cytokines.



- Remove all CCM and perform a cell viability assay by adding, for example, a proliferation reagent to the apical side.

### 7. Cleaning the AES

- Fill the exposure modules with water, wait for 1 min, and remove the water. Next, fill the modules with 70% ethanol, leave it for 10 min, and remove the ethanol. Clean the exposure trumpets also with 70% ethanol.
- Stop the 85% humidity control, but leave the temperature of the cabinet at 37 °C for the next experiment.

### Representative Results

This article provides a method for culturing and exposing human bronchial epithelial cells at the ALI that mimics realistic, repeated inhalation exposure conditions that can be used for toxicity testing. Characteristics of both the cell model and of the exposure system are essential for achieving a realistic inhalation exposure model that can be used for repeated exposures. Results on these characteristics are shown below.

#### Cell model requirements and selection

When selecting a suitable cell model, the following characteristics must be taken into account:

- The cell model should be able to form a confluent monolayer with functioning tight junctions to mimic the lung barrier.
- The cell model should show optimal performance when exposed repeatedly to conditioned (temperature and humidity) air.
- The cell model should respond to an exposure.

This study started with four different human bronchial epithelial cell lines: 16HBE, Calu-3, H292, and BEAS-2B. These are all widely used for toxicity testing of nanomaterials and chemicals. Of the four cell lines, only the Calu-3 cells fulfilled all the above requirements. The cells formed a monolayer with tight junctions (**Figure 3**) that remained a stable barrier over time as measured by TEER, whereas the other cell lines either did not form a barrier or showed a drop-in barrier function when cultured at the ALI (**Figure 4**). In addition, H292 and BEAS-2B tended to overgrow into multiple cell layers when cultured for a longer time period. Traditional submerged cell culturing and ALI culturing differed greatly, because at the ALI nutrients were only available from the basolateral side and the cells were exposed to dry conditions at the apical side. These conditions can cause stress to the cell models, which could be

observed by measuring the cell viability over time. Cell lines 16HBE, H292, and BEAS-2B all showed an increased LDH release when cultured at the ALI, while Calu-3 cells showed only a slight LDH release (**Figure 5**).

Next, the response of the Calu-3 model to substances was tested. As a positive control substance, LPS was administered via nebulization to the apical side of the model. The deposited dose was 0.25 µg/cm<sup>2</sup>. The Calu-3 cells showed a reaction to lipopolysaccharide (LPS) by an increase in LDH release and in tumor necrosis factor alpha (TNF-α) release (**Figure 6**).

Finally, the Calu-3 monolayer was exposed to quartz silica (DQ12) nanomaterials (IOM, Edinburgh). Crystalline silica can induce silicosis and may also cause lung tumors. Therefore, the International Agency for Research on Cancer (IARC) has classified crystalline silica as a Group I human carcinogen<sup>20</sup>. The mechanism of action of crystalline silica is thought to be via the induction of persistent inflammation caused by its reactive surface<sup>21,22,23</sup>. Several *in vivo* studies in both rats and mice report the induction of inflammation and histopathology changes, including tumors and fibrosis, after inhalation exposure to crystalline silica<sup>24,25,26,27,28,29</sup>. These effects are all observed after repeated exposure and/or long-term follow-up. The Calu-3 model was used to investigate whether the observations from the *in vivo* studies could be mimicked using an *in vitro* model that could be exposed repeatedly at the ALI. Calu-3 cells were exposed for 3 consecutive weeks, 5 days per week, 4 h per day to DQ12. The deposited dose was measured using a QCM. The average deposited dose was 120 ng/cm<sup>2</sup> per day, with a cumulative dose of 1.6 µg/cm<sup>2</sup>, similar to the doses inducing an effect *in vivo*.

Other particle characteristics are shown in Table 1. After 3 weeks of exposure, DQ12 induced no significant effects in TEER, cell viability, and monocyte chemoattractant protein 1 (MCP-1) release, compared to the clean air controls (**Figure 7**). As more toxicity of DQ12 was expected based on the *in vivo* data, the reactivity of the particles was checked using an acellular assay according to the protocol optimized within the EU-project GRACIOUS (deliverable 5.3). The reactivity of the DQ12 batch was lower than expected (**Figure 8**), orders of magnitudes lower compared to the positive control particles carbon black (CB). This lack of reactivity might explain the absence of a toxicity response in the Calu-3 model.

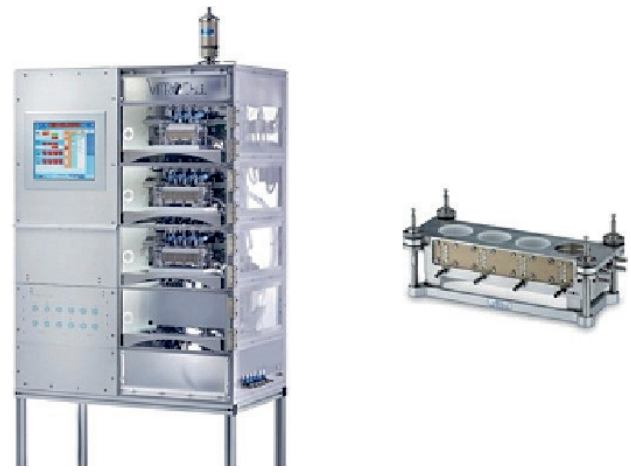


**Figure 1:** The automated exposure station (AES). The left figure shows the outside of the cabinet with the touch panel. The AES has three levels with exposure modules: the top level for clean air exposures, and the middle and bottom level for aerosol exposures. The right figure shows the exposure module in which inserts with cells are placed.

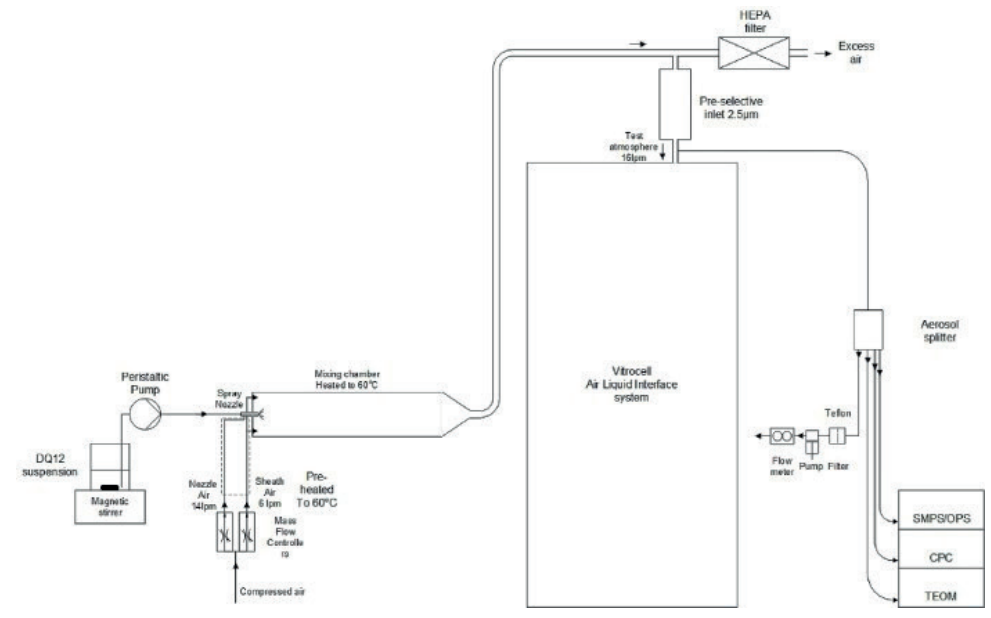


**Figure 2:** Schematic representation of the exposure setup. From left to right: 1) the ENM suspension connected to the spray nozzle via a peristaltic pump; 2) Using compressed air the spray nozzle nebulizes the ENM suspension and via a mixing chamber the aerosols are led to the AES; 3) Just before entering the AES, aerosol characterization instruments are connected: SMPS, OPS, CPC, and TEOM.

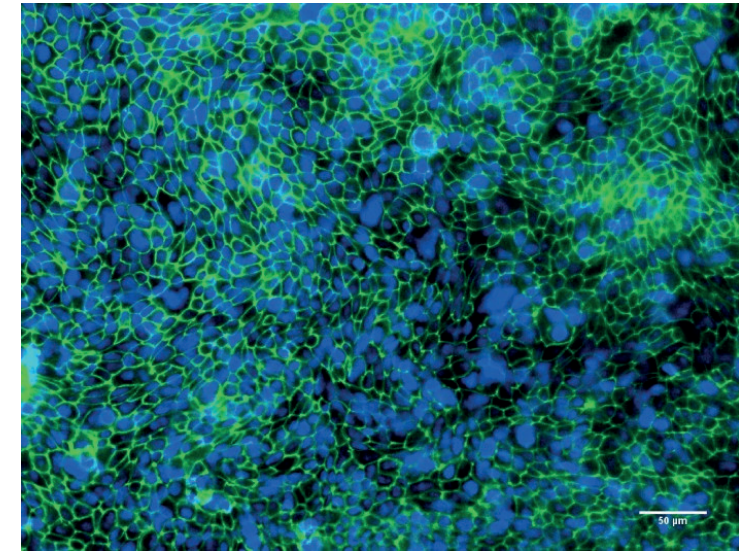


**Figure 3:** Representative image of Calu-3 cells after culturing at the air-liquid interface (ALI) for 10 days. Fluorescence microscopy image of Calu-3 cells after culturing at the ALI for 10 days. Tight junction protein ZO-1 is stained in green, nuclei of the cells are stained in blue.

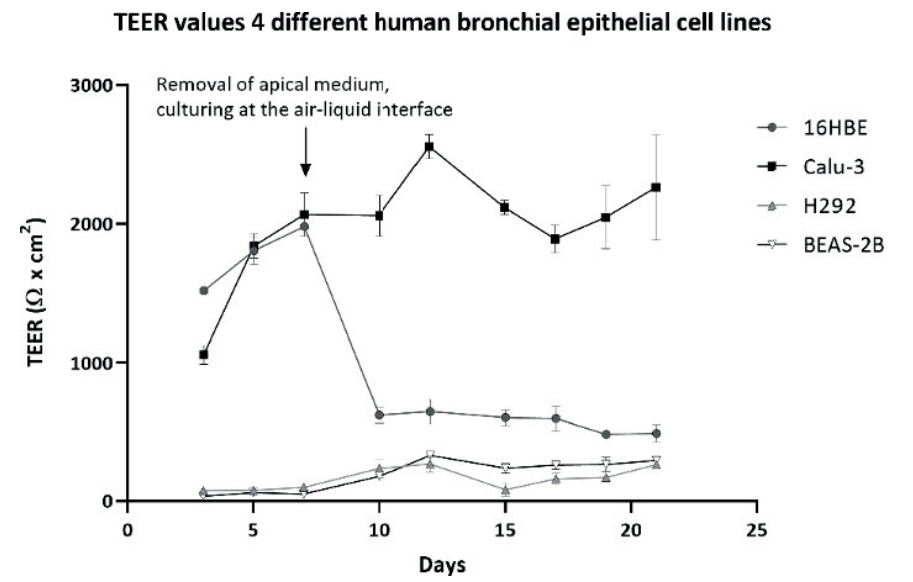


**Figure 4:** Transepithelial electrical resistance (TEER) of four different cell lines during a culture period of 21 days. TEER values of 16HBE, Calu-3, H292, and BEAS-2B when cultured for 21 days: first 7 days submerged, followed by 14 days at the ALI. TEER values were corrected for the background resistance of the insert and multiplied by the surface area of the insert. The symbols and error bars represent the average value and standard deviation of six inserts.



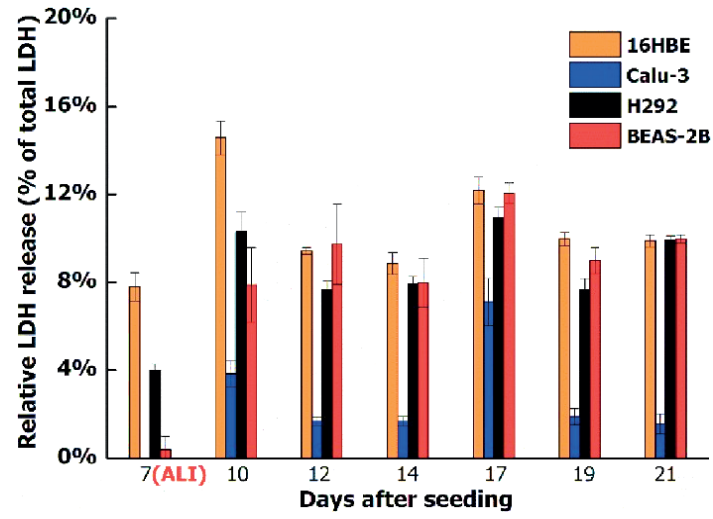


**Figure 5:** LDH release of four different cell lines during a culture period of 21 days. LDH release of 16HBE, Calu-3, H292, and BEAS-2B when cultured for 21 days: 7 days submerged, followed by 14 days at the ALI. LDH values shown are relative to the maximum LDH release per cell type. The symbols and error bars represent the average value and standard deviation of five inserts.

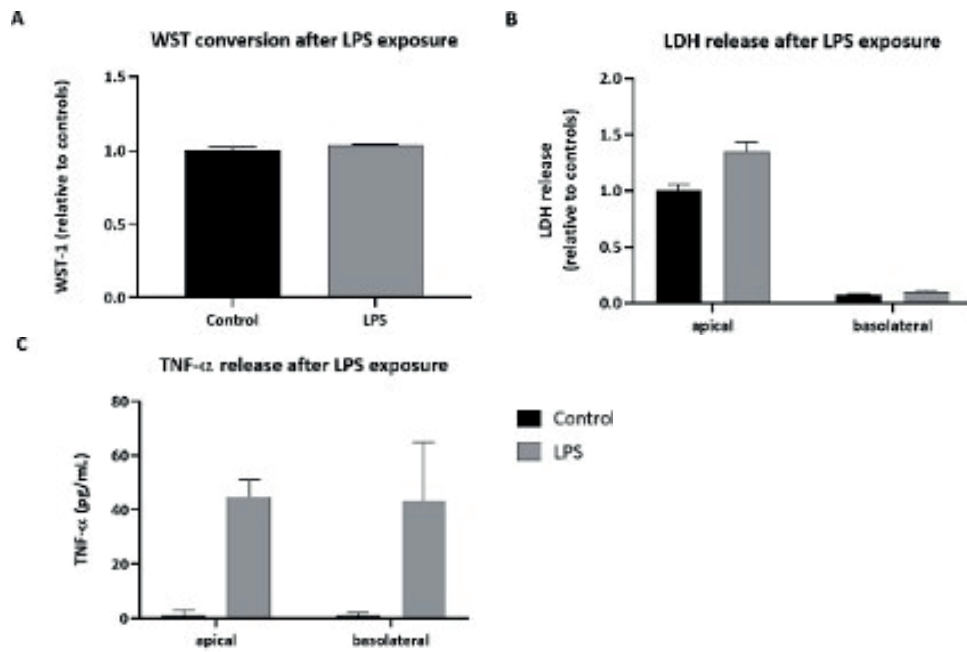


**Figure 6:** Cellular effects in Calu-3 cells exposed to LPS. Calu-3 cells were exposed via cloud nebulization to 0.25  $\mu\text{g}/\text{cm}^2$  LPS. (A) The WST-1 conversion. (B) LDH release. (C) TNF- $\alpha$  release after LPS exposure. The symbols and error bars represent average values and standard deviations of three inserts.

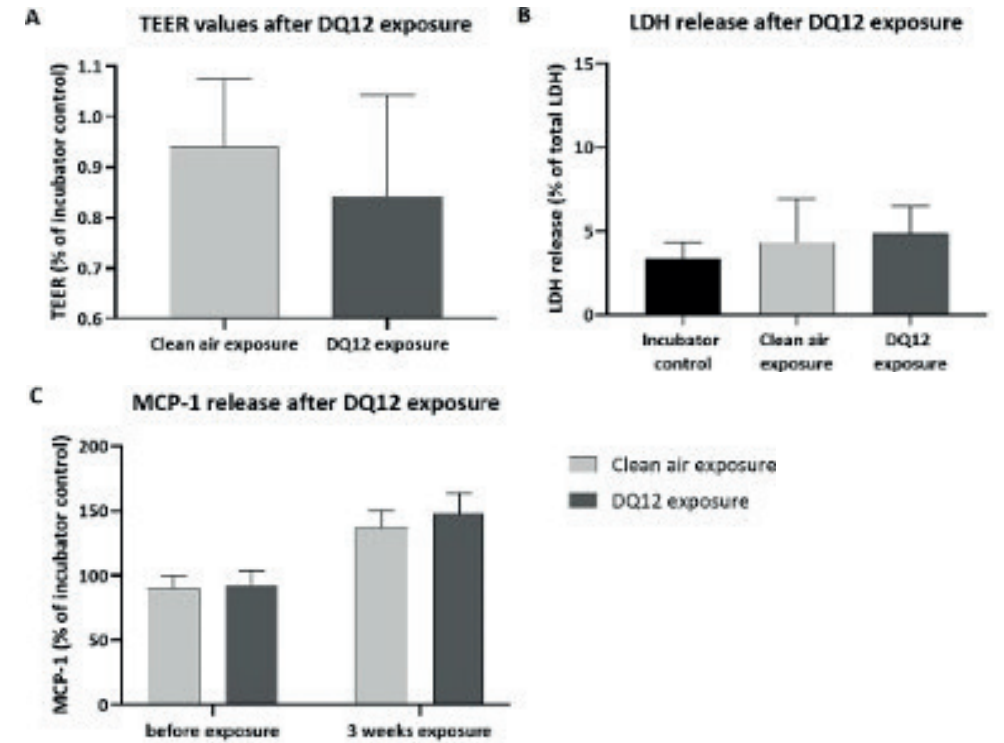


**Figure 7:** Cellular effects in Calu-3 cells exposed to DQ12 nanomaterials. Calu-3 cells were exposed for 3 weeks (4 h per day, 5 days per week) to DQ12 nanomaterials, about 120  $\text{ng}/\text{cm}^2$  per day, cumulative dose of 1.6  $\mu\text{g}/\text{cm}^2$ . (A) TEER values. (B) LDH release. (C) MCP-1 release after DQ12 exposure. All symbols and error bars represent average values and standard deviations of three inserts for the controls and six inserts for the DQ12 exposure

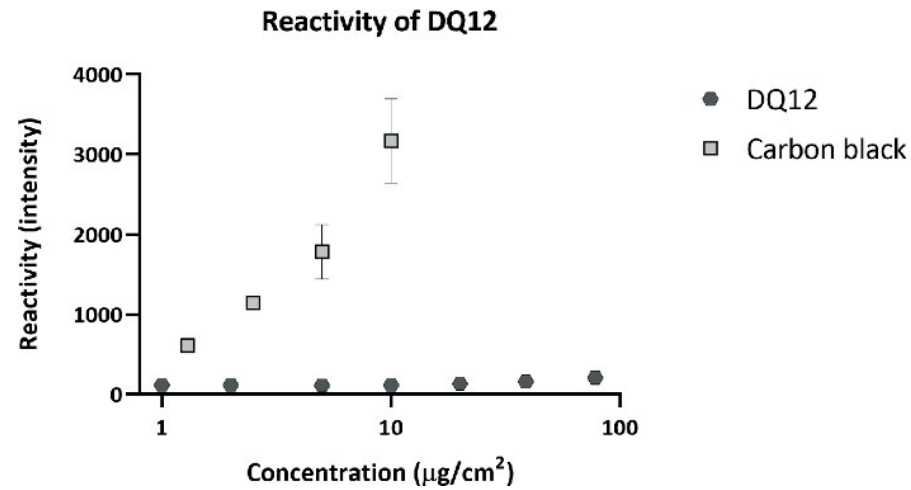


**Figure 8:** Acellular reactivity of DQ12. DQ12 was incubated with a 2',7'-Dichlorofluorescein Diacetate (DCFH-DA) probe to detect its surface reactivity. As a positive control, carbon black (CB) particles were included. Compared to CB, DQ12 has very low surface reactivity.

**Table 1:** DQ12 exposure characteristics. Values are shown as average with standard deviation in brackets.

Particle mass (µg/m³)	Particle number (#/cm³)	Mobility particle size (nm)	Geometric standard deviation	Optical particle size (µm)
2969 (418)	83983 (10215)	66.6	2.5	1.1 (1.3)

## Discussion

This paper describes a method for culturing human bronchial epithelial cells under ALI and exposing this bronchial model to aerosols or gases. The advantage of using Calu-3 cells is that they form tight junctions, remain a monolayer, are able to withstand the air flow, and can be cultured for weeks at the ALI, unlike many other cell types (e.g., 16HBE, H292, and BEAS-2B). Using the VITROCELL® automated exposure station (AES) has the advantage that the cells can be exposed under realistic and relevant conditions as low concentrations can be applied using a continuous airflow.

Continued flow systems, such as the AES, have advantages compared to using cloud systems<sup>3,30</sup>, which use a single nebulization of a suspension. The continuous flow is more realistic and many variables like flow rate, humidity, and temperature are

controlled. In addition, deposition can be enhanced using an electrical field. Finally, aerosol characteristics like size, number concentration, and mass are monitored online. A disadvantage is that continued flow systems are more complex compared to cloud systems. Therefore, it is important to run preparatory experiments that focus on the particle characteristics of the aerosol and the delivered dose on the insert. The initial starting concentration of the particles and the AES settings can then be adjusted to achieve the desired dose on the cells<sup>31</sup>. Depending on the type of particles being tested, the aerosol generation method can differ. The use of electrostatic deposition depends on the particle type and works best for metallic particles. For particles with a positive surface charge a negative electrostatic field should be applied and vice versa.

Selection of exposure concentrations can be difficult for any air-liquid exposure experiment. For the DQ12 exposures, the aim was to achieve a total cumulative dose of 1 µg/cm² after 3 weeks exposure, 5 days per week, 4 h per day. This dose is similar to doses that induced an effect *in vivo*<sup>21,25,27,30,31</sup>. When performing the exposures, there was some variation between different exposure days. Although the actual deposited dose of 1.6 µg/cm² is higher than the 1 µg/cm² that was aimed for, the dose might have been too low to observe effects in the Calu-3 model. Only minor differences in TEER, viability, and cytokine response were observed between the clean air exposure and the DQ12 exposure, and these differences were not statistically significant. An explanation for the observation that DQ12 exposure for 3 weeks did not induce significant effects in the Calu-3 cells is that macrophages were lacking from the Calu-3 model. Possibly, after DQ12 uptake macrophages produce proinflammatory cytokines that may affect Calu-3 cells. Another explanation is that the DQ12 batch that was used for the experiments was not as reactive as expected. When using LPS as a positive control substance, Calu-3 does show a response, as measured by an increase in LDH release and an increase in TNF-α release. This indicates that the model can detect toxicity.

The Calu-3 cell model has many advantages, as discussed in the results section. Moreover, when cultured for a longer time at the ALI, the Calu-3 cells can grow cilia/cilia-like structures<sup>13</sup> and produce mucus<sup>11,12,13</sup>. Despite these advantages, the model has limitations with respect to its physiological relevance. The Calu-3 cell lines originate from an adenocarcinoma, whereas 16HBE and BEAS-2B originate from healthy tissue. Unfortunately, the latter two are not suitable for repeated ALI exposure as they do not remain a stable monolayer over time. Another limitation of the Calu-3 model is that it only represents a single cell type. In the human lung, multiple cell types that interact and respond differently to exposure are present. Inhaled particles will deposit in different regions of the lungs depending on their aerodynamic size. This is where the particles contact the epithelial cell barrier, as mimicked by the Calu-3 model. In the human lung, alveolar macrophages are attracted to the particles,

engulf them, and clear them from the lungs. Macrophages also play an essential role in the inflammation response to particle exposure. Therefore, efforts are being made to extend the Calu-3 model by adding primary macrophages to mimic the lung barrier more closely. The disadvantage of the macrophages is that they remain viable only for about 7 days when cultured on top of Calu-3 cells at the ALI. Therefore, macrophages should be re-added weekly to transform the current Calu-3 model into a coculture model. The optimization of the coculture protocol is currently ongoing.

Given the above, the Calu-3 bronchial model is a suitable model for repeated exposure to aerosols of partly soluble substances such as chemicals from cigarette smoke and LPS. These soluble substances induce significant increases in cytokine responses in the Calu-3 cells. For testing insoluble particles such as diesel exhaust and DQ12, a coculture model is needed, because the macrophages play a crucial role in the induction of effects by particle exposure.

For the exposures described, insert membranes with 3.0 µm pores were used. The main reason for choosing this type of insert is that it is possible to test the translocation of nanomaterials. When using smaller 0.4 µm pore size, particle agglomerates will not be able to cross the insert membrane. The disadvantage of using a large pore size is that the cells need a longer time to grow confluent and that it is more difficult to visualize the morphology of the cells using light microscopy. To check that the cells do form a confluent monolayer, the TEER should be >1,000 Ω x cm<sup>2</sup> before starting an exposure.

Taken together, the Calu-3 bronchial model presented here is suitable to use for repeated exposure to aerosols, at least up to 3 weeks. The model can withstand being cultured and exposed via a continuous airflow and is capable to detect toxicity to the bronchial epithelium.

## Disclosures

The authors have nothing to disclose.

## Acknowledgments

This work is funded by EU-project PATROLS (Physiologically Anchored Tools for Realistic nanomaterial hazard assessment) and the Dutch Ministry of Health, Welfare and Sport (project V/050012). We would like to thank Dr. Yvonne Staal and Dr. Jan van Benthem for critically reviewing the manuscript.

## References

- Geiser, M., Jeannot, N., Fierz, M., Burtscher, H. Evaluating Adverse Effects of Inhaled Nanoparticles by Realistic *In Vitro* Technology. *Nanomaterials (Basel)*. 7 (2), E49 (2017).
- Herzog, F. et al. Mimicking exposures to acute and lifetime concentrations of inhaled silver nanoparticles by two different *in vitro* approaches. *The Beilstein Journal of Nanotechnology*. 5, 1357-1370 (2014).
- Lenz, A. G. et al. A dose-controlled system for air-liquid interface cell exposure and application to zinc oxide nanoparticles. *Particle and Fibre Toxicology*. 6, 32 (2009).
- Paur, H.R. et al. In-vitro cell exposure studies for the assessment of nanoparticle toxicity in the lung—A dialog between aerosol science and biology. *Journal of Aerosol Science*. 42 (10), 668-692 (2011).
- Lacroix, G. et al. Air-Liquid Interface *In Vitro* Models for Respiratory Toxicology Research: Consensus Workshop and Recommendations. *Applied in vitro Toxicology*. 4 (2), 91-106 (2018).
- Loret, T. et al. Air-liquid interface exposure to aerosols of poorly soluble nanomaterials induces different biological activation levels compared to exposure to suspensions. *Particle and Fibre Toxicology*. 13 (1), 58 (2016).
- Zhu, Y., Chidekel, A., Shaffer, T. H. Cultured human airway epithelial cells (calu-3): a model of human respiratory function, structure, and inflammatory responses. *Critical Care Research and Practice*. 2010 (2010).
- Braakhuis, H. M. et al. Progress and future of *in vitro* models to study translocation of nanoparticles. *Archives in Toxicology*. 89 (9), 1469-1495 (2015).
- Ren, H., Birch, N. P., Suresh, V. An Optimised Human Cell Culture Model for Alveolar Epithelial Transport. *PLoS One*. 11 (10), e0165225- e0165225 (2016).
- Srinivasan, B. et al. TEER measurement techniques for *in vitro* barrier model systems. *Journal of Laboratory Automation*. 20 (2), 107-126 (2015).
- Papazian, D., Wurtzen, P. A., Hansen, S. W. Polarized Airway Epithelial Models for Immunological Co-Culture Studies. *International Archives of Allergy and Immunology*. 170 (1), 1-21 (2016).
- Jeong, M. H. et al. *In vitro* model for predicting acute inhalation toxicity by using a Calu-3 epithelium cytotoxicity assay. *Journal of Pharmacological and Toxicological Methods*. 98, 106576 (2019).
- Grainger, C. I., Greenwell, L. L., Lockley, D. J., Martin, G. P., Forbes, B. Culture of Calu-3 cells at the air interface provides a representative model of the airway epithelial barrier. *Pharmacology Research*. 23 (7), 1482-1490 (2006).
- Harcourt, J. L., Caidi, H., Anderson, L. J., Haynes, L. M. Evaluation of the Calu-3 cell line as a model of *in vitro* respiratory syncytial virus infection. *Journal of Virological Methods*. 174 (1-2), 144-149 (2011).
- Vitrocell VITROCELL® Automated Exposure Station (2019). <<https://www.vitrocell.com/inhalation-toxicology/exposure-systems/automated-exposure-station1>>.
- Mülhopt, S. et al. Toxicity testing of combustion aerosols at the air-liquid interface with a self-contained and easy-to-use exposure system. *Journal of Aerosol Science*. 96, 38-55 (2016).
- Vitrocell. VITROCELL® Cloud for the exposure to liquid aerosols (2019). <<https://www.vitrocell.com/inhalation-toxicology/exposure-systems/vitrocell-cloudsystem>>.
- Endes, C. et al. An *in vitro* testing strategy towards mimicking the inhalation of high aspect ratio nanoparticles. *Particle and Fibre Toxicology*. 11 (1), 40 (2014).
- Lenz, A. G. et al. Efficient bioactive delivery of aerosolized drugs to human pulmonary epithelial cells cultured in air-liquid interface conditions. *Am J Respir Cell Mol Biol*. 51 (4), 526-535 (2014).
- Borm, P. J., Tran, L., Donaldson, K. The carcinogenic action of crystalline silica: a review of the evidence supporting secondary inflammation-driven genotoxicity as a principal mechanism. *Critical Reviews in Toxicology*. 41 (9), 756-770 (2011).
- Borm, P. J. A., Fowler, P., Kirkland, D. An updated review of the genotoxicity of respirable crystalline silica. *Particle and Fibre Toxicology*. 15 (1), 23 (2018).
- Kawasaki, H. A mechanistic review of silica-induced inhalation toxicity. *Inhalation Toxicology*. 27 (8), 363-377 (2015).
- Sayes, C. M. et al. Changing the dose metric for inhalation toxicity studies: short-term study in rats with engineered aerosolized amorphous silica nanoparticles. *Inhalation Toxicology*. 22 (4), 348-354 (2010).

24. Driscoll, K. E. et al. Pulmonary response to inhaled silica or titanium dioxide. *Toxicology and Applied Pharmacology*. 111 (2), 201-210 (1991).
25. Muhle, H., Kittel, B., Ernst, H., Mohr, U., Mermelstein, R. Neoplastic lung lesions in rat after chronic exposure to crystalline silica. *Scandinavian Journal of Work, Environment and Health*. 21 (Suppl 2) 27-29 (1995).
26. Peeters, P. M. et al. Silica-induced NLRP3 inflammasome activation *in vitro* and in rat lungs. *Particle and Fibre Toxicology*. 11, 58 (2014).
27. Reuzel, P. G., Bruijntjes, J. P., Feron, V. J., Woutersen, R. A. Subchronic inhalation toxicity of amorphous silicas and quartz dust in rats. *Food and Chemical Toxicology*. 29 (5), 341-354 (1991).
28. Arts, J. H., Muijser, H., Duistermaat, E., Junker, K., Kuper, C. F. Five-day inhalation toxicity study of three types of synthetic amorphous silicas in Wistar rats and post-exposure evaluations for up to 3 months. *Food and Chemical Toxicology*. 45 (10), 1856-1867 (2007).
29. Mülhopt, S., Diabate, S., Krebs, T., Weiss, C., Paur, H. R. Lung toxicity determination by *in vitro* exposure at the air liquid interface with an integrated online dose measurement. *Journal of Physics: Conference Series*. 170, 012008 (2009).
30. van Ravenzwaay, B. et al. Comparing fate and effects of three particles of different surface properties: nano-TiO<sub>2</sub>, pigmentary TiO<sub>2</sub> and quartz. *Toxicology Letters*. 186 (3), 152-159 (2009).
31. Henderson, R. F. et al. A comparison of the inflammatory response of the lung to inhaled versus instilled particles in F344 rats. *Fundamental and Applied Toxicology*. 24 (2), 183-197 (1995).

# Chapter 3

## Part II

### **Optimization of an air-liquid interface *in vitro* cell co-culture model to estimate the hazard of aerosol exposures**

Rui-Wen He <sup>a,b</sup>, Hedwig M. Braakhuis <sup>a</sup>, Rob J. Vandebriel <sup>a</sup>, Yvonne C. M. Staal <sup>a</sup>, Eric R. Gremmer <sup>a</sup>, Paul H.B. Fokkens <sup>a</sup>, Claudia Kemp <sup>a</sup>, Jolanda Vermeulen <sup>a</sup>, Remco H. S. Westerink <sup>b</sup>, Flemming R. Cassee <sup>ab\*</sup>

<sup>a</sup> National Institute for Public Health and the Environment (RIVM), P.O. Box 1, 3720 BA, Bilthoven, The Netherlands

<sup>b</sup> Institute for Risk Assessment Sciences, Utrecht University, P.O. Box 80178, 3508 TD, Utrecht, The Netherlands

(Journal of Aerosol Science, 2021, Volume 153, 105703, ISSN 0021-8502)



## Highlights

Calu-3+MDM model shows the epithelial monolayer integrity under prolonged ALI culture.

Calu-3+MDM model has an increased sensitivity in inflammatory responses to LPS aerosol.

Combination of Calu-3+MDM model is a preferred option for long-term ALI exposure to inhaled aerosols.

## Abstract

Inhalation exposure to environmental and occupational aerosol contaminants is associated with many respiratory health problems. To realistically mimic long-term inhalation exposure for toxicity testing, lung epithelial cells need to be maintained and exposed under air-liquid interface (ALI) conditions for a prolonged period of time. In addition, to study cellular responses to aerosol particles, lung epithelial cells have to be co-cultured with macrophages. To that aim, we evaluated human bronchial epithelial Calu-3, 16HBE140- (16HBE), H292, and BEAS-2B cell lines with respect to epithelial morphology, barrier function and cell viability under prolonged ALI culture conditions. Only the Calu-3 cells can retain the monolayer structure and maintain a strong tight junction under long-term ALI culture at least up to 2 weeks. As such, Calu-3 cells were applied as the structural barrier to create co-culture models with human monocyte-derived macrophages (MDMs) and THP-1 derived macrophages (TDMs). Adhesion of macrophages onto the epithelial monolayer was allowed for 4 hrs with a density of  $5 \times 10^4$  macrophages/cm<sup>2</sup>. In comparison to the Calu-3 mono-culture model, Calu-3 + TDM and Calu-3 + MDM co-culture models showed an increased sensitivity in inflammatory responses to lipopolysaccharide (LPS) aerosol at Day 1 of co-culture, with the Calu-3 + MDM model giving a stronger response than Calu-3 + TDM. Therefore, the epithelial monolayer integrity and increased sensitivity make the Calu-3 + MDM co-culture model a preferred option for ALI exposure to inhaled aerosols for toxicity testing.

**Keywords:** Aerosol exposures; Co-culture; Epithelial cells; Macrophages; Air-liquid interface; Barrier function;

1.

## 1. Introduction

Humans constantly inhale various exogenous substances such as nanoparticles, traffic emissions, and cigarette smoking aerosols (Almstrand et al. 2009; Phillips et al. 1999). Inhalation exposure to environmental and occupational aerosol contaminants is related to a wide range of public health problems such as chronic respiratory diseases and airway dysfunction (Bakand et al. 2012; Samet and Krewski 2007). These effects on respiratory health can be studied using *in vivo* and *in vitro* methods. Due to limitations of *in vivo* experiments including ethical issues, inter-species differences and operational difficulties, *in vitro* models have increasingly been applied for hazard assessment of aerosol exposures (BéruBé et al. 2010; Braakhuis et al. 2016). The commonly used *in vitro* approach involves dissolving the aerosols of interest in culture medium to expose lung cells under submerged conditions. However, submerged exposure conditions do not adequately resemble the *in vivo* situation, as under realistic conditions a gradual delivery and deposition from the air onto the respiratory tract lining the epithelium will occur (Berube et al. 2009). Besides, characteristics and kinetics of the test substances will likely change during submerged exposure. Therefore, the relevance of biological responses observed following submerged exposure has been debated (Limbach et al. 2005; Mühlhopt et al. 2016).

To minimize these limitations, air-liquid interface (ALI) exposure of cells has been developed. ALI exposure of cells is applied by the exposure systems, which use a continuous flow or single cloud to expose cells to aerosols containing test substances, enabling a more relevant and realistic inhalation exposure (BéruBé et al. 2010; Mühlhopt et al. 2016). A single layer of epithelial cells covers the surface of bronchioles, the first target of exposure to inhaled substances (BéruBé et al. 2010; Hiemstra et al. 2018). Consequently, the corresponding characteristics of epithelium such as single-layer morphology and barrier functions are regarded as essential criteria for cell selection at the ALI (Hermans and Bernard 1999). For ALI conditions, cells are cultured on the apical side of membrane fitted in an insert, which is exposed to air to simulate human airway conditions (de Jong et al. 1994; Paur et al. 2011). Culture medium is added to the basolateral side of the insert to be in contact with cells for nutrient supply via the membrane. Such an approach requires careful selection of the appropriate cell types/lines, since not that many cell types can be cultured under ALI conditions and still remain viable for a sufficiently long period of time. While current epithelial cell models have been evaluated for their suitability for culture under ALI conditions for only a few days (Heijink et al. 2010), there is an increasing need to expose these cell models for multiple days to resemble repeated and even long-term exposure to inhaled aerosols (PATROLS-Website 2018).

Macrophages, the most abundant immune-cell type present in healthy lungs, play an important role in the clearance of foreign substance and apoptotic cells (Hu and Christman 2019; Septiadi et al. 2018). To mimic the lung epithelium more closely, co-culture models have been designed by adding macrophages on the top of the epithelial cell layer (Ji et al. 2018; Lehmann et al. 2011). These macrophages are intended to produce inflammatory responses that can affect epithelial cells, probably increasing the sensitivity of co-culture models to inhaled aerosol particles in comparison to mono-culture models (Tao and Kobzik 2002; Wottrich et al. 2004). Due to easy handling and high reproducibility, macrophages differentiated from THP-1 human monocytes (THP-1 derived macrophages, TDMs) were mostly used in co-cultures (Chanput et al. 2014), whereas human monocyte-derived macrophages (MDMs) can provide more realistic cellular responses (Lehmann et al. 2011). However, information on the number of days that MDMs and TDMs are viable is currently lacking and it is unknown if they retain their functions in co-culture models.

We therefore evaluated widely-used epithelial cell models including 16HBE140-(16HBE), Calu-3, H292 and BEAS-2B cells under prolonged ALI culture conditions in terms of their epithelial morphology, barrier function and cell viability. In addition, MDMs and TDMs were used to create co-culture models and to evaluate the number of days that they remained viable as well as their functional responses to LPS aerosol.

## 2. Materials and methods

### 2.1 Cell cultures

16HBE, Calu-3, H292 and BEAS-2B cells are widely used as lung epithelial cell models in submerged and ALI culture (see the supplementary information for additional details). 16HBE cells were kindly provided by Dr. Gruenert (University of California, San Francisco, CA). Calu-3, H292 and BEAS-2B cells were purchased from the American Tissue Culture Collection (ATCC, Rockville, MD). 16HBE cells (passage 12-18) were cultured in Dulbecco's Modified Eagle Medium (DMEM) /F-12 supplemented with 1% L-Glutamine, 1% Fungizone, 5% Fetal Bovine Serum (FBS), and 1% Penicillin-Streptomycin (P-S); Calu-3 cells (passage 05-12) were cultured in minimum essential medium (MEM) with 10% FBS, 1% Non-Essential Amino Acid (NEAA) solution and 1% P-S; H292 cells (passage 05-09) were cultured in RPMI-1640 medium with 10% FBS, 1% P-S and 1% sodium pyruvate; BEAS-2B cells (passage 05-09) were cultured in DMEM medium with 10% FBS and 1% P-S.

THP-1 monocyte-like cells (ATCC, Rockville, MD) and primary human CD14<sup>+</sup> monocytes isolated from buffy coats (Sanquin, Amsterdam, the Netherlands) were differentiated to macrophages. THP-1 cells (passage 08-13) were differentiated to TDMs by addition of phorbol 12-myristate 13-acetate (PMA, 30 ng/mL, Sigma, the Netherlands) for 5 days, followed by culturing with fresh medium for two more days. Primary human CD14<sup>+</sup> monocytes were differentiated to MDMs by addition of macrophage colony-stimulating factor (M-CSF, 50 ng/mL, Sigma, the Netherlands) for 6 days (Lehmann et al. 2011). Monocytes and macrophages were cultured in RPMI-1640 medium with 10% FBS and 1% P-S. To avoid the variation between donors, the isolated primary human CD14<sup>+</sup> monocytes were frozen in separate tubes until use to ensure MDMs used in this study were from the same donor. Cells were cultured in the flask in an incubator at 37°C with 5% CO<sub>2</sub>. All culture medium and supplements were purchased from Life Technologies (Thermo Fisher Scientific Inc., the Netherlands).

### 2.2 Preparation of air-liquid interface (ALI) culture

A schematic overview on the cell seeding and exposure is shown in **Figure 1**. When reaching approximately 80% confluency in the cell culture flask, 16HBE, Calu-3, H292, and BEAS-2B cells were detached enzymatically (0.05% trypsin-EDTA, Thermo Fisher Scientific Inc., the Netherlands) and subsequently seeded on the apical side of inserts (0.4 μm pore membrane, Polyester, Corning Inc., Germany) fitted in a 6- or 12- wells plate with respectively 1 or 0.5 mL corresponding culture medium on the apical side and 2 or 1.5 mL culture medium was added into the basolateral side. The submerged culture period to reach confluence was set at 7 days. H292 and BEAS-2B cells grow much faster in submerged conditions compared to 16HBE and Calu-3 cells. To prevent overgrowing before ALI culture, seeding densities were set at  $1.0 \times 10^5$  cells/cm<sup>2</sup> for 16HBE and Calu-3 cells, and  $2.0 \times 10^4$  cells/cm<sup>2</sup> for H292 and BEAS-2B cells. After submerged culture for 7 days, apical medium was removed from the inserts to obtain the ALI conditions. Morphology of the epithelial cell models in the inserts was monitored over time via an optical microscope (OM) (CKX41 Inverted Microscope, Olympus, Waltham, USA) with a 4-time objective lens.

To create co-culture models, macrophages were added onto the epithelial cell layer at the fourth day of ALI culture, which was set as day 0 (Do) for co-culture. MDMs were gently scraped from the flask with cell dissociation buffer (Thermo Fisher Scientific Inc., the Netherlands), while TDMs were detached enzymatically with Accutase (Thermo Fisher Scientific Inc., the Netherlands) due to their low cell viability after scraping. After re-suspension, 1 or 0.5 mL of macrophage suspension ( $2.0 \times 10^4$  or  $5 \times 10^4$  macrophages/cm<sup>2</sup>, some with labelling as described in 2.5) was added onto the epithelial cell layer in 6- or 12 -wells inserts to allow the adhesion of macrophages. In our pilot experiments we used a minimum of 2 hrs for macrophages adhesion.

However, microscopic observation showed that the majority of the cells was not able to adhere to the epithelial carpet within 2 hrs of adhesion. We therefore increased the adhesion time from 2 hrs to 4 hrs. To evaluate the influence of re-added apical medium on the morphology of the cell models and the adhesion efficiency of the macrophages, we prolonged the adhesion time to 24 hrs. From a practical point of view, we did not select an adhesion time between 4 and 24 hrs, as it will make the removal of apical medium as well as the following ALI exposure less convenient. The Calu-3 mono-culture model was also treated using same protocol, but adding 1 or 0.5 mL of culture medium. Mono- and co-culture models in 6-well inserts were evaluated over the co-culture time while in 12-well inserts the cells were exposed to LPS aerosol at D1 of the co-culture.

For all cell models in inserts, apical and basolateral medium was refreshed every 2-3 days and collected separately. To collect the apical medium at the ALI for measuring LDH and cytokine release (see 2.7), 1 and 0.5 mL of corresponding medium was added to the apical side of 6- and 12 -wells inserts respectively, incubated for around 30 mins, and harvested.

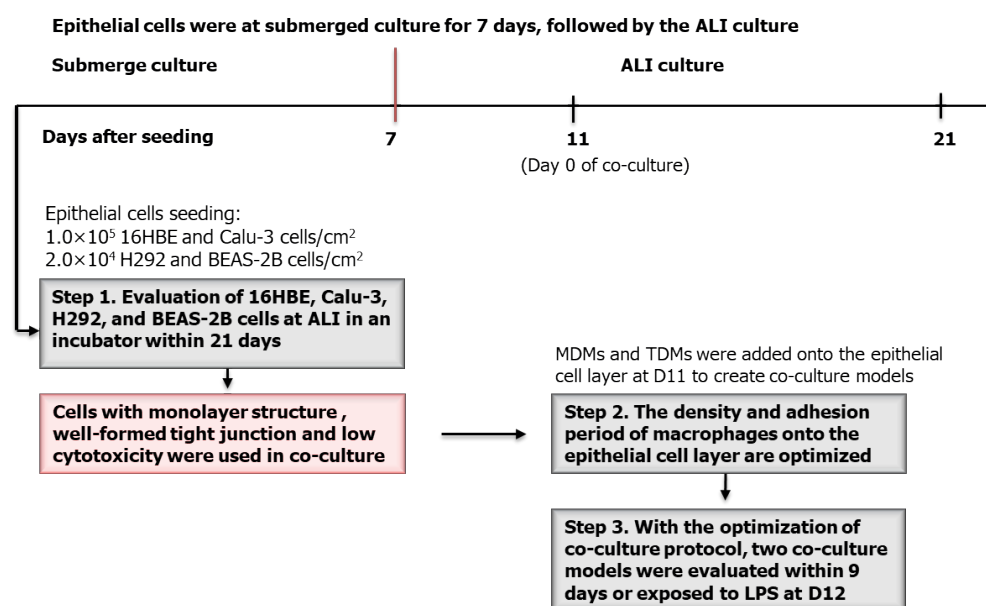


**Figure 1.** A schematic overview of the procedures including cell seeding, creating co-culture models and LPS exposure for the mono-culture and macrophage/epithelial cell co-culture models. Epithelial cells were at submerged culture for 7 days, followed by ALI culture.

### 2.3 Lipopolysaccharide (LPS) aerosol exposure

LPS (Thermo Fisher Scientific Inc., the Netherlands) as a positive control substance was sprayed onto the apical side of mono- and co-culture models in 12 well inserts via the VITROCELL® cloud exposure system (**Figure S1**, Vitrocell, Waldkirch, Germany) at D1 of the co-culture. The injection volume of LPS solution (175 µg/mL) for nebulization was 200 µL and the deposited dose in each insert was 0.25 µg/cm<sup>2</sup> as measured using a microbalance. The LPS exposure in the Cloud exposure system takes about 15 minutes. 3-4 inserts were used for LPS exposure in Calu-3 mono-culture, Calu-3 + MDM, and Calu-3 + TDM models; Due to the similar cellular responses between air control and incubator control (**Figure S7**) (He et al 2020), we chose to place 3 inserts under ALI conditions in an incubator as control. Apical and basolateral medium were collected separately (described in 2.2) after exposure for 24 hrs.

### 2.4 Transepithelial electrical resistance (TEER) measurement

As an important indicator of barrier integrity, transepithelial electrical resistance (TEER) was measured using an Evom2 Voltohmmeter equipped with 4 mm chopstick electrodes (World Precision Instruments Inc., FL, USA). To measure TEER at the ALI, 1 mL of corresponding medium was added onto the apical side of a 6-well insert. All TEER values were corrected for the resistance of cell-free insert ( $\approx 130$  ohm) and the surface area of a 6-well insert (4.67 cm<sup>2</sup>).

### 2.5 Zonula Occludens protein-1 (ZO-1) staining

Tight junctions play a crucial role in epithelial barrier function, therefore cultures were stained for the tight-junction protein ZO-1 in two ways, depending on the microscope used and research aim. To visualize tight junctions and the monolayer structure of epithelial cells, method 1 was used with confocal laser scanning fluorescence microscopy (CLSM); to visualize the epithelial cell layer in Calu-3 mono-culture and co-culture models, method 2 was used with fluorescence microscopy (FM). Cells were washed 3 times with phosphate buffered saline (PBS) and fixed in 4% paraformaldehyde (Thermo Fisher Scientific Inc., the Netherlands) for 5 mins, then permeabilized with 0.1% Triton X-100 (Thermo Fisher Scientific Inc., the Netherlands) for 15 mins.

Method 1: cells were incubated with the ZO-1 rabbit polyclonal antibody (Thermo Fisher Scientific, Switzerland, 1:100 in 0.1% bovine serum albumin (BSA) in PBS) for 2 hrs, followed by another 2 hrs incubation with a mixture of secondary antibodies in 0.1% BSA in PBS: goat anti-rabbit immunoglobulin G (IgG) DyLight 488 conjugated (Agrisera, Sweden, 1:100 dilution), rhodamine-phalloidin (Thermo Fisher Scientific, Switzerland, 1:100 dilution) and 1 µg/mL 4' 6-diamidino-2-phenylindole (DAPI) (Sigma Aldrich, Switzerland). All the staining steps were performed in the dark at room

temperature. After staining, the cells were washed with PBS, and mounted in glycergel (DAKO Schweiz AG, Switzerland) in microscopy slides, subsequently visualized via CLSM (Carl Zeiss, Switzerland) equipped with a 40-times objective lens.

Method 2: cells were incubated with the ZO1-1A12 monoclonal antibody (Thermo Fisher Scientific Inc., the Netherlands, 1:500 in 0.2% Triton X-100) for 30 mins, followed by another 30 mins incubation in the dark with a secondary antibody, fluorescein FITC anti-mouse IgG (Thermo Fisher Scientific Inc., the Netherlands, 1:100 in PBS). Cell nuclei were counter-stained afterwards by 1 µg/mL DAPI (Thermo Fisher Scientific Inc., the Netherlands) in PBS for 7 mins. In between all steps, cells were washed 2 or 3 times with PBS. Culture inserts were carefully mounted on a microscope slide with a glycerol-based liquid (Thermo Fisher Scientific Inc., the Netherlands) and examined via FM (Olympus BX51, Shinjuku, Japan) with a 10-time objective lens.

## 2.6 Macrophages morphology

Before adding onto the epithelial carpet, the morphology of MDMs and TDMs was assessed via the May Grünwald Giemsa stain. Briefly, macrophages were stained with May-Grünwald solution (Merck, Germany) for 5 mins on slides. After rinsing with Milli-Q water, macrophages were subsequently stained with 0.8 % (V/V) Giemsa solution in Sorensen's phosphate buffer (Thermo Fisher Scientific Inc., the Netherlands) for 20 mins. Afterwards, slides were rinsed thoroughly with Milli-Q water and air dried, which were then assessed with an OM (Leitz Laborlux D, Leica, Germany) at a 50-time objective lens.

To visualize macrophages in the co-culture models, macrophages were pre-labelled with Vybrant DiI dye (Thermo Fisher Scientific Inc., the Netherlands) according to Septiadi et al. (2018). After detachment from the flask, macrophages ( $10^5$  macrophages/mL < density <  $10^7$  macrophages /mL) were incubated in the dye-containing medium (dye : medium=1:200, v/v) for approximately 25 mins, followed by washing 3 times with culture medium. By counting cells under the OM and FM, the dye labelling efficiency of macrophages was calculated:

$$\text{Dye labeling efficiency (\%)} = \frac{\text{Macrophages number under FM}}{\text{Macrophages number under OM}} \times 100\%$$

As described in 2.2, the labelled macrophages were added onto the epithelial cell layer ( $2 \times 10^4$  macrophages/cm<sup>2</sup>). After adhesion of macrophages for 4 or 24 hrs, inserts were examined under the FM, with 4-6 images of macrophages being taken at random areas of the membrane. By counting the number of macrophages in each image, the efficiency of macrophages adhesion can be calculated as follows:

$$\text{Adhesion efficiency (\%)} = \frac{\text{Macrophages number in image} \times \frac{4.67}{0.0059}}{\text{Total adding number} \times \text{Dye labeling efficiency}} \times 100\%$$

in which the correction from image area (0.59 mm<sup>2</sup>) to surface area of the 6-well insert (4.67 cm<sup>2</sup>) is included.

## 2.7 Cell viability, LDH release and inflammatory cytokine release

The MTS assay was used to test the cell viability (Promega, Fitchburg, Wisconsin, USA). Briefly, cells on the apical side of the inserts were incubated with the MTS solution (medium: MTS reagent = 9: 1, v/v) for 60 mins before absorbance measurement by a microplate reader (SpectraMax M2: Molecular Devices, Sunnyvale CA, USA). Values of cell viability were corrected for the incubator controls.

To study cytotoxicity and cell membrane integrity, lactate dehydrogenase (LDH) release in the apical and basolateral medium was measured (Roche Diagnostics GmbH, Mannheim, Germany). Briefly, 100 µL of supernatant and 100 µL reaction reagent were successively added into a 96-well flat-bottomed plate and incubated in the dark for 20 minutes at room temperature. After adding 50 µL stop solution (HCl, 1.0 M, Sigma, Netherlands) per well, the absorbance was measured. All LDH values were corrected for the maximum LDH release per cell type or for the incubator controls. To measure the maximum LDH release, cells were incubated with lysis buffer (2% triton X-100, Thermo Fisher Scientific Inc., the Netherlands) for 5 mins. The lysate was collected for LDH measurement.

To test the inflammatory response, inflammatory cytokines (interleukin (IL)-1β, IL-8, IL-10 and tumor necrosis factor (TNF)-α) in the apical and basolateral medium were measured using an enzyme-linked immunosorbent assay (ELISA) (Thermo Fisher Scientific Inc., the Netherlands) according to the manufacturer's protocol.

## 2.8 Statistical analysis

Results from mono-culture models were obtained from two independent experiments, with 3-6 parallel inserts/supernatants in each experiment; results from co-culturing with macrophages were obtained from one experiment, with 6-12 parallel inserts/supernatant. Results from LPS exposure were obtained from one experiment, with 3-4 parallel inserts. Error bars indicate standard deviation of the mean (SD). Differences between groups were compared by one-way analysis of variance (ANOVA), a p-value ≤ 0.05 is considered statistically significant. Data analysis was conducted using GraphPad software (version 8.2.1).



### 3. Results

#### 3.1 Mono-culture models at the ALI

TEER changes of 16HBE, Calu-3, H292 and BEAS-2B cells were followed and their morphology was assessed over the 21-day culture period, and tight junctions of 16 HBE cells (D10) and Calu-3 cells (D12) were visualized with ZO-1 staining method 1 (**Figure 2**). In line with previous studies (Chen et al. 2015; Srinivasan et al. 2015), we classified barrier function of respiratory epithelial cell models in 6-well insert as “tight” with TEER values higher than  $1000 \text{ ohm} \times \text{cm}^2$ , as “intermediate” with values between  $300\text{--}1000 \text{ ohm} \times \text{cm}^2$ , and as “leaky” with values below  $300 \text{ ohm} \times \text{cm}^2$ . During submerged culture, 16HBE and Calu-3 cells showed similar trends of increasing TEER values over time, reaching around  $2000 \text{ ohm} \times \text{cm}^2$  (**Figure 2A**). When changing to ALI conditions, TEER values for 16HBE cells dropped 69% to around  $550 \text{ ohm} \times \text{cm}^2$  with the functional network of tight junction ZO-1 protein (stained with method 1) incompletely defined (**Figure 2C**, XY direction), while values for Calu-3 cells fluctuated around  $2000 \text{ ohm} \times \text{cm}^2$  with well-defined ZO-1 proteins expression around the cell periphery (**Figure 2D**, XY direction). H292 and BEAS-2B cells showed low TEER values (around  $300 \text{ ohm} \times \text{cm}^2$ ) in both culture conditions during the whole culture period.

After submerged culture for 7 days, confluent cell monolayers were seen for all cell lines (**Figure S2A**). However, H292 and BEAS-2B cells appeared as multilayers within 3 days culture at the ALI (D10, **Figure 2B**), which became more obvious at D12 (**Figure S2B**). A small scale of multilayers was also observed in 16HBE cells at D10 (**Figure 2C**, Z-stack section), indicating the loss of monolayer character. Only Calu-3 cells kept their monolayer structure (**Figure 2D**, Z-stack section) during long-term ALI culture ( $\approx 2$  weeks) that can be seen up to 5 weeks (**Figure S2C**).

Relative LDH release (corrected for the maximum LDH release) in the apical and basolateral medium was measured every 2 or 3 days, and the total LDH release was also calculated by adding the relative LDH levels on both sides (**Figure 3**). Overall, total LDH levels showed a slight increase for all cell lines when changing submerged culture conditions to the ALI, followed by fluctuations around 13% for 16HBE and BEAS-2B cells, and around 9% for Calu-3 and H292 cells. Among these cell lines, Calu-3 cells showed the highest LDH release ( $\approx 7\%$ ) in the apical medium and the lowest LDH release ( $\approx 2\%$ ) in the basolateral medium.

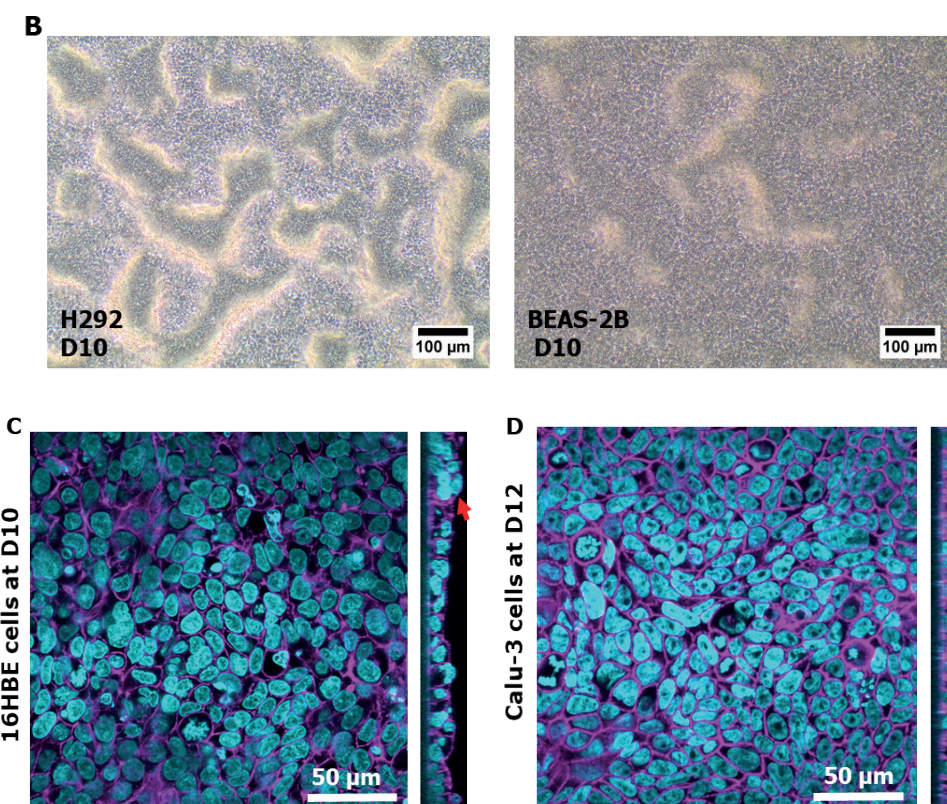
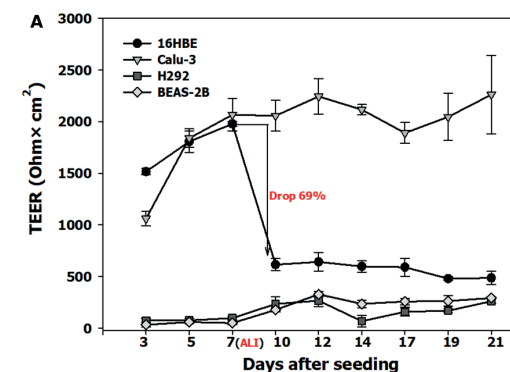


**Figure 2.** TEER (A) of 16HBE, Calu-3, H292 and BEAS-2B cells during the 21-day culture period, cells were at submerged culture for 7 days, followed by ALI culture; error bars indicate the standard deviation of 6 parallel inserts with cells. Cell morphology (B) of H292 and BEAS-2B cells at Day 10; Confocal fluorescence microscopy images of 16HBE cells at Day 10 (C) and Calu-3 cells at Day 12 (D); left: XY viewing direction; right: Z-stack section. Tight junction ZO-1 proteins (C and D) were stained in purple and the nuclei in turquoise. Multilayers in 16HBE cells at D10 (red arrow). Scale bars in B:  $100 \mu\text{m}$ ; in C and D:  $50 \mu\text{m}$ .



Due to the inability to develop a significant TEER, the occurrence of obvious multilayer structure and relatively higher LDH levels under ALI conditions, 16HBE, H292 and BEAS-2B cells were disregarded for additional experiments in this study, whereas Calu-3 culture model was used for subsequent co-cultures experiment.

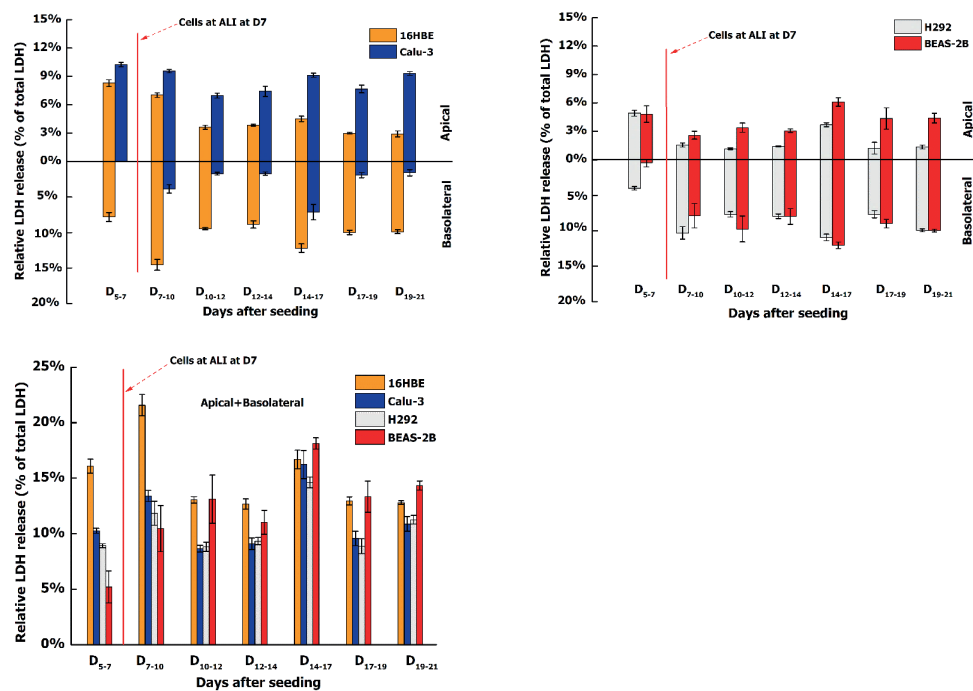


**Figure 3.** Relative LDH release on the apical (A) and basolateral (B) side of 16HBE, Calu-3, H292 and BEAS-2B cells as well as their total LDH levels (C) during the 21-day culture period. LDH release was measured during 2 or 3 days. The total LDH release was calculated by adding the relative LDH levels on both sides. Error bars indicate the standard deviation of 5 or 6 parallel inserts with cells.

### 3.2 Creating co-culture models

Before co-culture, MDMs and TDMs were stained in chamber slides to characterize morphology. As shown in **Figure S3**, the round and oval nuclei were peripherally and centrally located in macrophages, with the larger nuclei in TDMs. Some of MDMs and TDMs developed irregular cytoplasm and pseudopodia, suggesting differentiation of macrophages (Vordenbäumen et al. 2013).

After culturing with macrophages for 4 or 24 hrs (adhesion period), tight junctions of the epithelial cell layer were visualized (**Figure 4**, ZO-1 staining method 2, see 2.5). The strong ZO-1 expression around the cell periphery was observed in mono- and co-culture models, while cell fusions occurred as well, leading to the formation of some large cells with multiple nuclei or a single larger nucleus. Compared to 4 hrs, cell fusions appeared at a larger scale in mono- and co-culture models with 24 hrs adhesion period, resulting in the formation of multilayers of cells, in particular for the Calu-3+TDM model. The number of MDMs and TDMs on the epithelial cell layer as well as their adhesion efficiency were also related to the adhesion time periods (**Figure 5** and **Figure S4**). Overall, the larger number of adherent macrophages was seen in the co-culture models after 24 hrs adhesion, resulting in a higher adhesion efficiency ( $\approx 55\%$ ) of MDMs and TDMs in comparison to their efficiency after 4 hrs ( $\approx 20\%$ ).

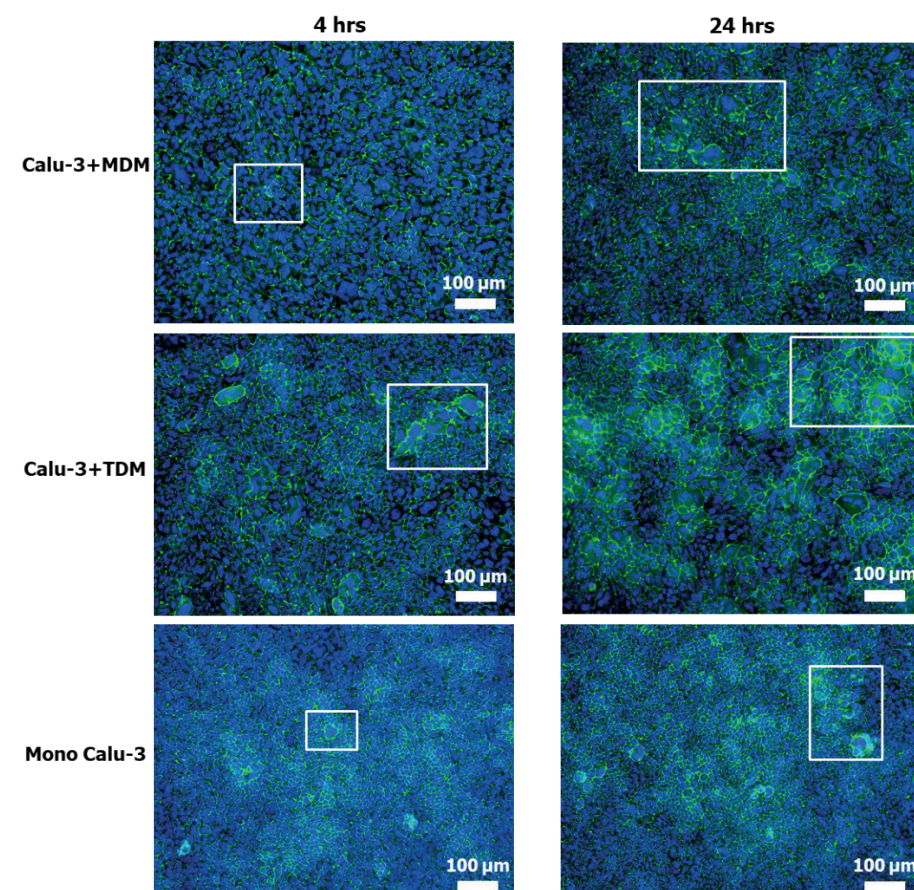


**Figure 4.** Fluorescence microscopy images of epithelial cell layer in mono-culture Calu-3 and co-culture models after 4 (left) and 24 hrs (right) adhesion period. The tight junction ZO-1 proteins were stained in green and nuclei in blue. White squares are examples of cell fusion. Scale bars: 100  $\mu\text{m}$ .

To avoid the large-scale formation of multilayers in the co-culture models, 4 hrs adhesion of macrophages was used for creating the co-culture models. In our pilot study no IL-1 $\beta$ , an inflammatory indicator for macrophages, was detected in the co-culture models in response to LPS aerosol when using a density of  $2.0 \times 10^4$  macrophages/cm<sup>2</sup>. Since the number of adherent macrophages can influence the sensitivity of co-culture models (Bodet et al. 2005), we increased the seeding density from  $2 \times 10^4$  to  $5 \times 10^4$  macrophages/cm<sup>2</sup> to enhance the sensitivity of the co-culture models. The adherence efficiency of MDMs and TDMs at a seeding density of  $5 \times 10^4$  macrophages/cm<sup>2</sup> after 4 hrs was  $17\% \pm 9\%$  and  $13\% \pm 7\%$ , respectively, which was rather similar with their efficiency at a seeding density of  $2 \times 10^4$  macrophages/cm<sup>2</sup>.

### 3.3 Co-culture models at the ALI

To determine the number of days that macrophages remained viable, morphology of MDMs and TDMs on the epithelial carpet was assessed during the 9-day co-culture period (Figure 6A and 6B). Overall, MDMs and TDMs showed similar morphological changes. At D1 and D3 of the co-culture, morphological differentiation was seen in MDMs and TDMs that formed aggregates and developed pseudopodia. During the 6 days co-culture, the numbers of macrophages as well as Calu-3 cells were similar at Day 1, 3, and 6 (Figure 6C and Table S1), suggesting that the ratio between Calu-3 cells and macrophages in our co-culture models remained stable ( $\approx 20$ ). However, increased apoptotic cell debris appeared after a longer period of the co-culture (D6 and D9) with a drop-in macrophage numbers at D9 (Figure 6C), indicating that more macrophages, particularly TDMs, had died after the long culture period at the ALI (> 6 days).

To evaluate the responses of co-culture models to ALI conditions, TEER changes and total IL-8 and IL-1 $\beta$  release in mono- and co-culture models after two time periods (D<sub>1-3</sub> and D<sub>3-6</sub>) were measured (Figure 6D and 6E). All cell models showed a comparable increase in TEER values from D<sub>0</sub> to D<sub>1</sub> that resulted in a level of around 1500 ohm $\times$ cm<sup>2</sup> (Figure 6D). IL-1 $\beta$  could not be detected in mono- and co-culture models after each time period (data not shown), while IL-8 could be detected in each cell model and showed no difference between D<sub>1-3</sub> and D<sub>3-6</sub> (Figure 6E). All cell models showed a comparable IL-8 level at D<sub>1-3</sub>, while a significant increase ( $p < 0.05$ ) was seen in the Calu-3+TDM model at D<sub>3-6</sub> in comparison to the mono-culture and Calu-3 + MDM models.

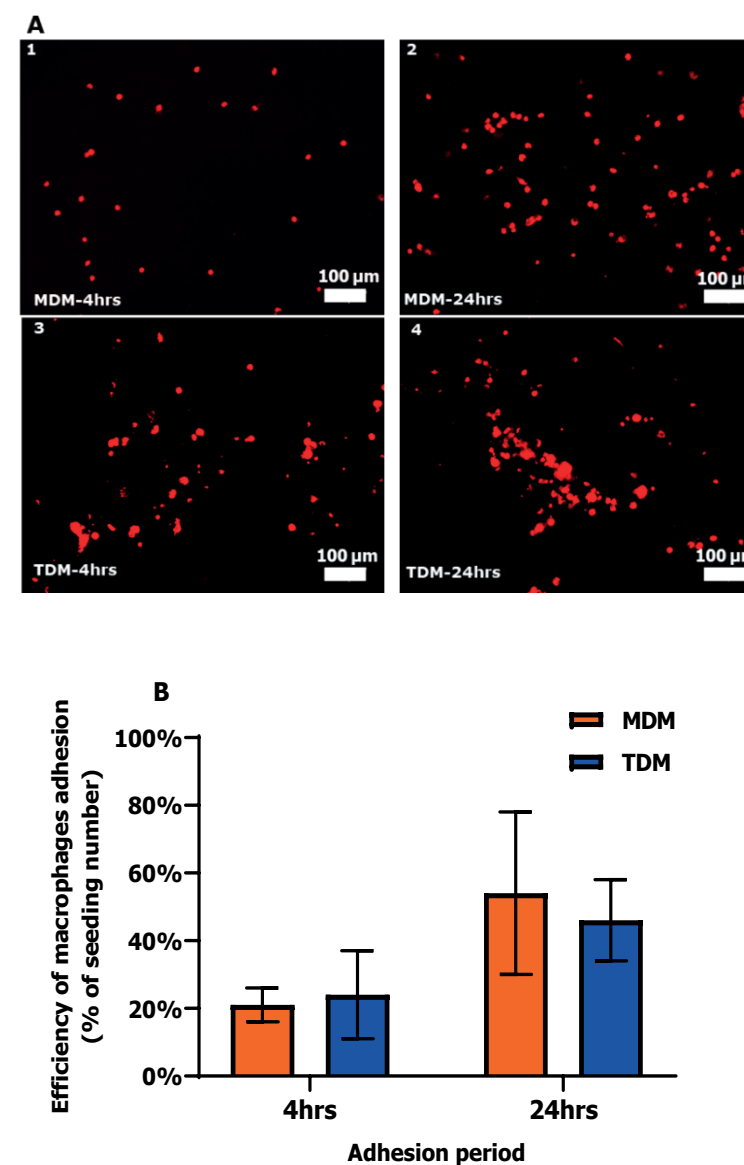


**Figure 5.** Fluorescence microscopy images (A) of MDMs and TDMs ( $2.0 \times 10^4$  cells/cm<sup>2</sup>) after 4 (left) and 24 hrs (right) adhesion onto the Calu-3 epithelial carpet and their adhesion efficiency (B). Macrophages were labelled with Vybrant DiI dye (in red, A). Scale bars in A: 100 μm. B: Error bars indicate the standard deviation of macrophages number in 4 or 6 random areas of the insert membrane. More images of MDMs and TDMs in Figure S4.

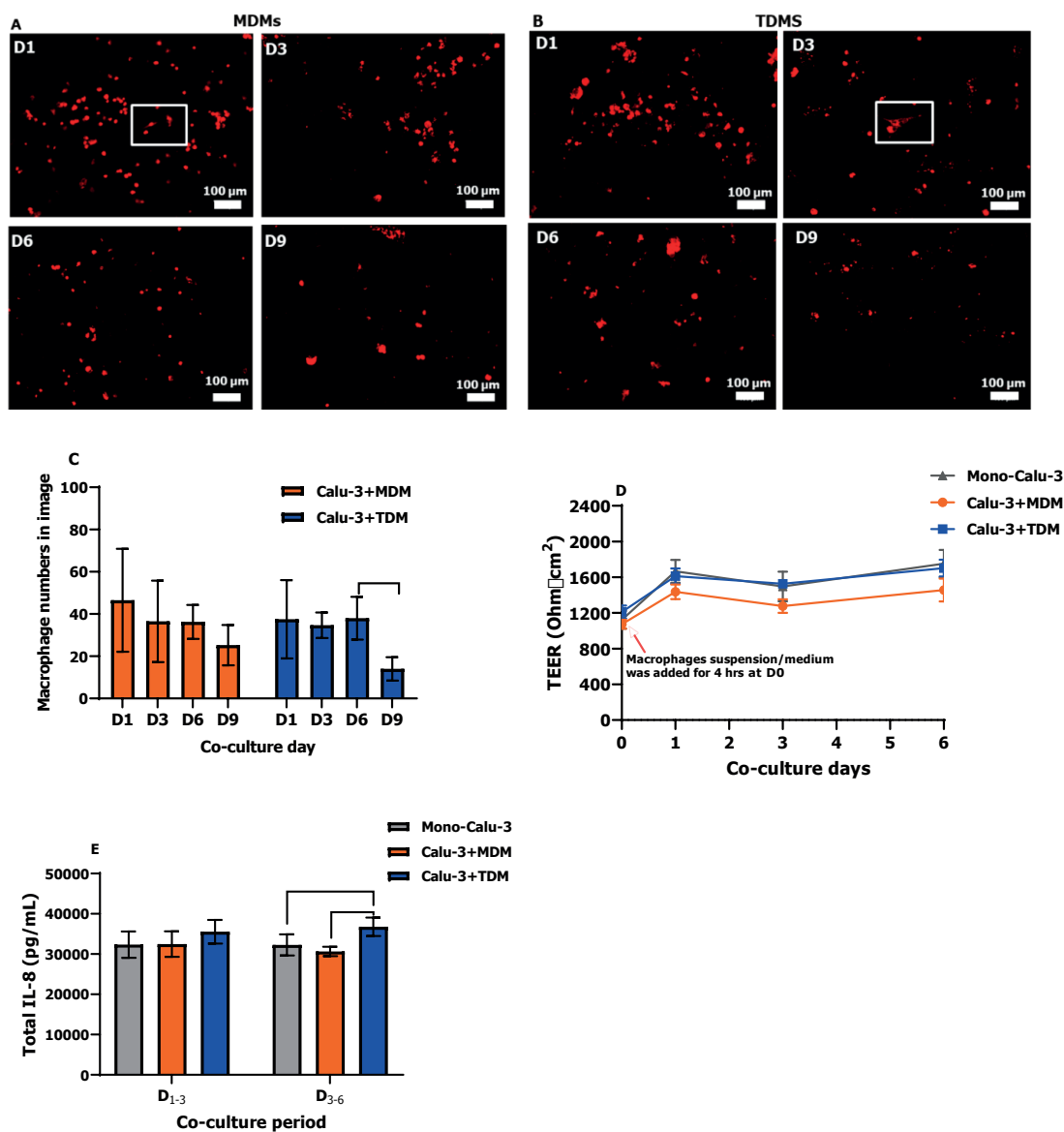


**Figure 6.** Fluorescence microscopy images of MDMs (A) and TDMs (B) (4 hrs adhesion, density:  $5.0 \times 10^4$  cells/cm<sup>2</sup>) and their average number in images (C) after co-culture for 1, 3, 6, and 9 days at the ALL, as well as the TEER (D) and IL-8 production (E) during the 6-day co-culture period. White squares in (A) and (B) are morphological examples of the MDMs and TDMs differentiation. Scale bars in (A) and (B): 100  $\mu$ m. Error bars in (C) indicate the standard deviation of macrophage numbers in 3 or 4 random areas of the insert membrane; Error bars in (D) and (E) indicate the standard deviation of 6 or 12 parallel inserts with cells. \* represents  $p < 0.05$ .

### 3.4 Functional responses of co-culture models to LPS aerosol

Cell viability, LDH release and production of the inflammatory cytokines IL-1 $\beta$ , IL-10 and TNF- $\alpha$  in mono- and co-culture models were measured after LPS exposure (D1 of the co-culture) for 24 hrs (**Figure 7**). All cell models showed high cell viability ( $> 90\%$ ) and no changes in LDH release upon LPS exposure (**Figure 7A** and **7B**), indicating no cytotoxicity. No effect of LPS on the release of IL-1 $\beta$  and IL-10 was seen in the mono-culture model. A comparable level of IL-1 $\beta$  was detected on the apical side of both co-culture models, while IL-10 was only detected on the apical side of the Calu-3 + MDM model ( $\approx 150$  pg/mL) (**Figure 7C** and **7D**). TNF- $\alpha$  that can be produced by both macrophages and Calu-3 cells was detected on both sides of all cell models (**Figure 7E** and **7F**). On the apical side, the Calu-3 + MDM model showed the highest concentration of TNF- $\alpha$  ( $\approx 1150$  pg/mL,  $p < 0.0001$ ), followed by the Calu-3 + TDM model ( $\approx 115$  pg/mL), which was significantly higher than the concentration in the mono-culture ( $\approx 45$  pg/mL,  $p < 0.0001$ ). No significant difference ( $p > 0.05$ ) was seen in the TNF- $\alpha$  levels on the basolateral side of all cell models.

For all cell models, no LDH was detected on the basolateral side of the incubator controls and exposed samples; IL-1 $\beta$ , IL-10 and TNF- $\alpha$  were not detected on either side of the incubator controls, and also no IL-1 $\beta$  and IL-10 on the basolateral side of exposed samples.



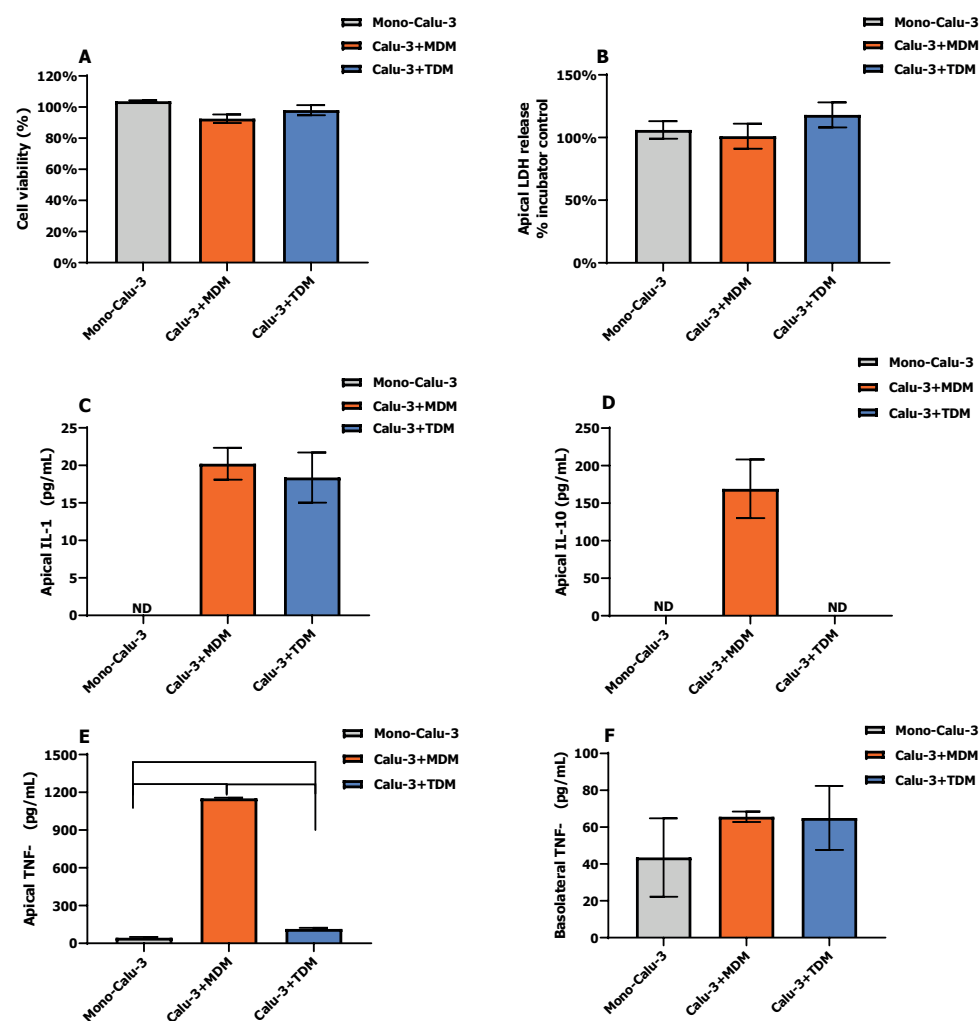


**Figure 7.** Effects of LPS exposure in mono- and co-culture models in 12 well inserts including cell viability (A), LDH release (B) and the production of IL-1 $\beta$  (C), IL-10 (D) and TNF- $\alpha$  (E) on the apical side and TNF- $\alpha$  (F) on the basolateral side. Error bars indicate the standard deviation of 3 or 4 parallel inserts with cells. ND represents not detected; \*\*\*\* represents  $p < 0.0001$ .

## 4. Discussion

Our results demonstrate the substantial differences in cellular responses including cell morphology, TEER changes, and cytotoxicity for epithelial mono-culture of 16HBE, Calu-3, H292 and BEAS-2B cells as well as the macrophage/epithelial cell co-culture models under ALI conditions. The Calu-3 epithelial model can retain its monolayer structure and develop a strong tight junction under long-term ALI culture, which was subsequently used as the structural barrier to create co-culture models in combination with MDMs and TDMs. With the optimization of the co-culture procedure at the ALI, our cell co-culture models showed epithelial monolayer integrity, and increased sensitivity in inflammatory responses to LPS exposure, with the Calu-3 + MDM model giving the strongest responses.

### 4.1 Mono-culture models at the ALI

Human bronchial epithelial and alveolar epithelial cell models are both viable options for *in vitro* exposure, especially to ultrafine particles (UFPs), since both the tracheobronchial and alveolar regions will receive UFPs on their epithelial surface. Deposition of UFPs is not limited to the alveoli, and with decreasing air velocity, substantial deposition can also occur on the terminal bronchial epithelium (Braakhuis et al. 2014). Therefore, human bronchial epithelial cell lines such as 16HBE, Calu-3, H292 and BEAS-2B cells are suitable lung models to study inhalation exposure (BéruBé et al. 2010; Hiemstra et al. 2018). Primary bronchial epithelial cells that can be cultured at the ALI for weeks with well-formed tight junctions might be a good alternative to the lung epithelial cell lines (Pezzulo et al. 2011). However, they have some disadvantages including the high cost, difficult handling procedures and donor variations, which make them less suitable as a basis for a co-culture model from an economical, reproducible and practical point of view. Indeed, to comprehensively evaluate inhalation toxicity of, for example, UFPs *in vitro*, it is warranted to study their effects both in bronchial epithelial models and alveolar epithelial cell models. Therefore, further investigation on which is the best alveolar model is also needed.

When culturing epithelial cell models at the ALI, we assessed the formation of monolayer structure and barrier function as markers of the ability to resist the transport of xenobiotics (BéruBé et al. 2010; Holgate 2008; Kidney and Proud 2000). According to our findings, Calu-3 epithelial cells can act as basis for the co-culture models, since they can develop a strong barrier function and keep their monolayer structure for long-term ALI culture with low cytotoxicity. Depending on the surface and pore size of insert membrane, culture period and medium refreshment frequency, TEER values of Calu-3 cells can differ widely varying from 100 to 2500  $\text{ohm} \times \text{cm}^2$  (Srinivasan et al. 2015). In this study, we set TEER values  $> 1000 \text{ ohm} \times \text{cm}^2$

in a 6-well insert before starting the co-culture as the criterion for the Calu-3 cell model. When forming a high barrier integrity at the ALI, the permeability coefficient of compounds across the Calu-3 monolayer would decrease with increasing molecular weight (Grainger et al. 2006). This might be an explanation for the observation that LDH ( $\approx 140$  kDa) accumulated on the apical side of the Calu-3 monolayer, while the level of LDH detected in the basolateral medium was only limited (**Figure 3**). In comparison, for 16HBE, H292 and BEAS-2B cells with a weak barrier function, the LDH level on the basolateral side was generally higher than that on the apical side. A similar finding was also reported for A549 cells that lack functional tight junctions at the ALI and showed higher LDH levels in basolateral than in apical medium after exposure to polluted air (Zavala et al. 2016). These findings indicate that LDH has a high permeability across cell layers with a weak barrier function, therefore LDH levels in the basolateral medium could be an indicator to evaluate the barrier function of cells at the ALI. Also, when evaluating and comparing the cytotoxicity at the ALI, LDH levels on the apical and basolateral side should be considered respectively depending on the barrier function of cells.

#### 4.2 Co-culture models at the ALI

The beneficial properties of the Calu-3 epithelial monolayer barrier can be increased by addition of pulmonary macrophages, which play an important role in the defence of airways (Byrne et al. 2015). In the present study, improvements were made by adding MDMs and TDMs onto the Calu-3 monolayer to create the co-culture models. However, there is no consensus regarding the optimal number of macrophages and their adhesion time to the epithelial cell layer. The commonly used seeding ratio between macrophages and epithelial cells ranges from 1:1 to 1:5 with an adhesion time from 2 hrs to 24 hrs (Bodet et al. 2005; Grabowski et al. 2016; Lehmann et al. 2011; Tao and Kobzik 2002; Ugonna et al. 2014). Our results demonstrate that a long time period (e.g. 24 hrs) with medium on top of the monolayer can affect its structure. To avoid this negative effect on the monolayer, a relatively short incubation period (e.g.  $\approx 4$  hrs) should be used for preparing co-cultures. However, the efficiency of macrophages adhesion decreased with a shorter incubation period. We calculated that the efficiency of MDMs and TDMs adhesion for 4 hrs is around 20%, thus the actual number of macrophages that adhered to the epithelial carpet was much lower than the added number. When taking this adhesion efficiency into consideration, the density of macrophages onto the epithelial carpet in our co-culture models (seeding density:  $5 \times 10^4$  macrophages/cm<sup>2</sup>) was around  $1.0 \times 10^4$  macrophages/cm<sup>2</sup>, slightly lower than that in human airway wall ( $\approx 3.5 \times 10^4$  macrophages/cm<sup>2</sup>) from the lung tissue sections (Grashoff et al. 1997). However, at a seeding number of  $2 \times 10^4$  macrophages/cm<sup>2</sup>, macrophages may already cover around 70 % of the insert membrane (**Figure S5**), especially at the centre of the membrane. In order to avoid a too high

density of macrophages on the epithelial layer, we increased the seeding density to  $5 \times 10^4$  macrophages/cm<sup>2</sup>. Still the density of adherent macrophages is lower than in lungs *in vivo*.

After the optimization of the co-culture procedure, the co-culture models showed a stronger inflammatory response (IL-1 $\beta$ , IL-10 and TNF- $\alpha$ ) to LPS aerosol compared to the mono-culture (**Figure 7**). Similar findings were reported in *in vitro* studies on air pollutants, in which inflammatory responses were increased when macrophages had been added to the epithelial cells (Bauer et al. 2015; Tao and Kobzik 2002; Wottrich et al. 2004). The macrophage-specific cytokines IL-1 $\beta$  and IL-10 were abundantly produced in our co-culture models, suggesting the activation of macrophages. Importantly, IL-1 $\beta$  and IL-10 only accumulated on the apical side (**Figure 7C** and **7D**). It is likely that the tight junction in the co-culture models blocks the passage of the cytokines from the apical to the basolateral side. This lack of passage can be seen as another read-out of proper barrier function. In line with this observation, upon LPS exposure the TNF- $\alpha$  concentration on the apical side of the co-culture models was significantly higher than that in mono-culture model, while the TNF- $\alpha$  level was comparable on the basolateral sides for mono-culture and co-culture models (**Figure 7E** and **7F**). This may suggest that TNF- $\alpha$  on the apical side of co-culture models, majorly produced by macrophages in response to LPS aerosol, does not cross the epithelial barrier. Also, it indicates that TNF- $\alpha$  on the basolateral side of co-culture models is mainly due to the release from Calu-3 cells as a similar level was observed for the mono-culture model.

The use of MDMs and TDMs in co-cultures was previously compared in terms of their availability, differentiation protocols and donor variations (Chanput et al. 2014; Kooter et al. 2017). We further investigated their morphological changes over the co-culture time period and their response to LPS aerosol. Similar morphological changes of MDMs and TDMs were observed within the 9-day co-culture period. Most of the macrophages remained viable until around D6 of co-culture. During the first 3 days of co-culture some of macrophages seemed to be more active with the developed arrow-like cytoplasm and pseudopodia (**Figure 6A** and **Figure 6B**). After co-culture for 6 days, macrophages started to detach and float upwards, moving out of focus, which were seen as blurry spots (**Figure S6**), indicating the loss of viability. A lack of medium supply due to the tight barrier formed by the epithelial carpet during co-culture for 6 days may explain this loss of viability. It suggests that our co-culture models can be used up to 6 days, while for more prolonged exposures macrophages need to be re-added weekly to ensure characteristics of the co-culture model. Cytokine responses to LPS aerosol varied between the Calu-3 + TDM and Calu-3 + MDM models (**Figure 7**). Upon LPS exposure an increased concentration of the anti-inflammatory cytokine IL-10 was detected on the apical side of the Calu-3 + MDM model in keeping



with M2 polarization by M-CSF (Mosser and Edwards 2008). In contrast, no IL-10 was detected in the Calu-3 + TDM model, which was possibly due to the M1 state of PMA-differentiated THP-1 monocytes (Maeß et al. 2014). In line with previous studies that proposed TNF- $\alpha$  as a marker for M1 macrophages (Mosser and Edwards 2008), a clear concentration-response relationship in TDMs monocultures (M1 macrophages) was observed at LPS levels ranging from 0.08 to 5.12  $\mu\text{g}/\text{cm}^2$ , while TNF- $\alpha$  was not detectable in MDMs monocultures (M2 macrophages) (**Figure S8**). Interestingly, on the apical side of the co-culture models, the Calu-3 + MDM model produced more TNF- $\alpha$  compared to the Calu-3 + TDM model. Interactions between macrophages and epithelial cells might play an essential role in promoting the TNF- $\alpha$  release on the apical side, as reported in several studies (Fizeşan et al. 2019; Ji et al. 2018). However, the mechanism of bidirectional communication underlying inflammatory responses in the current co-culture models is still unclear and needs to be further studied.

Taken together, an optimized Calu-3 + MDM co-culture model was created by allowing 4 hrs adhesion of macrophages onto the epithelial monolayer with the density of  $5 \times 10^4$  macrophages/ $\text{cm}^2$ . Our model showed epithelial barrier integrity under prolonged ALI culture conditions, as well as an increased sensitivity to LPS aerosol in comparison to the Calu-3 mono-culture and Calu-3 + TDM co-culture models at D1 of co-culture. Therefore, we propose this model, provided weekly seeding of MDMs, to be applied in the prolonged ALI exposure to estimate the hazard of aerosols exposures.

### Conflict of interest statement

The authors have no conflict of interest to disclose.

### Acknowledgements

This work is funded by the EU-project PATROLS (No. 760813) and the Dutch Ministry of Health, Welfare and Sport (project 5.1.2). We thank Marc Bazan, Victoria de Leeuw and Liset de la Fonteyne-Blankestijn from the National Institute for Public Health and the Environment (RIVM) for their valuable assistance with cell culture, cell staining and fluorescence microscopy. We are also grateful to Dr. Barbara Rothen-Rutishauser, Barbara Drasler and Anne Bannuscher from the Adolphe Merkle Institute, University of Fribourg for their kind assistance with the confocal microscopy. The support provided by China Scholarship Council (CSC) during the PhD period of Rui-Wen He in Utrecht University-Institute for Risk Assessment Studies is also acknowledged.

### References

- Almstrand A-C, Ljungström E, Lausmaa J, Bake B, Sjövall P, Olin A-C (2009) Airway monitoring by collection and mass spectrometric analysis of exhaled particles. *Analytical chemistry* 81(2):662-668
- Bakand S, Hayes A, Dechsakulthorn F (2012) Nanoparticles: a review of particle toxicology following inhalation exposure. *Inhalation toxicology* 24(2):125-135
- Bauer RN, Müller L, Brighton LE, Duncan KE, Jaspers I (2015) Interaction with epithelial cells modifies airway macrophage response to ozone. *American journal of respiratory cell and molecular biology* 52(3):285-294
- BeruBe K, Aufderheide M, Breheny D, et al. (2009) *In vitro* models of inhalation toxicity and disease. *Alternatives to Laboratory Animals* 37(1):89-141
- BéruBé K, Prytherch Z, Job C, Hughes T (2010) Human primary bronchial lung cell constructs: the new respiratory models. *Toxicology* 278(3):311-318
- Bodet C, Chandad F, Grenier D (2005) Modulation of cytokine production by *Porphyromonas gingivalis* in a macrophage and epithelial cell co-culture model. *Microbes and infection* 7(3):448-456
- Braakhuis HM, Park MV, Gosens I, De Jong WH, Cassee FR. (2014) Physicochemical characteristics of nanomaterials that affect pulmonary inflammation. *Particle and fibre toxicology* 11(1):18
- Braakhuis HM, Giannakou C, Peijnenburg WJ, Vermeulen J, van Loveren H, Park MV (2016) Simple *in vitro* models can predict pulmonary toxicity of silver nanoparticles. *Nanotoxicology* 10(6):770-779
- Byrne AJ, Mathie SA, Gregory LG, Lloyd CM (2015) Pulmonary macrophages: key players in the innate defence of the airways. *Thorax* 70(12):1189-1196
- Chanput W, Mes JJ, Wichers HJ (2014) THP-1 cell line: an *in vitro* cell model for immune modulation approach. *International immunopharmacology* 23(1):37-45
- Chen S, Einspanier R, Schoen J (2015) Transepithelial electrical resistance (TEER): a functional parameter to monitor the quality of oviduct epithelial cells cultured on filter supports. *Histochemistry and cell biology* 144(5):509-515
- de Jong PM, Van Sterkenburg M, Hesselting SC, et al. (1994) Ciliogenesis in human bronchial epithelial cells cultured at the air-liquid interface. *American journal of respiratory cell and molecular biology* 10(3):271-277
- Fizeşan I, Cambier S, Moschini E, et al. (2019) *In vitro* exposure of a 3D-tetraculture representative for the alveolar barrier at the air-liquid interface to silver particles and nanowires. *Particle and fibre toxicology* 16(1):14
- Grabowski N, Hillaireau H, Vergnaud-Gauduchon J, et al. (2016) Surface-modified biodegradable nanoparticles' impact on cytotoxicity and inflammation response on a co-culture of lung epithelial cells and human-like macrophages. *Journal of biomedical nanotechnology* 12(1):135-146
- Grainger CI, Greenwell LL, Lockley DJ, Martin GP, Forbes B (2006) Culture of Calu-3 cells at the air interface provides a representative model of the airway epithelial barrier. *Pharmaceutical research* 23(7):1482-1490
- Grashoff W, Sont JK, Sterk PJ, et al. (1997) Chronic obstructive pulmonary disease: role of bronchiolar mast cells and macrophages. *The American journal of pathology* 151(6):1785
- Heijink IH, Brandenburg SM, Noordhoek JA, Postma DS, Slebos D-J, van Oosterhout AJ (2010) Characterisation of cell adhesion in airway epithelial cell types using electric cell-substrate impedance sensing. *European Respiratory Journal* 35(4):894-903
- Hermans C, Bernard A (1999) Lung epithelium-specific proteins: characteristics and potential applications as markers. *American journal of respiratory and critical care medicine* 159(2):646-678
- He R-W, Gerlofs-Nijland ME, Boere J, Fokkens P, Leseman D, et al. (2020) Comparative toxicity of ultrafine particles around a major airport in human bronchial epithelial (Calu-3) cell model at the air-liquid interface. *Toxicology in Vitro*:104950
- Hiemstra PS, Grootaers G, van der Does AM, Krul CA, Kooter IM (2018) Human lung epithelial cell cultures for analysis of inhaled toxicants: Lessons learned and future directions. *Toxicology in vitro* 47:137-146
- Holgate ST (2008) The airway epithelium is central to the pathogenesis of asthma. *Allergology International* 57(1):1-10
- Hu G, Christman JW (2019) Alveolar Macrophages in Lung Inflammation and Resolution. *Frontiers in Immunology* 10:2275

- Ji J, Upadhyay S, Xiong X, et al. (2018) Multi-cellular human bronchial models exposed to diesel exhaust particles: assessment of inflammation, oxidative stress and macrophage polarization. *Particle and fibre toxicology* 15(1):19
- Kidney JC, Proud D (2000) Neutrophil transmigration across human airway epithelial monolayers: mechanisms and dependence on electrical resistance. *American journal of respiratory cell and molecular biology* 23(3):389-395
- Kooter IM, Gröllers-Mulderij M, Duistermaat E, Kuper F, Schoen ED (2017) Factors of concern in a human 3D cellular airway model exposed to aerosols of nanoparticles. *Toxicology in Vitro* 44:339-348
- Lehmann AD, Daum N, Bur M, Lehr C-M, Gehr P, Rothen-Rutishauser BM (2011) An *in vitro* triple cell co-culture model with primary cells mimicking the human alveolar epithelial barrier. *European Journal of Pharmaceutics and Biopharmaceutics* 77(3):398-406
- Limbach LK, Li Y, Grass RN, et al. (2005) Oxide nanoparticle uptake in human lung fibroblasts: effects of particle size, agglomeration, and diffusion at low concentrations. *Environmental science & technology* 39(23):9370-9376
- Maeß MB, Wittig B, Cignarella A, Lorkowski S (2014) Reduced PMA enhances the responsiveness of transfected THP-1 macrophages to polarizing stimuli. *Journal of immunological methods* 402(1-2):76-81
- Mosser DM, Edwards JP (2008) Exploring the full spectrum of macrophage activation. *Nature reviews immunology* 8(12):958-969
- Mülhopt S, Dilger M, Diabaté S, et al. (2016) Toxicity testing of combustion aerosols at the air-liquid interface with a self-contained and easy-to-use exposure system. *Journal of Aerosol Science* 96:38-55
- PATROLS-Website (2018) <https://www.patrols-h2o2o.eu/>
- Paur H-R, Cassee FR, Teeguarden J, et al. (2011) In-vitro cell exposure studies for the assessment of nanoparticle toxicity in the lung—A dialog between aerosol science and biology. *Journal of Aerosol Science* 42(10):668-692
- Pezzulo AA, Starner TD, Scheetz TE, et al. (2011) The air-liquid interface and use of primary cell cultures are important to recapitulate the transcriptional profile of *in vivo* airway epithelia. *American Journal of Physiology-Lung Cellular and Molecular Physiology* 300(1):L25-L31
- Phillips M, Herrera J, Krishnan S, Zain M, Greenberg J, Cataneo RN (1999) Variation in volatile organic compounds in the breath of normal humans. *Journal of Chromatography B: Biomedical Sciences and Applications* 729(1-2):75-88
- Samet J, Krewski D (2007) Health effects associated with exposure to ambient air pollution. *Journal of toxicology and environmental health, Part A* 70(3-4):227-242
- Septiadi D, Abdussalam W, Rodriguez-Lorenzo L, et al. (2018) Revealing the role of epithelial mechanics and macrophage clearance during pulmonary epithelial injury recovery in the presence of carbon nanotubes. *Advanced Materials* 30(52):1806181
- Srinivasan B, Kolli AR, Esch MB, Abaci HE, Shuler ML, Hickman JJ (2015) TEER measurement techniques for *in vitro* barrier model systems. *Journal of laboratory automation* 20(2):107-126
- Tao F, Kobzik L (2002) Lung macrophage-epithelial cell interactions amplify particle-mediated cytokine release. *American journal of respiratory cell and molecular biology* 26(4):499-505
- Ugonna K, Bingle CD, Plant K, Wilson K, Everard ML (2014) Macrophages are required for dendritic cell uptake of respiratory syncytial virus from an infected epithelium. *PloS one* 9(3)
- Vordenbäumen S, Braukmann A, Altendorfer I, Bleck E, Jose J, Schneider M (2013) Human casein alpha s1 (CSN1S1) skews *in vitro* differentiation of monocytes towards macrophages. *BMC immunology* 14(1):46
- Wottrich R, Diabaté S, Krug HF (2004) Biological effects of ultrafine model particles in human macrophages and epithelial cells in mono- and co-culture. *International journal of hygiene and environmental health* 207(4):353-361
- Zavala J, O'Brien B, Lichtveld K, et al. (2016) Assessment of biological responses of EpiAirway 3-D cell constructs versus A549 cells for determining toxicity of ambient air pollution. *Inhalation toxicology* 28(6):251-259

## Supplementary Material

### Materials and methods

#### Description of epithelial cell lines

Cell lines 16HBE and BEAS-2B are immortalized from normal human bronchial epithelial cells and widely used in lung research. The 16HBE cells can form well-defined tight junction with highly organized actin filaments (Ehrhardt et al. 2002) while BEAS-2B cells can form a confluent monolayer faster and exhibit higher homology in gene expression pattern compared to primary cells (Heijink et al. 2010). Calu-3 cells can produce features of differentiated, functional human airway epithelial cells, allowing them to be used for modelling the respiratory epithelial barrier (Grainger et al. 2006). Although the H292 cell line is generated from the salivary gland carcinoma cell, it has been often used as lung cell model to study effects of inhalation exposure on gene expression due to high reactivity to total particulate matter and gas/vapor phase (Courcot et al. 2012; Sekine et al. 2015).

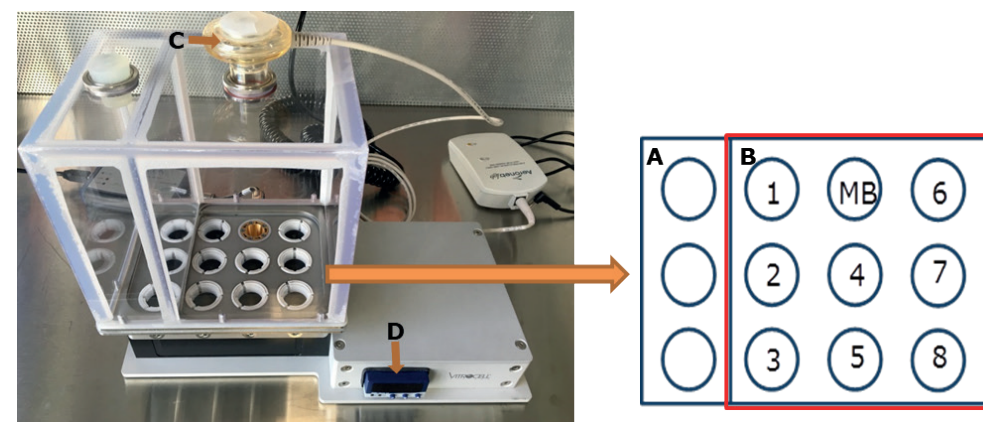


**Figure S1.** Air-liquid interface (ALI) Cloud exposure system. A: Chamber for exposure controls, which were not used in this study; B: Chamber for LPS exposure, number 1-8 represents each position, MB represents a microbalance; C: Aerosol nebulizer; D: Temperature controller. More information can be found via <https://www.vitrocell.com/inhalation-toxicology/exposure-systems/vitrocell-cloud-system>



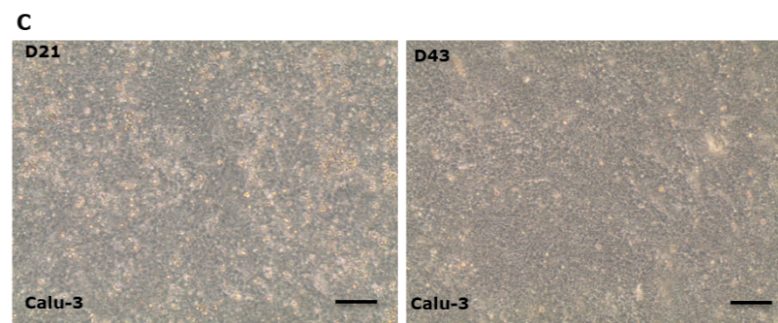
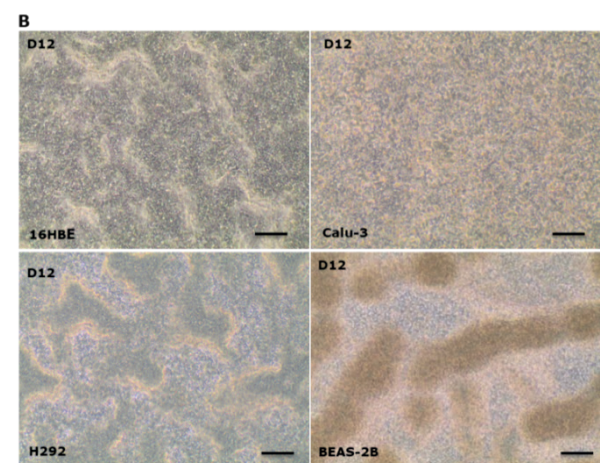
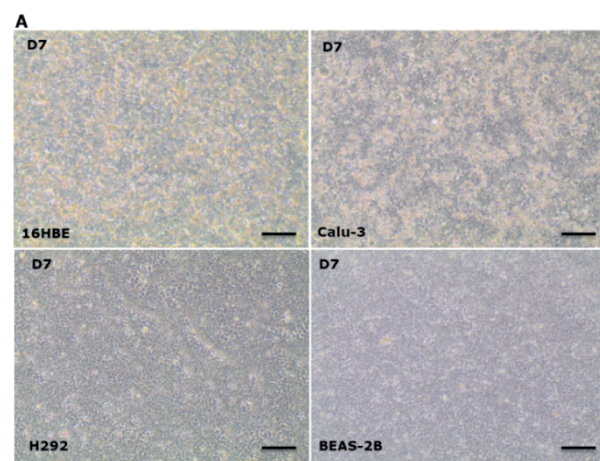


**Figure S2.** Cell morphology of 16HBE, Calu-3, H292 and BEAS-2B cells at day 7 (A) and 12 (B) as well as Calu-3 cells at day 21 and 43 (C). Cells were at submerged culture for 7 days, followed by ALI culture. Scale bars: 100  $\mu$ m.

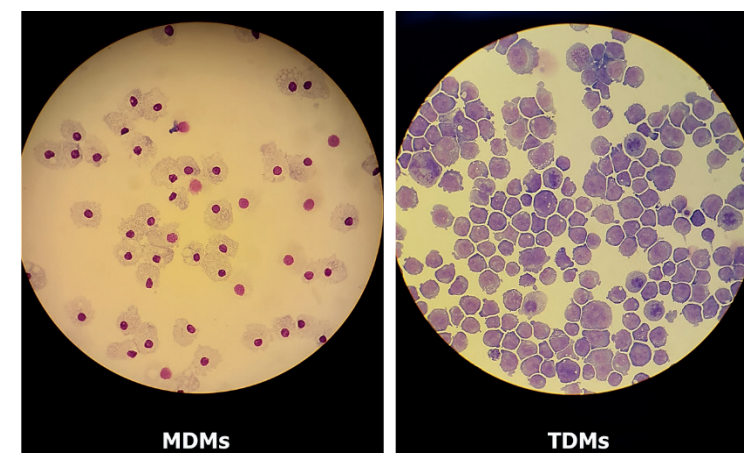


**Figure S3.** May-Grunwald Giemsa stained cytosmears of MDMs (left) and TDMs (right) before adding onto Calu-3 cells.

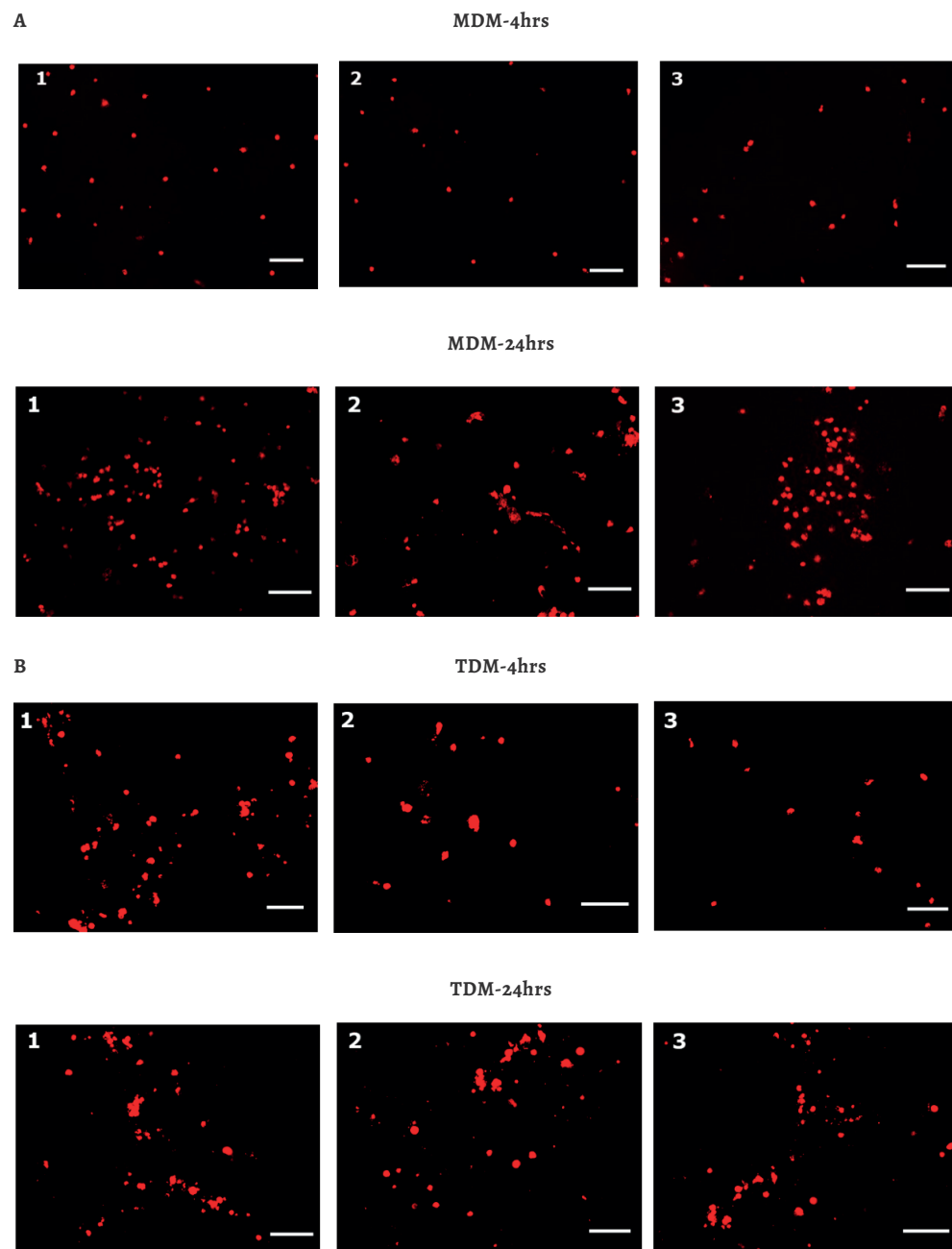


**Figure S4.** Fluorescence microscopy images of MDMs (A) and TDMs (B) after 4 or 24 hrs adhesion onto the Calu-3 epithelial carpet. The seeding density of MDMs and TDMs is  $2.0 \times 10^4$  cells/cm<sup>2</sup>. Macrophages were labelled with Vybrant DiI dye in red. Scale bars: 100  $\mu$ m. Number 1, 2, and 3 represent the images taken at random areas of the membrane.

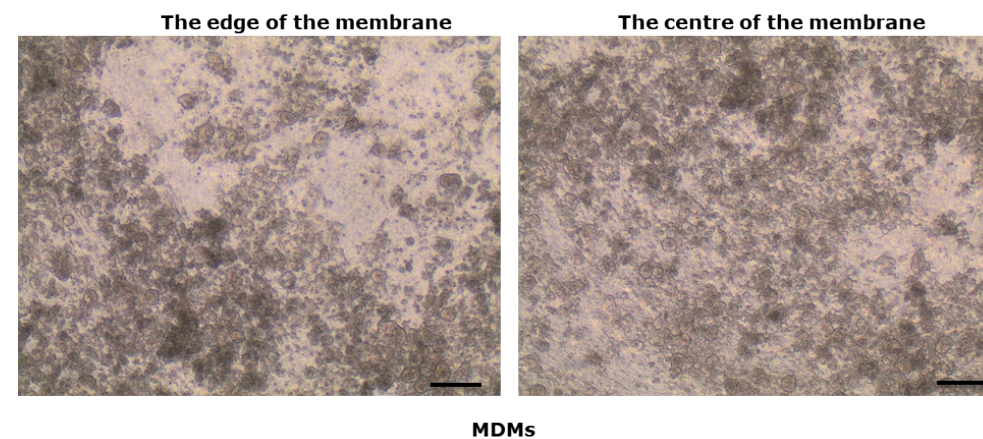


**Figure S5.** Microscopy images of MDMs (density:  $2.0 \times 10^4$  cells/cm<sup>2</sup>) after seeding onto the epithelial carpet. Scale bars: 100  $\mu$ m.

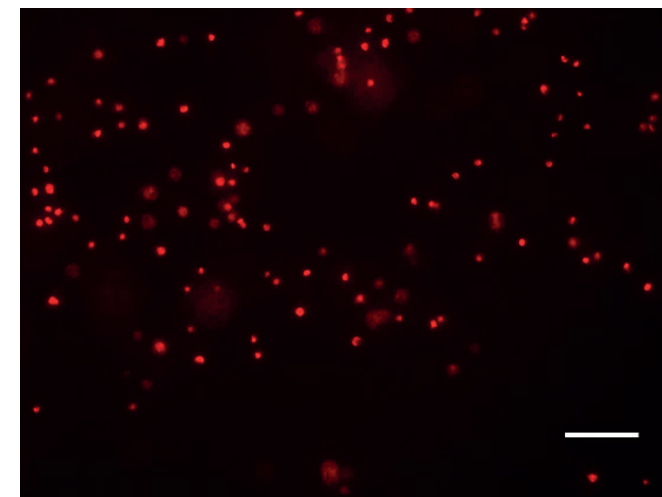


**Figure S6.** Fluorescence microscopy images of MDMs (4 hrs adhesion, density:  $5.0 \times 10^4$  cells/cm<sup>2</sup>) at D6 of co-culture. Scale bars: 200  $\mu$ m.



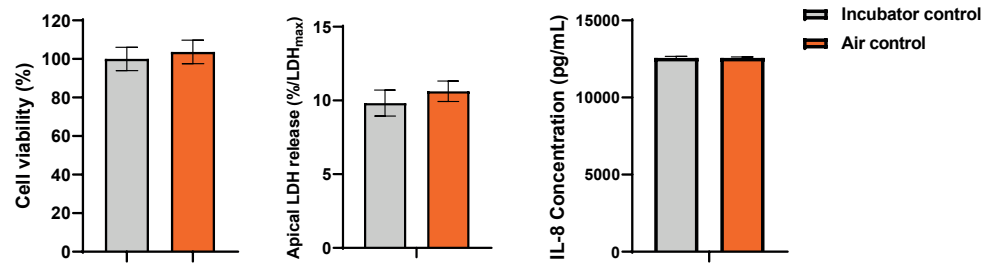


**Figure S7.** Effects of exposure to Milli Q water aerosol in co-culture models in 12 well inserts including cell viability, LDH release and the production of IL-8. Error bars indicate the standard deviation of 3 or 4 parallel inserts with cells.

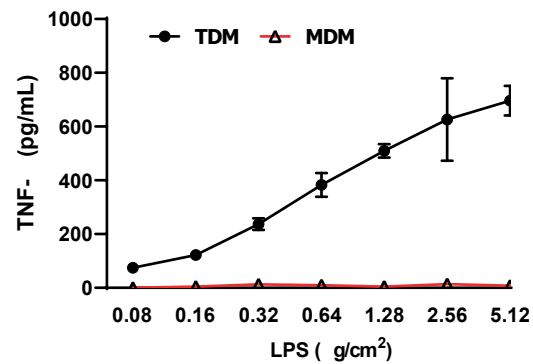


**Figure S8.** TNF- $\alpha$  release from TDMs and MDMs after exposure to LPS at concentrations from 0.08 to 5.12  $\mu\text{g}/\text{cm}^2$ . Error bars indicate the standard deviation of 3 parallel inserts with cells.

**Table S1.** The density of the Calu-3 cells and the ratio between Calu-3 cells and macrophages ( $1.0 \times 10^4$  macrophages/ $\text{cm}^2$ ) at Day 0, 1, 3, and 6 for the co-culture. Results for the Calu-3 cells density were obtained from 3 parallel inserts.

Co-culture day	Day 0	Day 1	Day 3	Day 6
Density (Calu-3 cells/ $\text{cm}^2$ )	176421 $\pm$ 2389	192798 $\pm$ 7421	207211 $\pm$ 16925	226842 $\pm$ 7421
Ratio (Calu-3 cells: macrophages)	$\approx$ 18	$\approx$ 19	$\approx$ 20	$\approx$ 22

## References

- Courcot E, Leclerc J, Lafitte J-J, et al. (2012) Xenobiotic metabolism and disposition in human lung cell models: comparison with *in vivo* expression profiles. *Drug Metabolism and Disposition* 40(10):1953-1965
- Ehrhardt C, Kneuer C, Fiegel J, et al. (2002) Influence of apical fluid volume on the development of functional intercellular junctions in the human epithelial cell line 16HBE140-: implications for the use of this cell line as an *in vitro* model for bronchial drug absorption studies. *Cell and tissue research* 308(3):391-400
- Grainger CI, Greenwell LL, Lockley DJ, Martin GP, Forbes B (2006) Culture of Calu-3 cells at the air interface provides a representative model of the airway epithelial barrier. *Pharmaceutical research* 23(7):1482-1490
- Heijink IH, Brandenburg SM, Noordhoek JA, Postma DS, Slebos D-J, van Oosterhout AJ (2010) Characterisation of cell adhesion in airway epithelial cell types using electric cell-substrate impedance sensing. *European Respiratory Journal* 35(4):894-903
- Sekine T, Sakaguchi C, Fukano Y (2015) Investigation by microarray analysis of effects of cigarette design characteristics on gene expression in human lung mucoepidermoid cancer cells NCI-H292 exposed to cigarette smoke. *Experimental and Toxicologic Pathology* 67(2):143-151

# Chapter 4

## **Comparative toxicity of ultrafine particles around a major airport in human bronchial epithelial (Calu-3) cell model at the air–liquid interface**

Rui-Wen He <sup>ab</sup>, Miriam E. Gerlofs-Nijland <sup>a</sup>, John Boere <sup>a</sup>, Paul Fokkens <sup>a</sup>,  
Daan Leleman <sup>a</sup>, Nicole A.H. Janssen <sup>a</sup>, Flemming R Cassee <sup>ab\*</sup>

<sup>a</sup> Department for Environmental Health, National Institute for Public Health and the Environment (RIVM), P.O. Box, 3720 BA, Bilthoven, The Netherlands

<sup>b</sup> Institute for Risk Assessment Sciences, Utrecht University, P.O. Box 80178, 3508 TD Utrecht, The Netherlands

(Toxicology in Vitro, 2020, Volume 68, 104950, ISSN 0887-2333)

## Highlights

Airport and road traffic UFPs can activate inflammation in Calu-3 cells

Airport UFPs exert similar toxicity compared to UFPs from road traffic emission

ALI condition promotes cellular responses to particles at low exposed dose

## Abstract

Relatively high concentrations of ultrafine particles (UFPs) have been observed around airports, in which aviation and road traffic emissions are the major sources. This raises concerns about the potential health impacts of airport UFPs, particularly in comparison to those emitted by road traffic. UFPs mainly derived from aviation or road traffic emissions were collected from a location near a major international airport, Amsterdam-Schiphol airport (AMS), depending on the wind direction, along with UFPs from an aircraft turbine engine at low and full thrust. Human bronchial epithelial cells (Calu-3) model in combination with an air-liquid interface (ALI) Cloud system was used for the *in vitro* exposure to UFPs at low doses ranging from 0.09 to 2.07  $\mu\text{g}/\text{cm}^2$ . Particle size distribution was measured. Cell viability, cytotoxicity and inflammatory potential (interleukin (IL) 6 and 8 secretion) on Calu-3 cells were assessed after exposure for 24 hrs. The biological measurements on Calu-3 cells confirm that pro-inflammatory responses still can be activated at the high cell viability (>80%) and low cytotoxicity. By the Benchmark Dose (BMD) analysis, Airport and Non-Airport (road traffic) UFPs as well as UFPs samples from a turbine engine have similar toxic properties. Our results suggest that UFPs from aviation and road traffic in airport surroundings may have similar adverse effects on public health.

**Keywords:** UFPs; Airport emission; Road traffic emission; Calu-3 cell; Air-liquid interface; BMD analysis.

## 1. Introduction

Relatively high concentrations of ultrafine particles (UFPs, particle size < 100 nm), expressed as number per volume, have been observed around airports primarily linked with aviation activities (Hudda and Fruin 2016, Keuken et al 2015, Masiol and Harrison 2014, Ren et al 2018, Riley et al 2016, Winther et al 2015). Although characteristics (e.g. size distribution) and sources of the airport UFPs are becoming clear (Stacey 2019), little is known about their toxicity as well as the comparison of their toxicity with UFPs from other sources such as road traffic.

Large airports are usually surrounded by major motorways. Consequently, aviation activity and road traffic are the major sources to the particles in airport surroundings (He et al 2018). A recent study reported total particles number concentrations (PNCs) of around 35,000 particles/cm<sup>3</sup> at a monitoring site nearby the Amsterdam-Schiphol airport (AMS, the Netherlands), in which aviation activity was estimated to account for 79% and road traffic for 18% of PNCs (Pirhadi et al 2020). Aircraft emissions are characterized by a smaller particle size compared to other combustion sources, such as road traffic (Stacey 2019). The small class of UFPs contributes mostly to the size distribution for aviation emissions with a strong increase in the range of 10-20 nm, while the size of UFPs from road traffic is generally larger than 50 nm (Keuken et al 2015, Pirhadi et al 2020, Shirmohammadi et al 2017). The size of particles is an important characteristic, which can influence not only their toxic potency, but also where particles exert their toxicity (Heusinkveld et al 2016, Miller et al 2017, Stone et al 2017, Terzano et al 2010). Depending on the size distribution of UFPs, the exposure risks may differ. Therefore, understanding the associated risks due to exposure to UFPs from aviation and road traffic emissions is of great significance to gain better insight into the extent of their contributions to health effects.

To better assess the potential toxicity of inhaled UFPs, the air-liquid-interface (ALI) exposure via exposure systems was developed. Compared to the traditional *in vitro* exposure by adding the particles suspension into medium, ALI exposure allows particles to be deposited on semi-dry apical cell surface via a continuous flow or single cloud to adequately resemble the realistic inhalation exposure in lungs (BéruBé et al 2010, Kim et al 2016), thereby being applicable in many toxicity studies (Antherieu et al., 2017; Fizeşan et al., 2019; Müllhopt et al., 2016). UFPs can deposit in the respiratory tract mainly by diffusion, which increases with decreasing air velocity. Model calculation using the Multiple Path Particle Dosimetry (MPPD) model suggests that both tracheobronchial and alveolar regions would receive UFPs (1 - 100 nm) on the epithelial surface (Braakhuis et al. 2014). Human bronchial and alveolar epithelial cells were consequently the preferred options for toxicity testing of UFPs. However,

there are at present only a few human lung cell models available that are resistant to being cultured at ALI, as well as have a good performance on biological barrier (i.e. well-formed tight junctions). The careful selection of the appropriate cell lines was consequently required before starting an exposure.

The aim of this study is to investigate the toxicity of UFPs from aviation and road traffic emissions. We collected UFPs from airport and non-airport emissions (mostly impacted by road traffic) around AMS, as well as UFPs directly from an aircraft turbine engine. An optimized human bronchial epithelial Calu-3 cell model was used in combination with the ALI Cloud system to test the toxicity of UFPs samples at 5 exposure doses. The adverse effects as tested by cell viability, lactate dehydrogenase (LDH) release and pro-inflammatory responses were measured at 24 hrs post exposure and evaluated by the benchmark dose (BMD) analysis.

## 2. Materials and methods

### 2.1 Collection of UFPs samples

#### 2.1.1 Airport and Non-Airport UFPs sample

UFPs from aviation is usually mixed with that of road traffic in airport surroundings, making it difficult to separate the two sources into specific UFPs fractions. To solve this problem, we positioned a UFP sampler at a location (52°19'15.2"N 4°47'07.5"E) between the AMS and two major motorways (A4 and A9), and very close to two major runways within no other major sources in between the sampler and aircrafts (**Figure 1**). **Figure 1** illustrated the location of the sampling site, which is as same as the sampling site described in Lammers et al (2020). Additionally, we took the advantage of the change of wind directions, allowing sampling UFPs on separate filters at times downwind of airport runways or the major motorways. Samples collected under southern and western wind from direction of the airport were labeled as "Airport" UFPs sample, whereas if the wind was blowing from the direction of the motorways (eastern and northern wind) the samples were labeled as road traffic dominated UFPs (Non-Airport UFPs).

Airport and Non-Airport UFPs samples were collected in 2018, the detailed collecting time can be found in **Table 1**. Two modified high-volume cascade impactors (HVCI) were used to collect UFPs samples from airport and non-airport emissions respectively using only the final stage with a mass median aerodynamic diameter (MMAD) of less than 0.18  $\mu\text{m}$  as previously described (Demokritou et al 2002). The decision which HVCI was turned on was made after checking the wind direction. To obtain sufficient UFPs on filters, the sampling time for each filter was for several days, from 9 a.m.

to 4 p.m per day. All filters were weighed by an analytical balance before and after collection (after overnight stabilization at 40-60% humidity and 20°C) and then stored at -20°C in the dark.

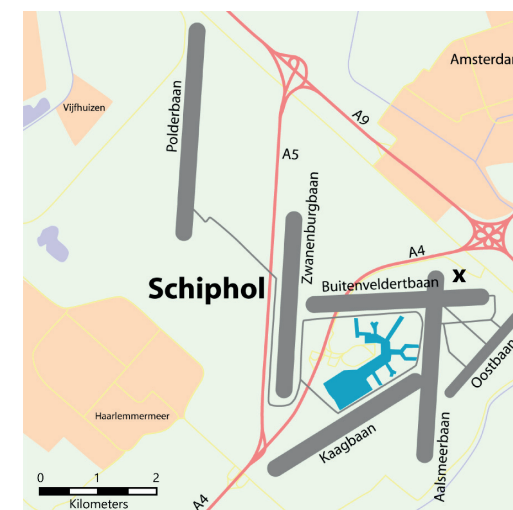


**Figure.1** Location of the sampling site (x) near Amsterdam Airport Schiphol (AMS), same as the sampling site described in Lammers et al (2020), northeastern of airport runways and southwestern of two major motorways (A4 and A9).

**Table 1.** Description and characteristics of particle samples.

Particle samples	Collection period (2018)	Dominating source of emission	Mean size (nm) <sup>1</sup>	Size peaks (nm) <sup>2</sup>
Diesel	N/A	NIST Diesel (reference sample)	177±91	27, 42, 188
Turbine 1	26 April	F100 (low thrust)	204±158	42, 103, 223
Turbine 2	26 April	F100 (full thrust)	70±75	17, 24, 32
Non-airport 1	23, 24 May; 8 June	road traffic contribution	51±64	13, 9, 21
Non-airport 2	12, 13 June; 4-6, 9, 12, 20 July	Road traffic contribution	45±40	29
Non-airport 3	16 October	Road traffic contribution	45±43	30
Airport 1	14, 15 June; 17, 18, 24 July	Aviation contribution	97±102	31, 77
Airport 2	31 July; 8, 15, 22, 29 August; 10, 26 September	Aviation contribution	47±36	32

N/A = not applicable

<sup>1</sup>. This is the mean size of particles in suspension and the size can deviate from particle size in the outside air

<sup>2</sup>. These are the major peaks in the size distribution



### 2.1.2 UFPs samples for turbine and diesel engines

UFPs were also collected directly from the exhaust of a turbine engine (Pratt & Whitney F100) when running at low thrust (ground-idle or taxi operation, Turbine 1) and at full thrust (Turbine 2) using a HVCI. In addition, a standard reference diesel particulate matter (NIST® SRM® 2975) for diesel engine exhaust emissions was purchased (Sigma Aldrich, the Netherlands). Although the NIST diesel sample cannot be used for the direct comparison of the toxicity with the other UFPs samples because of different collection methods, this diesel sample can be used as a benchmark material to assess whether the used biological measurement works and to allow comparison with past and future study findings.

## 2.2 Preparation of particle suspension and characterization

Filters containing UFPs were extracted with methanol by sonication according to the earlier protocol (Gerlofs-Nijland et al 2013). The extraction procedure was repeated three times. The combined extract from three times was collected in a glass bottle and concentrated using a rotary evaporator (IKA® RV10, Germany) to almost dry matter. 1 mL of methanol was then added to rinse the bottle by an ultrasonic treatment. The remaining suspension was collected into a pre-weighed glass vial, subsequently evaporated overnight at 25°C, followed by acclimatization (40-60% humidity at 20°C) for 24 hrs. The glass vial with residue was then weighed. A clean Teflon TE38 filter was also extracted using the same protocol and included as a negative control. All extracted UFPs samples were stored at -20°C.

Immediately prior to exposure, the extracted UFPs as well as NIST diesel particles were suspended by ultrasonic treatment in 1 mL of Milli-Q water with 0.01% NaCl solution (for nebulization in Cloud system). The particle size distribution of each suspension was measured by a tracing analysis of the Brownian motion with a laser illuminated microscope (LM20, NanoSight Ltd, UK).

## 2.3 ALI culture and TEER measurement

Human bronchial epithelium Calu-3 cell line purchased from the American Tissue Culture Collection (ATCC, Rockville, US) was used for *in vitro* exposure. Calu-3 cell line was cultured with minimal essential medium (MEM) + GlutaMAX, supplemented with 10% fetal bovine serum (FBS), 1% non-essential amino acid (NEAA) solution and 1% penicillin/streptomycin in an incubator with 5% CO<sub>2</sub> at 37°C. Upon reaching about 80% confluence, Calu-3 cells were enzymatically detached from the culture flask with 0.05% trypsin-EDTA. 0.5 mL cells suspension with a density of  $2.5 \times 10^5$  cells/mL was seeded into the apical side of sterile 12 mm insert (3.0 µm pore size, 1.12 cm<sup>2</sup> polyester membrane, Costar, Germany) placed in a 12-well plate. 1.5 mL culture medium was added to the basolateral side of insert for nutrient supply. Cells in insert were cultured

under submerged condition for 7 days to achieve confluence. Apical medium was then removed, Calu-3 cells were cultured for an additional 7 days at ALI. Culture medium (only basolateral medium during ALI culture) was refreshed every 2-3 days. All culture medium and supplements were purchased from Life Technologies (Thermo Fisher Scientific Inc., the Netherlands). As an important indicator of barrier function, transepithelial electrical resistance (TEER) of Calu-3 cells was measured by the Evom2 Voltohmmeter with a 4mm chopstick electrodes (World Precision Instruments Inc., FL, USA) before ALI exposure. To measure TEER under ALI condition, 0.5 mL medium was added into the apical side of the insert. All TEER values were corrected for the resistance of cell-free inserts ( $\approx 130$  ohm) and insert surface area (1.12 cm<sup>2</sup>).

## 2.4 UFPs exposure in Cloud exposure system

The VITROCELL® Cloud Exposure System (Vitrocell, Waldkirch, Germany) was used for ALI *in vitro* exposure at 37°C. The system contains 12 cavities for 12 mm inserts including 3 cavities for exposure control inserts, 1 for determining the deposited mass of particles in an insert via a microbalance, and the rest for ALI exposure (Figure 2, Lenz et al., 2014). To achieve the ALI exposure to particles, this system uses a single nebulization to produce a dense cloud of droplets with particles in the chamber. The ultrasonic nebulization of the particle suspensions results in 4.0 – 6.0 µm droplets that are much larger than the size distribution of used particle samples. As such, we do not expect that the nebulization has an impact on the aggregation of the particles. Therefore, the particle size distribution of UFPs samples in suspension would be less affected due to the nebulization. Cells were then exposed to the particles by sedimentation of the droplets. Prior to the *in vitro* exposure, the fluorescein sodium salt (Sigma, the Netherlands) and a reference UFPs sample (DQ12 quartz, IOM, Edinburg) were sprayed via nebulizer respectively to assess the deposition of particles on the membrane of inserts at exposure positions. The detailed protocol can be found in the supplementary information.

Since pilot *in vitro* studies already indicated that the effect level was higher than 0.05 µg/cm<sup>2</sup> on the Calu-3 cell model, we designed the exposure procedure by successively nebulizing 100-400 µL of prepared suspension (1000 µg/mL) in the chamber to aim at the doses of UFPs approximately ranging from 0.1 to 1.5 µg/cm<sup>2</sup>. The experiment of each sample includes the following 3 steps: First, 3 inserts for exposure controls were exposed with the suspension of a blank filter extraction or re-suspension solution without particles; Second, 4 exposed doses tested in succession for each UFPs sample, with 2 inserts for each dose (duplicate measurement); Finally, 4 inserts that were not exposed in the Cloud system but, with the exception of exposure, treated in the same way including 3 for incubator controls and 1 for measuring the total amount of LDH in cells (see 2.6). The mass of deposited particles via a microbalance was recorded

after exposure to the particle aerosol. The actual applied doses in this study vary between the different samples due to the instrumental uncertainty. Overall, most UFPs samples reach the aimed dose range with the exception of Airport 1 sample, in which the highest dose ( $0.96 \mu\text{g}/\text{cm}^2$ ) is much lower compared to the highest dose of the other samples. After exposure, all inserts were transferred to a new 12-wells plates with 1.5 mL fresh culture medium on the basolateral side and cultured in an incubator for 24 hrs.

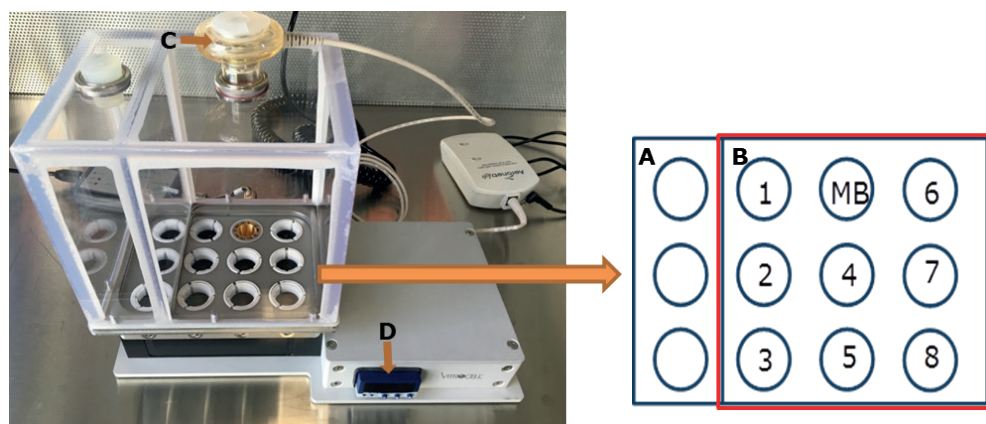


**Figure 2.** Air-liquid interface (ALI) Cloud exposure system. A: Chamber for exposure controls; B: Chamber for UFPs exposure, number 1-8 represents each exposure position, MB represents a microbalance; C: Aerosol nebulizer (pore size:  $4.0 - 6.0 \mu\text{m}$ ); D: Temperature controller. More detailed information can be found via the following link: <https://www.vitrocell.com/inhalation-toxicology/exposure-systems/vitrocell-cloud-system>

## 2.5 Cell viability

Cell viability was measured by the MTS assay (Promega, Fitchburg, Wisconsin, USA) as previously described (He et al 2018). Briefly, Calu-3 cells on the membrane after 24 hrs exposure were washed with culture medium, apical and basolateral medium was collected and stored at  $4^\circ\text{C}$  or  $-20^\circ\text{C}$  for analysis. Subsequently, cells were incubated with  $500 \mu\text{L}$  fresh MTS solution (medium: MTS reagent = 9: 1). After 30 minutes incubation,  $100 \mu\text{L}$  MTS solution was transferred into 96-well flat bottom plates (Thermo Fisher Scientific Inc., the Netherlands) for absorption measurement. MTS solution was used as a blank control. The viability of exposed cells was corrected for incubator controls.

## 2.6 LDH leakage

The leakage of total lactate dehydrogenase (LDH) in culture medium was measured with the LDH cytotoxicity detection kit (Roche Diagnostics GmbH, Mannheim, Germany).  $100 \mu\text{L}$  of collected apical or basolateral medium and reaction reagent were successively added into 96-well flat bottom plates and incubated in dark at room temperature for 20 minutes. After adding  $50 \mu\text{L}$  stop solution (HCl,  $1.0 \text{ M}$ , Sigma, the Netherlands), absorbance was measured at  $490 \text{ nm}$  (with background subtraction at  $650 \text{ nm}$ ). Culture medium was tested as a blank control. All LDH values are corrected for the total amount of LDH in cells. To measure the total amount of LDH, cells in an insert (incubator control) were lysed with 2% triton X-100 (Thermo Fisher Scientific Inc., the Netherlands) for 5 minutes.

## 2.7 Release of pro-inflammatory mediators

To investigate effects of particles on pro-inflammatory responses, the production of pro-inflammatory mediators (IL-6 and IL-8) in basolateral medium was measured using the enzyme-linked immunosorbent assay (ELISA) kit (eBioscience, San Diego, USA). As a positive control substance, lipopolysaccharide (LPS) was sprayed to the apical side of Calu-3 model for inducing pro-inflammatory responses. The detailed exposure protocol can be found in the supplementary information.

## 2.8 Statistical analysis

Applying the adverse responses at 5 dose groups, the benchmark dose (BMD) analysis (EFSA 2009) was performed with PROAST (version 65.2 [www.rivm.nl/proast](http://www.rivm.nl/proast)) to create a dose-response relationship for each UFPs sample. This analysis has the advantage that it estimates the BMD with a confidence interval, increasing the reliability of outcomes and allowing to compare the toxicity of UFPs samples. The detailed description of BMD analysis can be found in our earlier study (Gosens et al., 2016). The analysis was performed at a defined effect size (benchmark response (BMR)). For the release of LDH and inflammatory mediators (IL-6 and IL-8), a BMR of 10% change compared to the incubator control level was chosen according to the EFSA (2009). When applying this statistical analysis at the predefined BMR, several dose-response models were fitted to results and the optimal model would be turned out after modeling. The Hill model was used in the present study and lower 5% and upper 95% confidence limits (one sided, BMDL and BMDU, respectively) of the corresponding BMD as well as mean BMD were derived with the Hill model. The 90% BMD confidence interval ( $\text{BMD}_{\text{c.i.}}$ ) including BMDL, BMDU, and average BMD values was presented per effect marker that represented the degree of toxicity. The narrower the  $\text{BMD}_{\text{c.i.}}$  is, the more certain this dose interval can lead to the predefined effect. The  $\text{BMD}_{\text{c.i.}}$  was also used for potency comparison between UFPs samples (EFSA 2009).

The more overlapping between  $BMD_{c.i.}$  implies less difference in the potency of UFPs samples. If there is no 10% change or no BDMU determined at applied doses, the UFPs sample was not included in the comparison.

### 3. Results

#### 3.1 UFPs samples description

The description and size distributions of the particle samples are presented in **Table 1**. It should be noticed that this is the size distribution of the particles in suspension that can deviate from particle size in the outside air. The mean size of the particles samples in suspension falls within the ultrafine range as defined in this study (<180 nm) with the exception of Turbine 1 sample (204 nm). The mean size of each Non-Airport sample is approximately 50 nm, which is similar to the mean size of the Airport 2 sample. In comparison, the mean size of the Airport 1 sample (97 nm) is twice as large.

#### 3.2 Particles deposition in ALI Cloud system and TEER of Calu-3 cells

A fluorescein sodium salt was used to assess the deposition of parties in ALI Cloud system. Although it is a soluble chemical, as we have generated an aerosol that either included the fluorescein or the collected/purchased particles, we have used this to demonstrate if the droplets themselves were uniformly distributed. On the basis of the fluorescence images, distributions of the fluorescein salt were homogeneous on the membrane of each insert in exposure position. The fluorescence intensity was similar between exposure inserts as well (**Figure S1**). It indicates the fluorescein deposition was uniform within each exposure well and constant across the different wells. Moreover, after nebulization with the Cloud system the deposition of DQ12 quartz ( $\approx 150$  nm in suspension) on membranes of inserts, as a reference, was also analyzed via a TEM. As shown in **Figure S2**, most of particles were evenly deposited on the membrane, while several particles cluster appeared, probably because of the agglomeration and aggregation of particles in the suspension.

To check that Calu-3 cells do form the tight barrier after 14 days (7 days at submerge and 7 days at ALI) culture, TEER of Calu-3 cells was measured before starting the exposure. As shown in **Figure 3A**, Calu-3 cells used for *in vitro* exposure can express high TEER ( $> 800$  ohm $\times$ cm $^2$ ) levels, indicating well-formed tight junction and suitability for particles exposure via ALI Cloud system. TEER of Calu-3 cells was also measured after 24 hrs exposure to Airport and Non-Airport UFPs (**Figure 3B**). All TEER values at each exposed dose showed a slight drop to around 600 ohm $\times$ cm $^2$ , indicating the barrier function in Calu-3 cells still remained upon exposure.

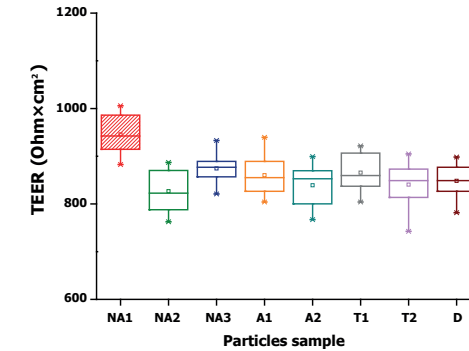


**Figure 3A.** TEER of Calu-3 cells at the ALI before being used for *in vitro* exposure to UFPs samples. NA and A represent Non-Airport and Airport samples, T represents Turbine sample, D represents Diesel sample. Calu-3 cells were at submerged culture for 7 days, followed by ALI culture for 7 days.

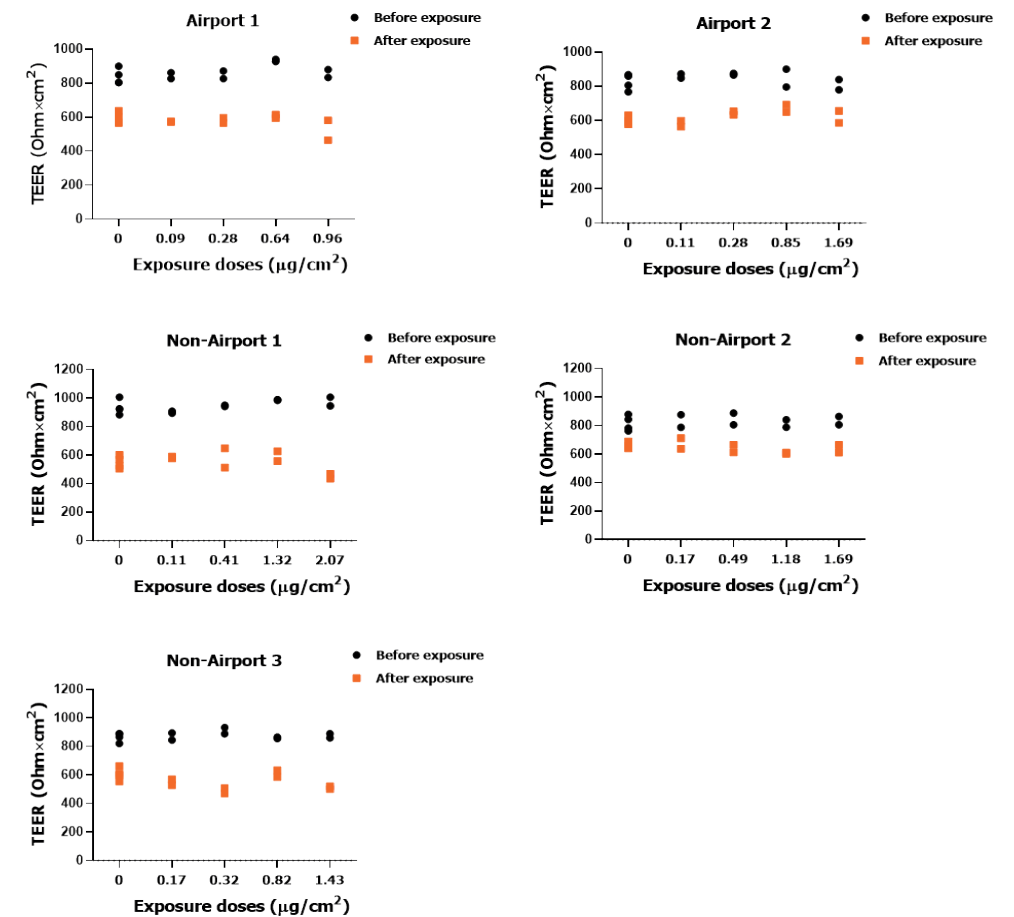


**Figure 3B.** TEER changes of Calu-3 cells after 24 hrs exposure to Airport and Non-Airport UFPs at the ALI.

### 3.3 Cell viability and cytotoxicity

After 24 hrs exposure, cell viabilities are higher than 80% for all particle samples at the exposed doses (Figure 4). LDH release in the medium (apical + basolateral) was also measured (Figure 5) as a marker for cell membrane damage and cytotoxicity. In general, an increased LDH release is only observed at the highest exposed dose around 1.5  $\mu\text{g}/\text{cm}^2$  for most of UFPs samples. For the reference sample (NIST diesel), a clear dose-response relationship can be observed at exposure levels ranging from 0 to 3.6  $\mu\text{g}/\text{cm}^2$ .

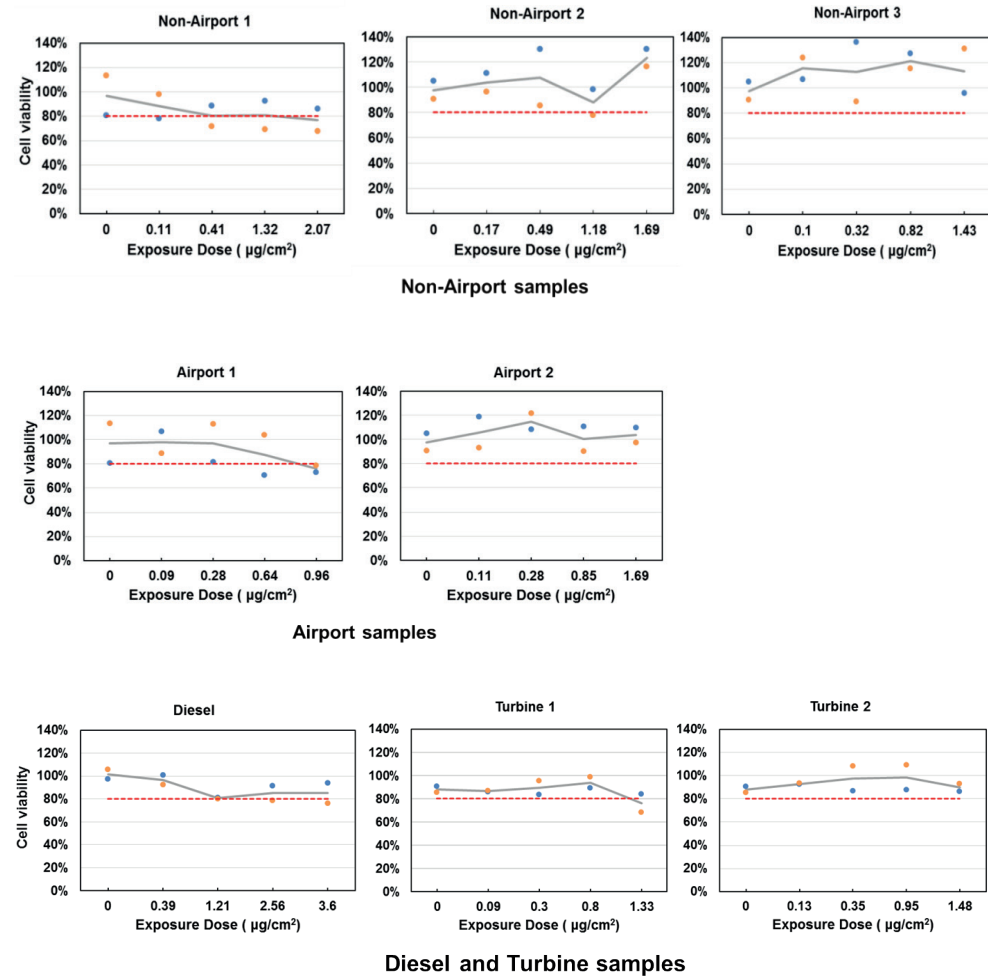


**Figure 4.** Cell viability tested by MTS after exposing to UFPs samples for 24 hrs. The dots represent viability values from the duplicate measurement at applied doses and the trend line was made by average cell viability values at each dose. The dotted line is 80% viability, above which indicates few effects on cell death.

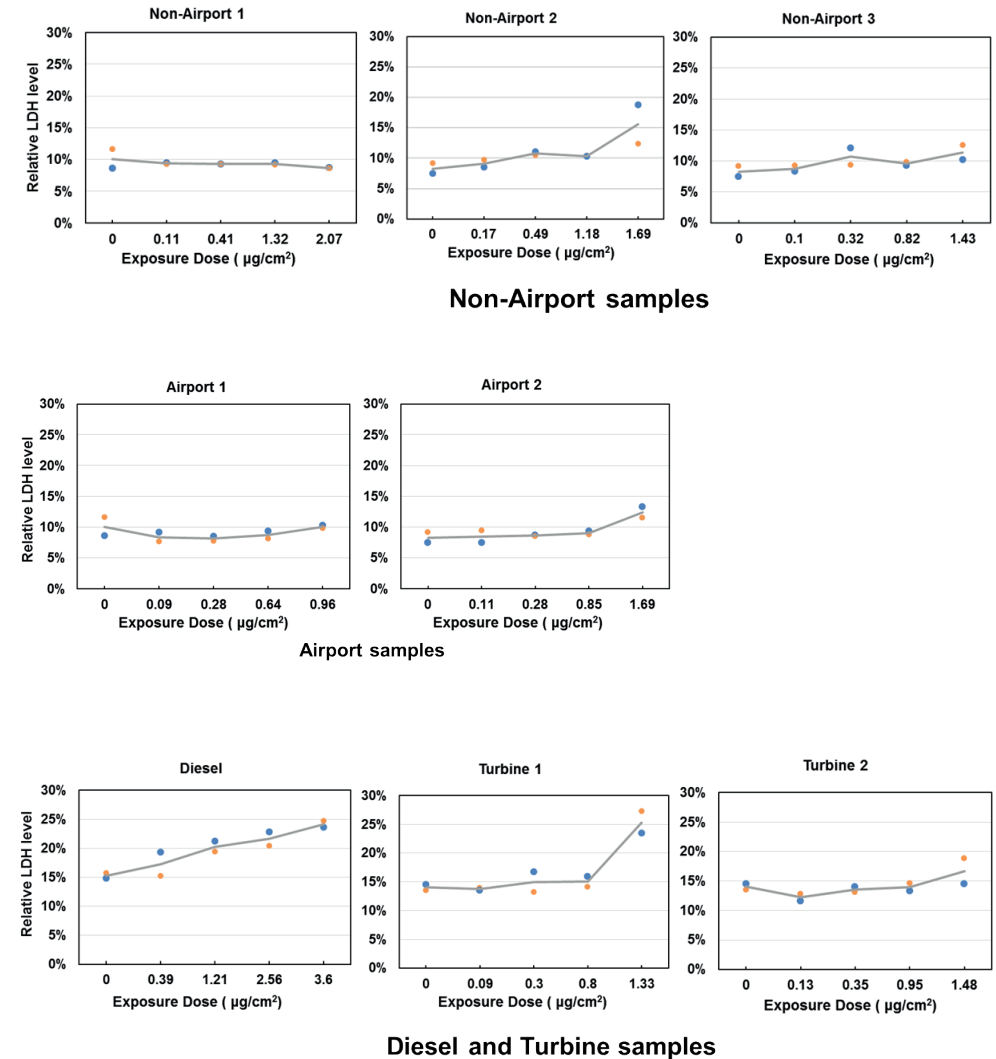


**Figure 5.** Relative LDH release of Calu-3 cells after exposing to UFPs samples for 24 hrs. The dots represent LDH levels from the duplicate measurement at applied doses and the trend line was made by the average LDH levels at each dose.

A BMD analysis was performed to rank the UFPs samples based on the degree of cytotoxicity, BMD values inducing a 10% increase in LDH level were obtained, including the mean BMD, the lower (BMDL) and upper (BMDU) limits of the BMD<sub>c.i.</sub> (Figure 6 and Table 3). The BMDU for Airport 1 sample could not be determined and



Non-Airport 1 sample dose not induce the BMR at exposed doses. It indicates the low cytotoxicity of Airport 1 and Non-Airport 1 samples, which are not included in the comparison. BMDs for the other Airport and Non-Airport samples as well as turbine and diesel samples can be determined, however, no distinctions in LDH levels could be made because of the substantial overlap between their BMDc.i (NIST diesel sample is not used for the comparison because of different collection methods).

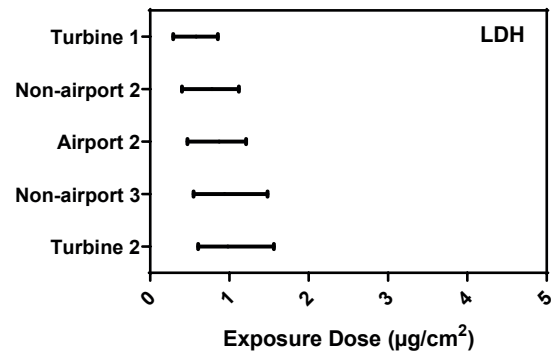


**Figure 6.** Summary of derived BMDs and confidence interval in LDH levels for which a dose-response was found within applied doses. The BMDU for Airport 1 sample could not be determined and Non-Airport 1 sample did not induce the BMR. Both samples were not included in the comparison.

### 3.4 IL-6 and IL-8 production

The production of pro-inflammatory mediators (IL-6 and IL-8) in Calu-3 cells was measured after 24 hrs exposure (**Table 2**). Exposure to UFPs collected from airport and non-airport emissions as well as from a turbine engine at low thrust (Turbine 1) can promote the production of IL-6 and IL-8 mainly at the highest applied dose. When using LPS as a positive control substance to induce pro-inflammatory response (IL-8), Calu-3 cells do show an increased IL-8 secretion (> 2.5 folds), which gives confidence that Calu-3 model is capable of detecting pro-inflammatory responses (**Figure S3**).

According to the outcomes of the performed “BMD analysis” (**Figure 7** and **Table 3**), a 10% BMR could be identified for all particle samples with the exception of Turbine 2 and NIST diesel, indicating few effects on IL-6 and IL-8 production for Turbine 2 and diesel samples at used doses. However, due to the substantial overlapped BMDc.i. between Airport and Non-Airport UFPs samples, no distinctions in cytokines IL-6 and IL-8 levels could be made.

**Table 2.** The concentration of pro-inflammatory mediators (IL-6 and IL-8) in basolateral side medium after exposing to UFPs samples at 5 doses for 24 hrs.

Particle samples	Exposure Dose (µg/cm <sup>2</sup> )	Concentration (pg/mL)	
		IL-6	IL-8
Diesel	0	2891	15926
	0.39	2569	14151
	1.21	2910	16027
	2.56	2816	15509
	3.60	3081	16971
Turbine 1	0	2517	13866
	0.09	2640	14541
	0.30	3003	16543
	0.80	2726	15016
	1.33	3045	16770
Turbine 2	0	2517	13866
	0.13	1821	11529
	0.35	2058	13031
	0.95	2117	13402
	1.48	1977	12515
Non-airport 1	0	1108	6663
	0.11	999	6321
	0.41	957	6056
	1.32	1053	6665
	2.07	1350	8549
Non-airport 2	0	1489	10687
	0.17	1333	9563
	0.49	1615	11585
	1.18	1600	11476
	1.69	1866	13389
Non-airport 3	0	1489	10687
	0.10	1522	10923
	0.32	1788	12825
	0.82	1737	12464
	1.43	1928	13830
Airport 1	0	1108	6663
	0.09	909	5753
	0.28	955	6045
	0.64	1166	7379
	0.96	1496	9469

	0	1489	10687
	0.11	1562	11208
Airport 2	0.28	1599	11474
	0.85	1965	14096
	1.69	2024	14519

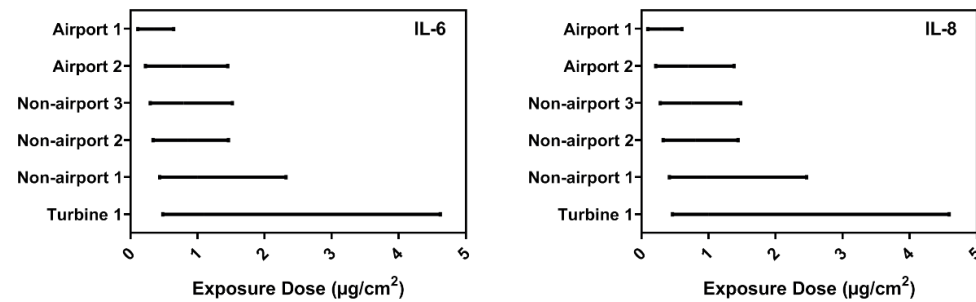


**Figure 7.** Summary of derived BMDs and confidence interval in IL-6 and IL-8 levels for which a dose–response was found within applied doses. Turbine 2 sample did not induce a BMR and was therefore not included in the comparison.

**Table 3.** Summary of derived BMDs in LDH, IL-6 and IL-8 levels including the mean BMD, lower (BMDL) and upper (BMDU) limits of the confidence interval inducing a 10% BMR.

BMR:10%	BMDs ( $\mu\text{g}/\text{cm}^2$ )								
	LDH			IL-6			IL-8		
	Mean	BMDL	BMDU	Mean	BMDL	BMDU	Mean	BMDL	BMDU
Turbine 1	0.58	0.29	0.84	1.1	0.48	4.62	1.0	0.46	4.59
Turbine 2	0.98	0.62	1.56	-	-	-	-	-	-
Non-airport 1	-	-	-	1.0	0.43	2.32	0.98	0.42	2.46
Non-airport 2	0.78	0.40	1.12	0.86	0.34	1.46	0.81	0.32	1.44
Non-airport 3	0.94	0.55	1.48	0.79	0.29	1.52	0.75	0.28	1.45
Airport 1	0.87	0.55	-	0.35	0.11	0.66	0.31	0.09	0.60
Airport 2	0.87	0.47	1.21	0.76	0.22	1.45	0.7	0.21	1.38
Diesel <sup>1</sup>	1.9	1.01	2.69	3.5	1.7	-	3.5	1.65	-

“-”: could not be determined

<sup>1</sup>. NIST diesel sample is not used for the direct comparison of the toxicity to the other UFPs samples because of different collection methods

## 4. Discussion

Our findings show that cell damage and the secretion of pro-inflammatory mediators can occur in a Calu-3 model after exposure to UFPs from airport a non-airport emission as well as from an aircraft turbine engine. There are no indications that the health effects of airport emission are substantially different from those caused by road traffic emissions applying similar exposure doses (on a mass basis).

The exposed doses (0.09 to 2.07  $\mu\text{g}/\text{cm}^2$ ) of particles in this study are substantially lower than those have been previously reported in other *in vitro* studies. For example, the research on Los Angeles International Airport (LAX), in which the toxicity of PM <0.25  $\mu\text{m}$  collected from aviation activities and urban traffic area was compared, assumed a dosage of 3.13  $\mu\text{g}/\text{cm}^2$  (He et al 2018). In the RAPTES study (Steenhof et al 2011), increasing doses from 3.68 to 58.8  $\mu\text{g}/\text{cm}^2$  were used to compare the *in vitro* toxicity of PM samples with three size fractions and from different sources in the Netherlands. Comparable doses of particles used in our study were also used in a recent *in vitro* study, in which human bronchial epithelial (BEAS-2B) cells were directly exposed to diluted emissions from a turbine engine under stationary condition at very low doses (2.1 - 6.9  $\text{ng}/\text{cm}^2$ ) and at doses of 0.3-0.4  $\mu\text{g}/\text{cm}^2$  with the engine speed corresponding to ascending airplanes (Jonsdottir et al 2019). Comparing the exposure levels used in those *in vitro* studies to levels people are actually exposed to in the environment, including airport surroundings, is difficult. Especially for UFPs when exposure doses related to mass concentrations are used, while for ultrafine particles particle size and particle number concentrations may be more relevant.

To our knowledge, this is the first ALI exposure to air pollution UFPs done with Calu-3 model. For the reference diesel sample a clear increase in LDH release was seen with the exposure doses increase, however, production of IL-6 and IL-8 induced at each dose were at comparable level to the exposure control (0  $\mu\text{g}/\text{cm}^2$ ). This low production of pro-inflammatory cytokines was also observed in another bronchial epithelial (BEAS-2B) cells line after exposure to diesel particles (SRM 2975) at doses ranging from 1.0  $\mu\text{g}/\text{cm}^2$  to 110  $\mu\text{g}/\text{cm}^2$  (Chaudhuri et al 2010). A possible explanation for the limited induction of pro-inflammatory response is that the large size distribution of diesel particles ( $\approx 177\pm 91$  nm) might lead to the less cellular internalization of particles, thus limiting the release of pro-inflammatory cytokines in Calu-3 cells (Hussain et al., 2009, He et al 2018). In line with the growing awareness that cellular adverse effects including the inflammation can still be induced at high cell viability (Bitterle et al 2006, He et al 2018), up-regulation of pro-inflammatory mediators (10% increase of IL-6 and IL-8 secretion) was observed in Calu-3 cells after Airport and Non-Airport UFPs exposure at levels ranging from 0.35 to 1.0  $\mu\text{g}/\text{cm}^2$  (Table 3). The effect doses of

UFPs on Calu-3 cells that cause the pro-inflammatory responses under ALI exposure are substantially lower in comparison with those on Calu-3 cells using submerged exposure (Mura et al 2011, Puisney et al 2018). For example, Puisney et al (2018) reported only limited up-regulation of inflammatory marker (IL-6) in Calu-3 cells after submerged exposure to the nano-sized particles at dose of 1.0 - 10  $\mu\text{g}/\text{cm}^2$ . The exposure method may be a critical factor influencing the effect dose. Compared to the traditional submerged exposure via medium, ALI exposure reflects more relevant and realistic human inhalation exposure, allowing particles to be deposited at the epithelial cell surface instead of agglomeration and diffusion in the medium (Limbach et al 2005), consequently resulting in the lower effect doses of UFPs under ALI exposure. A recent review about *in vitro* exposures also concluded that in relation to the production of the inflammatory marker (IL-8) after particles exposure, the deposited dose recorded at ALI exposure is more informative than the administered dose used for submerged exposure (Secondo et al 2017).

Besides the exposure method, effect doses can also be influenced by cell types used in ALI exposure. Jonsdottir et al (2019) performed an *in vitro* exposure at ALI with similar design, which showed the over-production of inflammatory mediators (IL-6 and IL-8) in human bronchial epithelial (BEAS-2B) cells after exposing to diluted emissions from a stationary engine at very low doses (2.1 - 6.9  $\text{ng}/\text{cm}^2$ ). These low effect doses may indicate the higher sensitivity in BEAS-2B cells than that in Calu-3 cells when exposed to UFPs under ALI condition. The high resistance in Calu-3 cells at ALI might be an explanation. ALI condition promotes the differentiation of Calu-3 cells in producing the thick mucus and forming the tight junction, which are the functional characteristics in lungs (Grainger et al 2006, Vllasaliu et al 2011). The mucociliary clearance and well-formed tight junction can therefore provide much more resistance to particles exposure in Calu-3 cells compared to other *in vitro* models (e.g. BEAS-2B and A549 cells) with the weak cellular clearance and tight junction formation at ALI (Bitterle et al 2006, Heijink et al 2010). Such high resistance in Calu-3 cells at ALI was also reported in Banga et al, (2012), showing that no changes were detected in levels of some cytokines including IL-8 in Calu-3 cells (ALI culture for 14 days) after exposing to nanoparticles (<100 nm) at 4  $\mu\text{g}/\text{cm}^2$  and 4  $\text{ng}/\text{cm}^2$ . However, that lack of macrophages, which is a limitation of the current epithelial Calu-3 model, might be another explanation of lower sensitivity of this cell type for cytokine production. Possibly, macrophages can produce pro-inflammatory mediators after the uptake of UFPs that subsequently may affect Calu-3 cells, promoting cellular responses to UFPs (Hu and Christman 2019).

When starting a risk assessment of exposure to UFPs, BMDs for various cellular responses can be used to identify the degree of toxicity (EFSA 2009). Substantial overlap between the  $\text{BMD}_{\text{c.i.}}$  of UFPs from airport and non-airport emissions was shown in LDH, IL-6 and IL-8 levels, which indicates the comparable ability of these UFPs samples to induce the

cytotoxicity and pro-inflammatory responses in Calu-3 cells. An explanation for their similar toxicity is the mild effects on the cytotoxicity and inflammation, which might be due to the low deposited dose. With the mild effects, the range of  $\text{BMD}_{\text{c.i.}}$  is wide, which makes the  $\text{BMD}_{\text{c.i.}}$  of UFPs samples difficult to distinguish. The insignificant difference on size distribution between Airport and Non-Airport UFPs might be another explanation. A large amount of research has reported differences in size can lead to different toxicity of particles. Particles in smaller size can absorb more organic and inorganic substances and deposit on the respiratory tract with higher efficiency, which increase their toxicity per unit of inhaled mass (Terzano et al., 2010, Li et al 2003, Schwarze et al 2006). Unlike previous findings that the particle size in airport emission was clearly smaller than that in road traffic emission (Keuken et al 2015, Shirmohammadi et al 2017), size distributions of airport and road traffic UFPs samples are similar in the present study with the exception of Airport 1 sample which is even twice as large as the mean size. This indicated that size distribution in UFPs suspension may differ from size distribution of UFPs in ambient air, since the smaller particles can easily clump together and form larger particles during collecting and extracting the UFPs in/from the filter (Yu et al 1997). To overcome this limitation, the combination of particles sampling system and ALI exposure system can be implemented to provide the real-time UFPs exposure. The optimization of the ALI exposure system is currently ongoing.

## Conclusion

UFPs from airport, non-airport (road traffic) origin as well as from a turbine engine can induce the cell damage and release of pro-inflammatory markers. No substantial differences are identified among UFPs samples in their toxic potency at the applied doses, suggesting that UFPs from airport and road traffic in airport surroundings may have similar adverse effects on public health.

## Acknowledgements

This research has been commissioned by the Dutch Ministry of Infrastructure and Water management for the research program M240045 “Gezondheidsrisico’s ultrafijn stof rond Schiphol”. We thank Eric Gremmer and Ilse Gosens from the National Institute for Public Health and the Environment (RIVM) for their valuable assistance with the *in vitro* measurements, BMD analysis. We thank Remco Westerink from the Institute for Risk Assessment Sciences (IRAS), Utrecht University for his insightful comments on the manuscript. We are also grateful to Barbara Drasler and Dimitri Vanhecke from the Adolphe Merkle Institute, University of Fribourg for their kind assistance with the TEM microscopy. The support provided by China Scholarship Council (CSC) during the PhD period of Rui-Wen He in Utrecht University- IRAS is also acknowledged.



## References

- A. Lammers, N.A.H. Janssen, A.J.F. Boere, M. Berger, C. Longo, S.J.H. Vijverberg, A.H. Neerinx, A.H. Maitland - van der Zee, F. R. Cassee. Effects of short-term exposures to ultrafine particles near an airport in healthy subjects. *Environment International*, in press
- Antherieu, S., Garat, A., Beauval, N., Soyeux, M., Allorge, D., Garcon, G., & Lo-Guidice, J.-M. (2017). Comparison of cellular and transcriptomic effects between electronic cigarette vapor and cigarette smoke in human bronchial epithelial cells. *Toxicology in Vitro*, 45, 417-425.
- Banga A, Witzmann FA, Petrache HI, Blazer-Yost BL. 2012. Functional effects of nanoparticle exposure on Calu-3 airway epithelial cells. *Cellular Physiology and Biochemistry* 29:197-212
- BéruBé K, Prytherch Z, Job C, Hughes T. 2010. Human primary bronchial lung cell constructs: the new respiratory models. *Toxicology* 278: 311-18
- Bitterle E, Karg E, Schroeppl A, Kreyling W, Tippe A, et al. 2006. Dose-controlled exposure of A549 epithelial cells at the air-liquid interface to airborne ultrafine carbonaceous particles. *Chemosphere* 65: 1784-90
- Braakhuis HM, Park MV, Gosens I, De Jong WH, Cassee FR. 2014. Physicochemical characteristics of nanomaterials that affect pulmonary inflammation. *Particle and fibre toxicology* 11(1):18
- Chaudhuri N, Paiva C, Donaldson K, Duffin R, Parker LC, Sabroe I. 2010. Diesel exhaust particles override natural injury-limiting pathways in the lung. *American Journal of Physiology-Lung Cellular and Molecular Physiology* 299: L263-L71
- Demokritou P, Kavouras I, Ferguson S, Koutrakis P. 2002. Development of a high volume cascade impactor for toxicological and chemical characterization studies. *Aerosol Science & Technology* 36: 925-33
- EFSA. 2009. "Guidance of the Scientific Committee on Use of the benchmark dose approach in risk assessment." *EFSA Journal* 7(6): 1150.
- Fizeşan I, Cambier S, Moschini E, Chary A, Nelissen I, Ziebel J, Audinot J-N, Wirtz T, Kruszewski M, Pop A. 2019. *In vitro* exposure of a 3D-tetraculture representative for the alveolar barrier at the air-liquid interface to silver particles and nanowires. *Particle and fibre toxicology* 16: 14
- Gerlofs-Nijland ME, Totlandsdal AI, Tzankiozis T, Leseman DLC, Samaras Z, et al. 2013. Cell toxicity and oxidative potential of engine exhaust particles: impact of using particulate filter or biodiesel fuel blend. *Environmental science & technology* 47: 5931-38
- Gosens I, Cassee FR, Zanella M, Manodori L, Brunelli A, et al. 2016. Organ burden and pulmonary toxicity of nano-sized copper (II) oxide particles after short-term inhalation exposure. *Nanotoxicology* 10: 1084-95
- Grainger CI, Greenwell LL, Lockley DJ, Martin GP, Forbes B. 2006. Culture of Calu-3 cells at the air interface provides a representative model of the airway epithelial barrier. *Pharmaceutical research* 23: 1482-90
- Heijink IH, Brandenburg SM, Noordhoek JA, Postma DS, Slebos D-J, van Oosterhout AJ. 2010. Characterisation of cell adhesion in airway epithelial cell types using electric cell-substrate impedance sensing. *European Respiratory Journal* 35: 894-903
- He R-W, Shirmohammadi F, Gerlofs-Nijland ME, Sioutas C, Cassee FR. 2018. Pro-inflammatory responses to PM<sub>0.25</sub> from airport and urban traffic emissions. *Science of the Total Environment* 640: 997-1003
- Heusinkveld HJ, Wahle T, Campbell A, Westerink RH, Tran L, et al. 2016. Neurodegenerative and neurological disorders by small inhaled particles. *Neurotoxicology* 56: 94-106
- Hudda N, Fruin S. 2016. International airport impacts to air quality: size and related properties of large increases in ultrafine particle number concentrations. *Environmental science & technology* 50: 3362-70
- Hu G, CHRISTMAN JW. 2019. Alveolar Macrophages in Lung Inflammation and Resolution. *Frontiers in Immunology* 10: 2275
- Hussain S, Boland S, Baeza-Squiban A, Hamel R, Thomassen LC, Martens JA, Billon-Galland MA, Fleury-Feith J, Moisan F, Pairon J-C. 2009. Oxidative stress and proinflammatory effects of carbon black and titanium dioxide nanoparticles: Role of particle surface area and internalized amount. *Toxicology* 260:142-149.
- Jonsdottir HR, Delaval M, Leni Z, Keller A, Brem BT, et al. 2019. Non-volatile particle emissions from aircraft turbine engines at ground-idle induce oxidative stress in bronchial cells. *Communications Biology* 2: 90
- Keuken M, Moerman M, Zandveld P, Henzing J, Hoek G. 2015. Total and size-resolved particle number and black carbon concentrations in urban areas near Schiphol airport (the Netherlands). *Atmospheric Environment* 104: 132-42
- Kim HR, Lee K, Park CW, Song JA, Park YJ, Chung KH. 2016. Polyhexamethylene guanidine phosphate aerosol particles induce pulmonary inflammatory and fibrotic responses. *Archives of toxicology* 90: 617-32
- Lenz A-G, Stoeger T, Cei D, Schmidmeir M, Semren N, et al. 2014. Efficient bioactive delivery of aerosolized drugs to human pulmonary epithelial cells cultured in air-liquid interface conditions. *American journal of respiratory cell and molecular biology* 51: 526-35
- Li N, Sioutas C, Cho A, Schmitz D, Misra C, et al. 2003. Ultrafine particulate pollutants induce oxidative stress and mitochondrial damage. *Environmental health perspectives* 111: 455
- Limbach LK, Li Y, Grass RN, Brunner TJ, Hintermann MA, et al. 2005. Oxide nanoparticle uptake in human lung fibroblasts: effects of particle size, agglomeration, and diffusion at low concentrations. *Environmental science & technology* 39: 9370-76
- Maier KL, Alessandrini F, Beck-Speier I, Josef Hofer TP, Diabaté S, et al. 2008. Health effects of ambient particulate matter—biological mechanisms and inflammatory responses to *in vitro* and *in vivo* particle exposures. *Inhalation toxicology* 20: 319-37
- Masiol M, Harrison RM. 2014. Aircraft engine exhaust emissions and other airport-related contributions to ambient air pollution: a review. *Atmospheric Environment* 95: 409-55
- Miller MR, Raftis JB, Langrish JP, McLean SG, Samutrtai P, et al. 2017. Inhaled nanoparticles accumulate at sites of vascular disease. *ACS nano* 11: 4542-52
- Mülhopt S, Dilger M, Diabaté S, Schlager C, Krebs T, Zimmermann R, Buters J, Oeder S, Wäscher T, Weiss C. 2016. Toxicity testing of combustion aerosols at the air-liquid interface with a self-contained and easy-to-use exposure system. *Journal of Aerosol Science* 96: 38-55
- Mura S, Hillaireau H, Nicolas J, Le Droumaguet B, Gueutin C, et al. 2011. Influence of surface charge on the potential toxicity of PLGA nanoparticles towards Calu-3 cells. *International journal of nanomedicine* 6: 2591
- Pirhadi M, Mousavi A, Sowlat MH, Janssen NA, Cassee FR, Sioutas C. 2020. Relative contributions of a major international airport activities and other urban sources to the particle number concentrations (PNCs) at a nearby monitoring site. *Environmental Pollution*: 114027
- Puisney C, Oikonomou EK, Nowak S, Chevillot A, Casale S, et al. 2018. Brake wear (nano) particle characterization and toxicity on airway epithelial cells *in vitro*. *Environmental Science: Nano* 5: 1036-44
- Ren J, Cao X, Liu J. 2018. Impact of atmospheric particulate matter pollutants to IAQ of airport terminal buildings: A first field study at Tianjin Airport, China. *Atmospheric environment* 179: 222-26
- Riley EA, Gould T, Hartin K, Fruin SA, Simpson CD, et al. 2016. Ultrafine particle size as a tracer for aircraft turbine emissions. *Atmospheric environment* 139: 20-29
- Schwarze P, Øvreivik J, Låg M, Refsnes M, Nafstad P, et al. 2006. Particulate matter properties and health effects: consistency of epidemiological and toxicological studies. *Human & experimental toxicology* 25: 559-79
- Secondo LE, Liu NJ, Lewinski NA. 2017. Methodological considerations when conducting *in vitro*, air-liquid interface exposures to engineered nanoparticle aerosols. *Critical reviews in toxicology* 47: 225-62
- Shirmohammadi F, Lovett C, Sowlat M, Mousavi A, Verma V, et al. 2017. Chemical composition and redox activity of PM<sub>0.25</sub> near Los Angeles International Airport and comparisons to an urban traffic site. *The Science of the total environment* 610: 1336
- Stacey B. 2019. Measurement of ultrafine particles at airports: A review. *Atmospheric environment*
- Steenhof M, Gosens I, Strak M, Godri KJ, Hoek G, et al. 2011. *In vitro* toxicity of particulate matter (PM) collected at different sites in the Netherlands is associated with PM composition, size fraction and oxidative potential-the RAPTES project. *Particle and fibre toxicology* 8: 26
- Stone V, Miller MR, Clift MJ, Elder A, Mills NL, et al. 2017. Nanomaterials versus ambient ultrafine particles: an opportunity to exchange toxicology knowledge. *Environmental health perspectives* 125: 106002
- Terzano C, Di Stefano F, Conti V, Graziani E, Petroianni A. 2010. Air pollution ultrafine particles: toxicity beyond the lung. *Eur Rev Med Pharmacol Sci* 14: 809-21
- Vllasaliu D, Fowler R, Garnett M, Eaton M, Stolnik S. 2011. Barrier characteristics of epithelial cultures modelling the airway and intestinal mucosa: a comparison. *Biochemical and biophysical research communications* 415: 579-85
- Winther M, Kousgaard U, Ellermann T, Massling A, Nøjgaard JK, Ketzler M. 2015. Emissions of NO<sub>x</sub>, particle mass and particle numbers from aircraft main engines, APU's and handling equipment at Copenhagen Airport. *Atmospheric Environment* 100: 218-29
- Yu A-B, Bridgwater J, Burbidge A. 1997. On the modelling of the packing of fine particles. *Powder technology* 92: 185-94



## Supplementary Material

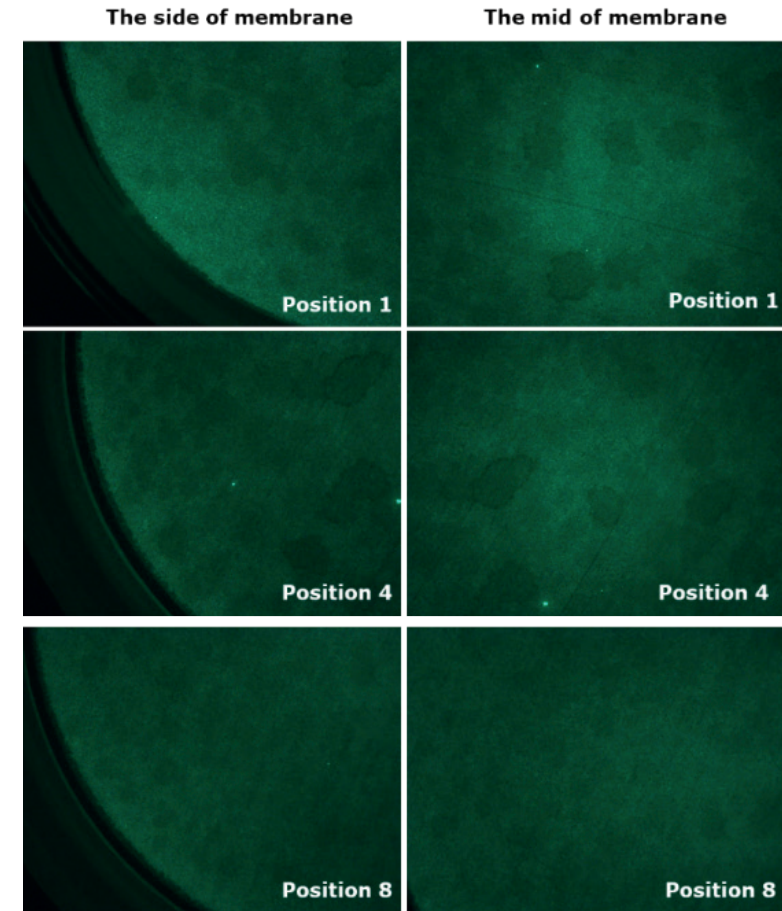
### Materials and methods

#### 1. Particles distribution in Cloud exposure system

The fluorescein sodium salt was dissolved into Milli-Q water with 0.01% NaCl solution to make the stock solution at 2.4 mM. Subsequently, 200  $\mu$ L of the stock solution was sprayed to a dense cloud of droplets with particles in Cloud exposure system, sodium salts were deposited into cell-free inserts by the sedimentation of droplets. After deposition, inserts were observed under the fluorescence microscope (Olympus BX51, Shinjuku, Japan). Each membrane was then washed by 2mL Milli-Q water, the collected wash solution was used for fluorescence intensity measurement. Besides, 100  $\mu$ L of DQ12 suspension (1000  $\mu$ g/mL in Milli-Q water with 0.01% NaCl solution) was also sprayed to a dense cloud of droplets with particles in Cloud exposure system. After deposition, inserts were observed under the a Tecnai spirit TEM (Thermo Fisher/FEI, Hillsboro, Oregon, US) with a 4096x4096 Eagle CCD camera (Thermo Fisher/FEI, Hillsboro, Oregon, US).

#### 2. Lipopolysaccharide (LPS) exposure

Calu-3 cells were prepared under ALI condition as described in 2.3. For ALI exposure to LPS substance, 0 and 350  $\mu$ g /mL LPS solution (Milli-Q water with 0.01% NaCl) was nebulized to the apical side of the Calu-3 model in the Cloud system, the exposed dose of LPS is around 0.45  $\mu$ g/cm<sup>2</sup> via a microbalance. Subsequently, all inserts were transferred to a new 12-wells plates with 1.5 mL fresh culture medium on the basolateral side and then cultured in an incubator for 24 hrs. The basolateral side medium was collected from each insert for measuring IL-8 production.



Position number	Fluorescence intensity ( $\mu$ M)
1	2.2 $\pm$ 0.4
2	2.6 $\pm$ 0.4
3	2.3 $\pm$ 0.4
4	2.7 $\pm$ 0.5
5	2.4 $\pm$ 0.4
6	2.2 $\pm$ 0.7
7	2.5 $\pm$ 0.6
8	2.2 $\pm$ 0.5

**Figure S1.** The distribution of fluorescein sodium salts on the side and in the middle of the membrane insert as well as the fluorescence intensity of membrane insert at each position. Number 1-8 represents the exposure position in Cloud system shown in **Figure 2A**.

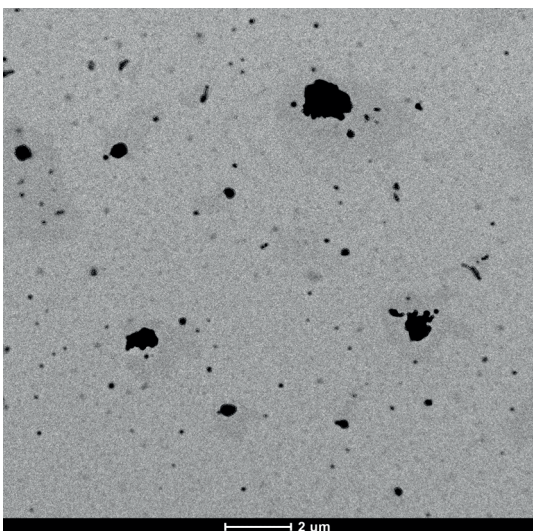


**Figure S2.** TEM image of DQ12 quartz after nebulization via the Cloud system. Scale bar: 2  $\mu\text{m}$ ;

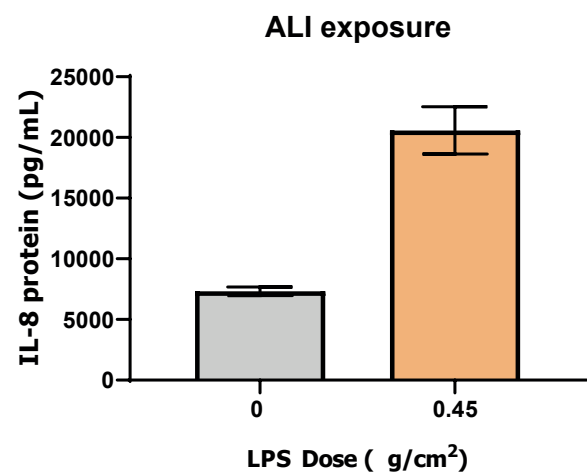


**Figure S3.** Production of cytokine IL-8 from Calu-3 cells after ALI exposure to LPS for 24 hrs. The dissolve solution, Milli-Q water with 0.01% NaCl, was used for exposure control (0  $\mu\text{g}/\text{cm}^2$ ).

# Chapter 5

## ***In vitro* hazard characterization of simulated aircraft cabin bleed-air contamination in lung models using an air-liquid interface (ALI) exposure system**

Rui-Wen He <sup>ab</sup>, Marc M.G. Houtzager <sup>c</sup>, W.P. Jongeneel <sup>a</sup>, Remco H. S. Westerink <sup>b</sup>, Flemming R. Cassee <sup>ab\*</sup>

<sup>a</sup> National Institute for Public Health and the Environment (RIVM), P.O. Box 1, 3720 BA, Bilthoven, The Netherlands

<sup>b</sup> Institute for Risk Assessment Sciences (IRAS), Toxicology Division, Faculty of Veterinary Medicine, Utrecht University, P.O. Box 80177, 3508 TD, Utrecht, The Netherlands

<sup>c</sup> The Netherlands Organisation for Applied Scientific Research, TNO, P.O. Box 80015, 3508 TA Utrecht, The Netherlands

(Environment International, 2021, Volume 156, 106718, ISSN 0160-4120)

## Highlights

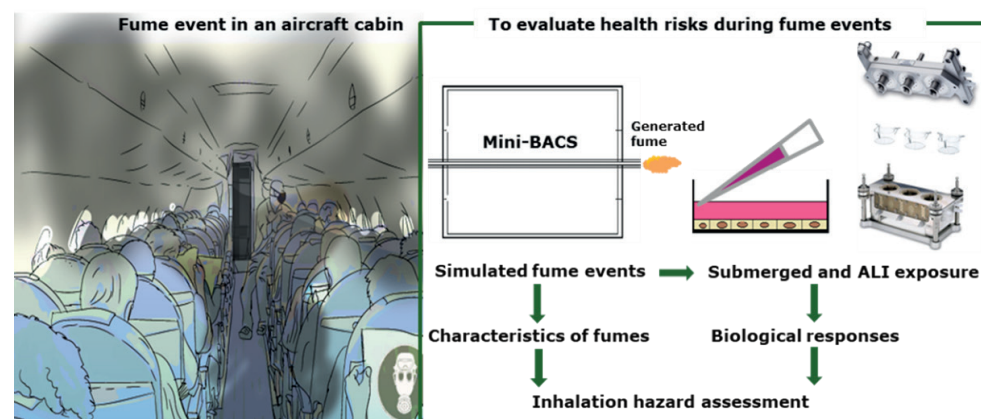
“Mini-BACS + AES” setup can be used for *in vitro* hazard characterization of simulated fume events.

Aircraft hydraulic fluid fumes are more harmful than engine oil fumes.

Higher OP level and smaller particle size may contribute to higher toxicity of hydraulic fluid fumes.

Our results clearly reflect potential health risks associated with fume events in aircraft cabins.

## Graphical abstract



## Abstract

Contamination of aircraft cabin air can result from leakage of engine oils and hydraulic fluids into bleed air. This may cause adverse health effects in cabin crews and passengers. To realistically mimic inhalation exposure to aircraft cabin bleed-air contaminants, a mini bleed-air contaminants simulator (Mini-BACS) was constructed and connected to an air-liquid interface (ALI) aerosol exposure system (AES). This unique “Mini-BACS + AES” setup provides steady conditions to perform ALI exposure of the mono- and co-culture lung models to fumes from pyrolysis of aircraft engine oils and hydraulic fluids at respectively 200 °C and 350 °C. Meanwhile, physicochemical characteristics of test atmospheres were continuously monitored during the entire ALI exposure, including chemical composition, particle number concentration (PNC) and particles size distribution (PSD). Additional off-line chemical characterization was also performed for the generated fume. We started with submerged exposure to fumes generated from 4 types of engine oil (Fume A, B, C, and D) and 2 types of hydraulic fluid (Fume E and F). Following submerged exposures, Fume E and F as well as Fume A and B exerted the highest toxicity, which were therefore further tested under ALI exposure conditions. ALI exposures reveal that these selected engine oil (0 – 100 mg/m<sup>3</sup>) and hydraulic fluid (0 – 90 mg/m<sup>3</sup>) fumes at tested dose-ranges can impair epithelial barrier functions, induce cytotoxicity, produce pro-inflammatory responses, and reduce cell viability. Hydraulic fluid fumes are more toxic than engine oil fumes on the mass concentration basis. This may be related to higher abundance of organophosphates (OPs, ≈ 2800 µg/m<sup>3</sup>) and smaller particle size (≈ 50 nm) of hydraulic fluid fumes. Our results suggest that exposure to engine oil and hydraulic fluid fumes can induce considerable lung toxicity, clearly reflecting the potential health risks of contaminated aircraft cabin air.

**Keywords:** Fume event; Aircraft cabin air; Mini-BACS; Organophosphates; Co-culture; BMD analysis.



## 1. Introduction

Concerns have been raised regarding the potential health risks of exposure to contaminated air in aircraft cabins (Michaelis, 2011; Ramsden, 2012; Winder and Michaelis, 2005). Health effects reported by a fraction of aircraft cabin crews include cough, sore throat, nausea, dizziness, disorientation, and tremors during flight. Those health complaints, which are sometimes collectively referred to as “aerotoxic syndrome” (Michaelis et al., 2017; Van Netten, 2005), have been associated with exposure to cabin air contaminants, particularly during so-called fume events (Abou-Donia et al., 2013; Brown et al., 2001; Reneman et al., 2016; Winder and Michaelis, 2005).

The primary source of outside air used to pressurize and ventilate the cabin and cockpit (so-called “bleed air”) is extracted from the main engine compressors (during flight) or from the Auxiliary Power Unit (on ground level). Bleed air passes through the air conditioning system (so-called “PACKs”) of the Environmental Control System (ECS) before being distributed to aircraft cabin and cockpit. However, during this process, bleed air contamination may occur, for example, due to oil leaks. Oils from those leaks are subjected to high temperatures and their thermal degradation products can contaminate bleed air, subsequently resulting in aircraft cabin air contamination (Michaelis, 2011; Michaelis, 2016). It has been reported that organophosphates (OPs), volatile organic compounds (VOCs), carbon monoxide (CO) and ultrafine particles (UFPs, particle size < 100 nm) are the main contaminants (Denola et al., 2011; Howard et al., 2018; Shehadi et al., 2016; Solbu et al., 2011).

Inhalation exposure to a complex mixture of those contaminants in an aircraft cabin may pose considerable health risks for crews and passengers (Michaelis et al., 2017). A large health survey on 4011 flight attendants, conducted by the Occupational Health Research Consortium in Aviation (OHRCA) in 2014, showed that almost 50% of flight attendants reported one or more symptoms, in which respiratory symptoms and neurological problems accounted for 23% and 17%, respectively (OHRCA, 2014). However, given the difficulties to capture fume events in real time in aircraft cabins, current information on characteristics of fume events as well as their inhalation toxicity is still scarce.

The use of a simulation setup for generating fumes under controlled laboratory conditions allows a steady output of test atmospheres to measure the composition (e.g. chemicals and particles) of fume events, regardless the type and state of the engine or ECS. It has been reported that various chemicals can be derived from simulated fume events, of which CO and tricresyl phosphate (TCP) isomers were

the most frequently reported compounds (Van Netten and Leung, 2001; Winder and Balouet, 2002). High concentrations of UFPs were also detected after pyrolysis of aircraft engine oils (Amiri et al., 2017; Mann et al., 2014). The chemical composition of fume emissions from laboratory pyrolysis can differ depending on oil types (Van Netten and Leung, 2001), which probably affects toxic properties of the generated fumes. Therefore, understanding the composition profile of fumes generated from different types of aircraft engine oil and hydraulic fluid is essential for further investigation of inhalation toxicity by cabin air contaminants.

Upon inhalation, particles can be gradually deposited onto human tracheobronchial epithelium based on the size and aerodynamic behaviour (Braakhuis et al., 2014). Therefore, human bronchial epithelial cell models are preferred for inhalation exposure studies. To more accurately evaluate the responses to UFPs originating from, for example, pyrolyzed oils, macrophages can be added onto the epithelial carpet (Ji et al., 2018; Wottrich et al., 2004), as macrophages are known to play an important role in the uptake and clearance of particles in the lungs (Hu and Christman, 2019). Importantly, cell models should allow for a continuous exposure to the generated fumes under air-liquid interface (ALI) exposure conditions to realistically mimic inhalation exposure of the bronchial epithelium.

The primary goal of this study is to investigate the hazards of simulated aircraft fume events under controlled laboratory conditions. We hypothesize that aircraft engine oil and hydraulic fluid fumes can induce cytotoxicity and inflammation responses in human lung cell models under ALI exposure conditions. To test this hypothesis, a mini bleed-air contaminants simulator (Mini-BACS) was set up for generating fumes, including 4 types of engine oil fumes (Fume A, B, C, and D) and 2 types of hydraulic fluid fumes (Fume E and F). Chemical composition, particle number concentration (PNC), and particles size distribution (PSD) of the generated fumes were investigated. For testing the toxicity of the generated fumes *in vitro*, we started with submerged exposure of the lung model to establish a dose-response relationship to gain a basic understanding of their toxic potency. In accordance with the results obtained from submerged exposure, the 4 types of fume samples that exerted the highest toxicity were selected and subsequently tested under ALI exposure conditions to further evaluate their toxicity. An aerosol exposure system (AES) was connected with the Mini-BACS to allow long-term ALI exposure to the generated fumes using a monoculture of human bronchial epithelial (Calu-3) cells and a co-culture of Calu-3 + human monocyte-derived macrophages (MDMs). Adverse effects on the cell models, including changes in transepithelial electrical resistance (TEER), cell viability, lactate dehydrogenase (LDH) release and inflammatory responses, were measured at 24 hours

post exposure. Additionally, the off-line chemical characterization was performed to measure the concentrations of aldehydes-ketones, OPs, VOCs, and organic acids in the generated aircraft cabin fumes.

## 2. Materials and methods

### 2.1 Chemicals and reagents

We selected 4 types of engine oil and 2 types of hydraulic fluid that are the most abundant based on market share. More information of those samples, provided by distributors of aviation oils and fluids, is shown in **Table S1**. Culture medium and supplements, as well as enzyme-linked immunosorbent assay (ELISA) kits for measuring interleukin (IL)-6, IL-8, IL-10 and tumor necrosis factor (TNF)- $\alpha$  were purchased from Life Technologies (Thermo Fisher Scientific Inc., the Netherlands); WST assay kit was purchased from Promega (Fitchburg, Wisconsin, USA); LDH detection kit was purchased from Roche Diagnostics (Mannheim, Germany); All other chemicals, unless otherwise noted, were purchased from Sigma Aldrich (the Netherlands).

### 2.2 Cell culture under submerged and ALI conditions

Calu-3 cells purchased from American Tissue Culture Collection (ATCC, Rockville, MD) were cultured in minimum essential medium (MEM) with 10% fetal bovine serum (FBS), 1% Non-Essential Amino Acid (NEAA) solution and 1% penicillin/streptomycin. Primary human CD14<sup>+</sup> monocytes isolated from buffy coats (Sanquin, the Netherlands) were differentiated to MDMs by addition of macrophage colony-stimulating factor (M-CSF, 50 ng/mL) for 6 days as previously described (He et al., 2021). Monocytes and macrophages were cultured in RPMI-1640 medium with 10% FBS and 1% penicillin/streptomycin. All cells were cultured in flasks in an incubator with 5% CO<sub>2</sub> at 37 °C.

When reaching approximately 80% confluence, Calu-3 cells were detached enzymatically by 0.05% trypsin-EDTA. Then, 0.5 mL of cell suspension (density:  $2.5 \times 10^5$  cells/mL) was seeded on the apical side of cell culture inserts (0.4  $\mu$ m pore membrane, 1.12 cm<sup>2</sup> polyester membrane, Costar, Germany) in 12-well plates, with 1.5 mL cell culture medium on the basolateral side of the inserts for nutrient supply. After submerged culture for 7 days to reach confluence, the apical medium was removed to obtain ALI conditions. Calu-3 cells on the inserts were cultured for an additional 7 days under ALI conditions before being used for subsequent ALI exposure or co-culture with MDMs. To create the Calu-3 + MDM co-culture model, 0.5 mL of MDMs suspension was added onto the Calu-3 epithelial carpet for 4 hours with a density of  $5 \times 10^4$  macrophages/cm<sup>2</sup>. After removing the apical medium, the Calu-3 + MDM co-

culture model was cultured for an additional 20 hours under ALI conditions. During cell culture on the inserts, the apical and basolateral medium were refreshed every 2 or 3 days.

### 2.3 Mini-BACS setup

As illustrated in **Figure 1**, aircraft engine oil and hydraulic fluid samples were guided to a spray nozzle (Schlick, Germany) by an adjustable motor driven syringe to be nebulized with pre-heated (90 °C) air into a heated mixing chamber (90 °C), controlled by a mass flow controller (MFC). The fumes then flowed through an oven (R50/500/12, Nabertherm, Germany) for pyrolysis and vaporization. In previous studies, pyrolysis experiments were performed at various temperatures in the range from 200 to 600 °C (Amiri et al., 2017; Mann et al., 2014; Van Netten and Leung, 2001). Different temperatures will most likely have an effect on aerosol characteristics, however, according to the report of National Research Council (NRC) (2002), typical conditions for bleed air of an aircraft engine do not exceed 350 °C (NRC, 2002). To realistically reflect conditions during fume events, we therefore used 350 °C and 200 °C as the pyrolysis temperature for aircraft engine oils and hydraulic fluids, respectively. The whole system was kept pressurized at around 3 bar using a critical orifice downstream of the oven and a back pressure regulator. After expanding through the critical orifice to atmospheric pressure, the generated fumes were diluted and cooled with compressed air controlled by a MFC to 20 - 25 °C measured by a temperature sensor, and transferred to a buffer tank made of anodized aluminum. To continuously monitor the characteristics of test atmospheres in the buffer tank, including PNC, PSD, and concentrations of VOCs and CO, we used a condensation particle counter (CPC) 3752 (TSI inc., St Paul MN, USA), a scanning mobility particle sizer (SMPS) 3936 (TSI inc., St Paul MN, USA), a total hydrocarbon analyser (THCA) RS 55-T (Ratfish Analysensysteme GmbH., Poing, Germany) and a gas filter correlation CO analyser model 300E (ENVIRO-TEC., Largo Lakes Blvd, USA).

### 2.4 Fume sampling, chemical analysis and submerged exposure

Fumes generated from aircraft engine oil and hydraulic fluid with the Mini-BACS were collected for chemical analysis and *in vitro* toxicity testing via submerged exposure. Concentrations of aldehydes-ketones (C1 - C6), OPs (32 OPs), VOCs (C6 - C12), and organic acids (C1 - C8) in collected fume samples were measured. Details of sampling, extraction and chemical analysis can be found in the Supplementary Material.

To perform submerged exposure, Calu-3 cell suspension (density:  $8 \times 10^5$  cells/mL) was added into 96-well plates (100  $\mu$ L per well) and cells were cultured for 24 hours to reach confluence. Before submerged exposure in 96-well plates, fume extracts in vials (described in the Supplementary Material) were dissolved in pure DMSO to make

stock solutions at 100 mg/mL. The solution of each fume sample was subsequently diluted in Calu-3 cell culture medium to 8 exposure doses ranging from 4 to 512 µg/mL containing 0.5% DMSO. Calu-3 cells were exposed to those samples at 8 doses in triplicate for 24 hours. The medium suspension of blank filter extracts containing 0.5% DMSO and the fresh culture medium were used as negative controls and medium controls, respectively.

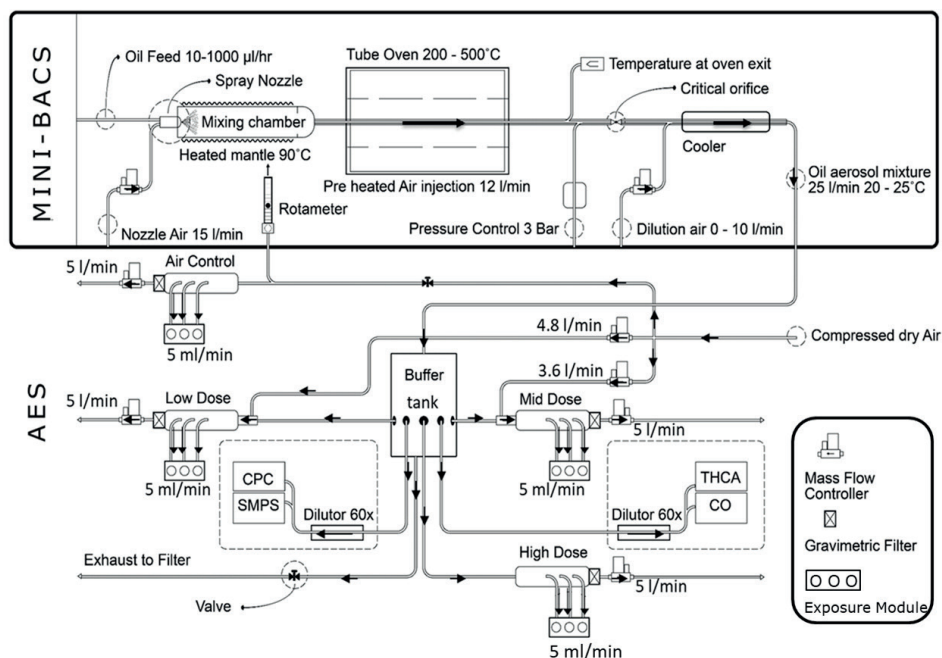


**Figure 1.** Schematic representation of the mini bleed-air contaminants simulator (Mini-BACS, top) and ALI aerosol exposure system (AES, bottom). The Mini-BACS is connected to the AES for exposure to the generated fumes in vitro. The AES contains 4 exposure modules including 1 module for exposure to clean air (air control) and 3 for exposure to the generated fumes at 3 doses each. For online measurement of particle number concentration (PNC), particle size distribution (PSD), and concentrations of volatile organic compounds (VOCs) and CO, the AES is connected to a condensation particle counter (CPC), a scanning mobility particle sizer (SMPS), a total hydrocarbon analyzer (THCA) and a gas filter correlation carbon monoxide (CO) analyzer.

## 2.5 ALI exposure to the generated fumes

The AES (Vitrocell, Waldkirch, Germany) used for this study has 4 exposure modules, including 1 module for exposure to clean air and 3 for exposure to the generated fumes at different doses (**Figure 1** and **Figure S1**). Before starting an exposure, we filled each well in the modules with 3.5 mL of Calu-3 cell culture medium and then transferred the inserts with the cells to each well. From the buffer tank (described in 2.3), streams of the generated fumes were fed into three manifolds where fumes were diluted with compressed air. A small volume of fume taken from each manifold was sprayed via the AES, with a flow-rate at 5 mL/min, onto the cells on the inserts for 4 hours at 37 °C and 85% humidity. Compressed clean air with the same flow-rate was used as clean air control. The main flow of fume or compressed air through each manifold (5 L/min) was collected on filters (PTFE Membrane Disc Filters - 2 µm, VWR, the Netherlands) for calculating their mass concentrations during exposure:

$$\text{Mass concentration (mg/m}^3\text{)} = \frac{\text{Fume mass on the filter (mg)} \times 1000}{5 \text{ L/min} \times 240 \text{ min}}$$

Notably, nucleation may occur when the emission of the oil vapor cools down to reach temperatures that also are present in aircraft cabins. In our study, particle agglomeration may mostly occur between the generation of oil fumes (after cooling down) and deposition onto the cells. This gives a very short residence time of the generated fumes (< 2 seconds) during this process, thus reducing chance of particle agglomeration. Meanwhile, 4 inserts were placed in an incubator: 3 for incubator controls and 1 for measuring the maximum LDH release ( $\text{LDH}_{\text{max}}$ ) in the cells. After exposure in the AES for 4 hours, the inserts with the cells were placed back to new 12-well plates with 1.5 mL culture medium on the basolateral side and transferred to an incubator for an additional 24-hour exposure.

## 2.6 Biological responses after submerged and ALI exposures

After submerged exposure to fume samples collected from pyrolysis of aircraft engine oils and hydraulic fluids for 24 hours, viability of Calu-3 cells was measured via the WST assay as previously described (He et al., 2018) to establish the dose-response relationship for engine oil and hydraulic fluid samples.

TEER values of the Calu-3 monoculture and the Calu-3 + MDMs co-culture on the inserts were measured after exposure under ALI conditions for 24 hours as an important indicator of barrier function and integrity in the lung cell models. The Evom2 Voltohmmeter with 4 mm chopstick electrodes (World Precision Instruments Inc., FL, USA) was used for TEER measurement by adding 0.5 mL culture medium to the apical side of the inserts. TEER values were corrected for the insert surface

area (1.12 cm<sup>2</sup>) and for the resistance of cell-free 12-well inserts ( $\approx$  130 Ohm). After measuring TEER, apical and basolateral medium were collected and viabilities of the cells on the inserts were measured using the WST assay. Briefly, cells on the inserts were incubated with 10% WST solution for 30 min before absorbance measurement was performed as previously described (He et al., 2020). To investigate cytotoxicity, LDH release in the apical and basolateral medium was measured. Briefly, 100  $\mu$ L of medium and 100  $\mu$ L of LDH reagent were successively added to a 96-well plate and then incubated at room temperature (in dark) for 20 minutes before absorbance measurement. LDH values were corrected for the maximum LDH release (LDH<sub>max</sub>) as previously described (He et al., 2020). In addition, production of cytokine IL-6, IL-8, IL-10 and TNF- $\alpha$  as markers for inflammatory responses in medium was measured using ELISA kits according to the manufacturer's protocol.

### 2.7 Statistical analysis

Results from submerged exposures were obtained from 2 independent experiments for each fume type, with 3 parallel inserts per experiment. Results from ALI exposures were obtained from 1 or 2 independent experiments for each fume type, with 3 or 4 parallel inserts per experiment. Differences between groups were compared by one-way analysis of variance (ANOVA), a  $p$ -value  $\leq$  0.05 is considered statistically significant. Data analysis was conducted using GraphPad software (version 8.2.1). Benchmark dose (BMD) analysis was used to derive a dose–response relationship for each fume sample (PROAST, version 67.0, www.rivm.nl/proast). More information of BMD analysis was described in our earlier study (He et al., 2020). In accordance with the European Food Safety Authority (EFSA) as well as taking the variation of the data into account, a 20% increase compared to incubator controls in total levels (apical + basolateral) of LDH release and inflammatory cytokines production was chosen as a benchmark response (BMR) for modelling (EFSA, 2009). After fitting the data to several models, the Exponential model turned out to be the optimal model for analysis. The lower 5% (BMDL) and upper 95% (BMDU) confidence limits (90% BMD confidence interval (BMDc.i.)) and the mean BMD of each fume were derived from the model analysis for effect markers. BMDc.i. was used for potency comparison between fume samples. More overlap between the BMDc.i of fume samples indicates less difference in their potency. If there was no 20% change or no BDMU determined at the tested dose-range, fume sample was not included in the rank order.

## 3. Results

### 3.1 Chemical profiles of fume samples

The concentration ( $\mu$ g/m<sup>3</sup>) of aldehydes-ketones (C1 - C6), OPs (32 OPs), VOCs (C6 - C12), and organic acids (C1 - C8) in the collected fume samples were measured and total levels of aldehydes-ketones, OPs, VOCs, and organic acids were calculated (Figure 2A and Table S2). Overall, engine oil fumes (Fume A, B, C and D) showed different concentration profiles. Total level of aldehydes-ketones was comparable among Fume A, B and D, around 6000  $\mu$ g/m<sup>3</sup>, which was higher than that of Fume C at 4257  $\mu$ g/m<sup>3</sup>. Fume B and C had a comparable OP level ( $\approx$  2400  $\mu$ g/m<sup>3</sup>), which was around 2 and 5 times as high as that of Fume D (1077  $\mu$ g/m<sup>3</sup>) and Fume A (495  $\mu$ g/m<sup>3</sup>), respectively. Fume D had the highest level of organic acids (1246  $\mu$ g/m<sup>3</sup>), followed by Fume B (825  $\mu$ g/m<sup>3</sup>), Fume A (709  $\mu$ g/m<sup>3</sup>), and Fume C (340  $\mu$ g/m<sup>3</sup>). Total VOCs levels of engine oil fumes were relatively low ranging from 93 to 378  $\mu$ g/m<sup>3</sup>. In comparison to engine oil fumes, hydraulic fluid fumes had much lower levels of aldehydes-ketones (< 80  $\mu$ g/m<sup>3</sup>) and organic acids (< 10  $\mu$ g/m<sup>3</sup>), but relatively high levels of OP ( $\approx$  2800  $\mu$ g/m<sup>3</sup>). The two hydraulic fluid fumes showed a comparable chemical profile, with the exception of total VOCs level which was around 60 times higher measured in Fume E ( $\approx$  600  $\mu$ g/m<sup>3</sup>) compared to Fume F ( $\approx$  10  $\mu$ g/m<sup>3</sup>).

### 3.2 Cell viability after submerged exposure

For viability of Calu-3 cells under submerged exposure conditions, a clear dose-response relationship was observed for all of fume samples at doses > 32  $\mu$ g/mL (Figure 2B). The median lethal concentration (LC<sub>50</sub>) of fume samples for Calu-3 cells was calculated to rank their potency. Fume E and F had relatively low LC<sub>50</sub> at 80 and 100  $\mu$ g/mL, respectively, followed by Fume A and B at around 250  $\mu$ g/mL, and Fume C and D at around 480  $\mu$ g/mL. This indicates the higher toxicity of Fume E and F (hydraulic fluid fumes) as well as Fume A and B (engine oil fumes), which were therefore selected for subsequent ALI exposure using the Calu-3 monoculture cell model. Fume F was also tested using the Calu-3 + MDM co-culture model.



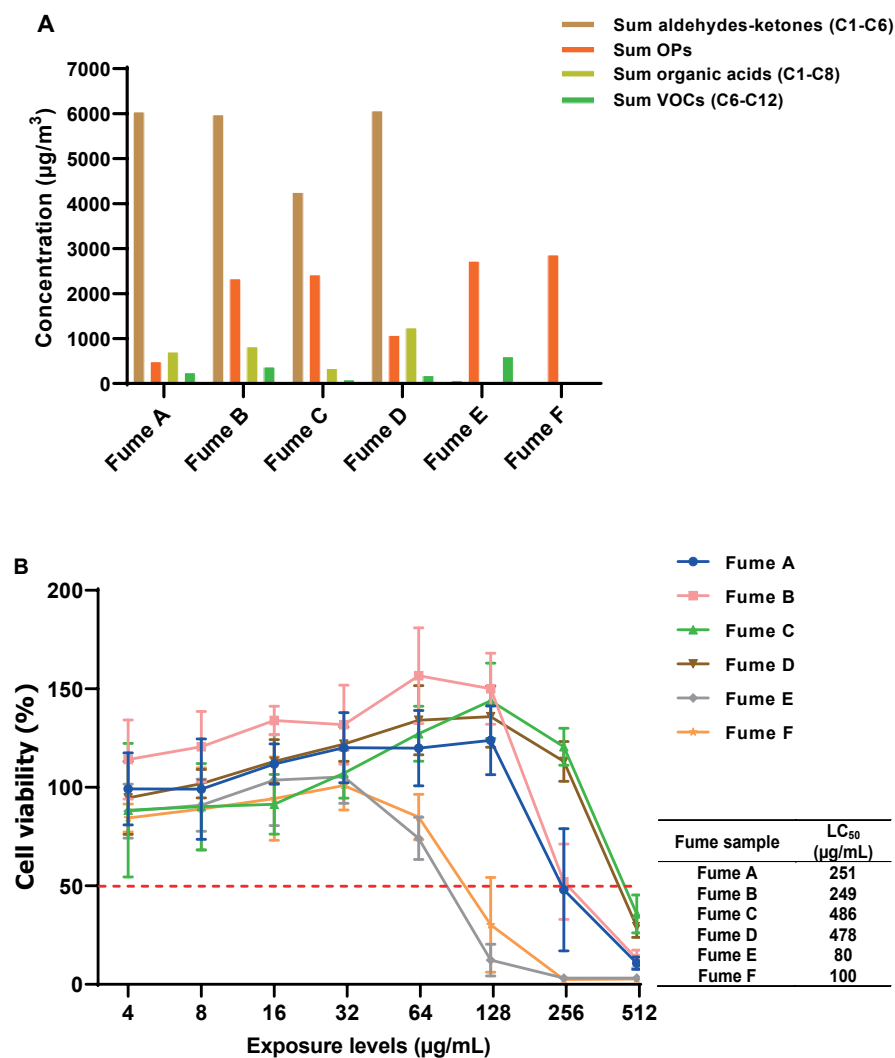


**Figure 2.** Chemical profiles of fume samples collected on filters (A) and cell viability after submerged exposure to fume samples (B). (A) Total concentrations of aldehyde-ketones (C1- C6), OPs (32 types of OPs), organic acids (C1 – C8), and VOCs (C6 – C12) in the collected engine oil (Fume A, B, C, and D) and hydraulic fluid (Fume E and F) fumes. (B) Viability of the Calu-3 cells, determined using the WST assay, after submerged exposure to each fume sample for 24 hours at 8 doses from 4 to 512 µg/mL. The red dotted line in (B) indicates 50% viability. LC<sub>50</sub> represents the median lethal concentration (µg/mL) of fume samples under submerged exposure conditions.

### 3.3 Characteristics of test atmospheres during ALI exposure

ALI exposure experiments were performed to more closely mimic inhalation exposure during a fume event. For ALI exposure, aircraft engine oils and hydraulic fluids were pyrolyzed at stable temperatures around 350 °C and 200 °C, respectively. In parallel, the characteristics of test atmospheres, including PNC, PSD and concentration of VOCs and CO, were continuously monitored during ALI exposure (Figure 3 and Table 1). The mean particle size of engine oil fumes ( $\approx 100$  nm) was twice as large as that of hydraulic fluid fumes ( $\approx 50$  nm). The mean PNC of engine oil fumes was around  $2.0 \times 10^8 / \text{cm}^3$ , which was higher than that of hydraulic fluid fumes ( $\approx 8.0 \times 10^7 / \text{cm}^3$ ). The mean concentrations of VOCs and CO measured in engine oil fumes were around 10 and 20 ppm, respectively, which were higher than VOCs and CO levels of hydraulic fluid fumes ( $\approx 5.5$  and  $0.7$  ppm, respectively). Mass concentrations of the generated fumes during ALI exposure were also calculated (Table 1). The highest exposure concentration was  $100 \text{ mg/m}^3$  for Fume A and B,  $55 \text{ mg/m}^3$  for Fume E,  $90 \text{ mg/m}^3$  for Fume F with the Calu-3 monoculture, and  $50 \text{ mg/m}^3$  Fume F with the Calu-3 + MDM co-culture.

**Table 1.** Characteristics of test atmospheres, including the particle number concentration (PNC), geometric mean (GM) mobility diameter  $\pm$  geometric standard deviation (GSD), concentrations of VOCs and CO, and mass concentration, during ALI exposure in the AES using the Calu-3 monoculture cell model. Fume F was also tested using the Calu-3 + MDM co-culture model.

Fume sample	Mean PNC (per $\text{cm}^3$ )	Mobility diameter GM $\pm$ GSD (nm)	Mean VOCs concentration (ppm)	Mean CO concentration (ppm)	Mass concentration range ( $\text{mg/m}^3$ )
Fume A	$\sim 2.0 \times 10^8$	$97 \pm 3.1$	$9.0 \pm 1.6$	$15 \pm 4.9$	0-100
Fume B	$\sim 2.3 \times 10^8$	$96 \pm 1.7$	$12 \pm 3.6$	$20 \pm 9.9$	0-100
Fume E	$\sim 8.1 \times 10^7$	$60 \pm 9.7$	$4.7 \pm 0.3$	$0.7 \pm 0.1$	0-55
Fume F (monoculture)	$\sim 7.8 \times 10^7$	$40 \pm 4.7$	$6.1 \pm 0.7$	$0.7 \pm 0.1$	0-90
Fume F (co-culture)	$\sim 9.1 \times 10^7$	$45 \pm 0.7$	$5.6 \pm 0.4$	$0.8 \pm 0.1$	0-50

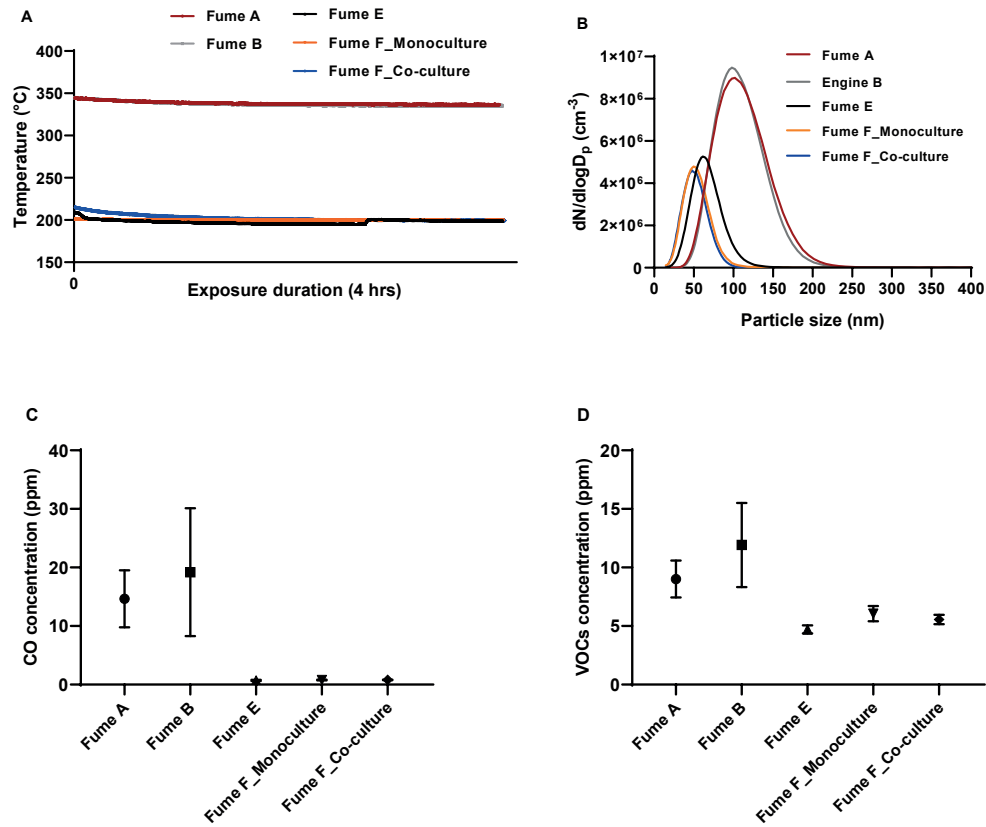


**Figure 3.** Characteristics of test atmospheres during ALI exposure in the AES for 4 hours. (A) Oven temperature for pyrolysis, (B) particle size distribution, (C) CO concentration, and (D) VOCs concentration of fumes generated from engine oils (Fume A and B) and hydraulic fluids (Fume E and F) during ALI exposure using the Calu-3 monoculture cell model. Fume F was also tested using the Calu-3 + MDM co-culture model.

### 3.4 Barrier functions and cell viability after ALI exposure

We measured TEER values and viabilities of the cells after ALI exposure to the different fumes for 24 hours (Figure 4). Compared to TEER values of controls, Calu-3 cells showed comparable TEER levels ( $\approx 1000 \text{ Ohm}\times\text{cm}^2$ ) after exposure to engine oil fumes at the tested dose-range. After exposure to hydraulic fluid fumes, a significant drop of the TEER value (lower than  $500 \text{ Ohm}\times\text{cm}^2$ ,  $p < 0.05$ ) was observed in the Calu-3 cells at the highest exposure dose. However, there was no significant change in TEER values of the Calu-3 + MDM co-culture in response to hydraulic fluid fume (Fume F) exposure (Figure 4A). After 24-hour exposure to engine oil fumes up to  $100 \text{ mg/m}^3$ , Calu-3 cells retained high cell viabilities ( $> 80\%$ ), indicating the absence of cytotoxic

effects. After exposure to hydraulic fluid fumes, viabilities of Calu-3 cells fell below  $80\%$  at  $> 55 \text{ mg/m}^3$  of Fume E and  $45 \text{ mg/m}^3$  of Fume F. In comparison to the Calu-3 monoculture, the Calu-3 + MDMs co-culture retained a high cell viability ( $> 80\%$ ) after exposure to Fume F up to  $50 \text{ mg/m}^3$  (Figure 4B).

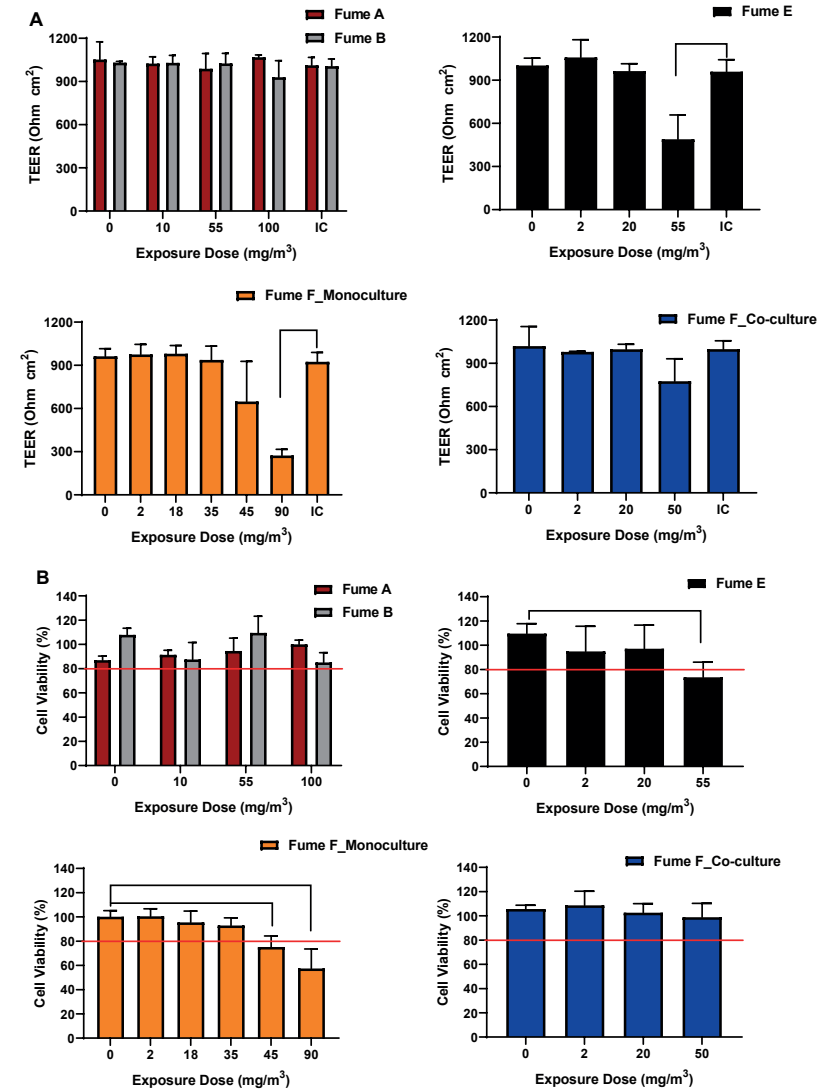


**Figure 4.** TEER values (A) and viabilities (B) of the cells after ALI exposure to fumes generated from aircraft engine oils (Fume A and B) and hydraulic fluids (Fume E and F) at different doses for 24 hours using the Calu-3 monoculture cell model. Fume F was also tested using the Calu-3 + MDM co-culture model. Error bars indicate the standard deviation of 3 or 6 parallel inserts with the cells. \* represents  $p < 0.05$ , \*\*  $p < 0.01$  and \*\*\*  $p < 0.001$ . The red line (B) indicates  $80\%$  viability.

### 3.5 LDH release under ALI exposure conditions

In response to aircraft engine oil and hydraulic fluid fumes exposure, LDH levels on the apical side of the Calu-3 monoculture and the Calu-3 + MDM co-culture were comparable ( $\approx 7\%$  of  $LDH_{max}$ ) over the tested dose-ranges (**Figure 5A**). In contrast, on the basolateral side, an increase in LDH release was observed at the highest dose for all of the generated fumes, with the exception of Fume A. BMD values of fume samples inducing a 20% increase in total level (apical + basolateral) of LDH release were derived from BMD analysis to rank their degree of cytotoxicity (**Figure 5A** and **Table 2**). The BMDU of Fume A could not be determined at the tested dose-range, indicating its low cytotoxicity. Fume A was consequently not included in the rank order. According to the BMD values of hydraulic fluid fumes for LDH release (**Table 2**), BMDc.i. of Fume F in the Calu-3 monoculture (23 - 28  $mg/m^3$ ) was comparable to that in the Calu-3 + MDMs co-culture (27 - 34  $mg/m^3$ ). Using the Calu-3 monoculture, the BMDc.i (23 - 28  $mg/m^3$ ) of Fume F was lower than that of Fume E (35 - 45  $mg/m^3$ ). The BMDc.i of hydraulic fluid Fume E and F in the Calu-3 monoculture was much lower compared to the BMDc.i of engine oil Fume B (67 - 78  $mg/m^3$ ), indicating higher cytotoxicity of hydraulic fluid fumes.

### 3.6 Inflammatory responses under ALI exposure conditions

Production of inflammatory cytokines (IL-6 and IL-8) in the apical and basolateral medium from mono- and co-culture cell models was measured after ALI exposure for 24 hours (**Figure 5B** and **Figure 5C**). In general, levels of IL-6 and IL-8 on the apical side were much higher than on the basolateral side. On both apical and basolateral sides, an increase in IL-6 production was clearly seen for all of the generated fumes at the highest dose, with the exception of engine oil Fume A (**Figure 5B**). For IL-8 production, an increase on both sides was observed only for hydraulic fluid Fume F at the highest dose using the Calu-3 monoculture model (**Figure 5C**). IL-10 and TNF- $\alpha$ , markers for macrophages, were not detected on either side of the Calu-3 monoculture and the Calu-3 + MDM co-culture models exposed to engine oil and hydraulic fluid fumes at the tested dose-range (data not shown).

BMD values of each fume sample evoking a 20% increase of total levels (apical + basolateral) of IL-6 and IL-8 production were obtained from BMD analysis (**Figure 5B**, **Figure 5C** and **Table 2**). For aircraft engine oil fumes, the BMDU of Fume A for IL-6 production could not be determined and Fume A and B were not able to induce a BMR for IL-8 production. Therefore, Fume A was not included in the rank order of IL-6 and IL-8 production and Fume B was not included in the rank order of IL-8 production. This also indicates few pro-inflammatory effects of engine oil fumes at the tested dose-range. In comparison, a 20% increase of IL-6 and IL-8 production was identified for hydraulic fluid fumes. However, no distinctions were observed due

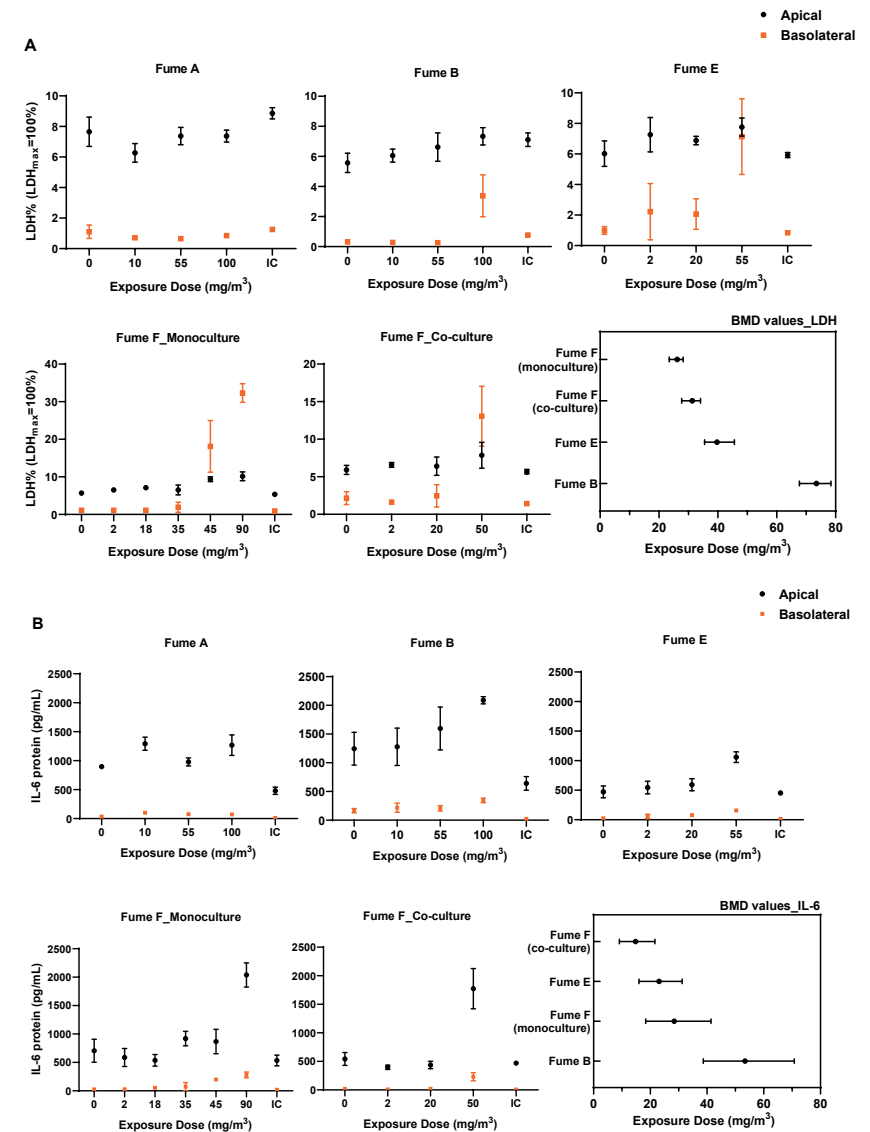


**Figure 5.** Induction of cytotoxicity and inflammatory responses after ALI exposure to fumes generated from engine oils (Fume A and B) and hydraulic fluids (Fume E and F) at different doses for 24 hours using the Calu-3 monoculture cell model. Fume F was also tested using the Calu-3 + MDM co-culture model. Relative LDH release (A) and production of IL-6 (B) and IL-8 (C) on the apical and basolateral sides of the inserts, combined with summary of the derived BMDc.i. and mean BMD of the different fumes for total level (apical + basolateral) of LDH release (A), IL-6 production (B) and IL-8 production (C). BMDU of Fume A could not be determined in LDH release (A) and IL-6 production (B). A 20% increase (BMR) of IL-8 production (C) could not be determined for Fume A and B. Error bars indicate the standard deviation of 3 or 6 parallel inserts with the cells. IC represents incubator control.

to the substantial overlap between BMDc.i. of Fume E and Fume F (monoculture). Also, minor differences in BMDc.i. for IL-6 and IL-8 production were seen between the Calu-3 monoculture and the Calu-3 + MDMs co-culture in response to Fume F exposure.

**Table 2.** Summary of the derived BMD values of the different fumes for total levels (apical + basolateral) of LDH release, IL-6 production, and IL-8 production, including the mean BMD, lower (BMDL) and upper (BMDU) limits of the confidence interval inducing a 20% BMR, after ALI exposure to fumes for 24 hours using the Calu-3 monoculture cell model. Fume F was also tested with the Calu-3 + MDM co-culture model.

BMR:20%	BMD values (mg/m <sup>3</sup> )								
	LDH			IL-6			IL-8		
	Mean	BMDL	BMDU	Mean	BMDL	BMDU	Mean	BMDL	BMDU
Fume A	140	99	-	107	64	-	-	-	-
Fume B	73	67	78	53	38	70	-	-	-
Fume E	39	35	45	23	16	31	44	35	56
Fume F (mono-culture)	26	23	28	28	18	41	59	44	74
Fume F (co-culture)	31	27	34	14	9.0	21	42	34	56

“-”: could not be determined

#### 4. Discussion

Earlier studies conducted with simulated fume events under laboratory conditions mainly focused on the composition (e.g. chemicals and particles) of aircraft engine oil and hydraulic fluid fumes (Amiri et al., 2017; Mann et al., 2014; Van Netten and Leung, 2001). Our unique combination of a Mini-BACS and an AES integrates generation of fumes from aircraft engine oils and hydraulic fluids via a bleed-air simulator under controlled conditions, deposition of the generated fumes onto the cells with a continuous airflow via the AES, and online physicochemical measurements of test atmospheres during the entire ALI exposure. This system thus provides a realistic inhalation exposure for testing toxicity of fume events *in vitro*. The toxicological data

demonstrate that, for the Calu-3 mono-culture and the Calu-3 + MDM co-culture lung cell models, fumes from hydraulic fluids are more harmful than fumes derived from engine oils.-

Under submerged exposure conditions, the values from the WST assay increased up to 150% of control after exposure to the generated fumes, particularly engine oil fumes, at 32 - 128 µg/mL for 24 hours. Values from the WST assay directly correlate to the metabolic activity of the cells in the culture. It thus suggests that the cells are experiencing (oxidative) stress under exposure to engine oil fumes at 32 - 128 µg/mL, resulting in enhanced mitochondrial activity. Notably, the cells were exposed to oil fumes under submerged conditions by adding the fume suspension into the cell culture medium. The fume suspension consists of a mixture of particles and chemicals, which may reach the cells by sedimentation/diffusion (particles) and dissolving (chemicals), depending on their characteristics (e.g. solubility) and kinetics. The delivered dose of fumes to the cells under submerged exposure conditions consequently remains unknown. Therefore, it is difficult to compare the delivered doses of fumes under submerged conditions to the doses under ALI conditions.

Many *in vitro* studies have shown the important role of macrophages for co-culture cell models in promoting cellular responses and increasing sensitivity to, for example, particulate matter (Ji et al., 2018; Rothen-Rutishauser et al., 2007; Wottrich et al., 2004). Despite the high PNC (mean PNC ≈ 9.1 × 10<sup>7</sup>) measured in Fume F, the presumed higher sensitivity of the co-culture model was not noted in our study in which we compared effects induced by Fume F in the Calu-3 + MDMs co-culture to those observed in the Calu-3 monoculture. Usually, increases in IL-10 and TNF-α production are regarded as markers for the activation of macrophages (Hoppstädter et al., 2015; Mosser and Edwards, 2008). When challenged with lipopolysaccharide (LPS) as a positive control, the Calu-3 + MDM co-culture model shows increases in IL-10 and TNF-α production and a higher sensitivity to LPS compared to the Calu-3 monoculture (He et al., 2021), indicating that MDMs in our co-culture model can be activated. However, IL-10 and TNF-α were not detected in the Calu-3 + MDM co-culture model after exposure to Fume F, suggesting that hydraulic fluid fumes did not activate macrophages under ALI exposure conditions in our study. It should be noted that during pyrolysis of hydraulic fluid at 200°C many unburned/unreacted fluid droplets were observed in fume emission. It is therefore possible that abundant particles in hydraulic fluid fumes stick to the surface and the interior of fluid droplets, which could limit the macrophages-particles interactions when deposited onto the cells.



In this study we used BMD analysis to identify the degree of toxicity of aircraft engine oil and hydraulic fluid fumes under ALI exposure conditions. Compared to engine oil fumes, hydraulic fluid fumes had a lower BMD<sub>c.i.</sub> for LDH release and inflammatory cytokines production, indicating their higher toxicity. Different chemical profiles between engine oil and hydraulic fluid fumes may be an explanation for their different toxic properties. A number of studies have discussed the possibility of OP formation from fume events and their potential harmful effects on cabin crews and passengers (Hood, 2001; Liyasova et al., 2011; NRC, 2002; Solbu et al., 2011). Additionally, tri-n-butyl phosphate (TBP) and triphenyl phosphate (TPP), which were detected in the generated fumes (**Table S2**), have previously been shown to reduce cell viability (200 μM of TBP and TPP) of the lung cell lines *in vitro* and induce cytotoxicity (5 μl TBP, 20% v/v in n-dodecane) in lungs of rats *in vivo* (An et al., 2016; Salovsky et al., 1998). To estimate the contribution of OPs from fumes on cytotoxicity in the lung cell models under ALI exposure conditions, we studied the relationship between total OP levels of the different fumes and the mean BMD values of those fumes for LDH release derived from ALI exposures. Total OP levels showed a significant negative correlation with the BMD values for LDH release ( $R^2 = 0.96$ ,  $p < 0.05$ , **Figure S1A**). Notably, TBP accounted for the largest fraction (> 95%) of total OP level for the different fumes (**Table S2**). To determine the influence of other OPs on cytotoxicity, we further conducted correlation analysis for total OP levels excluding TBP, where a significant negative correlation with the BMD values still existed ( $R^2 = 0.97$ ,  $p < 0.05$ , **Figure S1A**). Our data therefore suggest that under ALI exposure conditions higher cytotoxicity can be induced by fumes with higher total OP levels. As such, the relatively high OP level detected in hydraulic fluid fumes may explain their higher cytotoxicity under ALI exposure conditions compared to engine oil fumes. However, such significant correlations were not observed between total OP levels and the LC<sub>50</sub> values of fume samples derived from submerged exposures (**Figure S1B**). The poor water solubility of the most abundant OP detected in fumes (TBP and TPP: log Kow > 4, (Leo and Hoekman, 1995)) may provide an explanation for the absence of a correlation between total OP levels and cytotoxicity under submerged conditions, as it likely prevents OPs from dissolving in the cell culture medium to a sufficient degree. In addition, smaller sized particles have larger surface area to volume ratios and higher reactivity to absorb more chemicals, thereby increasing their *in vitro* toxicity (Jonsdottir et al., 2019; Stone et al., 2017). Therefore, the smaller particle size observed in hydraulic fluid fumes (mean size ≈ 50 nm) under pyrolysis may also contribute to their higher toxicity compared to engine oil fumes (mean size ≈ 100 nm).

Fume events are difficult to capture in real time, in part because it is not well understood under which conditions they are evoked. Consequently, there is limited knowledge on the composition and levels of inhaled fume during a fume event in an aircraft cabin.

Vasak (1992) has reported that mass concentrations of fumes were respectively 1.5 mg/m<sup>3</sup> and 1.3 mg/m<sup>3</sup> in the cockpit and in the passenger cabin during a fume event. This fume level reported 20 years ago may be not the actual cabin levels under current exposure conditions, as types of aircraft engine oil have been updated and changed in the past 20 years. However, no newer data on fume/particle concentrations have been published in the open literature, to our knowledge. According to the multiple path particle dosimetry (MPPD) model analysis, the deposition efficiency of particles (10 nm < particle size < 100 nm) onto the tracheobronchial epithelium ranges from 10% to 40% (Braakhuis et al., 2014). It can thus be estimated that the inhaled level of fume into the human tracheobronchial region theoretically ranges from 0.13 - 0.6 mg/m<sup>3</sup>. Although mass concentrations of engine oil (0 - 100 mg/m<sup>3</sup>) and hydraulic fluid (0 - 90 mg/m<sup>3</sup>) fumes during ALI exposure in our study are substantially higher, the deposition efficiency of aerosolized substances in the AES (with the same exposure parameters used for ALI exposure to fumes) is low at around 2% for aerosolized UFPs (particle size ≈ 60 nm, data not shown). Upper estimates for exposure levels of fumes onto the cells in our study thus amount to 2.0 mg/m<sup>3</sup>. Using the BMD values (**Table 2**), we can estimate that, after adjusting for deposition efficiency (2%), the BMDL values of Fume A for LDH release (1.98 mg/m<sup>3</sup>) and IL-6 production (1.28 mg/m<sup>3</sup>) in the Calu-3 cells differ slightly from the realistic exposure levels of fume in the lungs (0.13 - 0.6 mg/m<sup>3</sup>). For Fume B, this difference is even smaller with the BMDL for LDH release (1.34 mg/m<sup>3</sup>) and IL-6 production (0.76 mg/m<sup>3</sup>). For Fume E, the BMDL values for LDH release (0.70 mg/m<sup>3</sup>), IL-6 production (0.32 mg/m<sup>3</sup>), and IL-8 production (0.70 mg/m<sup>3</sup>) are substantially overlapping with realistic exposure levels of fume in the lungs. This also holds for the BMDL of Fume F for LDH release (0.46 mg/m<sup>3</sup>), IL-6 production (0.36 mg/m<sup>3</sup>), and IL-8 production (0.88 mg/m<sup>3</sup>) using the Calu-3 monoculture model as well as for LDH release (0.54 mg/m<sup>3</sup>), IL-6 production (0.18 mg/m<sup>3</sup>), and IL-8 production (0.68 mg/m<sup>3</sup>) using the Calu-3 + MDMs co-culture model. Additionally, cabin fume is a complex mixture of gases and particles, in which the gaseous part is likely also toxic to the lungs. Therefore, the main gaseous contaminants (CO and VOCs) during fume events should also be taken into consideration to comprehensively evaluate how the fume levels in test atmospheres *in vitro* relate to exposure conditions in aircraft cabins. The reported levels of CO ranged from < 1 to 9.4 ppm and VOCs ranged from below the limit of detection to ≈ 10 ppm in aircraft cabin air (Shehadi et al., 2016). It is clear that CO and VOCs levels measured in test atmospheres (CO: 0.7 - 20 ppm; VOCs: 4.7 - 12 ppm) during *in vitro* exposure substantially overlap with the realistic cabin levels. The toxicological data derived from ALI exposures in our study thus clearly reflect the potential health risks associated with fume events in aircraft cabins, particularly for hydraulic fluid fumes.

## Conclusion

Our unique experimental “Mini-BACS + AES” setup is able to provide steady conditions to perform *in vitro* exposure under ALI conditions to aircraft engine oil and hydraulic fluid fumes, generated at respectively 350°C and 200°C. Exposure of the Calu-3 monoculture and Calu-3 + MDM co-culture lung cell models to high levels of aircraft engine oil and hydraulic fluid fumes under ALI conditions can reduce TEER and viabilities of the cells, induce cytotoxicity, and increase production of pro-inflammatory cytokines. Hydraulic fluid fumes are more toxic than engine oil fumes on the mass concentration of fume basis, which may be related to higher abundance of OPs and smaller particle size of hydraulic fluid fumes. Our toxicological data clearly reflect the potential health risks during fume events in aircraft cabins.

## Acknowledgements

Part of this work was performed under the service contract MOVE/BE/SER/2016-363/SI2.748114 – “Investigation of the quality level of the air inside the cabin of large transport aeroplanes and its health implication” funded by the Directorate-General for Mobility and Transport (DG MOVE) of the European Commission. We thank Rob Vree Egberts, Paul H.B. Fokkens and Eric R. Gremmer from the National Institute for Public Health and the Environment (RIVM) for their valuable assistance with the “Mini-BACS + AES” setup and *in vitro* exposure. The support provided by China Scholarship Council (CSC) during the PhD period of Rui-Wen He in Utrecht University-Institute for Risk Assessment Studies is also acknowledged.

## References

- Abou-Donia, M.B., M.M. Abou-Donia, E.M. ElMasry, J.A. Monro, and M.F. Mulder. 2013. Autoantibodies to nervous system-specific proteins are elevated in sera of flight crew members: biomarkers for nervous system injury. *Journal of Toxicology and Environmental Health, Part A*. 76:363-380.
- Amiri, S.N., B. Jones, K.R. Mohan, C.P. Weisel, G. Mann, and J. Roth. 2017. Study of aldehydes, carbon monoxide, and particulate contaminants generated in bleed-air simulator. *Journal of Aircraft*. 54:1364-1374.
- An, J., J. Hu, Y. Shang, Y. Zhong, X. Zhang, and Z. Yu. 2016. The cytotoxicity of organophosphate flame retardants on HepG2, A549 and Caco-2 cells. *Journal of Environmental Science and Health, Part A*. 51:980-988.
- Braakhuis, H.M., M.V. Park, I. Gosens, W.H. De Jong, and F.R. Cassee. 2014. Physicochemical characteristics of nanomaterials that affect pulmonary inflammation. *Particle and fibre toxicology*. 11:18.
- Brown, T.P., L.K. Shuker, L. Rushton, F. Warren, and J. Stevens. 2001. The possible effects on health, comfort and safety of aircraft cabin environments. *The journal of the Royal Society for the Promotion of Health*. 121:177-184.
- Denola, G., P. Hanhela, and W. Mazurek. 2011. Determination of tricresyl phosphate air contamination in aircraft. *Annals of occupational hygiene*. 55:710-722.
- EFSA. 2009. Guidance of the Scientific Committee on Use of the benchmark dose approach in risk assessment. *EFSA Journal*. 7:1150.
- He, R.-W., H.M. Braakhuis, R.J. Vandebriel, Y.C.M. Staal, E.R. Gremmer, P.H.B. Fokkens, C. Kemp, J. Vermeulen, R.H.S. Westerink, and F.R. Cassee. 2021. Optimization of an air-liquid interface *in vitro* cell co-culture model to estimate the hazard of aerosol exposures. *Journal of Aerosol Science*. 153:105703.
- He, R.-W., M.E. Gerlofs-Nijland, J. Boere, P. Fokkens, D. Leseman, N.A. Janssen, and F.R. Cassee. 2020. Comparative toxicity of ultrafine particles around a major airport in human bronchial epithelial (Calu-3) cell model at the air-liquid interface. *Toxicology in Vitro*:104950.
- He, R.-W., F. Shirmohammadi, M.E. Gerlofs-Nijland, C. Sioutas, and F.R. Cassee. 2018. Pro-inflammatory responses to PM<sub>0.25</sub> from airport and urban traffic emissions. *Science of the Total Environment*. 640:997-1003.
- Hood, E. 2001. OPs cause bad trips? *Environmental health perspectives*. 109:A156-A156.
- Hoppstädter, J., M. Seif, A. Dembek, C. Cavelius, H. Huwer, A. Kraegeloh, and A.K. Kiemer. 2015. M2 polarization enhances silica nanoparticle uptake by macrophages. *Frontiers in pharmacology*. 6:55.
- Howard, C., D. Johnson, J. Morton, S. Michaelis, D. Supplee, and J. Burdon. 2018. Is a Cumulative Exposure to a Background Aerosol of Nanoparticles Part of the Causal Mechanism of Aerotoxic Syndrome. *J Nanomed Nanosci: JNAN-139*. DOI. 10.
- Hu, G., and J.W. Christman. 2019. Alveolar Macrophages in Lung Inflammation and Resolution. *Frontiers in Immunology*. 10:2275.
- Ji, J., S. Upadhyay, X. Xiong, M. Malmlöf, T. Sandström, P. Gerde, and L. Palmberg. 2018. Multi-cellular human bronchial models exposed to diesel exhaust particles: assessment of inflammation, oxidative stress and macrophage polarization. *Particle and fibre toxicology*. 15:19.
- Jonsdottir, H.R., M. Delaval, Z. Leni, A. Keller, B.T. Brem, F. Siegerist, D. Schönenberger, L. Durdina, M. Elser, and H. Burtscher. 2019. Non-volatile particle emissions from aircraft turbine engines at ground-idle induce oxidative stress in bronchial cells. *Communications biology*. 2:1-11.
- Leo, A., and D. Hoekman. 1995. Exploring QSAR. American Chemical Society.
- Liyasova, M., B. Li, L.M. Schopfer, F. Nachon, P. Masson, C.E. Furlong, and O. Lockridge. 2011. Exposure to tri-o-cresyl phosphate detected in jet airplane passengers. *Toxicology and applied pharmacology*. 256:337-347.
- Mann, G.W., S.J. Eckels, and B. W. Jones. 2014. Analysis of particulate size distribution and concentrations from simulated jet engine bleed air incidents. *HVAC&R Research*. 20:780-789.
- Michaelis, S. 2011. Contaminated aircraft cabin air. *J. Biol. Phys. Chem*. 11:132-145.
- Michaelis, S. 2016. Oil bearing seals and aircraft cabin air contamination. *Sealing Technology*. 2016:7-10.
- Michaelis, S., J. Burdon, C.V. Howard, and W.H. Organization. 2017. Aerotoxic syndrome: a new occupational disease? *Public health panorama*. 3:198-211.
- Mosser, D.M., and J.P. Edwards. 2008. Exploring the full spectrum of macrophage activation. *Nature reviews immunology*. 8:958-969.

- NRC. 2002. The airliner cabin environment and the health of passengers and crew. National Academies Press. <https://doi.org/10.17226/10238>.
- OHRCA. 2014. <http://www.ohrca.org/wpcontent/uploads/2014/08/finalreport.pdf>.
- Omaye, S.T. 2002. Metabolic modulation of carbon monoxide toxicity. *Toxicology*. 180:139-150.
- Ramsden, J.J. 2012. Contaminated aircraft cabin air: aspects of causation and acceptable risk. *J Biol Phys Chem*. 12:56-68.
- Reneman, L., S.B. Schagen, M. Mulder, H.J. Mutsaerts, G. Hageman, and M.B. de Ruiter. 2016. Cognitive impairment and associated loss in brain white microstructure in aircrew members exposed to engine oil fumes. *Brain imaging and behavior*. 10:437-444.
- Rothen-Rutishauser, B., C. Mühlfeld, F. Blank, C. Musso, and P. Gehr. 2007. Translocation of particles and inflammatory responses after exposure to fine particles and nanoparticles in an epithelial airway model. *Particle and fibre toxicology*. 4:1-9.
- Salovsky, P., V. Shopova, and V. Dancheva. 1998. Antioxidant defense mechanisms in the lung toxicity of tri-n-butyl phosphate. *American journal of industrial medicine*. 33:11-15.
- Shehadi, M., B. Jones, and M. Hosni. 2016. Characterization of the frequency and nature of bleed air contamination events in commercial aircraft. *Indoor air*. 26:478-488.
- Solbu, K., H.L. Daae, R. Olsen, S. Thorud, D.G. Ellingsen, T. Lindgren, B. Bakke, E. Lundanes, and P. Molander. 2011. Organophosphates in aircraft cabin and cockpit air—method development and measurements of contaminants. *Journal of Environmental Monitoring*. 13:1393-1403.
- Stone, V., M.R. Miller, M.J. Clift, A. Elder, N.L. Mills, P. Møller, R.P. Schins, U. Vogel, W.G. Kreyling, and K. Alstrup Jensen. 2017. Nanomaterials versus ambient ultrafine particles: an opportunity to exchange toxicology knowledge. *Environmental Health Perspectives*. 125:106002.
- Van Netten, C. 2005. Aircraft air quality incidents, symptoms, exposures and possible solutions. In *Air Quality in Airplane Cabins and Similar Enclosed Spaces*. Springer. 193-210.
- Van Netten, C., and V. Leung. 2001. Hydraulic fluids and jet engine oil: pyrolysis and aircraft air quality. *Archives of Environmental Health: An International Journal*. 56:181-186.
- Vasak, V. 1992. Cabin Air Contamination in BAe 146 in EastWest Airlines. *Industrial Hygiene and Environmental Service Laboratories, St Ives*.
- Winder, C., and J.-C. Balouet. 2002. The toxicity of commercial jet oils. *Environmental research*. 89:146-164.
- Winder, C., and S. Michaelis. 2005. Crew effects from toxic exposures on aircraft. In *Air Quality in Airplane Cabins and Similar Enclosed Spaces*. Springer. 229-248.
- Wottrich, R., S. Diabaté, and H.F. Krug. 2004. Biological effects of ultrafine model particles in human macrophages and epithelial cells in mono- and co-culture. *International journal of hygiene and environmental health*. 207:353-361.

## Supplementary Material

### Materials and methods

#### Sampling, extraction and chemical analysis of fumes

Aircraft engine oil and hydraulic fluid fumes generated with a Mini-BACs were collected in different ways depending on analysis methods of the target chemicals.

Aldehydes-ketones (C1 - C6):

The sampling and analysis of aldehydes and ketones is based on ISO16000-3 (2011). Sampling was performed with the use of a Dinitrophenyl-hydrazine (DNPH) cartridge based on the derivatization reaction between Dinitrophenylhydrazine and carbonyl or ketone groups. A hydrazone complex from the derivatization reaction was analysed by high pressure liquid chromatography (HPLC, Agilent 1100) followed by ultra-violet (UV, Model 785A, Separations) detection at 360 nm. Prior to sampling, all DNPH cartridges were moisturized with Milli-Q water in order to reach more stability for unsaturated aldehydes like acrolein.

Organophosphates (OPs):

To measure OPs, fumes were collected on glass fiber filters (Whatman, diameter 47 mm) in combination with Chromosorb 106 adsorption tubes. Before extraction, the internal standards, Triphenyl Phosphate-d15 and Triethyl Phosphate-d15, were added to filters. Filters and tubes were extracted via the accelerate solvent extractor (ASE 350, Dionex) with dichloromethane as extraction solvent. After extraction, the sample extract was concentrated and analysed by a gas chromatography (Agilent 7890A)/mass spectrometry (Agilent 5975C) (GC/MS). The method was capable of identifying and quantifying 32 OPs, including separation and quantification of 10 tricresyl phosphate (TCP) isomers based on Solbu et al. (2011).

VOCs (C6 - C12) and organic acids (C1 - C8):

Fumes were trapped on tenax GR thermal desorption (TD) tubes for VOCs and organic acids determination, which was performed by a TD-GC-MS (Agilent 7890 and Agilent 5977) based on ISO16000-5 (2007) and ISO16000-6 (2011). Compounds were identified based on retention time and mass spectra libraries (Automated Mass Spectral Deconvolution and Identification System (AMDIS), TNO library, and National Institute standards (NIST)). Quantification is performed by the substance specific calibration for compounds at a concentration above 3 µg/m<sup>3</sup>.

For submerged exposure, the generated fume was collected on 47-mm Teflon filters (2- $\mu\text{m}$  pore, VWR, the Netherlands) for 6 hours. For the first 3 hours of sampling, 4 parallel filters were used, after which 4 new filters were loaded. In total, 8 filters were collected for each type of fume. Filter extraction includes 3 steps. 1) Filters of each fume sample were cut into pieces and collected in a 50 mL tube, and 2) extracted with 5 mL of acetone (HPLC grade) by shaking for 5 mins. 3) After extraction, filters were rinsed with 3 mL acetone. The combined acetone from step 2 and 3 in the tube was evaporated at 25°C overnight. After evaporation, 2 mL acetone was added into the tube to re-dissolve fume extracts. The re-dissolved oil solution was collected in pre-weighed glass vials, then transferred to a stove at 25°C for evaporation overnight. After acclimatization (50% humidity at 20°C) for 24 hours, vials with fume extracts were weighed again and the mass of fume extracts was calculated. As control, 4 clean Teflon filters were extracted using the same protocol.

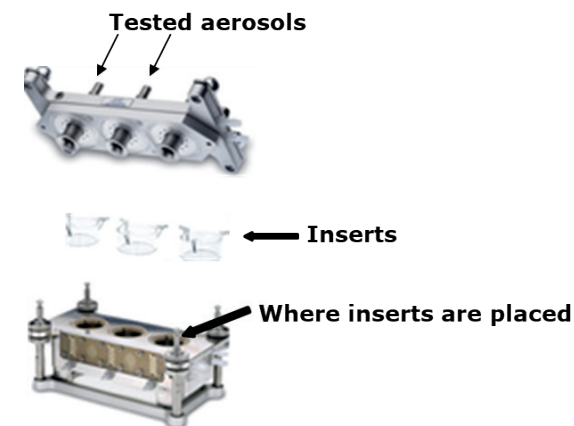


Figure S1. The exposure module in the AES.

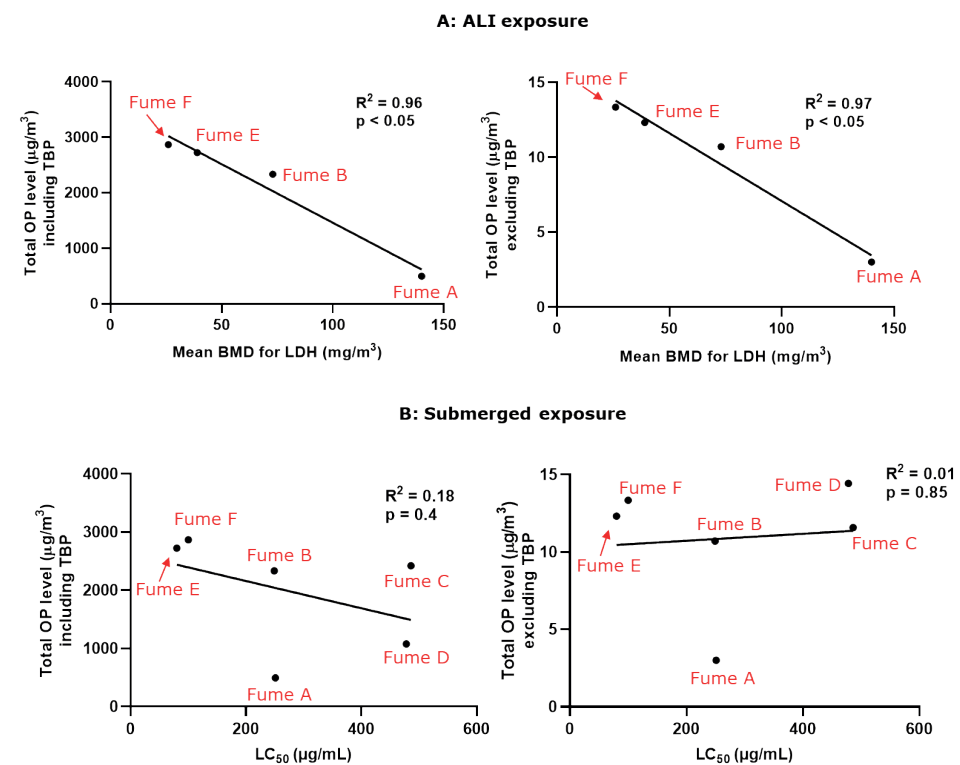


Figure S2. The correlations (A) between total OP levels of fume samples (left side: including TBP; right side: excluding TBP) and the mean BMD values of those fumes for LDH release derived from ALI exposures; (B) between total OP levels of fume samples (left side: including TBP; right side: excluding TBP) and the  $LC_{50}$  values of those fumes derived from submerged exposures.



**Table S1.** Description and characteristics of aircraft engine oil and hydraulic fluid samples used in this study.

Fume sample	Type	Flash point	TCP (% w/w)	Other OP-content (% w/w)	LD <sub>50</sub> * (oral, rat)
Fume A	Engine oil	>246 °C	TCP-free	-	-
Fume B			< 3%	-	> 5.0 mg/kg
Fume C			1% - 2.5%	-	> 5.0 mg/kg
Fume D			1% - 5%	TMPP (1% - < 3%)	-
Fume E	Hydraulic fluid	>160 °C	-	TBP (70% - < 80%)	> 1340 mg/kg
Fume F			>154 °C	-	TBP (60% - 100%)

\*-: No information

\*\* : median lethal dose

**Table S2.** The concentration ( $\mu\text{g}/\text{m}^3$ ) of organophosphates (OPs) measured in the different fumes.

OPs	Abbreviation	Concentration ( $\mu\text{g}/\text{m}^3$ )						
		Fume A	Fume B	Fume C	Fume D	Fume E	Fume F	LOD*
Trimethyl phosphate	TMP	-	-	-	-	-	-	0.002
Triethyl phosphate	TEP	0.796	-	-	-	0.378	0.020	0.012
Triisopropyl phosphate	TIPP	-	0.143	-	0.099	-	-	0.004
Tri-n-propyl phosphate	TnPP	-	-	-	-	-	-	0.016
Tri-n-butyl phosphate	TBP	492	2326	2411	1063	2713	2854	0.019
Tris(2-chloroethyl) phosphate	TCEP	-	-	-	0.022	-	0.082	0.007
Tris(2-chloro-1-methylethyl) phosphate	TCPP-1	0.210	0.119	1.034	0.693	0.153	0.356	0.012
Bis(2-chloro-1-methylethyl)2-chloro-1-propyl phosphate	TCPP-2	0.063	0.059	0.392	0.179	0.032	0.152	0.008
Trimethyl propane phosphate	TMPP	-	-	-	0.035	-	-	0.011
Bis(2-chloro-1-propyl)2-chloro-1-methylethyl phosphate	TCPP-3	-	-	-	-	-	-	0.002
Dibutyl phenyl phosphate	DBPP	-	-	0.031	-	0.023	0.081	0.004
Butyl diphenyl phosphate	BDPP	-	-	-	-	0.004	0.010	0.002
Tris(1,3-dichloro-2-propyl) phosphate	TDCPP	-	-	-	-	-	-	0.010
Tris(2-butoxyethyl) phosphate	TBEP	-	-	-	-	0.295	-	0.034
Triphenyl phosphate	TPP	1.656	0.759	1.117	0.580	11.2	12.3	0.003
2-Ethylhexyl diphenyl phosphate	EHDPP	0.106	0.059	0.369	0.144	0.072	0.066	0.002
Tris(2-ethylhexyl) phosphate	TEHP	-	-	-	-	-	0.090	0.004
Cresyl diphenyl phosphate	CDP-1	-	-	-	-	-	-	0.005
Cresyl diphenyl phosphate	CDP-2	-	-	-	-	-	-	0.007
Di-cresyl phenyl phosphate	DCP-1	-	0.038	0.024	0.039	0.009	-	0.004
Tri (o, o, o)-cresyl phosphate	ToCP	-	-	-	-	-	-	0.009

Di-cresyl phenyl phosphate	DCP-2	-	0.079	0.043	0.079	-	0.004
Di-cresyl phenyl phosphate	DCP-3	-	0.030	0.020	0.030	-	0.003
Tri (m, m, m)-cresyl phosphate	TmCP	0.032	1.313	1.118	1.788	0.111	0.005
Tri (m, m, p)-cresyl phosphate	T(m,m,p)CP	0.064	3.580	3.092	4.780	0.033	0.003
Tri (m, p, p)-cresyl phosphate	T(m,p,p)CP	0.057	3.402	3.257	4.489	0.029	0.003
Tri (p, p, p)-cresyl phosphate	TpCP	0.023	1.120	1.083	1.470	0.012	0.004
T(o,o,m)-cresyl phosphate	T(o,o,m)CP	-	-	-	-	-	0.005
T(m,m,o)-cresyl phosphate	T(m,m,o)CP	-	-	-	-	-	0.005
T(o,o,p)-cresyl phosphate	T(o,o,p)CP	-	-	-	-	-	0.005
T(o,p,m)-cresyl phosphate	T(o,p,m)CP	-	-	-	-	-	0.005
T(o,p,p)-cresyl phosphate	T(o,p,p)CP	-	-	-	-	-	0.005

"-": lower than detection limit

<sup>en</sup>: limits of detection

## References

- ISO16000-5. 2007. Indoor air—Part 5: sampling strategy for volatile organic compounds (VOCs).
- ISO16000-3. 2011. Indoor Air—Part 3: Determination of Formaldehyde and Other Carbonyl Compounds in Indoor Air and Test Chamber Air—Active Sampling Method.
- ISO160000-6. 2011. Indoor Air—Part. 6: Determination of Volatile Organic Compounds in Indoor and Test Chamber Air by Active Sampling on Tenax TA Sorbent, Thermal Desorption and Gas Chromatography Using MS or MS-FID. *Thermal Desorption and Gas Chromatography Using MS or MS-FID*.
- Solbu, K., H.L. Daae, R. Olsen, S. Thorud, D.G. Ellingsen, T. Lindgren, B. Bakke, E. Lundanes, and P. Molander. 2011. Organophosphates in aircraft cabin and cockpit air—method development and measurements of contaminants. *Journal of Environmental Monitoring*. 13:1393-1403.

# Chapter 6

## **General Discussion and Future Perspectives**

## General Discussion

The main objective of the research presented in this thesis is to optimize the lung cell models under air-liquid interface (ALI) conditions to assess inhalation toxicity of (aircraft-related) air pollutants *in vitro*. To achieve this objective, the following three research aims are formulated:

1. To investigate the chemical composition, potential sources, and *in vitro* toxicity of airport PM, in comparison to PM collected from urban traffic emissions.
2. To optimize the *in vitro* mono-/co-culture models of human airway barrier for aerosol exposure under ALI conditions.
3. To apply the optimized lung cell models for *in vitro* toxicity testing of aircraft-related air pollutants under ALI exposure conditions.

Those research aims are addressed in this thesis from Chapter 2 to Chapter 5. An overview of the thesis chapters including aim(s) that each chapter covers is presented in Table 1.

**Table 1.** Overview of the thesis chapters and their corresponding research aims.

Chapter	Title	Research aims		
		1	2	3
2	Pro-inflammatory responses to PM <sub>0.25</sub> from airport and urban traffic emissions	×		
3 Part I	An air-liquid interface bronchial epithelial model for realistic, repeated inhalation exposure to airborne particles for toxicity testing		×	
3 Part II	Optimization of an air-liquid interface <i>in vitro</i> cell co-culture model to estimate the hazard of aerosol exposures		×	
4	Comparative toxicity of ultrafine particles around a major airport in human bronchial epithelial (Calu-3) cell model at the air-liquid interface			×
5	<i>In vitro</i> hazard characterization of simulated aircraft cabin bleed-air contamination in lung models using a novel air-liquid interface (ALI) exposure system			×

According to the main findings drawn from Chapter 2 to Chapter 5 by those research aims, the general discussion in this section focuses on the following two perspectives:

1. Hazard assessment of exposure to aircraft-related air pollutants including airport UFPs in and around airports and bleed-air contaminants in aircraft cabin air.
2. Testing strategy to investigate *in vitro* toxicity of exposure to air pollutants.

### Hazard assessment of airport UFPs in and around airports

We investigated *in vitro* toxicity of UFPs from airport (Los Angeles International Airport (LAX) and Amsterdam-Schiphol airport (AMS)) emissions under submerged and ALI exposure conditions, in comparison to well-analyzed traffic emissions (**Chapter 2** and **Chapter 4**). In spite of differences in experimental design among studies at LAX and AMS, including lung cell type and culture/exposure method, results from both studies clearly indicate that short-term ( $\leq 24$  hours) exposure to airport UFPs at tested doses (LAX: 10  $\mu\text{g}/\text{mL}$ ; AMS: 0.09 – 1.69  $\mu\text{g}/\text{cm}^2$ ) can induce inflammation in lung cells. To our knowledge, information on *in vitro* toxicity of airport UFPs has been rarely reported. Jonsdottir et al. (2019) performed a short-term (1 hour) ALI exposure to UFP emissions directly from an aircraft turbine engine at very low doses (0 – 0.4  $\mu\text{g}/\text{cm}^2$ ). In their study significant cytotoxicity and enhanced pro-inflammatory responses were observed in the lung cells, suggesting acute lung toxicity of UFPs from aircraft emissions. As aircraft emissions are the major contributor to the total mass of airport UFPs, *in vitro* toxicity of UFPs from aircraft turbine engine emissions may to some extent represent toxic potency of airport UFPs. In accordance with a previous *in vivo* study (Bendtsen et al., 2019), acute lung inflammation can also be induced in mice after pulmonary exposure to 18 and 54  $\mu\text{g}$  of UFPs collected from the apron of Copenhagen Airport (CPH) for 1 day. Most notably, effects of airport UFPs on induction of acute inflammation, using interleukin (IL)-6 levels in blood samples as a marker, was also observed in volunteers (22 non-smoking adults with mild to moderate asthma) after exposure at the high LAX UFP zone (downwind of LAX, ~10 km) for 2 hours (Habre et al., 2018). Another recent study at AMS (same as sampling site described in **Chapter 4**) showed that short-term (5 hours) exposure to airport UFPs was associated with decreased lung function as well as decreased heart function in healthy volunteers (Lammers et al., 2020). However, according to an epidemiological study on airport staffs (baggage handlers, catering drivers, cabin cleaning staff, airside security and landside security) at CPH, no association was observed between chronic occupational exposure to UFPs at airport (from 1990 to 2012) and the increased risk of cardiovascular diseases (Møller et al., 2020). Taken those results from *in vitro*, *in vivo* and human exposures together, we can conclude that, compared to the background levels, short-term ( $\leq 24$  hours) elevated exposure to UFPs from airport emissions may



induce lung inflammation and negatively affect lung function. Our *in vitro* findings are in line with those reported using *in vivo* models or derived from volunteer exposures, suggesting that relatively simple models can already be informative for hazard assessment.

For short-term exposure to airport UFPs, to put exposure levels into perspective, we estimated the realistic inhaled dose delivered into the lungs during a single day (24 hours) as follows:

We assume the inhaled air volume for an adult of 25 m<sup>3</sup> per day (Paur et al., 2011), the human tracheobronchial surface area of 2471 cm<sup>2</sup> (Mercer et al., 1994), and the deposition fraction of airport UFPs (particle size ≈ 20 nm, Shirmohammadi et al. 2017) onto the tracheobronchial epithelium around 40% (Braakhuis et al., 2014). Mass concentrations of PM<sub>2.5</sub> measured at sampling sites near LAX and AMS during aircraft activities are respectively 35 µg/m<sup>3</sup> and 7.4 µg/m<sup>3</sup> (Pirhadi et al., 2020; Shirmohammadi et al., 2017). Also, according to the epidemiological studies in airport surroundings, PM<sub>2.5</sub> mass concentrations measured during volunteer exposures are 13.7 µg/m<sup>3</sup> at LAX (Habre et al., 2018) and 23.1 µg/m<sup>3</sup> at AMS (Lammers et al., 2020). Those values measured in airport surroundings (outside airport areas) may to some extent represent the residential exposure level. Mass concentrations of PM<sub>2.5</sub> were also measured inside a commercial airport in which PM<sub>2.5</sub> levels ranged from 105 to 385 µg/m<sup>3</sup> inside terminal buildings and from 156 to 400 µg/m<sup>3</sup> in ambient airport air (Ren et al., 2018). Those values measured inside airport areas may represent the occupational exposure level of PM<sub>2.5</sub> at airports. Lewis et al. (2018) have reported that for aviation emissions the mass fraction of PM<sub>0.1</sub> relative to PM<sub>2.5</sub> is around 15%. Accordingly, mass concentrations of UFPs can be estimated to be in a range of 1.11 to 5.25 µg/m<sup>3</sup> around airports (outside the airport area) and in a range of 15.8 to 60 µg/m<sup>3</sup> at airports (inside the airport area). According to the equation above, estimates for the realistic inhaled dose of UFPs for an adult after a single day exposure thus amount to 4.5 – 21 ng/cm<sup>2</sup> in airport surroundings and 64 - 243 ng/cm<sup>2</sup> at airports. Due to limitations of submerged exposure, toxicological results from submerged *in vitro* exposure could not be translated to real-life human exposures. We thus only use toxicological data from ALI exposures (**Chapter 4**) for inhalation risk assessment. Ideally, *in vitro* exposure to airport UFPs should be performed around the level to which a population can be exposed to. However, our pilot experiment in **Chapter 4** showed that the no-effect level using the Calu-3 cells was higher than 21 ng/cm<sup>2</sup> (the theoretically highest level around airports). We therefore increased the tested doses of UFPs to a range of 90 to 2070 ng/cm<sup>2</sup>. The BMDL values of airport UFPs for lactate dehydrogenase (LDH) release (470 – 550 ng/cm<sup>2</sup>) and pro-inflammatory responses (90 – 220 ng/cm<sup>2</sup>) derived from BMD analysis in our study were higher than the theoretical

inhaled level (4.5 – 21 ng/cm<sup>2</sup>) in airport surroundings, but substantially overlapping with the level (64 - 243 ng/cm<sup>2</sup>) at airports. Therefore, our *in vitro* toxicological data can closely reflect the potential health risks of short-term exposure to UFPs at airports, particularly for airport personnel who operate in airport taxiways.

Notably, we assessed health effects of airport UFPs on the basis of toxicological results from short-term exposures (24 hours), whereas under realistic environmental conditions airport personnel and surrounding residents are repeatedly exposed to airport UFPs over a long-term period. As clearance of UFPs in the lungs is a relatively slow mechanisms (up to several months to be completed, (Sturm, 2011)), cumulative exposure of airport UFPs may occur in airport personnel and surrounding residents. In theory that can result in persistent adverse effects on the lungs. Besides, retained UFPs in the lungs can gradually be translocated to the microvasculature and systemic circulation (Miller et al., 2017; Terzano et al., 2010), which may be a trigger of systemic diseases.

#### Hazard assessment of bleed-air contaminants in an aircraft cabin

It has been reported that fume events may occur once in about 200 - 5000 flights (Megson et al., 2016). Capturing fume events through an extensive commercial flight campaign would therefore be overly cost- and time-inefficient. Also, differences among aircrafts on engine conditions, used oil types, operational conditions and cabin air distribution systems may result in variable composition profiles of bleed-air contaminants in aircraft cabins during fume events. It is thus hard to clearly identify which marker substances can be used to investigate a potential association with adverse health effects. We therefore constructed a “Mini-BACS + AES” setup to mimic inhalation exposure to aircraft cabin bleed-air contaminants under controlled laboratory conditions (**Chapter 5**).

Our *in vitro* results revealed that fumes generated from aircraft engine oils (0 – 100 mg/m<sup>3</sup>) and hydraulic fluids (0 – 90 mg/m<sup>3</sup>) at the tested dose-ranges can induce significant toxicity in the lung cell models under ALI conditions. We also investigated the hazards of the generated fumes on the nervous system (data not shown in this thesis). The *in vitro* toxicological data showed that both acute (0.5 hour) and sub-chronic (24 - 48 hours) exposure to engine oil and hydraulic fluid fumes can cause an inhibition of neuronal activity in primary rat cortical cultures without affecting cell viability. There is currently a lack of data regarding lung toxicity after acute and chronic exposure to (simulated) aircraft cabin bleed-air contaminants. Neurotoxic effects of acute exposure to high levels of bleed-air contaminants in healthy volunteers were reported by Heutelbeck et al. (2016), in which an inhibition of neuropathy target esterase (NTE) activity was found in blood samples collected

from 11 flight crews 5 days post-exposure of a fume event. Also, clinical investigations suggested that chronic occupational exposure to low levels of bleed-air contaminants during flights can pose potential neurological effects on aircrews. Reneman et al. (2016) observed a relative reduction in brain white matter microstructure (associated with the extent of cognitive impairment) for aircrews with around 8000 flight hours compared to controls (healthy volunteers, predominantly racecar drivers), although the extent of the reductions in white matter seemed independent of the estimated total number of flight hours. Additionally, elevated levels of neuronal and glial auto-antibodies as biomarkers of central nervous system (CNS) injury were observed in blood samples obtained from three aircrews with more than 2600 flight hours (Hageman et al., 2020). Taken together, those results from *in vitro* and human exposures highlight the potential health risks, particularly functional neurotoxic effects, associated with exposure to contaminated aircraft cabin air.

As described in **Chapter 5**, the estimated inhaled fume level (0.13 - 0.6 mg/m<sup>3</sup>) into the human tracheobronchial region is comparable to the BMDL derived from the effect markers (LDH release and production of IL-6 and IL-8) in our study. This suggests that, on the mass concentration of fumes basis, our *in vitro* toxicological results can closely reflect the potential inhalation risks during fume events. Notably, the calculation in **Chapter 5** is made only on the mass basis of fumes and their deposition, while cabin fume is a complex mixture of gases and particles, in which the gaseous part is likely also toxic to the lungs. Therefore, the main gaseous contaminants (CO and VOCs) during fume events should also be taken into consideration to comprehensively evaluate how the levels of gaseous contaminants in test atmospheres *in vitro* relate to exposure conditions in aircraft cabins. The reported levels of CO ranged from < 1 ppm to 9.4 ppm and VOCs ranged from below the limit of detection to  $\approx$  10 ppm in aircraft cabin air (Shehadi et al., 2016). It is clear that CO and VOCs levels measured in test atmospheres (CO: 0.7 - 20 ppm; VOCs: 4.7 - 12 ppm) during *in vitro* exposure substantially overlap with the realistic cabin levels. EPA (2000) has established limits for CO of 9 ppm (around mean cabin CO level) for an 8-hour exposure to prevent carboxyhemoglobin (COHb) level in blood from rising > 2.5%. It suggests that acute exposure to CO during fume events might not induce significant toxicity in aircrew and passengers. In terms of exposure to VOCs during fume events, health monitoring of aircrews who suffer from complex symptoms after fume events showed that the individual VOC levels (in blood and urine), particularly octane and hexane, increased dramatically (around 100 times) after a fume event compared to those after a flight-free period (Heutelbeck, 2017). This implies that exposure to VOCs during a fume event can result in load and accumulation of VOCs in human body.

The use of a laboratory setup to simulate fume events has the advantage of being stable and independent under controlled conditions for characterization of test atmospheres and *in vitro* exposure to the generated fumes. However, it should be noted that such a simulator could not meet the exact aircraft engine circumstances and cabin conditions during fume events. In comparison to laboratory conditions, different aspects such as high ozone level, presence of combustion products (e.g. nitrogen oxides and sulfur oxides) emitted from aircraft engine, low humidity and low air pressure in aircraft cabins may increase the potential inhalation risks during fume events (Wolkoff et al., 2016). High level of ozone in the atmosphere at high altitude may enter into aircraft cabins, due to inadequate converters of ozone in many commercial aircrafts (Weisel et al., 2013). It has been reported that cabin ozone level is consistently associated with upper respiratory symptoms in aircrews and passengers (Bekö et al., 2015). High levels of ozone in aircraft cabins can also result in abundant ozone-initiated reaction products, particularly in presence of VOCs, which are abundantly formed during fume events. Those ozone-initiated reaction products can be more irritating than their precursors, thus increasing their inhalation risks (Weisel et al., 2013; Wolkoff et al., 2000). Combustion products, such as nitrogen oxides from high-temperature oxidation of nitrogen in combustion air and sulfur oxides from jet fuel, can be abundantly emitted from aircraft engines during take-off (Day, 2015). Exposure to those combustion products, in particular after reactions with cabin ozone, may exacerbate the development of respiratory symptoms in aircrews and passengers during flights (Strøm-Tejsen et al., 2008; Weschler, 2006). We therefore recommend to study chemical interactions between, for example, nitrogen oxides and ozone with possible bleed-air contaminants (e.g. VOCs) in a follow-up study. Aircraft cabin environment is also an important risk factor. The relatively low humidity and air pressure inside cabins, which can increased body fluid loss, is likely to result in adverse effects including irritation of the eyes and upper airways on aircrews and passengers (Hashiguchi et al., 2013; Nagda and Hodgson, 2001). Additionally, high level of occupancy and occasionally combined with frequent changes in gravitational forces can adversely influence comfort of aircrews and passengers, probably making them more susceptible to cabin bleed-air contaminants.

### Testing strategy to investigate *in vitro* toxicity of exposure to air pollutants

As mentioned in **Chapter 1**, *in vitro* exposure has become a widely applied method for inhalation hazard assessment as a potential alternative for testing in animals (BéruBé et al., 2010). In this thesis, we present results of studies in which we have used both submerged and ALI exposure conditions with different lung cell types in either monoculture or co-culture models for *in vitro* toxicity testing of particles with and without gases. In accordance with our findings, a testing strategy has been designed for air pollutants to present how to investigate *in vitro* toxicity of air pollutants

(Figure 1, using ambient UFPs as an example). Notably, the choice of type of lung cells for *in vitro* exposure may depend on region of the lung that relates to the objectives of the study. Therefore, the first important step is to select a suitable lung cell model for *in vitro* exposure. As inhaled UFPs can deposit onto the tracheobronchial and alveolar epithelium, depending on particle size and aerodynamic behavior, lung bronchial epithelial and alveolar epithelial cell models can be both used for inhalation toxicity testing of UFPs *in vitro*. Usually, those lung epithelial cell models are co-cultured with macrophages to investigate cellular responses to particles (Ji et al., 2018; Wottrich et al., 2004), as lung macrophages play an important role in the defense against inhaled particles (Joshi et al., 2018). Furthermore, to closely investigate mechanisms of particles uptake by immune cells of airway wall, more complex *in vitro* lung models can be designed on the co-culture of macrophages and lung epithelial cells basis for toxicity testing. For example, macrophages and epithelial cells collaborate with dendritic cells in the human airways by building a transepithelial network against inhaled particles. On the co-culture of macrophages and lung epithelial cells basis, dendritic cells can be cultured underneath the membrane of the inserts to create the triple cell culture model (Blank et al., 2007; Rothen-Rutishauser et al., 2005). Additionally, to recapitulate the air/blood barrier and investigate translocation of inhaled particles from the lungs to the blood stream, the co-cultures of alveolar epithelial cells and human umbilical vein endothelial cells (HUVEC) can be created by culturing HUVEC underneath the membrane of the inserts (Liyasova et al., 2011).

For testing the toxicity of the less-investigated UFP samples *in vitro*, it is suggested to start with submerged exposure to establish a dose-response relationship with a wide dose-range. The lethal doses (e.g. the median lethal dose,  $LD_{50}$ ) of UFP samples can be accordingly derived from the dose-response curve to gain a basic understanding of their toxic potency. ALI exposure of lung cell models can be subsequently performed to further accurately evaluate their toxicity. The exposure concentration for ALI exposure is usually determined according to the lethal doses (e.g.  $LD_{20}$  and  $LD_{50}$ ) from submerged exposure as well as the human realistic inhaled dose.

After ALI exposure, various biological responses can be measured to assess lung toxicity of inhaled UFPs, depending on the research aims. Cytotoxicity refers to the ability of, for example, UFPs to destroy living cells. Therefore, it is of vital importance to accurately measure cytotoxicity after inhalation exposure to identify if tested substances can pose certain health risks. The LDH release assay is the most commonly used method to determine cytotoxicity. Barrier function of airway epithelium plays a critical role in preventing inhaled UFPs from injuring the lungs. As an important indicator of barrier function, transepithelial electrical resistance (TEER) of lung cell models can be monitored after exposure to identify barrier integrity in lung cell

models. Some follow-up experiments such as visualization of tight junction proteins can also be considered, as tight junctions contribute significantly to barrier function of the bronchial epithelium (Ganesan et al., 2013). A combination of UFPs deposition and interactions in the lungs can result in the induction of lung inflammation. To monitor the inflammation induced by inhaled UFPs, inflammatory response in lung cell models can be determined on basis of the production of cytokines, including IL-6, IL-8 and tumor necrosis factor (TNF)- $\alpha$ . Besides, additional biological responses to inhaled UFPs such as reactive oxygen species (ROS) activity and surfactant production in lung models can also be measured for hazard assessment.

Ambient UFPs can vary in size, shape, chemical composition and other characteristics, depending on their potential sources. In parallel with toxicity testing, important physicochemical properties of particles, such as size distribution, shape and chemical composition that have been suggested to affect their toxic potency, should also be characterized for hazard assessment (Braakhuis et al., 2016; Kelly and Fussell, 2012). It has been reported that the translocation and clearance of particles in the lungs are strongly related to their size distribution, shape and chemical composition (Braakhuis et al., 2016; Li et al., 2003). During those processes, particle interactions with cell membrane, subcellular organelles and biological systems can occur, catalyzing ROS production and inflammatory responses in lung cell models (Braakhuis et al., 2016; Li et al., 2003). Also, particles consisting of relatively toxic chemicals such as polycyclic aromatic hydrocarbons (PAHs) and transition metals (e.g. Ni, V, Fe, and Cu) can significantly induce severe inflammation, particularly for UFPs with large surface-to-volume ratio and high surface activity to absorb those chemicals (Li et al., 2003; Masiol and Harrison, 2014). Overall, knowledge on characteristics of particles in combination with the obtained *in vitro* toxicity data will help to assess inhalation risks of UFPs and identify which marker characteristics dominantly contribute to toxicity.

## Future perspectives

As particle aggregation and alteration of the chemical composition of PM can usually occur during sampling and extraction processes (Chapter 2 and Chapter 4), *in vitro* toxicity of PM derived from particle suspensions may differ from PM in ambient air. A possible solution to minimize this limitation in future experiments is to combine PM sampling and ALI exposure, allowing for a direct exposure of the cells to collected aerosols. Moreover, we applied only single and short-term exposures of airport UFPs to assess their potential health risks, whereas under realistic environmental conditions airport personnel and residents living close to airports are probably exposed to airport UFPs over a long period of time. Therefore, inhalation toxicity of

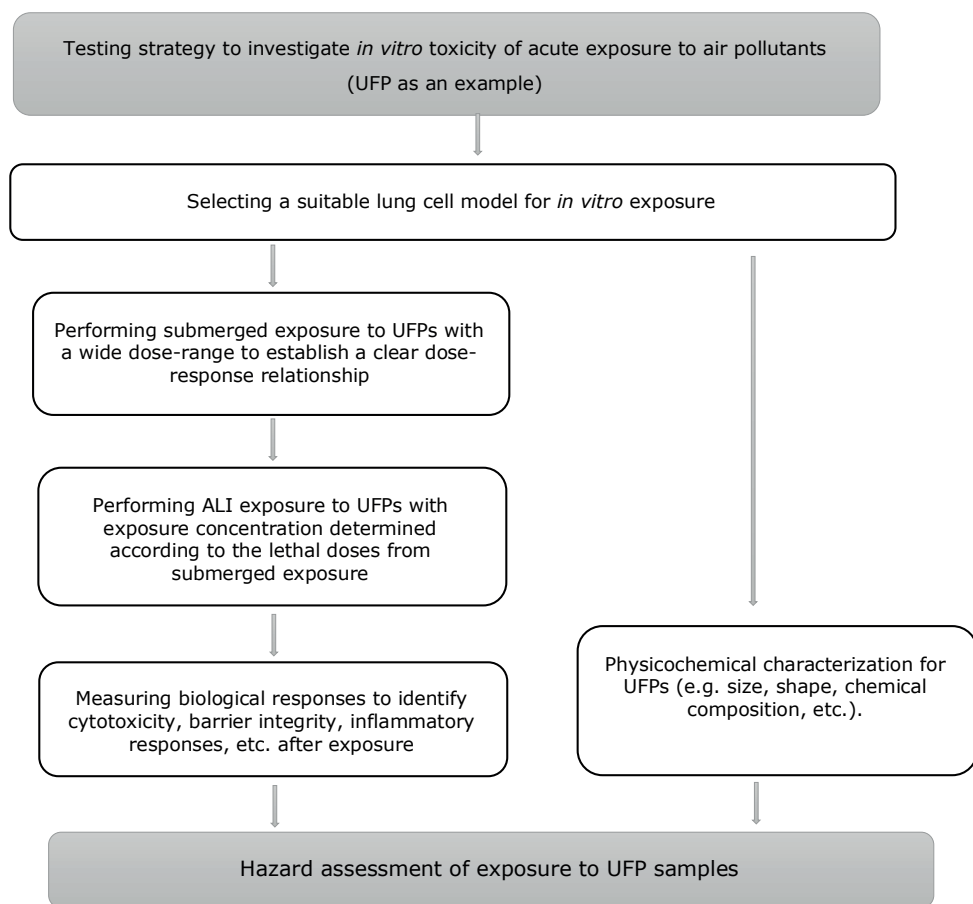


**Figure 1.** Testing strategy to investigate *in vitro* toxicity of acute exposure to ambient UFPs.

long-term and repeated exposures to airport UFPs needs to be further investigated. It is warranted to use not only human bronchial epithelial cell models but also alveolar epithelial models for inhalation toxicity testing to comprehensively evaluate toxic effects of inhaled UFPs. As such, a further study to investigate which is the best alveolar cell model under ALI conditions needs to be performed. Besides, to closely mimic *in vivo*-like conditions and accurately investigate cellular responses to test substances, progress should be made to develop complex *in vitro* lung models with more types of cells (e.g. lung vascular cells, primary bronchial and alveolar epithelial cells) under ALI conditions. For those established multicellular models, particularly involving primary cells, stability under long-term ALI exposure conditions will be a challenge. Therefore, comprehensive evaluations with respect to cell viability,

cell layer integrity, inflammatory responses and surfactant properties should be monitored for those multicellular models over prolonged ALI culture to identify their feasibility for toxicity testing. Notably, organ-on-a-chip (OOC) technology that integrates *in vitro* models and a micro-engineered environment on a single chip has recently taken *in vitro* toxicity testing to an unprecedented level (Bovard et al., 2017). Multiple lung-on-a-chip microsystems have been designed, which can reproduce not only the morphology but also mechanical properties (e.g. physical movement) of the lung epithelium (Benam et al., 2016; Huh, 2015). Those lung-on-a-chip microsystems in combination with ALI exposure systems may offer new opportunities to accurately evaluate the toxicity of e.g. inhaled particles *in vitro*.

The outcomes of this thesis mainly contribute to refine our understanding of the potential lung toxicity of exposure to airport UFPs and aircraft cabin bleed-air contaminants, referred as aircraft-related air pollutants in this thesis. Notably, increasing evidence indicates that UFPs and gaseous chemicals can pass through the lungs and go into the blood stream, eventually diffusing throughout the body including the brain (Park et al., 2014; Terzano et al., 2010). Therefore, further *in vitro* studies on cardiovascular toxicity and neurotoxicity of those aircraft-related pollutants should also be performed by linking, for example, lung OOC with heart OOC or brain OOC. Additionally, in this thesis, toxicological data were derived from *in vitro* exposures alone, which might not perfectly reflect inhalation risks of those aircraft-related air pollutants under real-life exposure conditions. Additional *in vivo* and clinical studies are expected in the future to validate our findings.

Last but not least, given the increasing number of associations between exposure to aircraft-related air pollutants and potential health risks, concerns on regulations of aircraft emissions and cabin air quality have been raised in recent years. Information summarized and discussed in this thesis regarding the hazardous properties of aircraft-related air pollutants and their possible inhalation risks may provide guidance and contribute to policy-making on air quality monitoring and improvement at airports and in aircraft cabins. Also, certain measures should be taken to minimize the occupational exposure risks for airport personnel and cabin crews who work in physical conditions with long-term and repeated exposures to airport UFPs and aircraft cabin bleed-air contaminants. For example, requiring airport personnel to wear masks when operating in airport taxiways, updating aircraft cabin ventilation standards to effectively control cabin bleed-air contaminants, setting a health-based shift system and working duration, and operating a routine health surveillance system.



## References

- Bekö, G., J.G. Allen, C.J. Weschler, J. Vallarino, and J.D. Spengler. 2015. Impact of cabin ozone concentrations on passenger reported symptoms in commercial aircraft. *PLoS one*. 10:e0128454.
- Benam, K.H., R. Villenave, C. Lucchesi, A. Varone, C. Hubeau, H.-H. Lee, S.E. Alves, M. Salmon, T.C. Ferrante, and J.C. Weaver. 2016. Small airway-on-a-chip enables analysis of human lung inflammation and drug responses *in vitro*. *Nature methods*. 13:151-157.
- Bendtsen, K.M., A. Broström, A.J. Koivisto, I. Koponen, T. Berthing, N. Bertram, K.I. Kling, M. Dal Maso, O. Kangasniemi, and M. Poikkimäki. 2019. Airport emission particles: exposure characterization and toxicity following intratracheal instillation in mice. *Particle and fibre toxicology*. 16:1-23.
- BéruBé, K., Z. Prytherch, C. Job, and T. Hughes. 2010. Human primary bronchial lung cell constructs: the new respiratory models. *Toxicology*. 278:311-318.
- Blank, F., B. Rothen-Rutishauser, and P. Gehr. 2007. Dendritic cells and macrophages form a transepithelial network against foreign particulate antigens. *American journal of respiratory cell and molecular biology*. 36:669-677.
- Bovard, D., A. Iskandar, K. Luettich, J. Hoeng, and M.C. Peitsch. 2017. Organs-on-a-chip: A new paradigm for toxicological assessment and preclinical drug development. *Toxicology Research and Application*. 1:2397847317726351.
- Braakhuis, H.M., M.V. Park, I. Gosens, W.H. De Jong, and F.R. Cassee. 2014. Physicochemical characteristics of nanomaterials that affect pulmonary inflammation. *Particle and fibre toxicology*. 11:18.
- Braakhuis HM, Giannakou C, Peijnenburg WJ, Vermeulen J, van Loveren H, Park MV. 2016. Simple *in vitro* models can predict pulmonary toxicity of silver nanoparticles. *Nanotoxicology* 10:770-779.
- CAA. 2004. Safety Regulation Group: cabin air quality. *Report No. Civil Aviation Authority (CAA) Paper 2004/04*.
- Day, G.A. 2015. Aircraft cabin bleed air contaminants: A review. Federal Aviation Administration: Report No. DOT/FAA/Am-15/20.
- EPA. 2000. Air quality criteria for carbon monoxide. *Final Report. EPA 600/P-99/001F*.
- Ganesan, S., A.T. Comstock, and U.S. Sajjan. 2013. Barrier function of airway tract epithelium. *Tissue barriers*. 1:e24997.
- Habre, R., H. Zhou, S.P. Eckel, T. Enebish, S. Fruin, T. Bastain, E. Rappaport, and F. Gilliland. 2018. Short-term effects of airport-associated ultrafine particle exposure on lung function and inflammation in adults with asthma. *Environment international*. 118:48-59.
- Hageman, G., T. Pal, J. Nihom, S. MackenzieRoss, and M. van den Berg. 2020. Three patients with probable aerotoxic syndrome. *Clinical Toxicology*. 58:139-142.
- Hashiguchi, N., A. Takeda, Y. Yasuyama, A. Chishaki, and Y. Tochihiro. 2013. Effects of 6-h exposure to low relative humidity and low air pressure on body fluid loss and blood viscosity. *Indoor air*. 23:430-436.
- Heutelbeck, A.R., C. Bornemann, M. Lange, A. Seeckts, and M.M. Müller. 2016. Acetylcholinesterase and neuropathy target esterase activities in 11 cases of symptomatic flight crew members after fume events. *Journal of Toxicology and Environmental Health, Part A*. 79:1050-1056.
- Heutelbeck, A.R.R. 2017. Progress Report: Diagnostics of Health Disorders and Bio Monitoring in Aircraft Crew Members after “Fume Events”—Preliminary Results After Analyzing Patient Files. 2017INTERNATIONAL AIRCRAFT:38.
- Huh, D. 2015. A human breathing lung-on-a-chip. *Annals of the American Thoracic Society*. 12:S42-S44.
- Ji, J., S. Upadhyay, X. Xiong, M. Malmlöf, T. Sandström, P. Gerde, and L. Palmberg. 2018. Multi-cellular human bronchial models exposed to diesel exhaust particles: assessment of inflammation, oxidative stress and macrophage polarization. *Particle and fibre toxicology*. 15:19.
- Jonsdottir, H.R., M. Delaval, Z. Leni, A. Keller, B.T. Brem, F. Siegerist, D. Schönenberger, L. Durdina, M. Elser, and H. Burtcher. 2019. Non-volatile particle emissions from aircraft turbine engines at ground-idle induce oxidative stress in bronchial cells. *Communications biology*. 2:1-11.
- Joshi, N., J.M. Walter, and A.V. Misharin. 2018. Alveolar macrophages. *Cellular immunology*. 330:86-90.
- Kelly, F.J., and J.C. Fussell. 2012. Size, source and chemical composition as determinants of toxicity attributable to ambient particulate matter. *Atmospheric environment*. 60:504-526.
- Lammers, A., N. Janssen, A. Boere, M. Berger, C. Longo, S. Vijverberg, A. Neerinx, A. Maitland-van der Zee, and F. Cassee. 2020. Effects of short-term exposures to ultrafine particles near an airport in healthy subjects. *Environment International*. 141:105779.
- Lewis, A., D. Carslaw, and S.J. Moller. 2018. Ultrafine Particles (UFP) in the UK.
- Li, N., C. Sioutas, A. Cho, D. Schmitz, C. Misra, J. Sempf, M. Wang, T. Oberley, J. Froines, and A. Nel. 2003. Ultrafine particulate pollutants induce oxidative stress and mitochondrial damage. *Environmental health perspectives*. 111:455.
- Liyasova, M., B. Li, L.M. Schopfer, F. Nachon, P. Masson, C.E. Furlong, and O. Lockridge. 2011. Exposure to tri-o-cresyl phosphate detected in jet airplane passengers. *Toxicology and Applied Pharmacology*. 256:337-347.
- Masiol M, Harrison RM. 2014. Aircraft engine exhaust emissions and other airport-related contributions to ambient air pollution: a review. *Atmos. Environ*. 95: 409-55.
- Megson, D., X. Ortiz, K.J. Jobst, E.J. Reiner, M.F. Mulder, and J.-C. Balouet. 2016. A comparison of fresh and used aircraft oil for the identification of toxic substances linked to aerotoxic syndrome. *Chemosphere*. 158:116-123.
- Mercer, R.R., M.L. Russell, V.L. Roggli, and J.D. Crapo. 1994. Cell number and distribution in human and rat airways. *American journal of respiratory cell and molecular biology*. 10:613-624.
- Miller, M.R., J.B. Raftis, J.P. Langrish, S.G. McLean, P. Samutrtai, S.P. Connell, S. Wilson, A.T. Vesey, P.H. Fokkens, and A.J.F. Boere. 2017. Inhaled nanoparticles accumulate at sites of vascular disease. *ACS nano*. 11:4542-4552.
- Møller, K.L., C. Brauer, S. Mikkelsen, J.P. Bonde, S. Loft, K. Helweg-Larsen, and L.C. Thygesen. 2020. Cardiovascular disease and long-term occupational exposure to ultrafine particles: A cohort study of airport workers. *International Journal of Hygiene and Environmental Health*. 223:214-219.
- Nagda, N.L., and M. Hodgson. 2001. Low relative humidity and aircraft cabin air quality. *Indoor air*. 11:200-214.
- Park, E.-J., Y.-G. Min, G.-w. Kim, J.-p. Cho, W.-j. Maeng, and S.-c. Choi. 2014. Pathophysiology of brain injuries in acute carbon monoxide poisoning: a novel hypothesis. *Medical hypotheses*. 83:186-189.
- Paur, H.-R., F.R. Cassee, J. Teeguarden, H. Fissan, S. Diabate, M. Aufderheide, W.G. Kreyling, O. Hänninen, G. Kasper, and M. Riediker. 2011. In-vitro cell exposure studies for the assessment of nanoparticle toxicity in the lung—A dialog between aerosol science and biology. *Journal of Aerosol Science*. 42:668-692.
- Pirhadi, M., A. Mousavi, M.H. Sowlat, N.A. Janssen, F.R. Cassee, and C. Sioutas. 2020. Relative contributions of a major international airport activities and other urban sources to the particle number concentrations (PNCs) at a nearby monitoring site. *Environmental Pollution*. 260:114027.
- Ren, J., X. Cao, and J. Liu. 2018. Impact of atmospheric particulate matter pollutants to IAQ of airport terminal buildings: A first field study at Tianjin Airport, China. *Atmospheric Environment*. 179:222-226.
- Reneman, L., S.B. Schagen, M. Mulder, H.J. Mutsaerts, G. Hageman, and M.B. de Ruiter. 2016. Cognitive impairment and associated loss in brain white microstructure in aircrew members exposed to engine oil fumes. *Brain imaging and behavior*. 10:437-444.
- Rothen-Rutishauser, B.M., S.G. Kiama, and P. Gehr. 2005. A three-dimensional cellular model of the human respiratory tract to study the interaction with particles. *American journal of respiratory cell and molecular biology*. 32:281-289.
- Shehadi, M., B. Jones, and M. Hosni. 2016. Characterization of the frequency and nature of bleed air contamination events in commercial aircraft. *Indoor air*. 26:478-488.
- Shirmohammadi, F., M.H. Sowlat, S. Hasheminassab, A. Saffari, G. Ban-Weiss, and C. Sioutas. 2017. Emission rates of particle number, mass and black carbon by the Los Angeles International Airport (LAX) and its impact on air quality in Los Angeles. *Atmospheric Environment*. 151:82-93.
- Strøm-Tejse, P., C.J. Weschler, P. Wargocki, D. Myskó, and J. Zarzycka. 2008. The influence of ozone on self-evaluation of symptoms in a simulated aircraft cabin. *Journal of exposure science & environmental epidemiology*. 18:272-281.
- Sturm, R. 2011. Theoretical and experimental approaches to the deposition and clearance of ultrafine carcinogens in the human respiratory tract. *Thoracic Cancer*. 2:61-68.
- Terzano, C., F. Di Stefano, V. Conti, E. Graziani, and A. Petroiani. 2010. Air pollution ultrafine particles: toxicity beyond the lung. *Eur Rev Med Pharmacol Sci*. 14:809-821.
- Weisel, C., C.J. Weschler, K. Mohan, J. Vallarino, and J.D. Spengler. 2013. Ozone and ozone byproducts in the cabins of commercial aircraft. *Environmental science & technology*. 47:4711-4717.
- Weschler, C.J. 2006. Ozone's impact on public health: contributions from indoor exposures to ozone and products of ozone-initiated chemistry. *Environmental health perspectives*. 114:1489-1496.

- Wolkoff, P., P. Clausen, C. Wilkins, and G. Nielsen. 2000. Formation of strong airway irritants in terpene/ozone mixtures. *Indoor air*. 10:82-91.
- Wolkoff, P., D.R. Crump, and P.T. Harrison. 2016. Pollutant exposures and health symptoms in aircrew and office workers: Is there a link? *Environment international*. 87:74-84.
- Wottrich, R., S. Diabaté, and H.F. Krug. 2004. Biological effects of ultrafine model particles in human macrophages and epithelial cells in mono- and co-culture. *International journal of hygiene and environmental health*. 207:353-361.

# Summary

## Summary

Since the aviation industry has expanded rapidly over the past decades, aircraft-related air pollution, including airport ultrafine particles (UFPs) pollution and aircraft cabin bleed-air contamination, is considered as an increasing global problem for human health. Exposure to UFPs in/near airports for airport personnel and surrounding residents as well as to bleed-air contaminants in aircraft cabins for aircrews and passengers may be related to a wide spectrum of public health problems. However, scientific information on toxicity of those air pollutants is still incomplete and thus needs to be further investigated. As described in **Chapter 1**, *in vitro* toxicity testing models using direct exposure to air pollutants have gradually become available, avoiding extensive investigations in experimental animals. To realistically mimic inhalation exposure, lung cell models need to be continuously exposed to test atmospheres under air-liquid interface (ALI) conditions. Some of the lung epithelial cell models involve co-culturing with macrophages to construct physiological traits that closely resemble *in vivo* lung epithelium in response to inhaled particles. However, many immortalized cell lines do not remain viable over long-term ALI culture. Careful selection of *in vitro* lung models that meet the aims for ALI exposure is therefore required. The main goal of this thesis is to optimize *in vitro* lung models under prolonged ALI culture conditions for investigating the adverse health effects of air pollutants that are emitted by and in aircrafts. Our major findings are summarized in the following sections.

### Investigation of the chemical composition, potential sources, and *in vitro* toxicity of airport particulate matter (PM), in comparison to PM collected from urban traffic emissions.

In **Chapter 2**, we presented the physicochemical characteristics, potential sources, and *in vitro* toxicity of PM<sub>0.25</sub> collected from airport emissions, in comparison to well-analyzed urban traffic emissions. Aircraft emissions were found as the major contributor to the total PM<sub>0.25</sub> mass collected downwind Los Angeles International Airport (LAX). Compared to airport PM, urban traffic PM samples had a more complex elemental composition, suggesting multiple emission sources. To test toxicity of PM<sub>0.25</sub> from airport and urban traffic emissions *in vitro*, human bronchial epithelial 16HBE cells were exposed to PM<sub>0.25</sub> suspension at 10 µg/mL under submerged conditions. Our *in vitro* toxicological results indicate that PM<sub>0.25</sub> from airport and urban traffic emissions can increase the generation of reactive oxygen species (ROS) and induce pro-inflammatory responses in the bronchial epithelial cells, eventually resulting in cell death. Compared to urban traffic PM, *in vitro* exposure to airport PM increases higher production of pro-inflammatory mediators in the cells probably due to their smaller size range. Our findings highlight the potential health risks of aircraft emissions as a major source of PM<sub>0.25</sub> in airport surroundings.

### Optimization of the *in vitro* mono-/co-culture models of human airway barrier for aerosol exposure under ALI conditions.

In **Chapter 3**, we optimized the *in vitro* mono-/co-culture cell model of human airway barrier under ALI conditions for aerosol exposure. Human bronchial epithelial Calu-3, 16HBE, H292 and BEAS-2B cell lines were evaluated regarding epithelial morphology, barrier function and cell viability over long-term ALI culture. Only Calu-3 cells can exhibit a monolayer structure and maintain a strong barrier function with high cell viability at least up to 2 weeks. Therefore, Calu-3 cells were used as structural barrier to create different co-cultures with monocyte-derived macrophages (MDM) and THP-1 derived macrophages (TDM). Following optimization of the protocol for co-culture, adhesion of macrophages onto the epithelial carpet was allowed for 4 hours with a seeding density of  $5 \times 10^4$  macrophages/cm<sup>2</sup>. When challenged with lipopolysaccharide (LPS) as a positive control, the two co-culture models showed higher sensitivity in inflammatory responses compared to the monoculture of Calu-3 cells, in which the co-culture of Calu-3 + MDM gave a stronger response than the Calu-3 + TDM. Taken together, the optimized monoculture of Calu-3 cells and co-culture of Calu-3 + MDM are preferred for toxicity testing under ALI exposure conditions.

### Application of the optimized lung cell models for *in vitro* toxicity testing of aircraft-related air pollutants under ALI exposure conditions.

Using *in vitro* lung models optimized in **Chapter 3**, we tested *in vitro* toxicity of airport UFPs with an ALI Cloud Exposure System (CES) in **Chapter 4** and fumes generated from aircraft engine oils and hydraulic fluids with an ALI Aerosol Exposure System (AES) in **Chapter 5**.

In **Chapter 4**, we separately collected UFPs predominantly derived from airport emissions (Airport UFPs) or traffic emissions (Non-Airport UFPs) at a location near Amsterdam-Schiphol airport (AMS), depending on wind directions. The mean size of Airport and Non-Airport samples in suspension falls within the ultrafine range (particle size < 100 nm). Using a CES, the optimized monoculture of Calu-3 cells was exposed under ALI conditions to Airport and Non-Airport UFPs, ranging from 0.09 to 2.07 µg/cm<sup>2</sup>. ALI exposures revealed that pro-inflammatory responses can be induced in the lung cells at high viabilities (> 80%) after exposure to Airport and Non-Airport UFPs at doses > 0.09 µg/cm<sup>2</sup>. Airport and Non-Airport UFPs exerted a comparable *in vitro* toxicity in the Calu-3 cells under ALI exposure conditions.

In **Chapter 5**, we investigated toxic effects of exposure to cabin bleed-air contaminants under ALI conditions. To realistically mimic inhalation exposure to cabin bleed-air contaminants and subsequently evaluate their toxicity *in vitro*, a mini Bleed-Air Contaminants Simulator (Mini-BACS) system was connected to an AES. This unique



combination integrates generation of fumes from aircraft engine oils and hydraulic fluids under controlled conditions, deposition of fumes onto lung cell models with a continuous airflow, and online physicochemical measurements of test atmospheres. Our results indicate that exposure to high levels of engine oil and hydraulic fluid fumes under ALI conditions can reduce TEER and cell viability, induce LDH release and increase the production of pro-inflammatory cytokines in the Calu-3 monoculture and Calu-3 + MDM co-culture models. Hydraulic fluids fumes are more toxic than engine oil fumes, likely due to higher abundance of organophosphates (OPs) and smaller particle size distribution (PSD) of hydraulic fluid fumes.

Taken together, *in vitro* toxicological data in **Chapter 4** and **Chapter 5** reveal that exposure to aircraft-related air pollutants, airport UFPs and the generated cabin fumes, can induce considerable lung toxicity, highlighting their potential inhalation risks under real-life exposure conditions.

# Nederlandse Samenvatting

## Nederlandse Samenvatting

Aangezien de luchtvaartindustrie de laatste decennia snel is toegenomen, wordt de aan vliegtuigen gerelateerde luchtverontreiniging, inclusief verontreiniging door ultrafijne deeltjes (UFPs) op luchthavens en verontreiniging door afgevoerde lucht uit vliegtuigcabines, beschouwd als een toenemend wereldwijd probleem voor de gezondheid van de mens. Blootstelling aan UFPs in/nabij luchthavens door luchthavenpersoneel en omwonenden, en aan luchtverontreiniging in vliegtuigcabines door bemanning en passagiers, kan in verband worden gebracht met een breed spectrum van gezondheidsproblemen. De wetenschappelijke informatie over de schadelijkheid van deze luchtverontreinigende stoffen is echter nog onvolledig en moet dus verder worden onderzocht. Zoals beschreven in **hoofdstuk 1**, zijn er langzamerhand *in vitro* modellen voor het testen op schadelijkheid beschikbaar gekomen die gebruik maken van directe blootstelling aan luchtverontreinigende stoffen, waardoor uitgebreid onderzoek bij proefdieren wordt vermeden. Om blootstelling door inademing op realistische wijze na te bootsen, moeten longcellen deels aan de lucht (de testatmosfeer) worden blootgesteld, in zogenaamde air liquid interface (ALI) modellen. Sommige van de modellen met longepitheelcellen omvatten een co-cultuur met macrofagen, met als doel fysiologische reacties te krijgen die sterk lijken op die van *in vivo* longepitheel in reactie op geïnhaleerde deeltjes. Veel geïmmortaliseerde cellijnen blijven echter niet levend tijdens een langdurige ALI kweek. Zorgvuldige selectie van *in vitro* longmodellen die voldoen aan de doelstellingen voor ALI blootstelling is daarom vereist. Het hoofddoel van dit proefschrift is het optimaliseren van *in vitro* longmodellen onder langdurige ALI kweekomstandigheden voor het onderzoeken van de nadelige gezondheidseffecten van luchtverontreinigende stoffen die worden uitgestoten door en in vliegtuigen. Onze belangrijkste bevindingen worden in de volgende paragrafen samengevat.

### Onderzoek naar de chemische samenstelling, potentiële bronnen en *in vitro* toxiciteit van deeltjes (PM) afkomstig van emissies op luchthavens, in vergelijking met PM afkomstig van emissies door stadsverkeer.

In **hoofdstuk 2** presenteerden we de fysisch-chemische karakteristieken, potentiële bronnen, en *in vitro* schadelijkheid van PM<sub>0.25</sub> verzameld uit emissies op luchthavens, in vergelijking met goed geanalyseerde emissies door stadsverkeer. Vliegtuig emissies bleken de grootste bijdrage te leveren aan de totale PM<sub>0.25</sub> massa die werd verzameld benedenwinds van Los Angeles International Airport (LAX). Vergeleken met PM van luchthavens, hadden PM monsters van stedelijk verkeer een meer complexe elementaire samenstelling, wat meerdere emissiebronnen suggereert. Om de toxiciteit van PM<sub>0.25</sub> van luchthaven- en stadsverkeeremissies *in vitro* te testen, werden humane bronchiale epitheliale 16HBE cellen blootgesteld aan 10 µg/

mL PM<sub>0.25</sub>-suspensie in celkweekmedium. Onze *in vitro* toxicologische resultaten tonen aan dat PM<sub>0.25</sub> van luchthaven- en stadsverkeeremissies het ontstaan van reactieve zuurstofspecies (ROS) kan verhogen en ontstekingsreacties in de bronchiale epitheelcellen kan opwekken, uiteindelijk resulterend in celdood. In vergelijking met PM van stadsverkeer, geeft *in vitro* blootstelling aan PM van luchthavens een hogere productie van ontstekingsmoleculen in de cellen, waarschijnlijk als gevolg van hun kleinere omvang. Onze bevindingen wijzen op de potentiële gezondheidsrisico's van vliegtuigemissies als een belangrijke bron van PM<sub>0.25</sub> in de omgeving van luchthavens.

### Optimalisatie van de *in vitro* mono-/co-cultuur modellen van de barrière van de luchtwegen in de mens voor blootstelling aan aërosolen onder ALI condities.

In **hoofdstuk 3** hebben wij het *in vitro* mono-/co-cultuur celmodel van de humane luchtwegbarrière onder ALI omstandigheden geoptimaliseerd voor blootstelling aan aerosolen. Humane bronchiale epitheliale Calu-3, 16HBE, H292 en BEAS-2B cellijnen werden geëvalueerd met betrekking tot epitheliale morfologie, barrièrefunctie en levensvatbaarheid van de cellen gedurende langdurige ALI kweek. Alleen Calu-3 cellen kunnen een enkellaags structuur vertonen en een sterke barrièrefunctie behouden met een hoge levensvatbaarheid van de cellen, tot ten minste 2 weken. Daarom werden Calu-3 cellen gebruikt als structurele barrière om verschillende co-culturen te creëren met van monocytten afgeleide macrofagen (MDM) en van THP-1 cellen afgeleide macrofagen (TDM). Na optimalisatie van het protocol voor co-cultuur, werd adhesie van macrofagen op het epitheliale tapijt uitgevoerd gedurende 4 uur met een zaaidichtheid van  $5 \times 10^4$  macrofagen/cm<sup>2</sup>. Wanneer ze werden gechallenged met lipopolysaccharide (LPS) als positieve controle, vertoonden de twee co-cultuurmodellen een hogere gevoeligheid in ontstekingsreacties in vergelijking met de monocultuur van Calu-3 cellen, waarbij de co-cultuur van Calu-3 + MDM een sterkere respons gaf dan Calu-3 + TDM. Alles bijeen zijn de geoptimaliseerde monocultuur van Calu-3-cellen en de co-cultuur van Calu-3 + MDM te verkiezen voor testen voor schadelijkheid onder ALI omstandigheden.

### Toepassing van de geoptimaliseerde longcelmodellen voor *in vitro* testen voor schadelijkheid van vliegtuig gerelateerde luchtverontreinigende stoffen onder ALI-blootstellingscondities.

Met behulp van *in vitro* longmodellen geoptimaliseerd in **hoofdstuk 3**, testten wij *in vitro* de schadelijkheid van UFPs afkomstig van luchthavens met een ALI Cloud Exposure System (CES) in hoofdstuk 4 en dampen ontstaan uit vliegtuigmotoroliën en hydraulische vloeistoffen met een ALI Aerosol Exposure System (AES) in **hoofdstuk 5**.

In **hoofdstuk 4** hebben we afzonderlijk UFPs verzameld die voornamelijk afkomstig waren van luchthavenemissies of verkeersemisies op een locatie in de buurt van de luchthaven Amsterdam-Schiphol (AMS), afhankelijk van de windrichting. De gemiddelde grootte in suspensie van de monsters van de luchthavens het verkeer valt binnen het ultrafijne bereik (deeltjesgrootte < 100 nm). Met behulp van een CES werd de geoptimaliseerde monocultuur van Calu-3 cellen onder ALI omstandigheden blootgesteld aan UFPs afkomstig van de luchthaven en het verkeer, variërend van 0.09 tot 2.07  $\mu\text{g}/\text{cm}^2$ . Blootstellingen aan ALI toonden aan dat ontstekingsreacties kunnen worden opgewekt in de longcellen bij hoge levensvatbaarheid (> 80%) na blootstelling aan UFPs van de luchthaven en van het verkeer bij doses > 0.09  $\mu\text{g}/\text{cm}^2$ . UFPs van luchthavens en verkeer gaven een vergelijkbare *in vitro* schadelijkheid in de Calu-3 cellen onder ALI blootstellingscondities.

In **hoofdstuk 5** onderzochten we de schadelijke effecten van blootstelling aan verontreinigingen in de afgevoerde lucht uit vliegtuigcabines onder ALI omstandigheden. Om de blootstelling aan verontreinigingen in de afgevoerde lucht uit vliegtuigcabines op realistische wijze na te bootsen en vervolgens hun schadelijkheid *in vitro* na te gaan, werd een mini Bleed-Air Contaminants Simulator (Mini-BACS) systeem aangesloten op een AES. Deze unieke combinatie integreert het opwekken van dampen van vliegtuigmotoroliën en hydraulische vloeistoffen onder gecontroleerde omstandigheden, het afzetten van dampen op longcelmodellen met een continue luchtstroom, en online fysisch-chemische metingen van testatmosferen. Onze resultaten tonen aan dat blootstelling aan hoge niveaus van motorolie en hydraulische vloeistofdampen onder ALI omstandigheden de TEER en de levensvatbaarheid van de cellen kan verminderen, LDH afgifte kan induceren en de productie van ontstekingsbevorderende eiwitten kan verhogen in de Calu-3 monocultuur en Calu-3 + MDM co-cultuur modellen. De dampen van hydraulische vloeistoffen zijn giftiger dan de dampen van motorolie, wat waarschijnlijk te wijten is aan de grotere aanwezigheid van organofosfaten (OPs) en de kleinere deeltjesgrootteverdeling (PSD) van de dampen van hydraulische vloeistoffen.

Samenvattend blijkt uit de *in vitro* toxicologische gegevens in **hoofdstuk 4** en **hoofdstuk 5** dat blootstelling aan met vliegtuigen gerelateerde luchtverontreinigende stoffen, UFPs van luchthavens en de opgewekte cabinegassen, een aanzienlijke longtoxiciteit kunnen induceren, wat hun potentiële inhalatierisico's onder reële blootstellingsomstandigheden onderstreept.



# Acknowledgements

## Acknowledgement

“Was ist deine leidendste Erfahrung? Ist dir Trinken bitter, werde Wein.” Rilke has already helped me to express my feeling towards this long and tough PhD journey. Now, it is a moment of great relief to finally be able to thank all the people that have provided indispensable help and priceless companionship along the way.

I am most grateful to my first promotor Flemming Cassee for taking me in as his doctoral student and introducing me to an interesting research field. His rigorous and patient guidance has made my study at RIVM such a rewarding and fruitful experience of which this dissertation is only a partial reflection. Remco Westerink, my second promotor, is really good at distilling clear thoughts and poignant arguments from my needlessly complex writing. I thank him for the stimulating discussions concerning my dissertation and for reading through numerous drafts, making sure that every word serves its purpose. All in all, without the help and advice from both of them, this dissertation would not have been possible, and their comments and questions will continue to guide me from here.

It is my fortune to have a congenial and brilliant cohort at RIVM. I should first thank Liu Dingyu for her generous assistance, particularly at the start of my PhD. I still remember it is Dingyu that picked me up from the Central Station at the first day when I arrived in Utrecht. Special thanks go to Rob Vandebriel and Hedwig Braakhuis for their generosity for having me work on PATROLS project and offering a sympathetic ear and guiding hand in my work, especially Rob who also helped me in the summary translation from English to Dutch. Such gratitude extends to Eric Gremmer and Paul Fokkens, who contributed most to the completion of my lab work. Thank Eric, my best friend at RIVM, for his invaluable assistance during experiments, for his creative design projects such as my dissertation cover, and for his daily music recommendation at coffee breaks. Those moments occupy a special place in my heart. As an expert technician, Paul provided me the firmest support not only during my ALI exposure experiments but also when my bike broke down. Therefore, I would like to specially thank Paul for teaching me how to fix my bike during my PhD.

I have also received the timely and helpful assistances from many colleagues at RIVM and IRAS – Miriam Gerlofs-Nijland, Ilse Gosens, John Boere, Evert Duistermaat, Daan Leseman, Zhang Yongliang, Lora Gerber, Yvonne Staal, Jolanda Vermeulen, Claudia Kemp, Edwin Zwart, Victoria de Leeuw – Many thanks to all of you. Additionally, my intellectual journey at RIVM could not have been so enjoyable and rewarding without the help of those intern students and researchers – Li Yixuan, Marc Bazan, Rob Vree Egberts, Sonia Fraga – who have temporally worked at RIVM.

During my PhD journey, I met many friends in the Netherlands. Those encounters are as beautiful as the chance encounter of a sewing machine and an umbrella on an operating table. I should first thank Xu Yang and Yue Hui, who were not only my roommates but also my best friends in the Netherlands. It's my good fortune to have met both of them at the start of this new journey in search of meaning and self-worth. I benefited greatly from talks over beers with them. Du Wei, my friend and my elder brother, thanks for driving me to visit those lovely places in the Netherlands in the past years. Without his warm heart and candid character, my life in the Netherlands would definitely be different. My deep gratitude also goes to Ji Mi, Wu Wenyang, Gan Jin, Chen Jie, Meng Xianke, Huang Luhuan, Li Jia, Wu weiwei, Yang Dongsheng, Yang Min, Zhao Yujia, among others, for being my fellow travellers at various stages of my graduate study.

My sincere appreciation goes to the financial support provided by the China Scholarship Council (CSC) during my PhD period. Also, I will never forget the TivoliVredenburg, where I watched lots of great gigs and had the most memorable moments of night and life in the Netherlands. It is definitely my favourite music venue in the world.

Words could not express my thanks to my parents, XuYing and He Chaoqi, and my little sister He Ruiqi, for their love, blessings, and patience. My deepest gratitude goes to my wife, Wang Nijing. Without her support, companionship, and encouragement, I could not have completed this work. It is to her that I dedicate this book.

# Curriculum Vitae



## Curriculum Vitae

**Name:** Ruiwen HE

**Date of birth:** 16-07-1991

**Citizenship:** Chinese

**E-mail:** [hrwen520@live.cn](mailto:hrwen520@live.cn)

### Research Interests

Development of *in vitro* models; Inhalation toxicity; Human risk assessment

### Education and Research Experience

2016 - 2021 Ph.D in Toxicology, RIVM and Utrecht University, the Netherlands.

**Supervisors:** Prof. Dr. Flemming Cassee and Dr. Remco Westerink

**Thesis Title:** “Air-liquid interface (ALI) exposure of *in vitro* lung models: improvement and application to study inhalation toxicity of aircraft-related air pollutants”

2013 - 2016 Master in Environmental Science, Nanjing University, P. R. China

**Supervisors:** Prof. Dr. Lena Q Ma and Dr. Xinyi Cui

2009 - 2013 Bachelor in Environmental Science, Guangzhou University, P. R. China

### Involved projects

Physiologically anchored tools for realistic nanomaterial hazard assessment (EU-PATROLS)

Fresh Aircraft (EU-FACTS)

“Health risks of ultrafine particles around Amsterdam Airport Schiphol” commissioned by the Dutch Ministry of Infrastructure and Water management

### Conference Activities

2020.11.16-20 7th International Conference NANOSAFE 2020 (oral presentation)

2019.08.25-28 31st Annual Conference of the International Society for Environmental Epidemiology (volunteer)

2019.05.15-16 European Federation of Engineering Consultancy Associations symposium, ultrafine particles air quality and climate (oral presentation)

2018.09.02-05 54th Congress of the European Societies of Toxicology (poster)

2018.05.30-31 Nederlandse Vereniging voor Toxicologie (NVT) annual meeting (poster)

## Research Output

### Publications during the PhD period

- **Rui-Wen He**, Marc M.G. Houtzager, W.P. Jongeneel, Remco H. S. Westerink, Flemming R. Cassee (2021). “In vitro hazard characterization in lung cell models exposed to fumes from aircraft engine oils and hydraulic fluids using an air-liquid interface (ALI) exposure system.” *Environment International*, 156, 106718.
- **Rui-Wen He**, Hedwig M. Braakhuis, Rob J. Vandebriel, Yvonne C. M. Staal, Eric R. Gremmer, Paul H.B. Fokkens, Claudia Kemp, Jolanda Vermeulen, Remco H. S. Westerink, Flemming R. Cassee (2020). “Optimization of an air-liquid interface *in vitro* cell co-culture model to estimate the hazard of aerosol exposures.” *Journal of Aerosol Science* 105703.
- **Rui-Wen He**, Miriam E. Gerlofs-Nijland, John Boere, Paul Fokkens, Daan Leseman, Nicole A.H. Janssen, Flemming R Cassee. (2020). “Comparative toxicity of ultrafine particles around a major airport in human bronchial epithelial (Calu-3) cell model at the air-liquid interface.” *Toxicology in vitro*, 104950.
- **He, R.-W.**, F. Shirmohammadi, M. E. Gerlofs-Nijland, C. Sioutas and F. R. Cassee (2018). “Pro-inflammatory responses to PM<sub>0.25</sub> from airport and urban traffic emissions.” *Science of the Total Environment* 640: 997-1003.
- Braakhuis, H. M., **R. He**, R. J. Vandebriel, E. R. Gremmer, E. Zwart, J. P. Vermeulen, P. Fokkens, J. Boere, I. Gosens and F. R. Cassee (2020). “An Air-liquid Interface Bronchial Epithelial Model for Realistic, Repeated Inhalation Exposure to Airborne Particles for Toxicity Testing.” *JoVE (Journal of Visualized Experiments)* (159): e61210.
- Medina-Reyes, E. I., N. L. Delgado-Buenrostro, D. L. Leseman, A. Déciga-Alcaraz, **R. He**, E. R. Gremmer, P. H. Fokkens, J. O. Flores-Flores, F. R. Cassee and Y. I. Chirino (2020). “Differences in cytotoxicity of lung epithelial cells exposed to titanium dioxide nanofibers and nanoparticles: Comparison of air-liquid interface and submerged cell cultures.” *Toxicology in Vitro* 65: 104798.